THE UNIVERSITY *of* EDINBURGH

Novel fire testing frameworks
for
Phase Change Materials
and
hemp-lime insulation

Martyn Scott McLaggan

Doctor *of* Philosophy

The University *of* Edinburgh
2016

Novel fire testing frameworks
for
Phase Change Materials
and
hemp-lime insulation

by

Martyn Scott McLaggan

The thesis has been supervised by:
Dr Rory M. Hadden
Dr Martin Gillie
Dr Adam Cowlard
Prof. José L. Torero

The examining committee consisted of:
Prof. Patrick van Hees
Dr Stephen Welch

Declaration

The work in this thesis has been completed solely by Martyn S. M^{c}Laggan at The University of Edinburgh under the supervision of Dr Rory Hadden, Dr Martin Gillie, Dr Adam Cowlard, and Prof. José L. Torero. Full reference is given where other sources are used. This work has not been submitted for any other degree or professional qualification.

Martyn M^{c}Laggan
May 2016

Abstract

Modern buildings increasingly include the usage of innovative materials aimed at improving sustainability and reducing the carbon footprint of the built environment. Phase Change Materials (PCMs) are one such group of novel materials which reduce building energy consumption. These materials are typically flammable and contained within wall linings yet there has been no detailed assessment of their fire performance. Current standard fire test methods provide means to compare similar materials but do not deliver knowledge on how they would behave in the event of a real fire. Thus, the aim of this thesis is to develop a novel testing framework to assess the behaviour of these materials in realistic fire scenarios.

For PCMs, a flammability study is conducted in the bench-scale cone calorimeter to evaluate the fire risk associated with these materials. Then, micro-scale Thermogravimetric Analysis (TGA) is used to identify the fundamental chemical reactions to be able to confidently interpret the flammability results. Finally, intermediate-scale standard fire tests are conducted to evaluate the applicability of the bench-scale results to realistic fire scenarios. These take the form of modified Lateral Ignition and Flame spread Test (LIFT) and Single Burning Item (SBI) tests to understand flame spread and compartment fires respectively. Finally, a simplified method to combine this knowledge for use in building design is proposed. This method allows the balancing of potential energy benefits with quantified fire performance to achieve the specified goals of the designer.

Hemp-lime insulation is a material which has also becoming increasingly popular in the drive towards sustainability. The porous nature of the material means that smouldering combustions are the dominant reaction mode but there is currently no standardised test method for this type of behaviour. Thus, hemp-lime materials also represent an unquantified risk. The work in this thesis defines a simple, accessible and economically viable bench-scale method for quantifying the fire risk associated with rigid porous materials. This is applicable for both downward opposed flow and upward forward flow smoulder propagation conditions. The behaviour is then interpreted using micro-scale thermogravimetric analysis to understand the underlying pyrolysis and oxidation reactions. Designers can utilise this framework to quantify the smouldering risk associated with hemp-lime materials to enable their usage in the built environment.

The holistic fire risk assessment performed in this thesis has quantified the behaviour of PCMs and hemp-lime insulation applicable to realistic fire scenarios. The simplified design method empowers designers to be able to realise innovative buildings through fundamental understanding of the fire behaviour of these materials. The outcomes of this thesis allow designers to mitigate the fire risk associated with these materials and achieve optimised engineering solutions. Furthermore, the novel fire testing frameworks provide the economically viable means to assess the fire performance of future PCMs and hemp-lime products which ensures lasting relevance of this research in the future.

Lay Summary

Modern buildings increasingly include the usage of innovative materials aimed at improving sustainability and reducing the carbon footprint of the built environment. These new materials are radically different to traditional building materials on which existing fire safety standards are based. Furthermore, these standards only provide the means to compare similar materials and do not deliver knowledge on how they would behave in the event of a real fire. For one of the materials there is no currently applicable test method due to its smouldering nature.

The first of these materials studied are known as Phase Change Materials (PCMs) which are capable of saving energy in the built environment. These materials are typically flammable and contained within wall linings yet there has been no assessment of their fire performance. A novel framework has been developed in this thesis to quantify their behaviour applicable to realistic fire conditions. The fundamental thermal decomposition behaviour is first obtained on a micro-scale under highly controlled conditions. This is used to interpret a small-scale flammability study which forms the backbone of the framework. This quantifies how the material behaves in a variety of conditions, evaluating its burning rate, rate of heat release, time to ignition, minimum energy for ignition, thermal evolution, and gas emissions. This is finally then validated in the intermediate-scale to both understand the behaviour of these materials in the standard test method, as well as ensure that the study is scalable. Finally, the framework is summarised in the final chapter. This can be used by designers to balance the potential energy savings from using PCMs with complete understanding of the associated fire risks. This also allows them to employ any risk mitigation strategies which they desire.

The second of these materials is a porous insulation material formed from shivs and fibres from the hemp plant. These are combined with a cement-like material to form a rigid material which can be included in building walls. Due to the porous nature of the material the material is capable of both flaming and smouldering, but the latter represents the key risk. There is currently no standardised method for evaluating smouldering so a suitable small-scale test method which is cheap, cost effective and widely available was developed. This method quantifies the smouldering risk associated with this material using key metrics. These include the burning rate, spread rate, time to ignition, minimum energy required to sustain a smoulder, and gas emissions. Designers are then able to safely use these materials in buildings knowing how they will behave in representative fire scenarios.

Acknowledgements

First and foremost I would like to thank both of my primary supervisors, Dr Rory Hadden and Dr Martin Gillie. I would also like to thank my industrial supervisors Dr Corinne Williams and Dr Debbie Smith OBE from BRE for their support and constant useful input. I would also like to thank Dr Adam Cowlard for his assistance, support and encouragement, as well as introducing me to fire research. Dr Christine Switzer is also thanked for her role in introducing me to the field and her willingness to help. I am particularly thankful towards Prof. José Torero for hosting my visit to the University of Queensland and his incredibly helpful engagement in the closing stages of the PhD.

I gratefully acknowledge the support of the BRE Trust and EPSRC in enabling this research to go forward. I would also like to additionally thank BRE for allowing me to make use of their facilities.

I would like to thank the Royal Society of Edinburgh for awarding me a John Moyes Lessells scholarship to enable me to travel to the University of Queensland, Australia to improve the research and widen my experience. It proved even more valuable than I imagined.

Lime Technology, UK are thanked for their generous donation of material. Max Burbridge is additionally thanked for helping with the casting and curing procedures of the material.

I'd like to thank Prof. Albert Simeoni for his enthusiastic support and constant willingness to help throughout the project. Prof. Luke Bisby is thanked for his support throughout, and particularly in the closing stages. Dr Stephen Welch is also thanked for his various contributions throughout the project.

I owe a significant amount to Michal Krajčovič without whom the laboratory work would no doubt have gone astray. Jero Carrascal is thanked both for his assistance in conducting laboratory work and for his various other contributions at the University of Queensland.

Mauricio Fuentes and Viktor Angelovski are thanked for their help in casting some of the hemp-lime and PCM enhanced hemp-lime specimens. Jamie Maclean is thanked for his help in running the intermediate-scale standard fire tests at BRE which would have otherwise proven difficult to perform.

Various interlocutors within the University of Edinburgh firegroup and John Muir have been key both in contributing to the research aspects of this project as well as making it a thoroughly enjoyable and worthwhile experience. This includes Juan, Ime, Payam, Liming, Zafiris, Shaun, Cristián, Ieuan, Fabio, Emma, Eric, and Paolo, amongst many countless others.

Contents

List of Figures

List of Tables

1 Introduction

1.1 Background and research significance

The design of buildings is the combination of a multitude of topics and disciplines. These include, but are in no means limited to, aesthetics, function, cost, sustainability, acoustics, structural integrity, and fire performance (Law 1986). The overall importance of each of these aspects will vary depending upon the intent of the design and the background surrounding its inception. In recent times the role of sustainability has become increasingly important within the built environment and society as a whole. Stringent goals for reducing carbon emissions have been set by various countries which have forced the design of buildings to fundamentally change to be able to meet these tough targets.

In the UK, the Code for Sustainable Homes (Department for Communities and Local Government 2006) was introduced in 2006 and a series of EU directives were introduced at the start of the century (European Parliament 2010). These forced a radical rethink of buildings and the materials contained within them to be able to meet these goals.

This led to the development of highly insulating materials capable of saving significant amounts of energy and reducing the carbon footprint of buildings. Furthermore, the potential for net zero carbon or near zero carbon homes became a tangible goal. However, the thermal mass of these buildings was extremely low compared to traditional buildings such as those constructed from concrete or brick. These buildings react rapidly to external temperatures and experience large temperature fluctuations over the period of one day (Konuklu and Paksoy 2009).

1.1.1Phase change materials

The latent thermal storage properties of certain materials have been utilised for some time, particularly for applications involving hot water and heat exchangers (Abhat 1983). Typically these materials are used to retain the heat stored within water, and were found to be more effective than traditional insulation under certain circumstances. These materials have melting points at some temperature between ambient the boiling point for water, typically falling within 60 to 80°C.

The ambitious nature of the carbon reduction goals resulted in the adoption of these latent thermal storage materials into the built environment. Materials were selected with a melting point corresponding to the desired internal temperature. During the day as the temperature rises the material would melts and absorbs energy from its surroundings, thus reducing the peak temperature in the room. As the temperature then falls during the night the materials then re-solidify and release their stored energy. The net result is that less energy is required for cooling during the day and for heating at night. Thus, the carbon footprint of a building can be reduced and the diurnal temperature fluctuation is also reduced.

An effective phase change material requires a throng of thermal properties to be feasible. Firstly, the material must have high latent heat of fusion and possess a melting point close to the desired internal temperature. The material must also be chemically stable or easily containable, and economically viable. Other desirable attributes include appropriate thermal conductivity, little or no flammability, non-corrosive, non-toxic, no supercooling, no phase segregation, and no degradation or loss of efficiency over repeated cycling.

For building applications predominantly organic materials are found to be suitable. Inorganics tend to exhibit too many undesirable properties, namely phase segregation, corrosion, and subcooling. The most suitable organic material is typically a blend of paraffin waxes, whilst fatty acids are also increasingly viable but tend to be more expensive (Salyer *et al.* 1988).

Thus, organic materials which are potentially flammable are included within walls and ceiling tiles to be able to achieve the required energy savings. To assess their flammability they must be classified according to the European system, BS ISO 13501 (British Standards Institution 2009a), but there is no requirement for understanding of their actual behaviour in the event of a fire. Since these materials are highly sophisticated they do not behave in a manner consistent with traditional materials and thus the relevancy of the standard fire testing regime must be reviewed.

1.1.2Hemp-lime insulation

The theme of this thesis is focused on innovative building materials which represent unquantified fire risks. Like phase change materials, hemp-lime materials have become increasingly common in the built environment in the drive towards sustainability and reducing carbon emissions. Industrial hemp is a crop which is relatively cheap to harvest and can be formed into a rigid material if combined with lime binder. The resulting has a low thermal conductivity which allows it to be a suitable insulation material whilst the hemp is capable of absorbing carbon dioxide over time and can thus overset emissions elsewhere. This is a highly attractive property in net zero carbon buildings.

1.1.3Existing fire test methods

The standard fire test methods provide a means to compare similar materials but do not deliver knowledge on the behaviour in the event of a fire. Materials are given a classification based on their performance in a single test which is not capable of encapsulating all fire scenarios. Since the test method does not deliver knowledge on how the material behaves it is possible for very different materials to achieve the same classification. Furthermore, there is no scope for optimisation within this design path.

A bespoke testing framework is required to enable the implementation of innovative materials which fall outside the limitations of the existing standard fire test methods (Harmathy 1979). This framework must deliver knowledge on how the material behaves in a wide range of realistic conditions, and accurately encapsulate complex behaviour. From this, designers will

be able to balance potential energy savings with quantified fire performance, thereby enabling the safe usage of these materials in the built environment.

For hemp-lime insulation, its porous nature means that smouldering will be the dominant mode of combustion, as opposed to flaming. There is currently no standard fire test method for evaluating smouldering and its associated risks. Testing in a furnace is capable of giving a classification but is not capable of characterising the fire behaviour applicable to realistic fire scenarios. Thus, the development of a framework to quantify these materials will enable designers to employ suitable risk mitigation strategies and allow their safe usage in buildings.

1.2 Aims and objectives

The aim of this project is to develop a novel fire frameworks which is capable of quantifying the fire performance of phase change materials and hemp-lime insulation to enable their usage in the built environment.

This will be achieved through the following objectives:

- Characterise the change in fire risk caused by the addition of PCMs (Phase Change Materials) to a substrate material;
- Perform a holistic fire risk assessment on commercially viable building products;
- Analyse the chemical reactions to understand the fundamental behaviour of innovative building materials;
- Developing a suitable test method to be able to quantify the smouldering risk associated with hemp-lime insulation;
- Evaluate the behaviour of PCMs within the existing standard fire testing classification system.

1.3 Outline

Chapter two
Literature review
A state of the art review of phase change materials with respect to fire is given. The thermal properties of PCMs and their application within the built environment is described in-depth. The history, development and relevance of standard fire testing is explored. The limited research available on PCMs and hemp-lime in fire are also investigated, as well as any other materials relevant to the adoption of PCMs.

Chapter three
Thermal degradation framework and determination of thermal transport properties
A study on the thermal degradation steps and thermal transport properties is conducted on all of the materials used in the thesis. This provides understanding of the pyrolysis and oxidation behaviour, and is used to interpret the flammability results. Furthermore, thermal analysis provides fundamental understanding of the chemical reactions and how the material behaves on a micro-scale to complete the characterisation.

Chapter four

Characterisation of the smouldering risk of an innovative hemp-lime insulation material

A method for quantifying the smouldering behaviour of rigid materials in the cone calorimeter is developed. This is applied to hemp-lime insulation to characterise its ignitability, burning characteristics, spread rate, and describe the nature of the smouldering front. The method includes both downward opposed flow and upward forward flow configuration in an apparatus which is economically viable and widely available.

Chapter five

Smouldering combustion of hemp-lime insulation containing microencapsulated Phase Change Materials

The change in fire risk associated with the addition of PCMs is of key significance in understanding the overall material behaviour. In this chapter, microencapsulated PCMs are added into the matrix of the previously characterised hemp-lime insulation. Key smouldering metrics are used to evaluate the performance with and without PCMs to quantify the change in fire risk associated with the addition of these materials.

Chapter six

Flammability study of PCM plasterboard using bench-scale calorimetry

A flammability study of an end use and commercially available PCM plasterboard is conducted in the cone calorimeter. The fire performance of the material is quantified under a range of conditions and forms an integral part of the framework developed for studying PCMs in fire. The overall behaviour of the material is characterised and methods for modelling this are identified.

Chapter seven

Intermediate-scale fire testing of PCM plasterboard

The fire behaviour of the PCM plasterboard is analysed within two standard fire tests – flame spread using LIFT according to ISO 5658 and single burning item (SBI) ISO 13823. The motivation is twofold; firstly, to verify the behaviour of the material on a larger scale and obtain the flame spread parameter and secondly, interrogate the usefulness of the existing standard fire test methods.

Chapter eight

Novel linking frameworks

The final chapter represents the binding element of the thesis to develop frameworks capable of quantifying the fire performance of PCMs and hemp-lime insulation to enable their usage by designers. An integrated method to utilise the framework proposed in the thesis is outlined to be used as part of a performance-based fire design.

Chapter nine

Conclusions and further work

The main conclusions from the thesis as a whole are summarised, and recommendations for future work are made.

2 Literature review

2.1 Introduction

The material in this chapter covers a highly comprehensive review of both PCMs (Phase Change Materials) and hemp-lime insulation. The motivation and usage of these materials is first discussed at ambient conditions so their potential energy savings can be understood. The purpose of this thesis is to provide a relevant holistic fire risk study which will not compromise the ability of these materials to reduce energy.

An extensive review of the materials with respect to fire is then conducted. At present, there is little to no research on either of these materials in fire conditions. Existing fire test methods are reviewed to help prepare for developing appropriate frameworks for both materials.

Finally, some of the key fire science and engineering concepts are discussed which will be used throughout the thesis. These have been included within the literature review since they are applicable to multiple parts of the framework as it is developed.

2.2 Guide to innovative materials

2.2.1Phase change materials

There are a wide variety of applications of Phase Change Materials (PCMs) (Zalba *et al.* 2003, Mehling and Cabeza 2008) including textiles (Sarier and Onder 2012), electronics (Wuttig and Yamada 2007), renewable hot water systems (Farid *et al.* 2004), refrigeration (Braga *et al.* 2009, Ahmed *et al.* 2010), and building linings (Kuznik *et al.* 2011). This project focuses solely on the lattermost.

Phase change materials are still relatively novel and the field has not sufficiently matured for there to be clear cut and definitive choices for the selection of materials. A wide variety of materials with vastly different performance and applications are available and cannot all be the subject of fire testing within this project. Thus, a review of the currently perceived viable and upcoming materials is conducted.

2.2.1.1 Background and development

PCMs exploit the heat of fusion of a material. When a building is warm, the melting of a PCM in a building lining will cause it to absorb energy and prevent overheating. As the temperature reduces the material solidifies and it will release the energy stored as heat of fusion which helps keep the building warm at night. This reduces the need for conventional heating and cooling which reduces the associated carbon footprint, increases energy efficiency and reduces cost.

Traditional buildings have a large thermal inertia due to thick walls and the use of materials with high heat capacity such as concrete. In modern sustainable construction the trend continues towards highly efficient lightweight materials to achieve the necessary energy savings with the least amount of thickness to reduce cost (Tyagi *et al.* 2011). This results in lightweight buildings which are highly influenced by the external conditions (Konuklu and Paksoy 2009).

2.2.1.1.1 Effectiveness in buildings

To maximise the amount of energy which can be stored and released it is necessary to have a large surface area (Cabeza *et al.* 2011). For this reason, wall linings, ceilings and flooring have been the areas of most interest for the development of PCMs since they have the greatest surface area.

Phase change materials can also be useful in shifting peak demand loads and help distribute energy demands throughout the day. This is because the materials aim to reduce severe temperature fluctuations which not only makes demand more consistent and predictable but reduces the size of the peak load (Zhang *et al.* 2007).

2.2.1.1.2 Preferable properties

Most crucially the material must have a high heat of fusion and the melting point must be in the temperature range desired. If a material does not possess these properties then it is not viable for use in latent heat thermal storage. It is preferable for the material to have high thermal conductivity, high specific heat and high density. High thermal inertia in the form of thermal conductivity and density are desirable since they increase the heat flow from the room to the phase change material and vice versa, thereby increasing its effectiveness (Baetens *et al.* 2010). In addition to this, it is desirable to avoid supercooling, have no phase segregation, be chemically stable, compatible with building materials, non-corrosive, non-flammable and non-toxic (Zalba *et al.* 2003, Khudhair 2004, Tyagi and Buddhi 2007, Mehling and Cabeza 2008, Sharma *et al.* 2009, Cabeza *et al.* 2011, Kuznik *et al.* 2011, Tyagi *et al.* 2011). Supercooling and phase segregation result in a reduction in efficiency as some of the material becomes ineffective. In the case of supercooling this occurs on every solidification cycle while phase segregation is a process which takes place over the lifetime of the material.

2.2.1.2 Types of PCM

PCMs are commonly divided into two major categories: organic and inorganic (Abhat 1983). Within each branch the materials are generally mixed to give more desirable properties, most commonly to obtain a suitable melting point. The mixture of the two, organic and inorganic, are referred to as eutectics but little research has successfully been able to utilise a viable mixture, and there has been no commercial uptake.

2.2.1.2.1 Organic

Organic phase change materials are typically the most popular because of their advantageous properties with relatively few downsides. They have high heat of fusion, no phase

segregation, experience little or no supercooling, have appropriate melting points, are cheap, and have good compatibility with building materials. However, they have low thermal conductivity and are typically flammable.

Whilst some review papers correctly identify organic PCMs as potentially flammable (Zalba *et al.* 2003, Cabeza *et al.* 2011, Tyagi *et al.* 2011, Zhou, Zhao, *et al.* 2011) there are still some which describe the flammability as limited (Sharma *et al.* 2009) or make no reference at all (Tyagi and Buddhi 2007, Baetens *et al.* 2010). Others suggest that the flammability risk can be mitigated with the correct containment (Pasupathy *et al.* 2008, Kuznik *et al.* 2011) despite having not conducted non-standardised fire testing.

It should be clear that a material containing an organic component, often paraffin wax, at least has the potential to be combustible (Drysdale 1999). The potential flammability has been illustrated in a variety of studies, despite non-flammable containment materials such as gypsum (Banu, Feldman, Haghighat, *et al.* 1998, Asimakopoulou *et al.* 2015) or concrete (Salyer and Sircar 1990). The key however is to quantify the fire performance to enable the safe usage of the material in design. For reference, a list of some of the viable organic PCMs in the form of paraffin waxes and fatty acids are given in Table 2.1.

Table 2.1 – The latent heats and melting points of organic PCMs commonly used in buildings. Information taken from Sharma *et al.* (2009) and Abhat (1983).

Material	**Formula**	**Melting point**	**Latent heat**
-	-	°C	$J \cdot g^{-1}$
Paraffin waxes			
Hexadecane	$CH_3(CH_2)_{14}CH_3$	16.7	237.1
Heptadecane	$CH_3(CH_2)_{15}CH_3$	21.7	213
Octadecane	$CH_3(CH_2)_{16}CH_3$	28.0	244
Fatty acids			
Acetic acid	CH_3COOH	16.7	184
Capric acid	$CH_3(CH_2)_8 \cdot COOH$	31.5†	152
Lauric acid	$CH_3(CH_2)_{10} \cdot COOH$	42-44†	178
Myristic acid	$CH_3(CH_2)_{12} \cdot COOH$	54†	187†
Palmitic acid	$CH_3(CH_2)_{14} \cdot COOH$	63†	187†
Stearic acid	$CH_3(CH_2)_{16} \cdot COOH$	70†	203†

† (Abhat 1983)

2.2.1.2.1.1 Paraffin wax

The most commonly adopted PCM for use in the built environment is currently paraffin wax. The melting point can be designed to be anywhere from -50 to 80°C by modifying the number of chains or by blending different waxes (Salyer and Sircar 1990). Petroleum derivatives are cheaply available and do not suffer from supercooling, phase segregation, and are not corrosive or toxic. Furthermore, good chemical stability makes paraffin waxes a suitable option for the inclusion into other building materials. However, they are inherently highly

flammable materials and thus efforts are generally made to mitigate a potential fire risk. Often this is achieved through particular encapsulation methods or the addition of suitable flame retardants.

2.2.1.2.1.2 Fatty acids

Fatty acids include vegetable and animal oils and represent a renewable and organic phase change material capable of achieving good thermal storage. Fatty acids share many of the attractive properties of paraffin waxes, such as suitable and flexible melting points, and high latent heat storage properties but have the benefit that they are truly renewable (Suppes *et al.* 2003), whereas paraffin waxes are a finite resource. However, typically their latent heat is lower than other PCMs (see Table 2.1) and are slightly less compatible with other building materials. In addition, fatty acids are also flammable and require quantification of their potential fire risk to enable their safe usage within building walls.

Commonly utilised fatty acids include combinations of lauric acid, stearic acid, myristic acid, and palmitic acid (Alkan and Sari 2008), and capric acid (Rozanna *et al.* 2005). The precise combination and selection of these materials will depend upon the application and the desired melting point.

2.2.1.2.2 Inorganic – salt hydrates

One of the greatest advantages of inorganic PCMs is their very low price point, which is lower even than the relatively cheap paraffin waxes. Their thermal properties are generally good and the listed latent heat is often higher when compared to equivalent organic materials as can be seen in Table 2.2 and Table 2.1. However, they suffer from phase segregation and often experience supercooling which makes them difficult to utilise effectively in a building for room temperature regulation. Supercooling reduces the storage capacity of the PCM when solidifying while phase segregation causes a permanent reduction in capacity as the components within the material separate and phase change can no longer occur. This results in a massive decrease in efficiency and can be very difficult to overcome. However, the core inorganic component is non-flammable unlike their organic counterparts. There is still potential for the containment to be flammable, for example, through the use of a flammable plastic container.

Table 2.2 – The latent heats and melting points of inorganic PCMs commonly used in buildings. Information taken from Abhat (1983).

Formula	**Melting point**	**Latent heat**
-	°C	$J \cdot g^{-1}$
H_2O	0	333
$KF \cdot 4H_2O$	18.5	231
$CaCL_2 \cdot 6H_2O$	29.7	256
$Na_2SO_4 \cdot 10H_2O$	32.4	254
$Na_2HPO_4 \cdot 12H_2O$	35.0	281

2.2.1.3 Methods of encapsulation

The operation of PCMs involves the reversible transition of solid to liquid and thus some form of encapsulation or containment is required. In the simplest cases the liquid is added into the porous matrix of a cementitious material such as concrete (Hawes and Feldman 1992) or gypsum (Scalat *et al.* 1996) and surface tension is sufficient to retain the material without any other modification. Fabricating sheets of plastic or rubber containing very high amounts of paraffin wax (60 to 90%) also represents a relatively simple method of containment. More complicated methods involve microencapsulation where small amounts of paraffin wax, or other core PCM material, is contained within a typically plastic shell. The encapsulation method and material type will have a major effect on the fire behaviour since these can represent different fire risks.

2.2.1.3.1 Immersion

Immersion was an early method employed for incorporating liquid PCM into porous materials such as plasterboard. The plasterboard would be dipped in a bath of PCM and kept at a high temperature for an extended period of time before being removed (Salyer *et al.* 1988, Banu, Feldman, and Hawes 1998). The sample would be weighed before and after in order to calculate the amount of phase change material that was successfully absorbed into the plasterboard. Such a process was useful for carrying out small amounts of research but did not prove commercially viable (Salyer *et al.* 1988, Banu, Feldman, and Hawes 1998).

2.2.1.3.2 Direct incorporation

Another early method of impregnating materials is to simply add liquid PCM into the material mix, such as for gypsum (Scalat *et al.* 1996, Banu, Feldman, and Hawes 1998) or concrete (Hawes and Feldman 1992, Hawes *et al.* 1992, Lee *et al.* 2000). One of the major issues with this technique is that it is highly reliant on the compatibility of the PCM with the building material (Salyer *et al.* 1988). If they are not compatible then it is not possible to combine them and instead another technique must be used. The advantages of this technique are that it is very quick and easy to do, without requiring any specialist technology or equipment. The amount of PCM that has been impregnated can only be calculated assuming the amount added is known, and that of all of is absorbed. Leakage is also an issue with this method although often the surface tension prevents the liquid PCM from escaping in normal conditions.

2.2.1.3.3 Encapsulation

One of the most effective ways to prevent leakage of the PCM from the supporting material is to encapsulate the PCM into another material, typically some form of polymer casing. This also reduces compatibility issues between the PCM and the supporting material since it will instead be dependent on the shell material used. There are two ways in which encapsulation can generally be achieved, either by creating microcapsules to be homogeneously distributed within another material or by encapsulating significant portions of PCM to form standalone pouches attached to a sheet of polymeric material.

2.2.1.3.3.1 Microencapsulation

Microencapsulation has proven to be a very popular method for a variety of reasons. The very small size of the capsules means that the surface area of PCM is much greater within the material, and hence the rate of heat transfer is much higher (Tyagi *et al.* 2011). This helps ensure that the PCM absorbs large amounts of energy which in turn increases their efficiency. It is also relatively straightforward to include the capsules directly into a building mix since they are designed to be sufficiently durable to prevent breakage. In turn, this ensures that leakage does not occur.

A multitude of techniques exist to synthesise microcapsules (Boh and Šumiga 2008). The choice of method is usually limited by the monomer that has been selected for use as the shell material, as well as the compatibility with the PCM. Suspension polymerisation (Vivaldo-Lima *et al.* 1997) has been used for the synthesis of polystyrene shells containing a blend of paraffin waxes (Sánchez *et al.* 2007) or n-octadecane (Li *et al.* 2012). Interfacial polymerisation (MacRitchie 1969) has been used for polyurethane shells containing n-octadecane (Li *et al.* 2012). Interfacial polycondensation can be used to create shells using polyurea, polyurethane, polyester, polyamide or amine resins for use with paraffin waxes or fatty acids (Liang *et al.* 2009, Zhang and Wang 2009a). A sol-gel technique has been adopted within fire-resistant SiO2 shells containing paraffin (Fang *et al.* 2010) or n-octadecane (Zhang, Wang, *et al.* 2010). Emulsion polymerisation (Chern 2006) has been used to encapsulate n-octadecane within PMMA (Sarı *et al.* 2009). Melamine-formaldehyde based shells with paraffin wax cores have been synthesised using in-situ polymerisation (Su *et al.* 2005, 2010, 2011). For natural coco fatty acids it was found that gelatin-gum Arabic shells (Ozonur *et al.* 2006) formed using complex coacervation (Kissel *et al.* 2006) was suitable, and could also be used with n-octadecane core (Li *et al.* 2012).

2.2.1.3.3.2 Macroencapsulation

Macroencapsulation refers to encapsulation of PCM in sizes greater than one millimetre. This is often done using plastic sheets which contain pockets of pure PCM and is added to the insulation of the building. The encapsulating layer of plastic is typically very thin compared to the amount of PCM and hence the PCM is highly concentrated. This can result in a very high incorporation amount that can be achieved but as with plastic sheets it must be contained behind another material since they are not suitable as a lining.

2.2.1.3.4 Shape-stabilised or form stable

Shape stabilised phase change materials, or form stable phase change materials, are those which the PCM has been bound directly into the matrix of a polymer in order to form a single rigid sheet of plastic-PCM composite. The sheets typically have very high content of phase change material (up to around 80 to 90% by weight) and thus are an attractive option since this means that their potential storage capacity per area is high (Kenisarin and Kenisarina 2012). The polymers used have been shown to be compatible with both paraffin waxes (Zhang *et al.* 2006) and fatty acids (Sari and Alkan 2012). They are often included behind plasterboard since they are typically highly flammable.

Other materials can be added to the basic plastic-PCM mix in order to improve some of the properties. Expanded graphite can be added to improve its thermal conductivity since this increases heat exchange with the room and hence the efficiency of the PCM, (Sari and Karaipekli 2007, Zhang, Hu, *et al.* 2010) or fire retardants can be introduced (Cai *et al.* 2006) in order to attempt to improve the fire performance of a material.

2.2.1.4 Integration into built environment

Phase change materials which are used to stabilise indoor temperatures have been included within walls (Kuznik *et al.* 2011, Zhou, Yang, *et al.* 2011), solar walls (Stritih and Novak 1996), ceilings (Koschenz and Lehmann 2004, Oliver 2012) and floors (Entrop *et al.* 2011, Haurie *et al.* 2014). For each of these applications the detail will be slightly different. Often the same PCM lining is used in both walls and ceilings, but in the latter it will be part of a suspended ceiling. Floors often utilise hot water pipes as part of the heating system and do not form part of the lining.

A simplified wall detail of a typical PCM lining is given in Figure 2.1. This was used as part of a combined experimental and numerical study which evaluated the impact and effectiveness of PCMs in buildings (Kuznik *et al.* 2010). Two wall assemblies were tested – one with PCM and one without. The wall assembly without the PCM plasterboard instead had it replaced with cardboard. The detail shows the PCM immediately facing the interior of the room, then backed by a substantial amount of insulation.

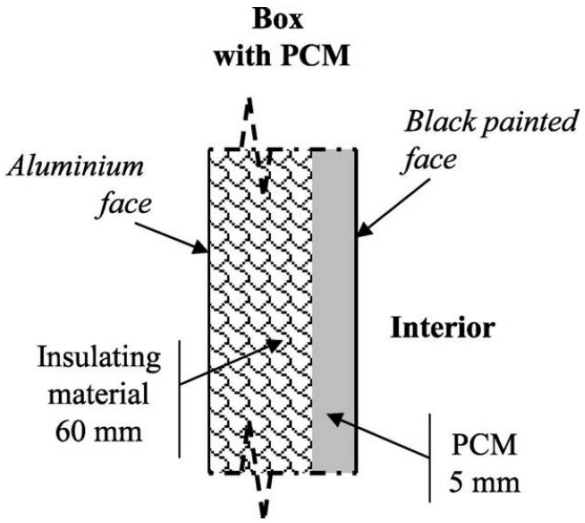

Figure 2.1 - Wall detail extracted from Kuznik *et al.* (2010).

Shape stabilised PCMs typically do not form the interior facing of the wall lining and are instead placed at depth, as illustrated in Figure 2.2. The PCM layer in this instance is 5mm thick and composed 60% paraffin wax and the rest polyethylene. This is positioned behind a 13mm thick protective layer of plaster. As with the PCM plasterboard, the backing is formed by insulation, which in this case is 50mm of polystyrene.

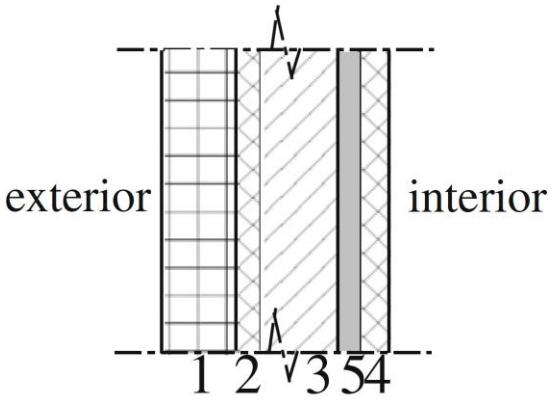

Figure 2.2 - Wall detail of an experimental investigation involving shape stabilised PCM. The layers are as follows: (1) wood plate (2) plaster (3) polystyrene (4) plaster (5) shape stabilised PCM. Extracted from Kuznik and Virgone (2009).

Wall details as adopted in practice are provided by a single PCM plasterboard manufacturer, as shown in Figure 2.3. These again show that the PCM plasterboard is positioned immediately facing the interior of the compartment, and is recommended to be backed by insulation. Thus, the wall details match those which have ordinary plasterboard and that, because the fire classification is the same, they can be used in the same role without modification.

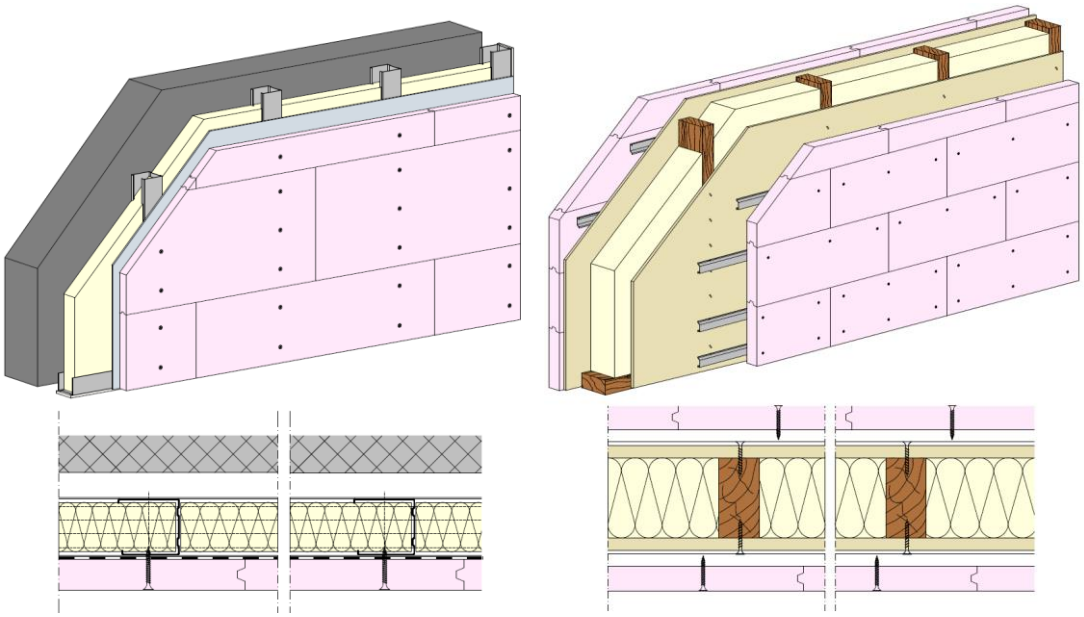

Figure 2.3 - Typical wall details for PCM plasterboard as part of (a) internal lining (b) timber framed building. Extracted from Rigips AG (2015).

The same manufacturer has also provided details for ceiling arrangements incorporating the same PCM plasterboard. It can be seen for a suspended ceiling (Figure 2.4a) that the detail is quite different and there is instead a large cavity as opposed to insulation. The heat losses to the back in this incident would be much higher and the material would take a longer time to

increase temperature. However, an oxidising environment is still present in this space and as such it presents a fire risk. The detail for a building containing wooden beams as part of the floor system (Figure 2.4b)

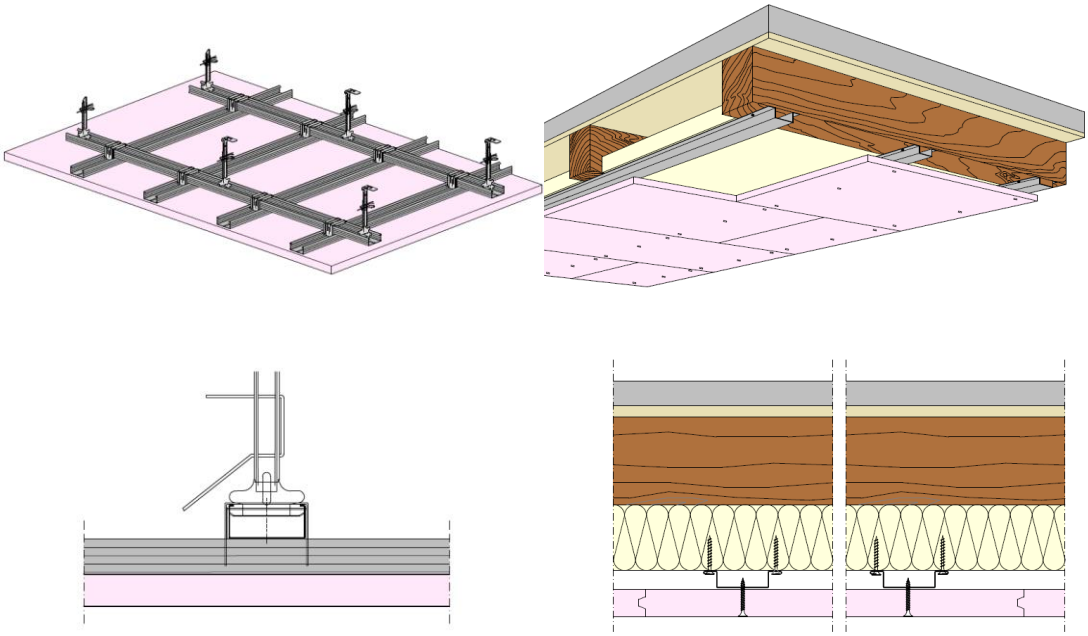

Figure 2.4 - PCM plasterboard details for two different ceiling systems - (a) suspended ceiling (b) timber frame. Extracted from Rigips AG (2015).

Traditional solar walls have taken the form of a Trombe-Michel Wall which incorporates a glass panel placed in front of a thick material with a high thermal inertia, such as concrete. The purpose is to absorb certain wavelengths of radiation through the glass and allowing the thermal wave to slowly penetrate through the wall behind. This reduces the peak exposure during the day and then slowly releases the heat during the evening. The net effect is much the same as PCMs despite relying on slightly different principles.

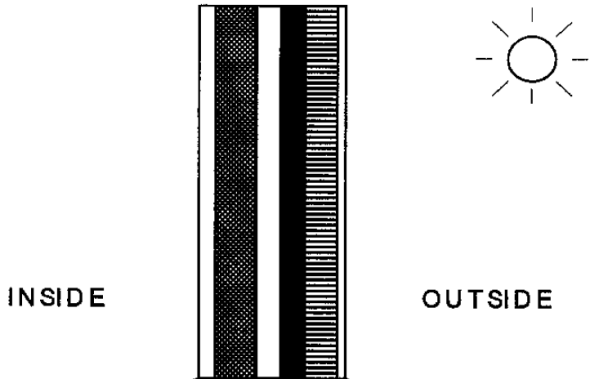

Figure 2.5 - The design of a PCM solar wall. From left to right the layers represent (i) ordinary plasterboard, (ii) insulation, (iii) air cavity for circulation, (iv) PCM-polycarbonate sheet, (v) transparent insulation material (TIM), and (vi) glass. Extracted from (Stritih and Novak 1996).

The design of a proposed PCM solar wall is given in Figure 2.5. The material with high thermal inertia, often concrete in a traditional solar wall, is replaced by the PCM. For this case the PCM is positioned closer to the exterior of the wall assembly and would not be directly exposed to a compartment fire. However, it does present a potentially highly flammable material deep within a wall and in proximity to a readily available source of oxygen in the form of an air cavity.

Finally, an example floor system with heating and shape stabilised PCM is shown in Figure 2.6. This type of system is significantly less prevalent in the literature when compared to the wall systems. The shape stabilised PCM is 15mm thick and composed of 75% paraffin and 25% polyethylene. This layer is placed in direct contact with electric heaters which are used to provide the underfloor heating for the compartment. Polystyrene insulation is placed underneath the PCM to reduce heat losses, whilst above is open to an air cavity. Wooden studs are located periodically to support the 8mm thick wooden flooring. Thus, the wood flooring is the only protective element for heat exposure above and if the heat is able to penetrate through this then it is able to reach the PCM, and beyond this, 100mm of polystyrene.

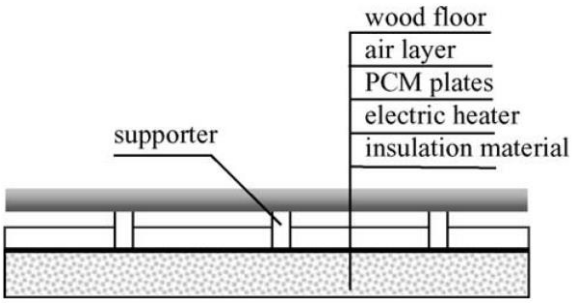

Figure 2.6 - Example section with underfloor heating and shape stabilised PCM. Extracted from Lin *et al.* (2005).

2.2.1.5 Potential for energy saving and optimisation

Early research focused on the feasibility and potential energy savings possible through the use of PCMs. This often involved the inclusion of as much PCM as possible, for example, finding the maximum amount of PCM which could be introduced into the matrix of a material. As the market has matured and the materials have been shown to be feasible it is then increasingly attractive to find the optimal amount of PCM which either provides the maximum benefit, or allows the design to reach its energy saving goals.

2.2.1.5.1 Thickness

One of the methods of optimisation which was explored was the concept of an optimal wall thickness (Kuznik *et al.* 2008). The distribution of PCM within the material is assumed to be homogeneous and that the thickness of the material can be varied to obtain the optimal amount. The wall area of the compartment linings containing PCM can be chosen as necessary. The amount of energy stored by the PCM layer is calculated through a numerical model and this provides the maximum amount per unit area possible.

2.2.1.5.2 Melting point and latent heat capacity

Another method of optimisation is based on finding the most suitable melting temperature and the latent heat capacity to evaluate the potential benefit of PCMs for a given compartment (Xiao *et al.* 2009). Sets of equations to achieve this are derived, and implemented in a simulation. This allows the effect of PCM surface area, convective heat coefficient, and external conditions to be evaluated. The tool is intended to be used by designers to optimise the energy efficiency application of PCMs within buildings.

2.2.1.5.3 Quantity of PCM

A single study has analysed how increasing the mass fraction of PCM within a given volume contributes to energy saving (Lee *et al.* 2011). Two rooms were built within a shipping container which contained a heater to regulate the temperature. One room contained no PCMs, whilst the other contained microencapsulated PCMs in the amounts of 1, 2, 3, and 4kg·m^{-2} over a series of tests. The amount of power required to maintain the reference temperature for simulated summer and winter conditions was measured for each of the above cases. It was found that in winter, where the main source of power consumption is heating, that small amounts of PCM (1 and 2kg·m^{-2}) increased the amount of energy required. This was due to the change in ambient thermal properties caused by the addition of PCMs, such as thermal mass, but the loading was not sufficient for the phase changes to have enough effect. At the higher amounts there was a 4% and 4.5% power ratio reduction for 3 and 4kg·m^{-2} respectively compared to the non-PCM room. For summer, where the main load is cooling, the ratio of power consumption was found to increase as the amount of PCM was increased. However, beyond 3kg·m^{-2} the benefit again decreased and thus this was the optimal amount for the specific configuration tested. These tests illustrate that increasing the mass fraction of PCM in a given volume may at some point experience diminishing returns and that the amount should be optimised for the desired energy saving goal.

2.2.2Hemp-lime insulation

Hemp-lime insulation is an innovative building material which is increasingly used in modern sustainable buildings. This material is formed by combining industrial grade hemp shivs and fibres (*cannabis sativa L.*), water, and a lime/cement binder. The resulting material is a rigid lightweight material which has low thermal conductivity owing to its porous nature (Bevan and Woolley 2008). The hemp crop, from which the shivs and fibres are farmed, absorbs carbon dioxide during its growth and thus is included in the calculations for the carbon footprint of a building. These beneficial carbon credentials mean that its usage is increasing as a sustainable alternative insulation material (Sutton *et al.* 2011a, 2011b). An example build containing hempcrete, which is a specific hemp-lime product, is shown in Figure 2.7.

Figure 2.7 – Project by the Greenlight Trust on an old timber framed foundry (a) detail showing hempcrete (b) overall view. Extracted from Bevan and Woolley (2008).

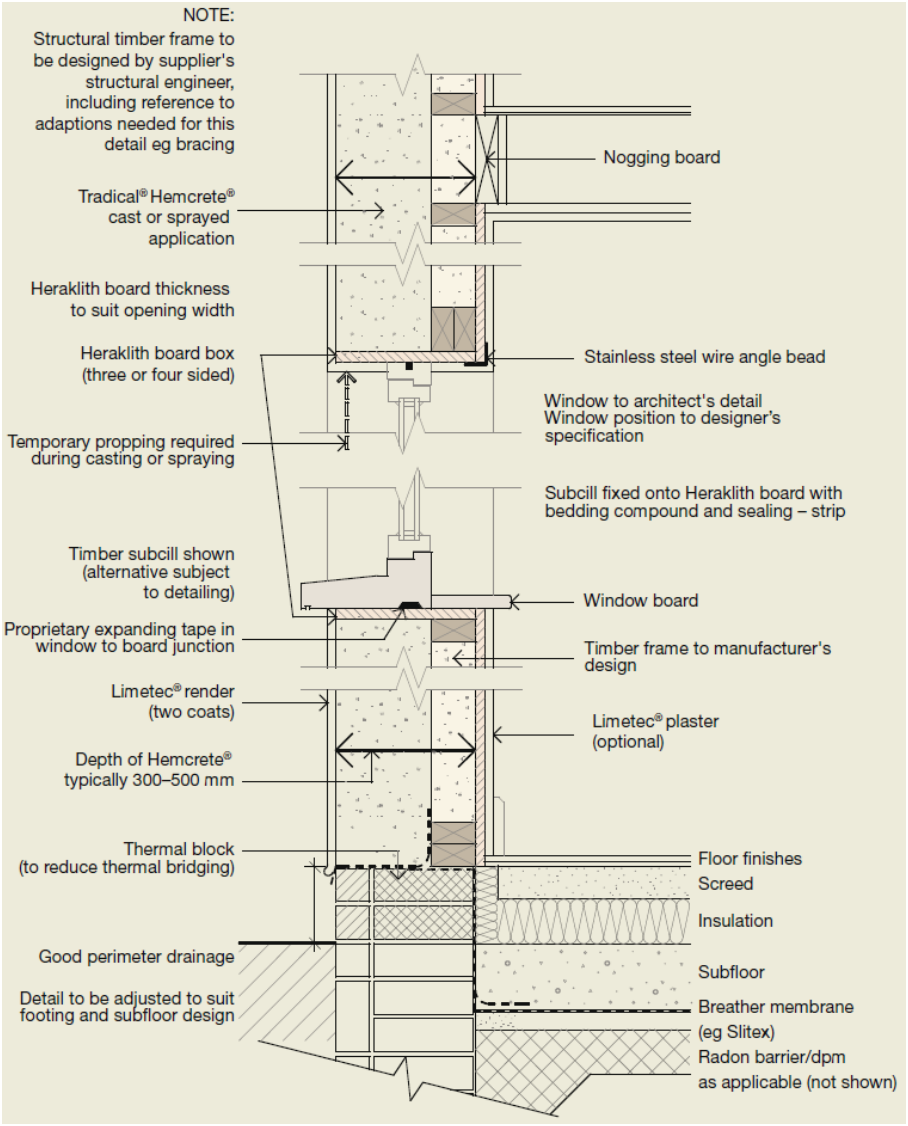

Figure 2.8 – Example section containing hemp-lime insulation in the wall of a timber framed building. Extracted from Bevan and Woolley (2008).

Similar to PCMs, hemp-lime is used within buildings to reduce the carbon footprint and achieve a higher standard in the Code for Sustainable Homes (Department for Communities and Local Government 2006) or equivalent guideline. Thus, the buildings in which hemp-lime is most often included as an insulation material tend to be of lightweight construction such as timber frame, as detailed in Figure 2.8, or masonry buildings.

2.2.2.1 Constituent components

The hemp shivs and fibres are processed from the straw component of industrial hemp. This contains a bast fibre surrounding a woody shiv and both have a variety of uses. The fibre is often used for textiles, paper and pulp, rope, and canvas, whilst the shiv can be used for animal bedding and fibreboard. Industrial hemp is a cheap and sustainable crop which can be easily grown and cultivated (Alaru *et al.* 2011) making it attractive for use. The seeds of the plant can also be used for oils, waxes, or directly as a food source therefore the shivs are often a waste stream from another process.

In some countries industrial hemp requires a licence or is prohibited due to its relation to marijuana. Any cultivation of the genus *Cannabis*, which includes industrial hemp, was previously banned in the United Kingdom under the Misuse of Drugs Act, 1971 Section 6 (1) & (2) (Elizabeth II 1971). This was later overturned in 1993 and now only a licence is required. Industrial hemp contains a very small amount (<0.2%) of the active ingredient tetrahydrocannabinoids (THC) and thus cannot be used for recreational purposes.

Hemp is a cellulosic material since it arises from plant matter. Cellulosic fuels in general are a common source of study in fire research, particularly wildfire problems, due to their abundance in nature. Typically organic materials are formed from a variety of organic compounds with varying chemical reactions and thermal degradation steps. The primary components of hemp are usually cellulose, hemicellulose, and a combination of lignin and pectins. Literature relating to the thermal degradation of hemp using TGA (Thermogravimetric Analysis) is available both as a complete material (Yao *et al.* 2008, Rachini *et al.* 2009), as well as studies on each of its constituent parts (Kashiwagi and Nambu 1992, Antal and Varhegyi 1995, Yang *et al.* 2007, Burhenne *et al.* 2013). A summary of the composition of hemp fibres and shivs found in Europe is given below in Table 2.3.

An appropriate binder is required to be able to form a rigid material. Cement, as is used to produce concrete, would prove adequate if specified to be compatible with the hemp but has large carbon costs associated with it (Bevan and Woolley 2008). Since the goal of using hemp-lime insulation is to lower the carbon footprint this proves a counterproductive issue. A suitable alternative is lime which has a lower embodied energy (Ip and Miller 2012). In reality, a combination of both lime bolstered by the quick setting properties of cement produces the most suitable binder. The embodied energy of the cement will be offset by the carbon sequestration of the hemp and produce a net benefit. The primary component of the resulting binder is lime, and cement is a secondary component (Bevan and Woolley 2008, Ip and Miller 2012). A number of unspecified additives are also included in commercial binder which are

not publicly disclosed. These could be pozzolanic materials (Elfordy *et al.* 2008), such as pulverised fuel ash (Sutton *et al.* 2011a), ground granulated blast-furnace slag, or metakaolin (Walker *et al.* 2014), which are recycled materials with a lower environmental impact than the cement which they displace.

Table 2.3 – Composition of industrial hemp (*cannabis sativa L.*).

Material	**Cellulose**	**Hemicellulose**	**Lignin**	**Pectin**	**Waxes**	**THC†**	**Ash**
-	%	%	%	%	%	%	%
Hemp (Spain)*	58.7	14.2	6	16.8	4.3	-	-
Hemp (France)*	56.1	10.9	6	20.1	7.9	-	-
Hemp (Estonia)**	53.86	10.60	8.76	-	-	73.22	5.25

† Total Hydrocarbon Content
*(Rachini *et al.* 2009)
**(Kikas *et al.* 2015)

2.2.2.2 Mix ratios

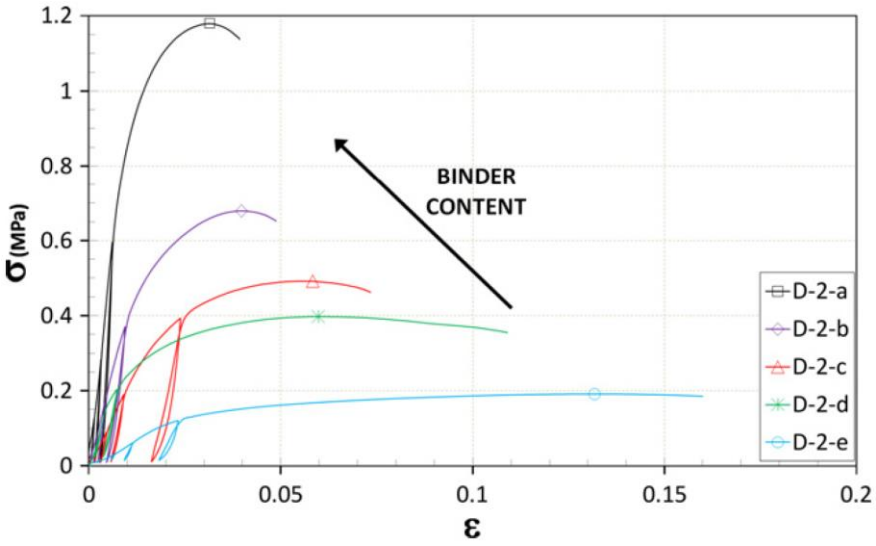

Figure 2.9 – Effect on increasing binder content on the stress-strain curves of hemp-lime insulation after curing for six months. Binder content by weight, from D-2-a to D-2-e, are 47.7%, 37.2%, 34.8%, 33.7%, and 24.6%. Extracted from Arnaud and Gourlay (2012).

Each binder is specifically designed for use with the hemp shivs provided by the same manufacturer, and will vary between different companies and regions. Thus, there is no general guidance which can be readily followed. Broadly, increasing the amount of the binder increases the strength of the resulting material but it also represents the most expensive component, and highest embodied energy. Thus, the quantity of binder cannot simply be increased indiscriminately and must be balanced with the other components to ensure the desired carbon capture and cost benefits are met. The increase in ultimate yield stress in

compression is shown as binder content increases in Figure 2.9 (Arnaud and Gourlay 2012). Sufficient water is required to maintain the hydration reaction during the curing process, as described later (*Section 2.2.2.3*).

Colinart *et al.* (2012) produced six mixtures which used quantities within the range of 16 to 23% hemp shivs by weight, 35 to 48% of various binders, and 33 to 48% water. Walker *et al.* (2014) investigated the effect of various binders on the mechanical strength of hemp-lime insulation and used a consistent mixture of 1 part (17%) hemp shiv, 2 parts (33%) binder, and 3 parts (50%) water. This also precisely matches the guidance given by the manufacturer for the specific hemp and lime binder which were used in this study.

2.2.2.3 Curing and conditioning

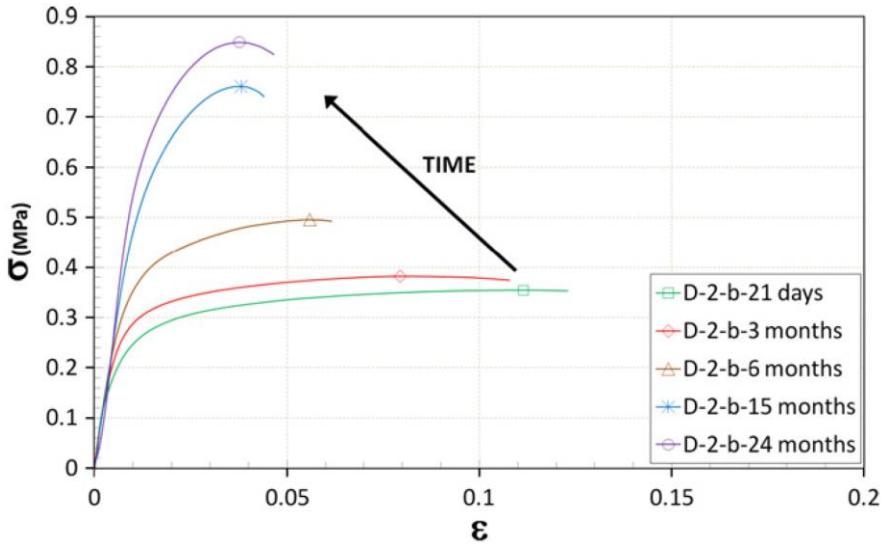

Figure 2.10 – Compressive strength of hemp-lime for various durations ranging from 21 days up to 24 months. Extracted from Arnaud and Gourlay (2012).

Unlike concrete, hemp-lime continues to exhibit a signifcant increase in compressive strength beyond six months, as seen in Figure 2.10 (Arnaud and Gourlay 2012). Literature on the curing of hydraulic lime mortars indicates two modes of curing over the space of a year (Lanas *et al.* 2004). Carbonation of the mortar occurs between 28 and 182 days which can be summarised by:

$$Ca(OH)_2 + CO_2 \rightarrow CaCO_3 + CO_2 \qquad \text{Eq. 1}$$

And a long-term curing process of the mortar, between 182 and 365 days, which further increases the compressive strength is then given by (Lanas *et al.* 2004):

$$2(2CaO \cdot SiO_2) + 4H_2O \rightarrow 3CaO \cdot 2SiO_2 \cdot 3H_2O + Ca(OH)_2 \qquad \text{Eq. 2}$$

2.2.2.4 Heat of combustion

The results from a literature review of general hemp and PCM products has been conducted to elucidate their possible values. This has found that the heat of combustion of the PCMs is higher than the hemp (Table 2.4). This is due to the paraffin wax within the capsules which, due to being a hydrocarbon, have an extremely high heat of combustion. Once absorbed into the matrix of the hemp it is theorised that the heat of combustion of the combined material will be higher. This increases the amount of energy released which in turn results in higher temperatures.

Table 2.4 – Summary of heat of combustion of some hemp materials, paraffin waxes and PCMs found in the literature. Note that no values representative for microencapsulated PCM were found.

Material	**Heat of combustion**	**Heat of combustion (dried)**
-	$MJ \cdot kg^{-1}$	$MJ \cdot kg^{-1}$
Dioecious hemp*	15.3-15.4	16.6-16.7
Monoecious hemp*	15.3-15.4	16.5-16.6
Hemp shivs**	18.3	-
Hexadecane‡	47.2490	-
Octadecane‡‡	47.1866	-
60% paraffin wax + 40% high density polyethylene†	34.5	-

*(Alaru *et al.* 2011)
**(Mankowski and Kolodziej 2008)
† (Cai *et al.* 2006)
‡ (Fraser and Prosen 1955)
‡‡ (Prosen and Rossini 1945)

2.3 Fire testing

Fire testing forms a critical part of the fire safety strategy within buildings. Materials must be certified and approved before they can be used, and failing to achieve adequate classification can prevent the material from being used in certain locations, such as in corridors or hospitals, or prevent its usage in the built environment entirely. The relevance, background, capabilities, and limitations of these methods are outlined in this section.

2.3.1Background and history

The start of the 20th century saw the first attempts of understanding the behaviour of buildings subject to fire exposures. This required the development of a test method which would be highly reproducible and capable of representing even the most severe fires. The equal fire load concept was developed by Ingberg (1928) as the first step of this process. A measure of fire severity could be approximated by the area under the Temperature-time curve of a compartment, and equivalent areas would be broadly similar levels of severity. The compartment was lined with non-combustible materials, and the rooms filled with furniture and materials typical of an office at the time. This generally included wooden desks and paper files, with some additional testing on wooden shelving. The aims of the research were

predominantly concerned with life safety and spread to neighbouring buildings by considering the fire resistance of structural elements.

A series of full-scale compartments were tested over eight years in Japan to develop the concept of fire safety further. Kawagoe (1958) developed the understanding of the role played by ventilation in determining the burning rate, and the duration of fires. This derived the opening factor which has been one of the key parameters in compartment fires. An international study (Thomas and Heselden 1972) was later conducted which defined the key parameters and shaped the fire safety strategy today. It was understood at the time that the framework was only applicable for the traditional and well understood materials which existed at the time, and that they would not necessarily be applicable to new materials which were being rapidly developed at the time (Harmathy 1979).

Ultimately this led to two branches of standard fire testing depending upon the function of a material. The first is the reaction to fire system (British Standards Institution 2009a) which is capable of comparing similar materials and providing a classification, and the second is furnace testing for isolated structural elements (British Standards Institution 2009b).

A more in-depth review of the development of the fire safety strategy and compartment fires is given by Majdalani (2014) and Torero *et al.* (2014).

2.3.2 European "reaction to fire" classification system

The current European classification system is given in BS EN 13501-1 (British Standards Institution 2009a) which determines the class of a material based on set test methods. The class will affect how the material can be used as part of a building.

The existing standard fire test methods provide a way to classify materials into flammability categories. The lowest of these is the non-combustible category, and after this the various levels of combustibility are classified. Table 2.5 summarises the different categories.

Table 2.5 – Euroclass categories for materials as part of standard fire testing.

Euroclass	**A1**	**A2**	**B**	**C**	**D**	**E**	**F**
Contribution	Non-combustible/ limited combustion		Combustible in increasing severity				No class

The first test in the series is the BS EN 13823 Single Burning Item (SBI) test which gives an initial indication of the classification that a product will ultimately receive. Additional testing is then required to confirm the class. If the product is determined to receive B in SBI, then ISO 1182 Non-combustibility (British Standards Institution 2010a) and ISO 1716 Heat of combustion (British Standards Institution 2010b) tests must be achieved to reach A1 or A2. For

all other classes the ISO 11925-2 Ignitability test (British Standards Institution 2010c) must instead be carried out to confirm the final classification of the product.

The PCM plasterboard used in this work has achieved B, S2, d0 when tested using this scheme, where SBI was according to DIN EN 13823:2002-06. This would typically be referred to as limited combustibility but falling short of the highest category, class A. The smoke yield, categorised as S2, relates to a moderate amount of smoke generation.

The results for other similar plasterboard products are not freely available for comparison despite their usage in the built environment. Nonetheless, the ratings which are available are given in Table 2.6.

Table 2.6 – Summary of available standard fire test results of PCM plasterboard products.

Product	Region	Standard	Test type	Result
Current plasterboard	Europe	DIN EN 13823:2002-06	SBI	B, S2, d0
Plasterboard 2	USA	ASTM E 136 ASTM E84	Combustibility Flame spread	Combustible B
Plasterboard 3	Europe	BS EN 13501-1	SBI/ignitability	D, S1, d0
Plasterboard 4	Europe	DIN EN 13501-1	SBI/ignitability	E

From the information that was available three separate classes were achieved for the different PCM plasterboard products. The range of classes achieved for the different products show that the test is successful in identifying different levels of fire risk for each of the products. However, there is no quantification of the fire performance which can be used as part of a design. Furthermore, within a single class there is no distinction of how the material would behave differently from another.

As an example, certain plasterboard products received a B classification during the round-robin development of the SBI (Hakkarainen *et al.* 1998), but the way in which they behave compared to PCM plasterboard cannot be inferred from the classification they have been granted.

For plasterboard containing organic PCM it would not be possible to pass the non-combustibility test (British Standards Institution 2010a) and thus B is the highest class that can be achieved. Gypsum without a combustible lining or additives is capable of achieving A.

2.3.3Fire resistance testing

Standard fire resistance testing in a furnace as part of BS ISO 13501-2 (British Standards Institution 2009b) is conducted in a small chamber which has a single side replaced with the material to be tested. The temperature-time curve produced by Ingberg (1928) is replicated by gas burners as measured by the temperature inside the furnace. No adjustments are made for

different thermal properties of either the specimen being tested, nor the linings of the furnace. As such, different furnaces and materials can experience vastly different exposures. Furthermore, combustible materials will generate pyrolysis gases which may burn in the chamber but because the temperature is regulated they will not contribute the exposure. Thus, the fire exposure of a combustible material is underrepresented and not suitable for testing in a furnace. Furthermore, this method does not allow the quantification of fire risk to be able to adequately compare PCM plasterboard with ordinary plasterboard. An in-depth review of standard fire testing for structural elements is given by Maluk (2014) and also Bisby *et al.* (2013).

2.4 Fire behaviour of relevant materials

2.4.1 Gypsum as a substrate for PCMs

For PCMs to be effective in construction they must be included within another substrate material. The fire behaviour of the substrate will therefore play an important factor in the overall fire performance of the finished PCM product. Since gypsum plasterboard is one of the most commonly adopted substrate materials the fire behaviour is reviewed.

Plasterboard is a generic term used to refer to a wide range of different products (Bénichou and Sultan 2005). There are no set guidelines or regulations which standardises the exact composition of the material. As such, each product may have different properties due to differing structure, of which there is little information available. These change between region and manufacturer, and are also developed over time.

The thermal degradation of gypsum plasterboard is a well-studied topic due to its role as a thermal barrier in fire safety. It is commonly employed as a fire protection material given its ability to absorb energy through its endothermic dehydration reactions at elevated temperatures. It is commonly used to protect structural elements and as a lining for compartments to prevent the spread of fire.

The thermal degradation and hence fire performance of gypsum plasterboard has typically been quantified using two main methods. Firstly, the use of Thermogravimetric Analysis (TGA) – potentially supplemented by Differential Scanning Calorimetry (DSC) – to understand the fundamental reactions leading to degradation. Secondly, the use of a furnace to analyse the time taken for the unexposed side to reach a specified temperature, as measured by a series of thermocouples as was previously described in *Section 2.3.3 Fire resistance* testing. The temperature of the unexposed face typically only exceeds the imposed limits when the structural integrity of the board begins to fail, and cracks begin to form. This allows heat to be transferred rapidly to the rear of the board. In some instances, cracking may occur near corners and fallout of material will follow.

The thermal degradation of gypsum board is highly dependent on the specific on the composition of the specific product. This varies depending upon the function of the board,

and also varies by company and country. For example, calcite is used to improve sound insulation and glass fibres are added to improve fire performance by reducing cracking. The exact composition of board is not known and the high variability makes it difficult to quantitatively compare gypsum boards. Nonetheless, a general description of the degradation of gypsum follows, covering the various additives and techniques employed for different effects as desired.

2.4.1.1.1 Decomposition steps

Gypsum typically has a moisture content of 25% by weight which is driven off in two reactions as the board is heated. The first dehydration reaction occurs between approximately 100 and 170°C as the calcium sulphate is converted into calcium sulphate hemihydrate and the free water, which accounts for around 75% of the total moisture, is removed. Between 150 and 170°C this is then converted into anhydrous calcium sulphate thus removing the remaining moisture in the form of chemically bound water (Manzello *et al.* 2007, Janssens 2011). Both of these reactions are endothermic and absorb significant amounts of energy due to the high heat of vaporisation of water. Furthermore, the reactions are reversible and the addition of water will restore the gypsum to its original state.

The dehydration reactions can be summarised as follows. The first dehydration reaction, dihydrate to hemihydrate, is given by:

$$CaSO_4 \cdot 2H_2O \rightarrow CaSO_4 \cdot \frac{1}{2}H_2O + \frac{3}{2}H_2O \qquad \text{Eq. 1}$$

And the second dehydration reaction, hemihydrate to anhydrite, is given by:

$$CaSO_4 \cdot \frac{1}{2}H_2O \rightarrow CaSO_4 + \frac{1}{2}H_2O \qquad \text{Eq. 2}$$

At higher temperatures there may be additional thermal degradation, including additive components. Ramachandran *et al.* (2003) lists an additional exothermic reaction due to the change in crystalline structure of the gypsum. However, this typically requires very specific conditions in thermogravimetric analysis for the reaction not to be masked. Under these conditions, a pinhole lid and higher sample mass result in a strong peak, where a low heating rate (2°C·min^{-1}) and an open atmosphere yield no peak whatsoever. This reaction is also noted by Manzello *et al.* (2010) and Lázaro *et al.* (2015):

$$CaSO_4(sol) \rightarrow CaSO_4(insol) \qquad \text{Eq. 3}$$

Depending on the composition of the specific board there may also be an additional degradation step at high temperatures. Between 600 and 700°C decarbonation of the calcium carbonate occurs (Ghazi Wakili *et al.* 2007). This is given by (Sanders and Gallagher 2002, 2005):

$$CaCO_3 \rightarrow CaO + CO_2 \qquad \text{Eq. 4}$$

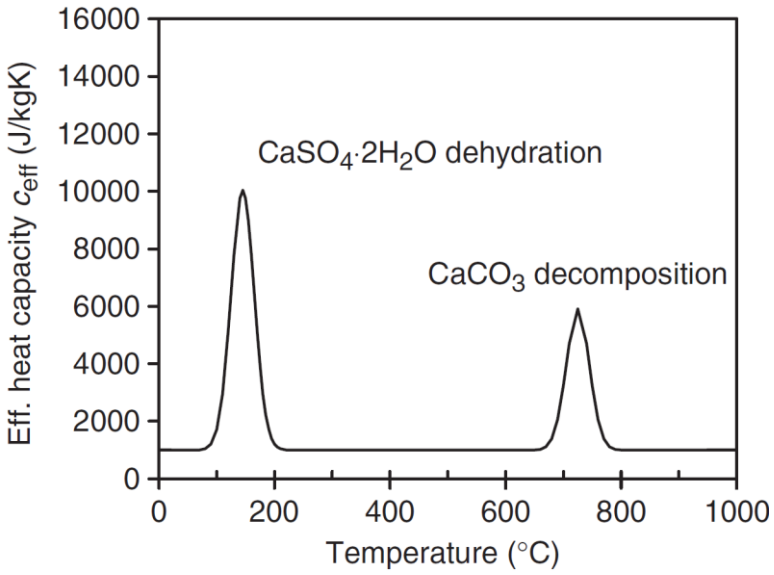

Figure 2.11 – Summary of the dehydration reactions (below 200°C) and the decarbonation of calcium carbonate (approximately 700 to 800°C). Extracted from Ghazi Wakili and Hugi (2009)

Earlier literature on the thermal degradation of gypsum listed the peak at 600 to 700°C as the second dehydration reaction. Recent research has confirmed that the dehydration reaction actually occurs at a much lower temperature, typically around 150 to 170°C (Ghazi Wakili and Hugi 2009, Manzello *et al.* 2010). However, it often overlaps with the first dehydration reaction and thus it is difficult or not possible to distinguish between the two steps.

An idealised illustration of the thermal decomposition as part of a numerical analysis by Ghazi Wakili and Hugi (2009) is shown in Figure 2.11. The dehydration reactions are lumped together and no other additives are present.

2.4.1.1.2 Thermal conductivity

A summary of the thermal conductivity as a function of temperature can be found in Figure 2.12. Preference has been given to discussing the most recent literature since they build upon the earlier testing and resolve some of the misconceptions. Thermal conductivity is initially in the range of 0.20 to 0.23W·m^{-1}·K^{-1} for heavy or type X boards, or 0.36W·m^{-1}·K^{-1} for ordinary plasterboard (Bénichou and Sultan 2005). Following the removal of moisture through the dehydration reactions the thermal conductivity will drop by up to 0.1W·m^{-1}·K^{-1}, to an absolute value of 0.10W·m^{-1}·K^{-1}. Within the range of 200 to 700°C, which corresponds to the region where often there are no reactions, there is only a slight increase in thermal conductivity as the temperature increases. This corresponds to approximately 0.1 to 0.15W·m^{-1}·K^{-1} (Mehaffey *et al.* 1994, Bénichou and Sultan 2005), or 0.18 to 0.26 W·m^{-1}·K^{-1} for both type C and X (Park *et al.* 2010). A substantial increase in the thermal conductivity then occurs again if the gypsum is heated to temperatures above around 700 to 800°C. This was previously noted as the approximate range of decarbonisation of calcium carbonate. Beyond this point the gypsum will reach its highest thermal conductivity, up to 1.10W·m^{-1}·K^{-1} for type X (Park *et al.* 2010) but

data for this stage is highly variable. Part of the reason for this variability is that the benefit of gypsum lies in its low temperature dehydration reactions, and thus the very high temperature behaviour is less important. Furthermore, failure of the board often occurs due to cracking and not solely due to heat conducting through the depth to the unexposed face.

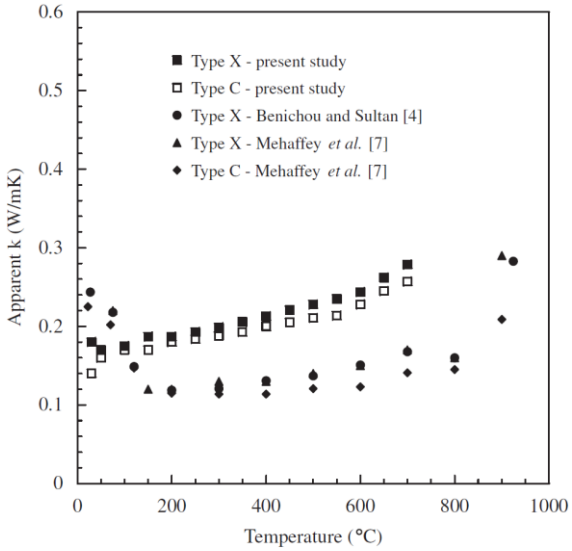

Figure 2.12 – Thermal conductivity of gypsum plasterboard from various studies as reported in the literature. Extracted from Park *et al.* (2010). Note that "present study" in the figure does not refer to this work.

2.4.1.1.3 Specific heat

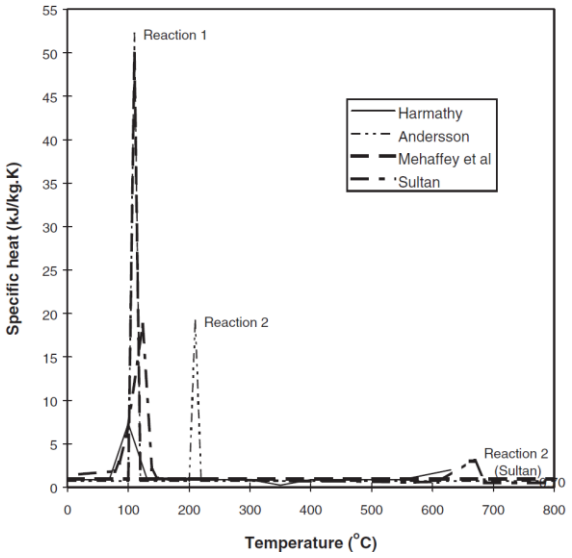

Figure 2.13 – Specific heat of gypsum plasterboard as reported by various authors. Extracted from Thomas (2002).

The specific heat capacity of gypsum is typically measured using Differential Scanning Calorimetry (DSC). This is a measure of the amount of energy required to increase the temperature of a sample, and can be used to find both the specific heat over a wide range of

temperatures as well as the heat flow during reactions. In the case of gypsum both the dehydration reactions are endothermic and therefore represent a large increase in the specific heat. Where calcium carbonate is present within the board matrix there will be a further peak in specific heat at higher temperatures. A collation of some of the literature as a function of temperature can be found in Figure 2.13.

The magnitude of the peaks in specific heat for the endothermic dehydration reaction illustrate gypsum's effectiveness as a fire protection material. Whilst at low temperatures this allows the plasterboard to absorb significant amounts of heat and delay the propagation of heat through the wall. This aids in protecting the wall assembly and removes energy from a compartment fire.

2.4.1.1.4 Density

Given that plasterboard does not shrink or expand significantly the density can be inferred from mass or mass loss measurements. The density of the plasterboard is highly dependent upon the exact composition of the material and will vary depending on the intended purpose. The density will decrease on mass loss due to chemical reactions in the material when exposed to elevated temperature. The specific amount of mass lost due to each of the reactions for a specific board can be conveniently obtained using Thermogravimetric Analysis (TGA). Bénichou and Sultan (2005) found a loss of 14 to 18% of mass on the combined dehydration reactions by 200°C, with a further loss of approximately 6% mass due to the decomposition of calcium carbonate between 650 and 750°C.

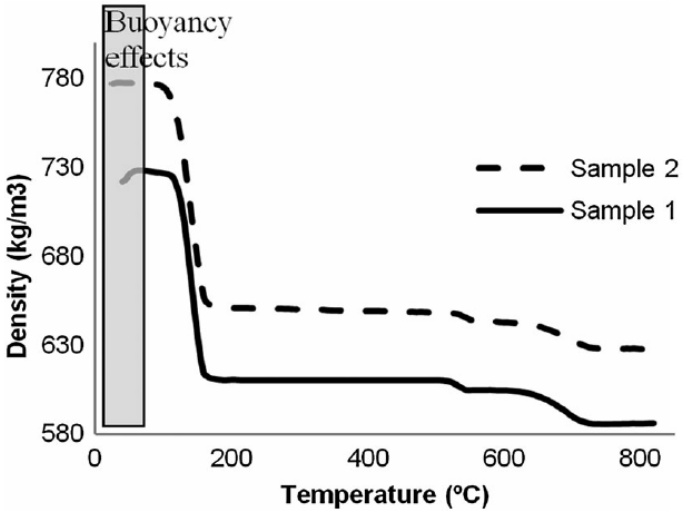

Figure 2.14 – Variation of density with temperature for two different types of plasterboard. Extracted from (Lázaro *et al.* 2015).

The change in density over temperature as inferred from TGA is given for two types of plasterboard from the same manufacturer in Figure 2.14 from Lázaro *et al.* (2015). This illustrates both how the density changes for two specific boards, as well as how the behaviour

of a board for the same function from the same manufacturer can vary. The changes in density, which are all decreases, all correspond to the previously identified chemical reactions.

2.4.1.1.5 Flammability assessment

The flammability of gypsum plasterboard is scarcely studied using bench-scale calorimetry but some data is available. The performance of the plasterboard is dominated by the facing, usually paper, which is the only combustible component. This is partially illustrated in Figure 2.15 where the heat release rate over time of a plasterboard with different types of wallpaper facing is shown. The fire behaviour is characterised by a sharp peak on ignition which rapidly decays to a short burnout. For this particular plasterboard the total flaming time is only around 30 seconds, regardless of the wallpaper facing. Thus, the total fuel load contributed by the facing is little despite some relatively high peak heat release rates. This short peak of flaming should be taken into consideration when comparing potential fire hazards with plasterboard.

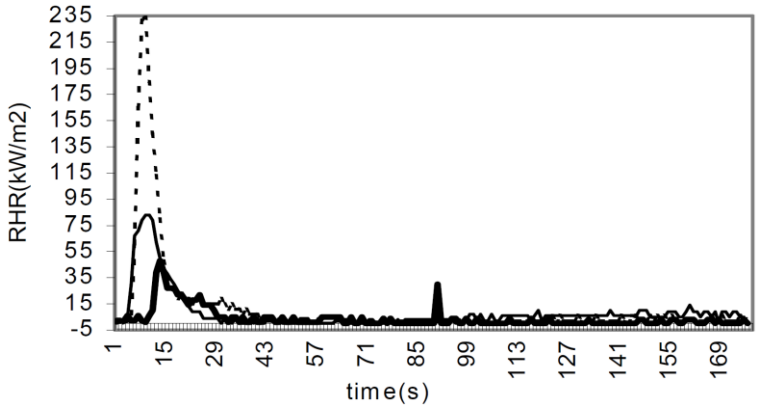

Figure 2.15 – Heat release rate over time for one plasterboard product which has no wallpaper (thick black line), unspecified wallpaper A (thin black line), and wallpaper B (dotted line). Extracted from Chew and Lim (2000).

Some of the flammability data available in the literature has been collated in Table 2.7. There is a large variance across each of the properties for the different properties, with up to 85% standard deviation in the total heat released. This would allude to differing fuel loads on the plasterboard, for example, due to different thicknesses of the lining material. Significant deviations are also noted in both the time to ignition and the peak heat release rate. Despite this, the values remain lower than other common building materials such as wood or PMMA.

Figure 2.16 portrays the spread of ignition times for the various plasterboards. The right-hand side of the figure shows how the variability increases when additional wallpaper and combustible facings are considered. In general these have been discounted since they are more representative of the facing than they are of ordinary faced plasterboard.

Table 2.7 – Summary of flammability properties of plasterboard in the literature, in addition to the PCM plasterboard in this study. Conditions and materials are not necessarily the same so care should be taken when making comparisons.

	Incident heat flux kW·m^{-2}	**Time to ignition** s	**Peak HRR** kW·m^{-2}	**Total heat released** MJ·m^{-2}	**Average** h_c kJ·g^{-1}
Type X plasterboard[1]	75	15	135	4.1	-
X-C gypsum board[2]	40	-	65	4	-
	50	-	70	4	-
Regular gypsum board[2]	40	-	0	0	-
	50	-	103	4	-
Ordinary gypsum board[3]	50	27	113.14	21.84	-
15mm gypsum board[4]	50	13	50.2	12.1	10.3
12.5mm gypsum board[4]	50	53	47.6	3.3	3.3
16mm FR gypsum[4]	50	72	63.2	3.0	5.1

[1] Carpenter and Janssens (2005)
[2] Richardson and Brooks (1991)
[3] Asimakopoulou *et al.* (2015)
[4] Chew and Lim (2000)

The peak heat release rate shows an upper limit of 100 to 140kW·m^{-2} for incident heat fluxes of 50 to 70kW·m^{-2} (Figure 2.17a). The distinction between ordinary plasterboard and fire resistant plasterboard is not evident in the peak heat release rate, but this may further illustrate that it is not necessarily the most suitable measure for evaluating fire risk. The total energy released over the duration (Figure 2.17b) shows that fire resistant plasterboard never releases more than 4.1MJ·m^{-2}. The ordinary plasterboard has a huge variance, which will depend upon the thickness of the combustible lining and hence the available fuel.

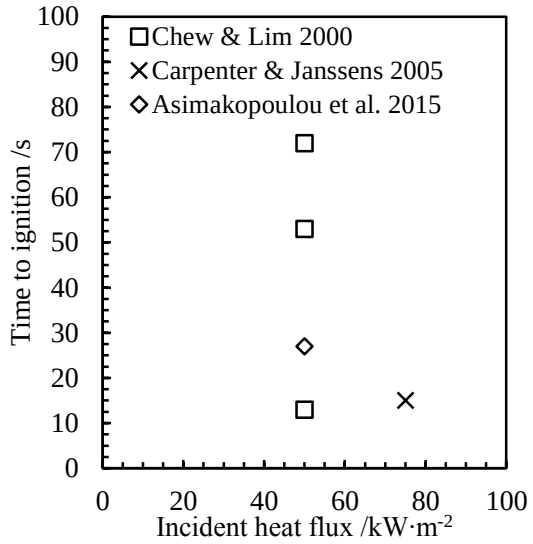

Figure 2.16 –Time to ignition of paper-faced based on data collated from Table 2.7.

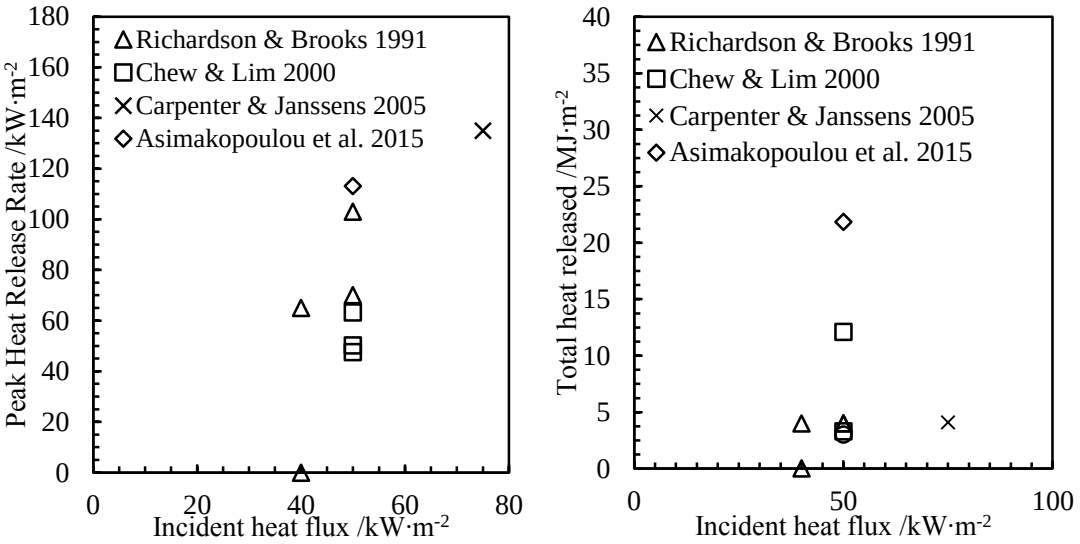

Figure 2.17 – (a) Peak heat release rate as a function of incident heat flux and (b) total heat released. Based on the data collated in Table 2.7.

2.4.2Existing PCMs in fire studies

PCMs have become increasingly popular in the energy industry but studies on their fire performance have been significantly less common. Only a portion of the research has identified fire as a potential issue, and only a fraction of that has performed studies to improve and evaluate the potential fire risk. Many of the studies use test methods which are outdated or are not particularly suited for effectively evaluating the fire performance. It is perhaps not surprising that this occurs given the complexity of the material and the quantity of fire test methods that exist between various regions which have been developed over several decades. Nonetheless, the studies that are available give some insight on how PCMs may behave in fire conditions.

2.4.2.1 PCM plasterboard

2.4.2.1.1 Formulation with fire retardants

A comprehensive study over an initial period of eight years was conducted to find the most effective PCMs, substrate materials, and encapsulation methods by Salyer *et al.* (1988). The results and conclusions are summarised in Salyer and Sircar (1990). This covered all aspects of PCMs including flammability and the addition of flame retardants. However, the fire testing was conducted using non-standard methods making it difficult to compare and evaluate. Tests typically took the form of exposure to a Bunsen burner for a prescribed period, and recording the time to ignition, and extinction. These were compared without flame retardants, and then for various formulations with flame retardants. The effect that the retardants had on the ambient thermal properties was also investigated.

Several methods were successfully implemented which reduced the perceived fire hazard associated with the PCMs that were produced. The guidance is partially outdated since microencapsulation was not used. To fire retard the PCM plasterboard there had to be

compatibility between all the components of the gypsum, raw PCM, flame retardant, and any potential synergists. With modern day microencapsulation some of these compatibility issues are resolved. Nonetheless, it was recommended that a liquid fire retardant with antimony oxide be added, or to add a fire retardant which will be present at the surface. This was to prevent combustible linings from acting as a wick for the PCM. The simplest of the suggestions was to reduce the amount of PCM impregnated within the board however this results in an obvious decrease in energy saving performance.

2.4.2.1.2 Early direct impregnation

Despite the fact that plasterboard is the most common substrate material for the addition of PCM, there is very little in the literature investigating the performance in fire. Of note, there is an early research paper which was produced before the current trend towards sustainability in modern times (Banu, Feldman, Haghighat, *et al.* 1998). At that time, PCM research was still at a very early stage and was investigating the different avenues for the inclusion into other materials. Two methods were adopted, direct immersion and dipping. Both these methods involve the production of ordinary gypsum plasterboard, 12.5mm thick in this case, and then adding the PCM afterwards. Over time, other encapsulated methods were developed and these became the preferred choice. With superior encapsulation in modern times, the fire behaviour of the materials is expected to be very different.

Testing was carried out in the cone calorimeter and a simple flammability study of the synthesised material was carried out. The research found that upon exposure to the imposed heat flux from the cone, either 35 or 50kW·m^{-2}, the paper lining ignited after some delay. This represented an initial peak in the heat release rate. A period of lesser burning would follow for around 5 to 10 minutes until the PCM then ignited. This caused another slightly larger HRR peak. The peak however is much wider showing the energetic nature of the PCM compared to the paper facing. The quantity of the PCM was much higher (23%) when compared to the paper facing (6%) and the other organic additives (2.5%). For reference, the amount of water lost due to crystallisation was given as 5.5%.

2.4.2.1.3 Recent microencapsulated PCM plasterboard

Near the beginning of the 21st century the interest in sustainability and thus PCMs grew rapidly. The number of publications was little to none from 1979 to 2002. This then increased to 9-13 publications per year from 2005 to 2010 (Kuznik *et al.* 2011). The commercial uptake has been delayed but has seen substantially increased usage in the built environment.

Thus, an initial study into the flammability of a modern PCM plasterboard was conducted by Asimakopoulou *et al.* (2015). A commercially available product was tested using TGA, DSC, the cone calorimeter, SEM and then a simple model was developed in FDS (Fire Dynamics Simulator, (McGrattan *et al.* 2014)). The plasterboard was 12.5mm thick and incorporated PCMs using microencapsulation. The microcapsules are believed to be the same as those that were tested in this thesis.

In the cone calorimeter the PCM was tested at both 50 and 75kW·m^{-2}, and then compared against a plasterboard tested in the same conditions. The behaviour was broadly similar to the synthesised material tested decades earlier, despite the vastly different incorporation methods. An initial HRR peak corresponded to the ignition of the paper, and was then followed by a period of lesser burning. The PCM then reached the critical temperature for it to be able to vaporise and escape from its shell, then burning upon mixing with oxygen. This resulted in a wide peak of almost equal magnitude to the HRR corresponding to the ignition of the paper. Again, the much greater width of the peak evidences the energetic nature of the PCM when compared to the paper.

2.4.2.1.4 Flammability comparison

The fire behaviour of the two materials tested using standardised methods (Banu, Feldman, Haghighat, *et al.* 1998, Asimakopoulou *et al.* 2015) have been summarised in Table 2.8. Despite a lower PCM content, and a lower still estimated wax content, the PCM enhanced plasterboard tested by Asimakopoulou *et al.* (2015) had a higher total mass lost as a percentage and around 45% more total heat released. The listed peak heat release rates are relatively similar but because there were peaks at both the start and end of the test this becomes a less informative measure. In both cases there was rapid ignition of the paper lining following exposure to the heat flux and apparent ignition of the paraffin wax was not until substantially later. This is perhaps an artefact of the test since a second peak is often observed in standardised cone testing due to the thermal thickness of the material (Schartel and Hull 2007, Carvel *et al.* 2011). Given that there is a constant HRR throughout the test it is possible that the PCM is burning and that the material generally acts as a charring material until the pyrolysis front reaches the opposite surface.

Table 2.8 – Summary of flammability properties in this study compared when previous results when tested at 50kW·m^{-2} in the horizontal orientation according to ISO 5660 (British Standards Institution 2015a) and ASTM 1354 (ASTM International 2014).

Quantity	Units	Plasterboard[1]	Plasterboard[2]
Thickness	mm	12.5	12.5
Est. PCM content	%	18	22.8
Est. wax content	%	12	22.8
Mass loss	%	43.31	36.78±0.21
Time to ignition	s	41	33±1
Peak HRR	kW·m^{-2}	181.38	170.75±12.66
Total heat released	MJ·m^{-2}	111.40	77.75±3.17
Average HRR	kW·m^{-2}	74.26	70.25±3.09
$H_{c,eff}$	kJ·g^{-1}	-	20.40±0.97

[1] Asimakopoulou *et al.* (2015)

[2] Banu, Feldman, Haghighat, *et al.* (1998)

2.4.2.1.5 Recent oven testing

A series of testing including constant temperature oven testing, DSC measurements, and thermal conductivity and mass loss for elevated oven temperatures were carried out (Kontogeorgos *et al.* 2015). The DSC measurements identified the characteristic endothermic peaks associated with the two step dehydration of gypsum between 100 and 200°C. In the PCM enhanced plasterboard additional exothermic reactions were identified both in an inert atmosphere and air. The peak was located at approximately 410°C, with at onset at around 280°C.

Specimens were placed in an oven which exposed both front and rear surfaces to the set oven temperature of 300°C. Specimens were two samples sandwiched together back to back, and were tested with and without the finishing. When tested with the finishing both the PCM and non-PCM case recorded substantial temperature increases. In the non-PCM case the peak temperature was 500°C whilst in the PCM case this was 800°C. A plateau at approximately 100°C was observed for both materials corresponding to the dehydration of the gypsum.

The tests were then repeated having removed the flammable lining. For the ordinary gypsum case the temperature stabilised at 300°C following the dehydration at 120°C. In the PCM case a peak of 500°C was observed after the temperature at depth reached 300°C, which could be attributed to the oxidation of PCM.

To obtain the mass loss and thermal conductivity at elevated temperatures samples were placed in an oven at the desired temperature and left to stabilise. After six hours they were then removed, placed in a bag and left to cool back down to ambient. Measurements were then take to be able to estimate the mass loss and thermal conductivity at high temperatures. Approximately 14% of mass lost for an oven temperature of 125°C which was attributed to the dehydration reactions. A further 16% mass loss by 160°C was attributed to the evaporation of paraffin wax and 4% mass loss by 250°C to the evaporation of PMMA. In each of these cases the oven temperature is significantly lower than the temperatures identified in the DSC. Given the more controlled boundary conditions in the DSC it would be believed that those temperatures are more accurate. The thermal conductivity noted a reduction of 40-50% in both PCM and non-PCM cases at an oven temperature of 120°C. The initial effective thermal conductivities at ambient were measured as 0.25 and 0.28$W \cdot m^{-1} \cdot K^{-1}$ for ordinary and PCM plasterboard respectively. The thermal conductivity of PCM plasterboard was within 10% of the ordinary plasterboard for oven temperatures above and below the dehydration reactions.

From this body of research the authors concluded that PCM plasterboard remained a suitable material for absorbing energy at temperatures below 300°C. At temperatures beyond this the PCM would be capable of evaporating and oxidising, thereby rapidly increasing the temperature within the board and representing a risk which should be carefully taken into account.

2.4.2.2 Shape stabilised

Shape stabilised PCMs, also known as form stabilised PCMs, are capable of supporting large quantities of organic PCM and thus show great potential for energy savings. The supporting material is typically a polymer material such as high density polyethylene (HDPE) or polymethylmethacrylate (PMMA) which constitutes around 10 to 40% of the total weight. In some instances rubber is used as the supporting material. The combustible nature of the materials, particularly with high quantities of organic PCM, made it necessary to investigate the flammability of such materials.

A collection of studies were performed which evaluated the performance of shape stabilised PCMs with and without flame retardants. A range of formulations with a variety of flame retardants were tested in the cone calorimeter at 35kW·m^{-2} to measure their mass loss rate, heat release rate, and total energy released. The first of these studies (Cai *et al.* 2006) considered paraffin wax and HDPE, with a selection of melamine phosphate (MPP), pentaerythritol (PER), 1,2-bis(pentabromophenyl) ethan (BPBE), antimony trioxide (AO) and melamine cyanurate (MCA). The thermal storage properties of the resultant material, as measured by DSC, were found to be unaffected by the addition of flame retardants for all cases. It should be noted that amount of PCM remains constant, and only the HDPE is displaced by the addition of the flame retardants.

For the base case of 60% paraffin wax and 40% HDPE the peak HRR was found to be approximately 900kW·m^{-2} over a period of 40 seconds. The total energy released as a function of the area was found to be 76.5MJ·m^{-2}. The addition of flame retardants was capable of reducing the peak HRR down to between 300 and 550kW·m^{-2} for different formulations. Similar decreases in peak MLR were noted for samples containing a concoction of MPP and PER. The results of the total energy released and the heat of combustion were more mixed. In some cases (60% paraffin wax, 15% HDPE, 19% BPBE, 6% AO) the total heat released was 30% lower whilst in other cases (60% paraffin wax, 15% HDPE, 25% MCA) it was as much as 15% higher.

The thermal stability was decreased by the addition of the flame retardants, thereby decreasing the temperature for the onset of pyrolysis. As such, this would typically be expected to increase the ignitability of the material and thus the fire risk would be modified.

The same material was then modified with expanded graphite (EG), ammonium polyphosphate (APP), and zinc borate (ZB) in various compositions (Cai, Wei, *et al.* 2008). The preferable properties of the additives compared to HDPE resulted in slightly superior thermal properties. The latent heat was higher, and improved properties during the freezing cycle. The peak HRR was reduced by 90% for the case of 60% paraffin wax, 20% HDPE and 20% EG. The case containing 10% EG and 10% APP also had a 90% reduction in the peak HRR, whilst 10% EG and 10% ZB reduced the peak by 70%. However, burning times were increased to 550s, 750s and >1200s for the three respective cases. In the base case the burning time was only 200s.

Time to ignition and total energy released were not given which may be important in determining and quantifying the change in fire risk.

An extension of this study was conducted on higher quantities of APP, 21 to 25%, and only very low quantities of EG, 0 to 4% (Cai *et al.* 2009). This clearly illustrated the influence of increasing amounts of EG. The peak HRR was substantially reduced in exchange for a longer burning time. In the case of 21% APP and 4% EG there was a secondary peak corresponding to the oxidation of the char. Since no figures are given for the time to ignition and total energy released it is again difficult to quantify the change in fire risk.

The next study investigated the effectiveness of organophilic montmorillonite (OMT) under the same conditions (Cai *et al.* 2007). It was mixed with both MPP and PER in varying quantities, and then tested in TGA, DSC and the cone calorimeter at 35kW·m^{-2}. The base case was the same 60% paraffin wax and 40% polyethylene material as previously.

The thermal stability was decreased and the latent heat storage was unaffected, as was the case with the other flame retardants previously studied. The addition of OMT reduced the peak HRR by 45 and 67% for two quantities of OMT. However, the time to ignition was reduced by 20 to 30% and the total heat released was increased by 6% for both quantities. Thus, the addition of flame retardants again changes the fire risk by increasing the ignitability and total energy released, but reducing the peak HRR.

The same study is then conducted on a composite material containing 75% paraffin wax, 15 to 25% HDPE modified with poly(ethylene-co-vinyl acetate) (EVA), and 0 to 10% OMT (Cai, Song, *et al.* 2008). The addition of OMT causes a decrease in the latent heat at ambient temperatures, thereby suggesting that the resultant PCM is less effective. The increase in the proportion of paraffin wax and the modification of the HDPE increases the peak HRR to 1575kW·m^{-2} for the same 35kW·m^{-2} exposure in the cone calorimeter. For values of 2.5, 5, and 10% of OMT the peak HRR is reduced by 12, 35, and 40% respectively. The time to ignition and total heat released are not listed in this instance but the thermal stability is increased. Thus would generally be expected to increase the time to ignition and therefore decrease the ignitability.

In summary, the addition of flame retardants to shape stabilised PCM boards were capable of modifying the fire risk by reducing the peak heat released but potentially increasing the ignitability and not reducing the total amount of energy released. For many of the cases studied the latent heat storage properties of the PCM were unaffected and thus it may prove an attractive option.

2.4.2.3 Fire retarded capsules

Work by Kośny *et al.* (2009) investigated the possibility of developing ignition resistance microcapsules for PCMs. Issues with the flammability of organic PCMs caused a particular issue in America since they were not capable of passing ASTM E2257 (ASTM International

2013a) and the room corner fire tests (British Standards Institution 1993) and thus could not be used.

Fatty acids were used over paraffin waxes because they were believed to be less flammable and thus made a better starting point. The plastic shell of the microcapsules was then altered to have fire retardants added in order to improve their fire performance. They found that after the alterations were made the material was then able to pass the ASTM critical radiant flux test and that there was little to no loss in the performance of the PCM at ambient conditions. This shows that they would be suitable for commercial use and their function remains intact even with the improved fire measures. Despite the apparent success of this research there have been no further developments and it has not been adopted elsewhere.

2.4.2.4 Concrete and mortars

2.4.2.4.1 Early direct flame impingement testing

Some simple testing on various concretes impregnated with PCMs were evaluated using ASTM D3806 (ASTM International 1998) by Hawes (1991). The PCM concrete was synthesised via immersion and incorporated one of butyl stearate (BS, fatty acid), dodecanol, or paraffin.

This test method subjects a 610mm long and 250mm sample to a direct flame with a temperature of 700±10°C. The specimen is inclined at 33° from the normal and the flame exposure lasts for ten minutes. The test procedure is intended to provide some limited information on the flame spread and extinction characteristics of paints.

The conclusions drawn by the authors were that the flame spread was highly restricted, extending no further than 100mm in the worst case. Upon removal of the flame there was no continued burning and thus no self-sustaining flaming was established.

This work was sufficient to identify that the fire hazard associated with PCMs in concrete is relatively low and potentially not an immediate danger. It also recognised that further large-scale testing would be required to properly characterise the behaviour. Recent fire testing of non-PCM concrete has shown that attempts to characterise its fire behaviour are not entirely straightforward Maluk (2014). The inclusion of PCMs would further complicate this. However, the maximum amount of PCM is in the region of 3 to 9% (Lee *et al.* 2000) by weight and thus its fire risk is very different to plasterboard and other materials.

2.4.2.4.2 Recent dripping, smoke and small-scale resistance testing

More recent testing has been conducted on concrete containing microencapsulated PCMs (Haurie *et al.* 2014). Thermal properties were evaluated using the T-history method (Hong *et al.* 2004) which is often used for PCMs. Fire testing was conducted using a Spanish standard for evaluating dripping and smoke generation (UNE 23725:1990) in addition to some small-scale fire resistance tests. These were used to understand how some thermal properties would change as the content of PCM in mortar was increased.

The T-history method was used to estimate that the thermal diffusivity decreased from 0.81±0.01mm^2·s^{-1} at 0% PCM content to 0.51±0.02mm^2·s^{-1} at 25% PCM content. This is due to the fact that the specific heat capacity is massively increased by the addition of the PCM, and the thermal conductivity is also reduced by some amount. This can clearly be seen when considering the definition of thermal diffusivity:

$$\alpha = \frac{k}{\rho \cdot c_p} \quad \text{Eq. 5}$$

Where α is the thermal diffusivity (mm^2·s^{-1}), k is the thermal conductivity (W·m^{-1}·K^{-1}), ρ is the density (kg·m^{-3}), and c_p is the specific heat capacity (J·kg^{-1}·K^{-1}).

The dripping test positions a 500W electrical heater in contact with a 100mm by 100mm specimen until ignition occurs. The heater is then removed and the time to extinguishment is recorded. The heater is again reintroduced and the process is repeated, recording each time ignition reoccurs. This test confirmed that the addition of PCM was sufficient to make an otherwise non-combustible material combustible. The times to ignition for both the 10% PCM and 25% PCM content were the same, at 38s. This contradicts the expected behaviour since typically a higher loading should mean that more material can be pyrolysed, and thus ignition is reached more rapidly. The number of ignitions at 10% content was higher, but the average flaming duration was shorter when compared to the tests at 25%. It was concluded from this test series that the lack of self-sustained flaming suggested a material which extinguishes easily.

The smoke test identified that the addition of PCMs produced smoke which reduced the light intensity by 15% at 10% content, and 40% light intensity reduction at 25% content. When there was no PCM present then there was no light obscuration.

Small-scale fire resistance tests were conducted and interpreted using the data gathered from tests in a pyrolysis combustion flow calorimeter (PCFC). The small-scale fire resistance test exposes on side of the specimen to a specified standard fire curve which reaches 1000°C after two hours. A minor deviation in the PCM test between 600 and 700°C was attributed to the combustion of the PCM. However, the PCFC identified the onset of the pyrolysis of the PCM at 100°C with a peak at 208°C. Furthermore, the flash point of the PCM was 146°C. The temperature otherwise between the non-PCM and PCM tests were the same.

The most useful information for these tests was the onset of pyrolysis and the flashpoint identified. These quantify the ignitability of PCMs, and show the low temperatures needed to achieve pyrolysis. Additional testing is still required to characterise the flammability of the materials.

2.4.3Hemp-lime in fire

Existing literature on the fire performance of hemp-based materials is limited. Some research relating to its use as a biofuel is available but this does not have applicability to fire science outside the determination of the heat of combustion (*Section 2.2.2.4*). An initial investigation into the use of hemp-lime insulation as a fire protection material was conducted recently (Hall 2013, Wright 2013). This evaluated the ability of the material to insulate steel members from fire exposure. It was found that the hemp-lime insulation has a high propensity to smoulder. In addition to this, there has been some standard fire resistance testing as part of accreditation, detailed below, but no further research in the literature. Furthermore, this testing does not give a complete characterisation or quantify the fire risk associated with these materials. The existing studies into the use of hemp-lime insulation as a fire protection material and a summary of some of the standard fire testing reports are given below.

2.4.3.1 Bespoke constant radiant heat flux testing

Studies of the thermal wave propagation and smouldering characteristics in hempcrete were conducted by Hall (2013) and Wright (2013). The aim of the project was to evaluate the performance of hempcrete as a potential alternative for the fire protection of steel structural elements. Thus, the focus of the research was on the thermal wave propagation and temperature reached at the unexposed face after a prescribed period of time.

In one series of tests samples of dimensions 320mm by 320mm by variable thickness, either 50 or 100mm, were exposed to constant external heat fluxes ranging from 25 to 40kW·m^{-2} from a radiant panel. The dimensions of the radiant panel were the same as the sample to provide a uniform heat flux to the surface, and the orientation was vertical. Smoulder spread rates were sufficiently low that the hempcrete was capable of preventing the unexposed face from reaching excessive temperatures for exposure durations of 60mins, which was the maximum considered in the study. The definition of excessive temperature was related to the loss of mechanical properties of the steel, which is in the region of 500°C. Spread rates for radiant panel tests across various heat flux have been derived as 1.53±0.21mm·min^{-1}. These were based on the time taken for thermocouples at each in-depth position to reach 300°C. Specimens were unsealed around the sides thereby permitting adequate oxygen diffusion to the smouldering front. Peak temperatures of up to 700°C were recorded as the smouldering front propagated through the specimen. For the 100mm thick specimens the rear face temperature did not exceed 100°C within the one hour testing timeframe. In some cases a smoulder was sufficiently established that a front continued to propagate for three hours after the panel was switched off. Furthermore, this reached temperatures of 800°C which was higher than any of the tests. This illustrates that there was potential for a self-sustaining smoulder to be established. Thermal evolution over 55 mins of a single test is illustrated in Figure 2.18.

An additional series of cone calorimeter tests were also conducted by the same authors using a constant heat flux of 40kW·m^{-2} on 100mm sized cube samples. This found that the peak HRR (Heat Release Rate) was 104.2kW·m^{-2} when calculated using oxygen consumption, or

62.5kW·m^{-2} when calculated using carbon dioxide generation. Both methods were conducted according to Biteau (2009). These peak values are similar to other fire protection materials, such as paper-faced plasterboard which are presented later in *Section 2.4.1.1.5*. However, the quantity of available fuel and the propensity for smouldering mean that the hempcrete represents a different type of fire risk which requires quantification.

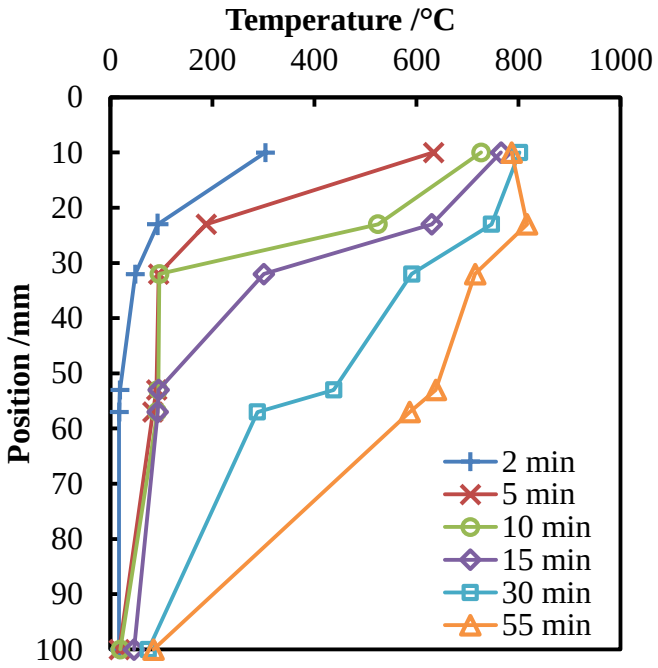

Figure 2.18 – Temperature-depth data profiles for a 100mm thick specimen exposed to a heat flux of 39.5kW·m^{-2}. Reproduced from Hall (2013).

2.4.3.2 Standard fire resistance testing

Some studies have been carried out to evaluate the fire performance of hemp-lime insulation using standard fire tests (Bevan and Woolley 2008). These have found that the material is capable of achieving fire resistance ratings of 60 and 120 mins, and or 240 mins for a thickness of 250mm.

Some testing has been carried out on by various manufacturers so that their products can be used within buildings. Lime Technology, UK have published their standard fire test results conducted by BRE Group, UK. Their Hempcrete was credited as providing a fire resistance of 60 minutes as a loadbearing element as per BS 476-21 (British Standards Institution 1987a). In accordance with BS 476-22 for non-loadbearing elements (British Standards Institution 1987b) the same material lasted 88 mins (integrity failure) and 180 mins (test manually terminated). The integrity failure was due to ignition of the timber frame (Hall 2013). In the latter case, cracking was observed at 127 mins but no failure was noted before the test was terminated.

Panels containing 120mm thick hempcrete backed by hemp-fibre insulation by the same company was capable of achieving 60 minutes after which time the timber frame ignited.

Other tests performed at CSTB, France and collated by Bevan and Woolley (2008) reached 100 minutes before failure of mortar joints. The test involved 250mm thick hemp-lime blocks constructed with lime mortar. Further testing by the same manufacturer suggested the possibility of reaching up to 240 mins without failure.

These tests indicate that although hemp-lime materials are susceptible to flaming and smouldering combustion, these risks are not adequately characterised by the standard testing. Whilst the temperature-time exposure in a furnace can be deemed severe, this is not particularly relevant to smouldering which is often limited by the rate of oxygen diffusion. This is partially evident from the fact that significant smouldering was observed in the cone calorimeter testing at only moderate heat fluxes by Hall (2013) and Wright (2013). Thus, a suitable method for characterising the smouldering risks are required.

2.5 Fire dynamics

Multiple fire dynamics theories are applied throughout the thesis and thus they are discussed here and the relevant parts are referred back to when necessary. Some of the assumptions and limitations of the various concepts are described but in general these are outlined to aid the understanding of the subject as opposed to a new fundamental study.

2.5.1Ignition

Ignitability is a key risk which is widely evaluated using bench-scale calorimetry. The flaming ignition of solids theory (Torero 2008) is widely applied to materials to give an indication of some of their intrinsic properties which can be compared with other materials. Additionally, the firepoint theory applied to solids (Rasbash 1975) is also briefly discussed due to its relevance to PCMs later in the thesis.

2.5.1.1 Flaming ignition of solids theory

The ignition theory of solids (Torero 2008) represents a fundamental concept in the ignitability of materials. It is capable of providing a representation of the ignition behaviour (including ignition temperature and the thermal inertia) obtained from testing in bench-scale calorimetry which can be used as a simple comparison between materials. In some cases these properties are labelled as “apparent” or “effective”, to differentiate from actual values. There are a number of reasons for the difference in these values, including the lack of heat losses, or non-linear treatment of losses; assumption of an inert solid; and non-temperature dependent properties. There are also issues for materials with low thermal inertia which cause rapid ignition and significant deviation from the theory is noted, which has been investigated and by Hidalgo-Medina (2015).

A simple method for determining the actual thermal inertia from the apparent thermal inertia is outlined by Mowrer (2005). This is useful when determining parameters for input into models such as FDS, but may not be necessary when simply comparing effective values in the literature. Furthermore, this still does not consider latent effects, for example due to moisture or phase changes nor the ability to determine temperature dependent properties.

The purpose of this thesis is to outline a framework for evaluating the fire risks associated with innovative materials. Therefore, there is not excessive focus on the assumptions and simplifications of ignition theory since this in itself is an entire topic. The materials studied violate many of the assumptions, including all those outlined above, and thus the results are expected to be highly inaccurate. Instead, the analyses are done so that simple comparisons can be made both to other construction materials in the literature, and changes in substrate behaviour due to the addition of PCMs. As a framework, the designer can choose whichever method they deem fit, and may wish to determine more accurate properties if modelling is the goal.

A complete description of the ignition theory including all the derivations, assumptions and limitations can be found elsewhere, for example, Torero (2008) or Steinhaus (2009). An abridged version is outlined below.

An energy balance is considered at the surface of the material (Eq. 6) and the following simplified boundary conditions are applied:

$$\rho \cdot c \frac{\partial T}{\partial t} = k \frac{\partial^2 T}{\partial x^2} \quad \text{Eq. 6}$$

$$\text{at } x = 0; \qquad 0 = \dot{q}_i'' + k \frac{\partial T}{\partial x} - h_T \left(T_{s,t} - T_0\right) \quad \text{Eq. 7}$$

$$\text{at } x = L; \qquad 0 = -k \frac{\partial T}{\partial x} \quad \text{Eq. 8}$$

Where ρ is the density, T is the temperature, t is the time, k is the thermal conductivity, x is the distance parallel to the heat source, where zero is the surface and the positive travels through the depth of the material, and h_T is the total heat transfer coefficient.

2.5.1.2 Ignition temperature

From the energy balance at the surface of the material (Eq. 7) the ignition temperature can be ascertained. This is based on the minimum heat flux required to achieve ignition, and the time to taken to reach this point is assumed to be infinite. Furthermore, the temperature of pyrolysis is assumed to be the temperature of ignition at this point since a strong pilot is used and the gases are assumed to be well mixed. Thus, the temperature of ignition is given by:

$$T_{ig} = T_0 + \frac{a \cdot \dot{q}_{cr}''}{h_T} \quad \text{Eq. 9}$$

Where T_{ig} is the ignition temperature, T_0 is the ambient temperature, a is the absorptivity and $\dot{q}_{cr}''$ is the critical heat flux. The convective heat transfer coefficient is included as part of the total heat transfer coefficient. This represents one of the greatest uncertainties in this analysis. An accurate value of the convective component is difficult to obtain and it is instead assumed to be 15 $W \cdot m^{-2} \cdot K^{-1}$ providing a total heat transfer coefficient of 45 $W \cdot m^{-2} \cdot K^{-1}$ (Torero 2016). This is based on other calculated heat coefficients for the cone calorimeter.

2.5.1.3 Apparent thermal inertia

Based on the set boundary conditions (Eq. 6, Eq. 7 and Eq. 8) a Laplace transform can be used to obtain the surface temperature at ignition:

$$T_{ig} = T_0 + \frac{a \cdot q_i''}{h_T}\left[1 - e^{\frac{t_{ig}}{t_c}} \cdot erfc\left(\left(\frac{t_{ig}}{t_c}\right)^{\frac{1}{2}}\right)\right] \quad \text{Eq. 10}$$

Where the temperature at ignition is assumed to be equal to the pyrolysis temperature. This pyrolysis temperature is the point at which flammable vapours are generated through material, and where the virgin material beyond the regression front is assumed to be inert. The characteristic time, which is the time taken for the thermal wave to penetrate through the material, is given by:

$$t_c = \frac{k\rho c}{{h_T}^2} \quad \text{Eq. 11}$$

At high heat fluxes the time to ignition is achieved rapidly compared to the characteristic time. This is valid for materials which have a large thermal gradient through their depth prior to ignition and are thermally thick. Thus, a first order Taylor series expansion around $t_{ig} << t_c$ in Eq. 10 yields:

$$\frac{1}{\sqrt{t_{ig}}} = \frac{2}{\sqrt{\pi}} \frac{a}{\sqrt{k\rho c}} \frac{\dot{q}_i''}{(T_{ig} - T_0)} \quad \text{Eq. 12}$$

This then allows the calculation of $k\rho c$ through a regression analysis for a given set of heat fluxes and ignition times. The absorptivity, *a*, is assumed to be 1 where no better data is available. For this approach the phase changes are lumped into the specific heat capacity and there is no variation with temperature. In reality, each phase change could be characterised through the latent heat of fusion for a reaction at a given temperature. However, this would require a more complex application of the ignition theory. Furthermore, the complicated and unknown formulation of both gypsum and PCM would result in a large number of reactions and would introduce additional errors where the input data is poor.

2.5.1.4 Ignition properties of common materials

For the sake of comparison a collation of ignition temperatures and thermal inertias for common building materials are given in

Table 2.9. Whilst these do not fully evaluate the ignition risk that each material represents it provides a broad context for PCMs to fit into. The motivation and justification for this was given previously in *Section 2.5.1*. The information is collected from Quintiere (2006).

Table 2.9 – Summary of ignition temperature and apparent thermal inertia of some common materials.

Material	**Ignition temperature**	**Apparent thermal inertia**
-	°C	$kW^2 \cdot s \cdot m^{-4} \cdot K^{-2}$
Ordinary gypsum†	412	0.57
Fire resistant gypsum†	510	0.40
Gypsum w/ wallpaper†	565	0.45
Polystyrene†	630	0.38
Polyisocyanurate†	445	0.02
Plywood†	390	0.46-0.54
PMMA type G†	378	1.02
Fibre insulation board†	355	0.46
Douglas fir particle board†	382	0.94

† Quintiere (2006), materials tested according to ASTM 1321 (ASTM International 2013b).

2.5.1.5 Firepoint theory for solids

In some places it becomes more apparent that it is convenient to describe ignition behaviour using an alternative theory. Firepoint theory is a concept applied to the ignition of liquid fuels, where sustained flaming defines the firepoint temperature of the material, and periodic flaming prior to this point is referred to as the flashpoint temperature. This has been successfully applied to solids in a number of cases (Rasbash 1975, Rasbash *et al.* 1986, Thomson and Drysdale 1987, Drysdale and Thomson 1989). The basis of this theory is that when a critical surface temperature is reached volatile gases will be produced. If the mass flux of these products is sufficiently high then the lower flammability limit is exceeded in the gas phase, and, in the presence of a pilot, a flame can be established. Heat losses from the flame maintain the generation of pyrolysis gases, but may also reduce its temperature to the point of extinction and thus flaming cannot be maintained. When these losses are exceeded the flame can be sustained. The generation of pyrolysis gases is dependent on a critical value to sustain the flame and thus the concept of critical mass flux is also relevant (Rich *et al.* 2007).

2.5.2Effective heat of combustion

The effective heat of combustion provides a method of calculating the amount of energy produced during combustion. This is done so using the following equation:

$$Q_T = \chi \cdot m_L \cdot \Delta h_{c,eff} \qquad \text{Eq. 13}$$

Where Q_T is the total heat released (kJ), χ is the completeness of combustion (-), m_L is the total mass lost (g), and $\Delta h_{c,eff}$ is the effective heat of combustion ($kJ \cdot g^{-1}$). The effective heat of combustion obtained through this method is not a material property but is instead dependent upon the environmental conditions and test setup.

2.5.3Determination of heat release rate

Two of the primary methods of calculating the heat release rate (HRR) in bench-scale calorimetry are oxygen consumption (OC) and carbon dioxide generation (CDG). This

parameter often times labelled the more important parameter in fire science and thus the method to determine it is important (Babrauskas and Peacock 1992).

Oxygen consumption method measures the amount of the oxygen depleted in the gases generated by a specimen. It is based on Thornton's principle (Thornton 1917) which linked the relationship between oxygen depletion and heat of combustion. This was then extended further to find that for most materials the amount of energy released per unit of oxygen consumed is relatively constant (Huggett 1980). The energy constants, validity and uncertainties associated with the extrapolation of this method have been studied in detail by Biteau (2009).

Oxygen depletion can be used to calculate the heat release rate using the energy constant of 13.1 kJ·g_{02}^{-1} (Huggett 1980). Since the formulation of PCM is mostly hydrocarbon liquids, an energy constant of 13.1 kJ·g_{02}^{-1} is appropriate. The calculations for heat release rate are carried out as per Janssens (1991).

The principle, as outlined above, is based a constant amount of energy produced for an amount of oxygen consumed in the products from the material. For bench-scale calorimetry, it is necessary to know the mass flow rate of gases through the duct where the oxygen concentration is measured. In the cone calorimeter this can be achieved by measuring the pressure drop:

$$\dot{m}_e = C\sqrt{\frac{\Delta p}{T_e}} \qquad \text{Eq. 14}$$

Where $\dot{m_e}$ is the mass flow rate in the duct, C is the orifice plate coefficient, Δp is the pressure drop, T_e is the gas temperature measured at the plate.

The heat release rate can ultimately be derived by:

$$\dot{q} = \left[E \cdot \phi - (E_{CO} - E)\frac{1-\phi}{2}\frac{X_{CO}^{A}}{X_{O_2}^{A}}\right]\frac{\dot{m}_e}{1+\phi(\alpha-1)}\frac{M_{O_2}}{M_a}(1-X_{H_2O}^{\circ})X_{O_2}^{A^\circ} \qquad \text{Eq. 15}$$

Where E_{CO} is the energy released for the combustion of CO to CO_2, and α is a factor to account for the displacement of oxygen by combustion products in the duct, the subscript a denotes values pertaining to incoming gases, the subscript e denotes values from the exhaust, M is the molecular weight, and $\dot{m}$ is the mass flow rate.

The oxygen depletion factor when O_2, CO and CO_2 are measured is given by:

$$\phi = \frac{X_{O_2}^{Ai}\left(1 - X_{CO_2}^{A} - X_{CO}^{A}\right) - X_{O_2}^{A}\left(1 - X_{CO_2}^{A^\circ}\right)}{\left(1 - X_{O_2}^{A} - X_{CO_2}^{A} - X_{CO}^{A}\right)X_{O_2}^{A^\circ}} \qquad \text{Eq. 16}$$

Where ϕ is the oxygen depletion factor, X is the molar fraction, the superscript A represents quantities measured by the gas analyser, and the superscript $^\circ$ refers to incoming air.

2.5.4 Smouldering combustion

Smouldering is a heterogeneous form of flameless combustion which occurs between the reaction of condensed phase fuel and gas phase oxygen (Ohlemiller 2008, Rein 2009). Susceptible materials are typically porous and upon heating will pyrolyse releasing pyrolysis gases and forming a rigid, carbon-rich char. The solid phase char undergoes an exothermic reaction with gaseous oxygen providing additional energy required to drive the pyrolysis reaction and allow for self-sustained smoulder. Under certain conditions – namely sufficient heat, oxygen and an ignition source – the gaseous volatiles may ignite and flaming will occur.

Smouldering is a key phenomenon which is often neglected in the field of fire safety engineering. This is reflected in the fact that currently there is no British Standard to assess the smouldering propensity of a material. Flaming is typically regarded as the most severe combustion mode due to the higher temperatures and energy released and is considered during the design of infrastructure. However, smouldering presents unique risks which become prevalent as novel building materials are used. Despite relatively low temperatures, the yield of carbon monoxide is much higher, representing a toxicity hazard, and smouldering may propagate undetected for some time in concealed spaces. Smouldering also allows a pathway to flaming combustion from heat sources that are too weak to ignite flaming directly.

The cone calorimeter has previously been used to study the smouldering of various materials, including plywood (Gratkowski *et al.* 2006), peat (Rein *et al.* 2009), and polyurethane foam (Hadden *et al.* 2012). The peat experiments by Rein *et al.* (2009) followed the ISO 5660 standard (British Standards Institution 2015a) closely, but the pilot was not used since flaming was not interest. Incident heat fluxes of 30 to 70kW·m^{-2} were used and suitable smouldering propagations were found. The use of an external heat source was recommended since self-sustained smoulders were found to be too heavily affected by edge effects. Gratkowski *et al.* (2006) adopted a similar approach but with significantly lower heat fluxes, in the range of 6 to 15kW·m^{-2} for periods of up to eight hours. The work focussed primarily on ignition due to self-heating, and characterised the depth at which ignition occurred for each heat flux. Hadden *et al.* (2012) investigated the effect of sample size in a mass loss calorimeter. A flange was added to the top of the specimen holder to prevent excessive recirculation due to buoyant effects. The setup was designed to promote a one-dimensional downward smoulder, whilst still being able to investigate flaming in the same configuration. It was found that critical heat flux decreased as the sample size was increased. Good repeatability was found for each size for both smouldering and flaming, suggesting that the cone calorimeter is an appropriate apparatus for studying smouldering. Each of these studies show that smouldering can be successfully studied in the widely available cone calorimeter.

In smouldering, there are two major configurations which are studied in the laboratory. The first is opposed smoulder in which the smoulder front propagates towards the oxidiser flow (Torero *et al.* 1993). The other smouldering configuration is known as the forward smoulder

(Torero and Fernandez-Pello 1996). In this instance the oxidiser flow and smouldering front propagate in the same direction. An illustration of these two regimes is given in Figure 2.19.

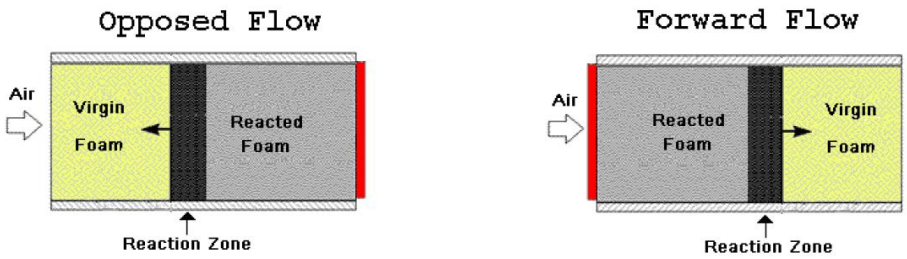

Figure 2.19 – Schematics illustrating opposed flow smouldering (left) and forward flow smouldering (right) for a foam material. Extracted from Rein (2009).

2.5.4.1 Opposed flow

In opposed flow smouldering an endothermic pyrolysis front propagates away from the heat source, generating volatile gases and leaving behind a char. The oxidiser, often in the form of air, diffuses through the virgin material and reacts with the char. This exothermic oxidation releases energy which heats the material in front, thereby allowing a self-sustaining reaction to be established if the heat losses are sufficiently low. The dominant heat transfer mechanisms from the reaction front to virgin material upstream are conduction and radiation. Oxidiser diffuses through the virgin material at a rate governed by the permeability of the material. The rate of this oxidiser flow to the reaction front is then proportional to the spread rate (Ohlemiller 1985). As the oxygen arrives to the reaction front the pyrolysis reaction will take place in an oxidised environment. Adequate oxygen supply will allow the exothermic oxidation to take place in the same region as the oxidative pyrolysis reaction. This overlapping of the endothermic pyrolysis and exothermic oxidation have been shown in experimental studies (Torero *et al.* 1993). However, it has been shown that both processes are still present and can be adequately modelled (Rein *et al.* 2007). The diffusion of oxygen through the virgin material means that its temperature remains near ambient, and there is no opportunity for preheating.

2.5.4.2 Forward flow

In forward flow smouldering an endothermic pyrolysis front generates char in the direction leading away from the heat source. The presence of oxidiser flow then allows the exothermic char oxidation to occur immediately. In forced flow conditions two distinct planes for the endothermic pyrolysis and exothermic oxidation are observed (Torero and Fernandez-Pello 1996). Previous research on cellulose identified that forward flow conditions can cause different chemical pathways to be followed (Ohlemiller and Lucca 1983). Char oxidation at the reaction front will starve the upstream pyrolysis reaction of oxygen, causing a non-oxidative environment and thus different chemical decomposition compared to opposed flow as above. The oxidiser is preheated as it travels through the hot ash and reaction zone, and thus the smoulder propagates much more rapidly than in the opposed regime. Furthermore, hot post-combustion gases transport additional heat via mass diffusion ahead of the reaction zone, aiding preheating and the pyrolysis reactions. It has been shown that spread rates in the

forward smoulder are typically around ten times more rapid than those in the opposed smoulder for cellulosic fuels (Ohlemiller 1985), and similar figures can also be derived for foams (Torero *et al.* 1993, Torero and Fernandez-Pello 1996). In reality, neither of these modes exists in isolation and the smouldering is often dominated by buoyancy induced airflow (Torero and Fernandez-Pello 1995).

2.5.4.3 Liquid smouldering combustion

The potential for combustion of organic liquid fuels within an inert porous matrix has been shown previously by Pironi *et al.* (2009). This has successfully been implemented and characterised in a wider range of circumstances (Switzer *et al.* 2009, Pironi *et al.* 2011, Yermán *et al.* 2015). The bodies of work generally focus on the complete destruction through smouldering combustion of organic waste products contained within sand or soil.

2.6 Concluding remarks

A review of phase change materials has been conducted which covers their usage, thermal performance, and the limited existing literature of their fire behaviour. Additional literature on related materials and fire dynamics have also been reviewed. The following conclusions have been drawn:

- PCMs represent an attractive option for energy savings in an environment of increasingly stringent and difficult to reach sustainability goals. They can be used in a lightweight building to offset rapid temperature fluctuations that plague these buildings.
- Organic PCMs, specifically paraffin waxes, are the most commonly adopted material for use within building walls. These are often microencapsulated and included within gypsum plasterboard, then used as compartment linings.
- The existing standard fire test methods provide a means of comparing similar products but do not deliver knowledge of how a material would behave in the event of a real fire. It is necessary to be able to quantify the fire performance of these materials to enable their safe usage in the built environment.
- The thermal degradation of the most commonly used substrate material, gypsum plasterboard, is a well understood topic. However, less literature exists on the flammability and the formulation of the material varies widely based on the region, and desired function. Furthermore, these are developed over time and thus do not remain constant.
- There is some very limited knowledge available on the fire behaviour and thermal degradation of PCMs. These studies have confirmed that PCMs are flammable and that their fire behaviour needs to be quantified.
- Some simple tools exist to optimise the energy savings for different PCMs based on thickness, PCM content, melting temperature, and latent heat capacity. This allows potential energy savings to be optimised against quantified fire performance.

3 Thermal degradation framework and determination of thermal transport properties

3.1 Summary

The chemical reactions of each of the innovative materials in this thesis are studied using Thermogravimetric Analysis (TGA) and Differential Scanning Calorimetry (DSC). This also allows qualitative verification of the composition of the materials and identification of pyrolysis and oxidation reactions. Using existing literature, the likely components are identified for each of the above materials and, where possible, comparisons are made those previously studied. The application of this data to bench-scale calorimetry and as part of design guidance is highlighted. In addition, the Transient Plane Source (TPS) technique is evaluated for the determination of fundamental thermal transport properties with respect to fire conditions. Transport properties including thermal conductivity, k, thermal diffusivity, α, volumetric specific heat, C_v, and specific heat capacity, C_p, have been obtained for a PCM (Phase Change Material) enhanced plasterboard product. The accurate determination of these material properties has the potential to more accurately predict the onset of pyrolysis and ignition, as well as heat transfer through wall assemblies.

3.2 Introduction

TGA allows the measurement of sample mass as the specimen is heated in a controlled environment. The mass loss rate allows information on the pyrolysis and oxidation reactions, and some information on the composition of materials. DSC allows measurement of the energy input to the system therefore allowing the enthalpy of reaction to be evaluated under controlled conditions. A detailed discussion of these techniques is given below and results from previous studies of PCM capsules and PCM plasterboards are presented and discussed to allow interpretation of the PCM used in this work.

TPS can be used to adequately determine the thermal properties of materials to complete the characterisation. If an inert solid is assumed for ignition behaviour then ambient condition thermal transport properties can be used to more accurately predict ignition. In combination with the TGA and DSC results this provides part of a method to describe the ignition of the material.

The aim of this chapter is to obtain fundamental material properties to be able to interpret the results when tested at bench-scale. This is achieved by the following objectives:

- Determining of thermal degradation steps of each material;
- Identifying the pyrolysis and oxidation reactions and the temperature at which they occur;
- Evaluating the ability to determine thermal transport properties with respect to fire through use of the TPS technique.

3.3 Literature review

Each of the techniques used in this chapter – TGA, DSC and TPS – are individually reviewed and their assumptions and application are outlined. Relevant thermal properties for PCM microcapsules, PCM plasterboard, and hemp are also reviewed.

3.3.1TGA and DSC

TGA is a macroscopic thermal analysis technique which can be used to determine pyrolysis and oxidation reactions (van Ekeren 1998). Pyrolysis is the chemical process in which volatiles are generated by thermal decomposition (Drysdale 1999). Energy is required to sustain the reaction and thus it is endothermic. Volatile pyrolysate may react with oxygen and combust in the gas phase. Alternatively, chars generated by the pyrolysis process allow oxygen to directly react with the surface and release energy and volatile post-combustion products (Rein 2013).

The process of oxidation is governed by several factors. The rate at which oxygen can reach the surface or flammable air mixture, and the rate at which the volatiles can be produce are both diffusion-controlled (Galwey and Brown 1998). The rate at which pyrolysate can react with oxidiser is kinetics-controlled (Boonmee and Quintiere 2005). Thermogravimetry utilises specific assumptions to identify the chemical reactions.

The first of these assumptions is that there is no thermal gradient present in the system and that the heating rate is sufficiently low that both the diffusion-controlled and kinetics-controlled processes can take place at sufficient rate. Thermal lag will be present in materials where the heat is not able to penetrate to the centre of the specimen, and a thermal gradient is induced. This is often in the case with heavy samples, and more so when the material has highly insulating properties. To avoid this, adequately small sample weights should be used in tandem with relatively slow heating rates.

Buoyancy occurs in TGA due to the displacement of air by the presence of a sample material. This is most notable at low temperatures and causes an apparent increase in the mass recorded. It can be corrected for by measuring the mass of an empty reference crucible, and removing this from the results.

A common method of interpreting TGA data is to take the first derivative, which provides the rate of mass loss (Laye 2002). From this the thermal degradation steps corresponding to the pyrolysis and oxidation reactions of various components can be identified. Furthermore, this illustrates the magnitude of the mass lost due to the reaction. Typically reactions have an onset temperature which is when, for a given heating rate, the reactions will start to initiate. This reaches a peak rate of reactions which corresponds to the maximum decomposition rate. The rate of mass loss then drops as the temperature increases further until the upper temperature point is reached and reactions cease. In the case where multiple reactions occur at once it can be difficult to identify the specify reactions. The use both inert and oxidising environments

can be useful in separating the pyrolysis and oxidation reactions but in complex materials it cannot be guaranteed that the reactions for individual components can be easily identified. To be able to accurately identify the components it is first necessary to conduct a literature review of the likely materials. Then, by comparison of the onset, end and peak temperatures as well as the relative magnitude is should be possible to identify the reactions with some degree of confidence.

DSC is a similar technique which can be conducted at the same time as TGA, but its accuracy will be reduced (Warrington 2002). The technique involves measuring the heat flow to the specimen to maintain the heating rate specified by the user. When an endothermic reaction occurs, the heat flow needs to be increased to overcome this and maintain the heating rate. Typically endothermic reactions correspond to pyrolysis and play a key part in ignition. When an exothermic reaction occurs the heat flow is instead reduced to prevent the temperature from increasing too rapidly. In fire conditions exothermic reactions commonly correspond to oxidation reactions and can infer on the combustion behaviour and when the onset of ignition may be.

3.3.2PCM microcapsules

Thermal analysis of PCM microcapsules is focused almost solely on the characterisation of various combinations which have been synthesised within a laboratory. Manufacturers of commercial products do not willingly share information on the exact composition of their materials and thus far there has been no characterisation of available products in the literature. Furthermore, the thermal analysis is done as part of a characterisation of their performance at ambient conditions. The literature reviewed below has relevance to fire, despite the fact it is intended for ambient thermal characterisation.

3.3.2.1 n-octadecane with polyurea shells

Zhang and Wang (2009) synthesised PCM microcapsules via interfacial polycondensation (see *Literature review* chapter for description of techniques) which had n-octadecane as a core material and amine-modified polyurea shells. The thermal analysis was conducted with a heating rate of $10°C \cdot min^{-1}$ in a nitrogen atmosphere from 50 to 550°C. TGA and DTG was used to analyse the thermal stability of the resulting capsules, as part of a wider study to characterise the synthesised material.

Peaks corresponding to the leakage of n-octadecane occurred in a range of between 183.97 and 217.62°C depending on the amine that was used to modify the polyurea shell. The onset for 10% mass loss was 148.86 to 171.98°C, also dependent upon the amine. The shell then degraded at a higher temperature with an onset of between 200.62 to 232.84°C, and the residual mass was 0.79 to 1.50% by 550°C. The authors concluded that amine modification resulted in lower thermal stability of the PCM. They also found that the decrease in thermal stability was increased when a higher core to shell encapsulation ratio was used.

3.3.2.2 n-octadecane with silica shells

Zhang *et al.* (2011) then synthesised a variety of PCM microcapsules with an n-octadecane core and silica shell via interfacial polycondensation. The thermal analysis was conducted using the same method as Zhang and Wang (2009) above.

The authors identified a thermal degradation step from 130 to 200°C with a peak at 137°C which corresponded to the leakage of n-octadecane from the shells. Dehydration of the silica shell occurred at a higher temperature range of between 280 and 370°C, with a peak at 325°C. Only 5% of the total mass was lost through this dehydration process, despite the fact the shells were 20 to 30% of the total mass of the PCM. With the core n-octadecane completely depleted in a single degradation step, this left 25.6 to 36.2% residual char at 550°C, which is significantly higher than the polyurea shells in the previous study.

3.3.2.3 n-octadecane with MMA-based polymer shells

Qiu *et al.* (2012) similarly synthesised PCM microcapsules containing n-octadecane but instead used different methylmethacrylate (MMA) polymers for the shell material. The method used to synthesis the microcapsules was suspension-like polymerisation. Thermal analysis was conducted at 10°C·min^{-1} in an argon atmosphere from 50 to 500°C for a series of synthesised PCMs as well as 99% pure n-octadecane by itself.

Non-encapsulated n-octadecane was found to degrade from 165 to 277°C. In cases where the shell was crosslinked they found that the onset of octadecane degradation started between 182 and 239°C. The crosslinked shells then had onset degradation temperatures of 349 to 372°C, all of which were higher than the n-octadecane evaporation temperature. The evaporation temperatures of n-octadecane were found to be higher for crosslinked than non-crosslinked shells. It was concluded that this was due to the higher strength of crosslinked shells, which were more capable of resisting the thermal expansion due to the evaporation of n-octadecane. Thus, stronger shells increased the onset temperature for the diffusion of n-octadecane.

3.3.2.4 Paraffin composite with SiO_2 shells

Fang *et al.* (2010) characterised the behaviour of paraffin composites with SiO_2 (silicon dioxide) shells synthesised via the sol-gel technique. This inorganic shell material was chosen because of the flammability and environmental concerns raised through the use of melamine-formaldehyde and urea-formaldehyde shell materials based on a study by Cai *et al.* (2009). Thermal analysis was conducted at 20°C·min^{-1} in a nitrogen atmosphere (20ml·min^{-1} flow) up to 700°C.

The thermal degradation was a two-step process for the synthesised materials. Firstly, dehydration of the water absorbed by the SiO_2 shell occurred from 20 to 80°C. Thereafter, the paraffin chains degraded from 200 to 350°C, with a peak between 288.6 and 292.1°C for encapsulation ratios of 69.1 to 87.5% respectively. Residual mass at 700°C was found to be between 19.65 and 27.61%, again for the respective encapsulation ratios. The authors

suggested that the formation of char reduced heat transfer to the core paraffin wax thereby reducing the rate at which volatile gases could be produced. Furthermore, the build-up of the physical char layer further reduced the rate at which the flammable gases could escape the shells. However, this may be an artefact from using too rapid a heating rate and could be resolved by reducing the rate to within the range of 1 to 5°C·min^{-1}. There is still potential that the char could form an insulating layer which increases the temperature at which the paraffin wax would evaporate.

3.3.2.5 n-eicosane with PMMA shells

Alkan *et al.* (2011) characterised the thermal stability of n-eicosane contained within PMMA (polymethylmethacrylate) shells produced via emulsion polymerisation. Thermal analysis was conducted at a heating rate of 5°C·min^{-1} in a nitrogen atmosphere up to 500°C.

The onset of thermal degradation for non-encapsulated n-eicosane was around 170°C, and the endset was 275°C, which compares closely with the values obtained for n-octadecane by Qiu *et al.* (2012). After microencapsulation the degradation of the microcapsules becomes a three step process up to approximately 420°C. By approximately 200°C the total mass lost is 35% which is the same as the amount of n-eicosane contained within the capsules. This may suggest that the thermal stability of the n-eicosane was not improved through the microencapsulation process. However, the authors do not make comment on this since the aim of the study was to characterise the synthesised material at ambient conditions.

3.3.2.6 Summary

Table 3.1 – Summary of onset, endset and peaks of core and shell materials from the literature. Values are not necessarily directly comparable. All temperatures are in °C.

Source	**Core**			**Shell**			**Char**
-	Onset	Peak	End	Onset	Peak	End	%
n-octadecane/polyurea Zhang and Yang (2009)	148-172	184-217	-	200-232	-	-	0.79-1.5
n-octadecane/silica Zhang *et al.* (2011)	130	175	200	280	325	370	25.6-36.2
n-octadecane/MMA Qiu *et al.* (2012)	182-239, 278-280	-	-	349-372	-	-	-
Paraffin/SiO2 Fang *et al.* (2010)	200	288-292	350	-	-	-	19-27
n-eicosane/PMMA Alkan *et al.* (2011)	170	-	275	200	-	420	-

A summary of some of the PCMs discussed above is given in Table 3.1. It can be seen that for the majority of the materials the onset for the degradation of the core is 200°C or below. Both MMA based shells and SiO_2 shells are successful in increasing the thermal stability of the PCM, thereby increasing the degradation temperature of the paraffin wax contained within. In all cases the paraffin wax was found to degrade at a temperature below that of the shell. In

general, for paraffin materials and alkanes in the range C_{18} to C_{20}, the degradation of core materials starts below 130°C in accordance with the melting point. The degradation of the shell material begins at much higher temperatures, often in excess of 200°C.

The goal of the majority of the available literature has been to characterise the various PCMs. Only the five studies mentioned above have provided data up to temperatures beyond 100°C which would be relevant to fire conditions. However, the goal in doing this has been to provide further characterisation, particularly in evaluating char yield and thermal stability, and not to assess the fire performance. Thus, there has yet to be a thermogravimetric study of PCMs with the specific goal of assessing their fire performance.

3.3.3PCM plasterboard

3.3.3.1 Thermal analysis with respect to fire

Asimakopoulou *et al.* (2015) used TGA and DSC to characterise a modern plasterboard material containing microencapsulated PCM. For the TGA, specimens were tested in an inert helium environment (50ml·min^{-1} flow), heating rates of 5, 50 and 80°C·min^{-1} using aluminium crucibles with pinhole lids. The sample mass was 55mg and tested from 20 to 600°C. The upper heating rates relate to those believed to be representative of a fire (Witkowski *et al.* 2016), whilst the lowest is more suitable for fundamental characterisation of the chemical properties (Haines *et al.* 1998). The high weight of the specimen may induce thermal lag, particularly at the high heating rates. The weight used was identical to that of Wullschleger and Ghazi Wakili (2008) but in other studies lower weights have been used, for example, Manzello *et al.* (2010) tested 10mg specimens.

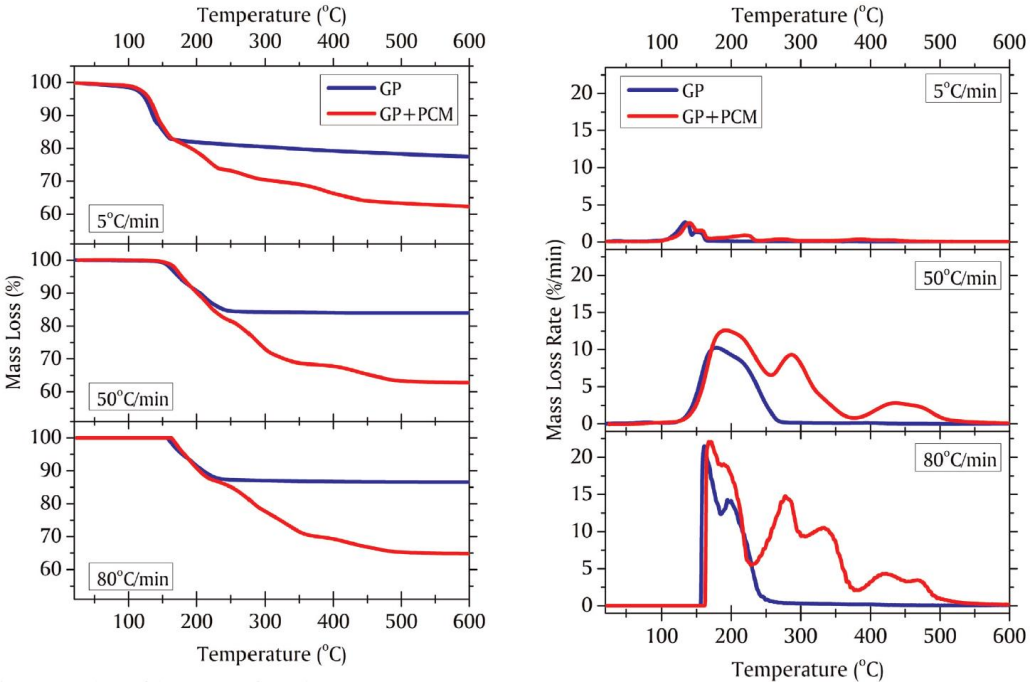

Figure 3.1 – Thermogravimetric results of PCM plasterboard testing at three heating rates showing (a) total mass loss and (b) mass loss rate. Extracted from Asimakopoulou *et al.* (2015).

This identified three thermal degradation steps, as illustrated in Figure 3.1. The first was attributed to the dehydration reactions of the gypsum, in which 18% of the total mass was lost. The next reaction was the evaporation of the paraffin wax from 227 to 347°C resulting in a further 12% mass loss. Finally, the shell melted from 280 to 450°C accounting for another 5% of the mass. From these mass loss steps, the estimated composition of the PCM is 42% shell and 58% core (paraffin wax).

The evaporation of the paraffin wax is notable in that at the highest heating rate, 80°C·min^{-1}, the degradation manifests itself with two peaks. This suggests that the paraffin wax may be a blend and not simply a single alkane. Similarly the decomposition pyrolysis of the shell at higher temperatures had two overlapping reactions, giving two peaks within the listed temperature range. The authors note that the plasterboard was paper faced, but the thermal analysis was focused on the core material.

Images of PCM plasterboard before and after combustion were taken using Scanning Electron Microscope (SEM). The materials were exposed to 75kW·m^{-2} in the cone calorimeter (Figure 3.2). This showed the presence of the microcapsules prior to testing distributed within the gypsum matrix. Only remnants of the capsules were present after testing, and thus it is assumed that the paraffin wax was able to escape to the environment outside of the gypsum and had the potential to react with air. In addition, thermally induced cracks were evident within the gypsum substrate.

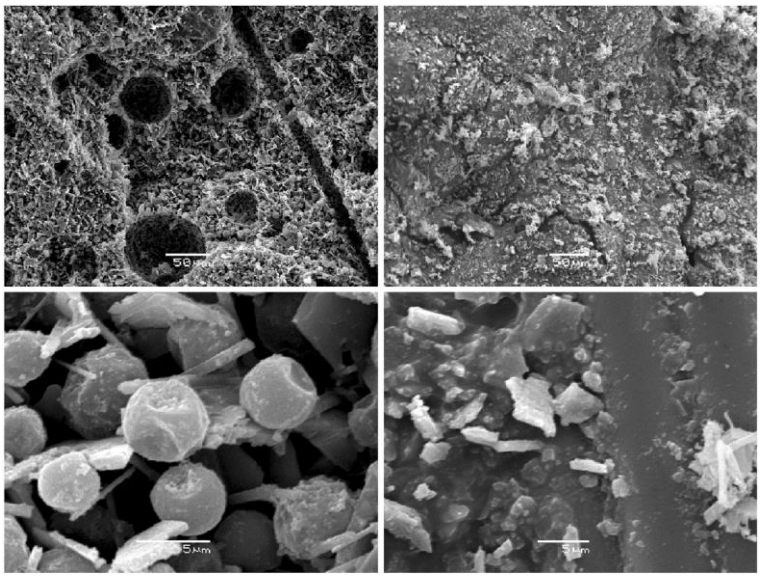

Figure 3.2 – SEM images of PCM plasterboard before (left) and after testing (right) in the cone calorimeter at 75kW·m^{-2}. Extracted from (Asimakopoulou *et al.* 2015).

DSC was also conducted on the same material to identify the composition and the enthalpy of reactions. This was done in nitrogen (200ml·min^{-1} flow) at 2°C·min^{-1} with a specimen weighing 14.11mg. The same temperature range was used as in the TGA experiments. The use of an

inert environment provides understanding of the pyrolysis reactions but is not able to inform on the exothermic oxidation reactions.

The endothermic evaporation of the PCM was found to occur from 204.29 to 251.74°C, with peak decomposition at 231.51°C. From this data the authors identified hexadecane as the closest matching alkane, and used its properties as the input to a fire model. The model used Arrhenius kinetics (Arrhenius 1889) of the form in Eq. 3 to simulate the dehydration and evaporation processes.

$$r_j = A_j \cdot Y_{s,i}^{nj} \cdot e^{\left(-\frac{E_j}{R \cdot T}\right)} \qquad \text{Eq. 3}$$

Where r_j is the rate of reactions, A_j is the pre-exponential factor, Y is the mass fraction of species, n is the order of reactions, E_j is the activation energy, R is the gas constant, and T is the temperature. The kinetic parameters used in the model are summarised in Table 3.2.

Table 3.2 – Chemical kinetics of a PCM plasterboard product. Extracted from Asimakopoulou *et al.* (2015).

Reaction	E_j	A_j	n	H
-	kJ·mol^{-1}	s^{-1}	-	kJ·kg^{-1}
Dehydration reaction 1	148600	$1.164 \cdot 10^{17}$	1	329.79
Dehydration reaction 2	78630	$2.957 \cdot 10^{7}$	1	109.93
Evaporation of hexadecane	40483	$1.408252 \cdot 10^{4}$	1	209.97

3.3.3.2 Thermal stability

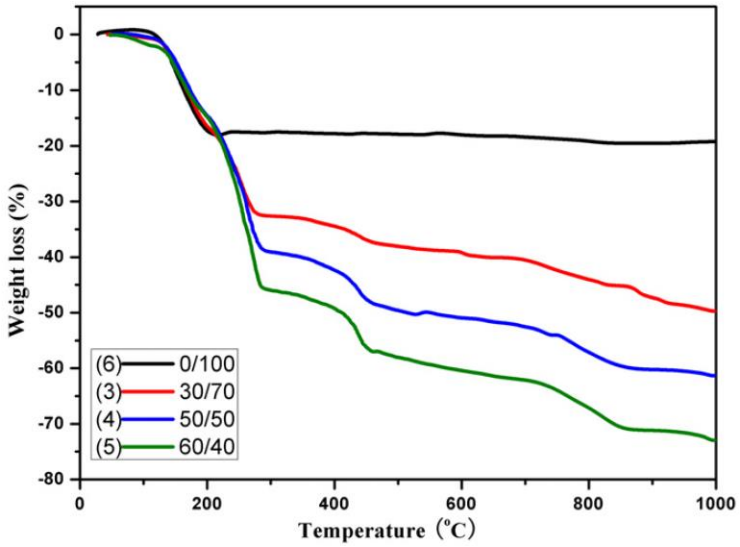

Figure 3.3 - TGA of gypsum board with microcapsules. The ratio in the legend is PCM to gypsum ratio. Extracted from Zhang *et al.* (2012).

Zhang *et al.* (2012) added n-octadecane core with melamine-formaldehyde shell PCMs (Zhang and Wang 2009b) into the matrix of gypsum to form a rigid board. The point of maximum decomposition was found within a range of 258.0 to 269.7°C for encapsulation ratios varying

from 30/70 to 60/40 (PCM/gypsum), as shown above in Figure 3.3). Thus, increasing the amount of PCM increased the point at which maximum decomposition occurred. Outside of the gypsum reactions the PCM was shown to degrade in a three step process. Decomposition up to 300°C was associated with the evaporation of the n-octadecane contained within the microcapsules. Degradation of the shells onset at 400°C, and a further decomposition of the shell occurred from 700 to 870°C.

3.3.4Hemp

Hemp is a natural material which contains a combination of cellulose, hemicellulose, lignin, pectins, and waxes. A comprehensive review of the thermal analysis of natural hemp shivs has previously been conducted (Rachini *et al.* 2009). In this work the constituent components were extracted and analysed by TGA and DSC. This way it was possible to identify the reactions corresponding to each of components, including overlapping and hidden reactions in the TGA data. A table summarising the degradation of the studied hemp fibre is given in Table 3.3 and Table 3.4.

The first reaction is the endothermic dehydration of the hemp as the absorbed water is vaporised. This reaction is evident in both air and argon. Then, under argon, there are a further two steps of degradation. A peak at 260°C corresponds to the simultaneous endothermic decomposition of pectin and hemicellulose. The latter dominants and thus it is only possible to identify if the materials are separated. The second peak is the pyrolysis of the cellulose at 333°C.

In air there are a total of three exothermic reactions. The peak corresponding to the overlapping degradation of pectin and hemicellulose is shifted slightly lower to 253°C. The pyrolysis and oxidation of cellulose is also lowered to 312°C where 51% of the hemp loss occurs. The final peaks at 395 and 427°C then correspond to the exothermic oxidation of the char residue.

The above gives an overall view of the decomposition of the hemp. However, the mechanisms behind two exothermic peaks, at 395 and 427°C, are not given and are instead listed as oxidation of char. To interpret these reactions requires additional literature. The exothermic oxidation of lignin in eucalyptus is listed as 370°C by Kifani-Sahban *et al.* (1996). Kashiwagi and Nambu (1992) undertook a detailed study of cellulose and identified three decomposition reactions. Firstly, the pyrolysis of cellulose was found to occur at 295°C for a heating rate of 1°C·min^{-1}. In air, the oxidation of cellulose was lower at 275°C. Then at 405°C was the oxidation of the char produced by the cellulose. Thus, it is possible that the first of the two reactions is the exothermic oxidation of lignin, and the second is the oxidation of char generated from cellulose.

Table 3.3 – Decomposition of natural hemp and various extracted components in an argon atmosphere. Positive heat flows indicate endothermic reactions, and negative values indicate exothermic reactions. Extracted from (Rachini *et al.* 2009).

Material	**Temperature range /°C**					
	40 to 150		130 to 380		380 to 600	
	Peaks	Weight loss (%)	Peaks	Weight loss (%)	Peaks	Weight loss (%)
Extracted pectins	+107	12.3	+224 +250	71.0 8.5	-	1.5
Extracted cellulose	+87	3.2	+333	61.3	-	8.0
Hemicellulose	-	-	-268†	-	-	-
Lignin	-	-	-365†	-	-	-
Hemp fibre bundles	+92	7.4	-260 -333	11.0 52.0	-	9.0

† from Yang *et al.* (2007)

Table 3.4 – Decomposition of natural hemp and various extracted components in an air atmosphere. Positive heat flows indicate endothermic reactions, and negative values indicate exothermic reactions. Extracted from (Rachini *et al.* 2009).

Material	**Temperature range /°C**					
	40 to 150		130 to 380		380 to 600	
	Peaks	Weight loss (%)	Peaks	Weight loss (%)	Peaks	Weight loss (%)
Extracted pectins	+113	11.8	+235 +277	66.0 15.5	-437	3.4
Extracted cellulose	+88	5.0	-344	75.0	-452	20.0
Hemicellulose	-	-	-265‡	-	-	-
Lignin	-	-	-225‡	-	-370†	27.3
Hemp fibre bundles	+87	7.2	-253 -312	10 51.0	-395 -427	27.3

† from Yang *et al.* (2007)

‡ from Kifani-Sahban *et al.* (1996)

In addition, the chemical kinetics for each of the reactions in cellulose are given in Table 3.5. These show the approximate magnitudes for each of the reactions. The endothermic pyrolysis has the smallest magnitude of the three reactions, and the exothermic nature of the char oxidation reaction dominates.

Table 3.5 – Chemical kinetics for cellulose. Extracted from Kashiwagi and Nambu (1992).

Reaction	E_a	A	n	ΔH
-	$kJ \cdot mol^{-1}$	min^{-1}	-	$J \cdot g^{-1}$
Pyrolysis	220	$1.2x10^{19}$	1.8	570
Oxidation	160	$1.5x10^{14}$	1.3	-5,700
Char oxidation	160	$3.4x10^{11}$	1	-25,000

3.3.5 Thermal transport analysis

Transient Plane Source (TPS) is an experimental technique for determining thermal transport properties using the hot disk apparatus. It is viable method for a wide range of materials and applications, and yields highly accurate results (Gustafsson 1991). A 10μm thick nickel element acts as both the heater and the sensing device, and is sandwiched between two specimens (Figure 3.4). The user chooses an appropriate input power and a constant current is supplied to the element to increase the temperature of the specimen by 1 to 5°K. The change in the electrical resistance of the sensor over time will be heavily influenced by the transport properties of the material which allows the thermal diffusivity and thermal conductivity to be calculated (Log and Gustafsson 1995).

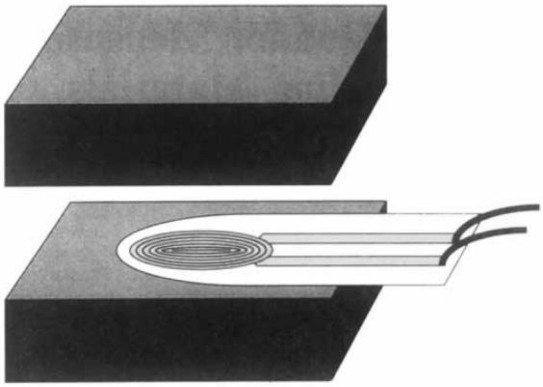

Figure 3.4 - Diagram of the hot disk method incorporating two sandwiched specimens and the nickel coiled sensor wrapped in polymeric material. Extracted from Log and Gustafsson (1995)

For the results to be valid the technique assumes that there are no phase changes at the temperature of data collection. If there is a phase change then the reading will not stabilise and the resulting properties will not be valid. If the material and the sensor are placed in a furnace then the thermal properties over a range of temperatures can be obtained.

The sensor can be either in the shape of a square or a circle, which will modify the heat transfer equations to be able to calculate the properties. These have already been derived for both geometries (Gustafsson 1991). The size of the sensor will determine the depth in which the thermal wave will penetrate. Shallow depths run the risk of capturing localised effects, for example, being excessively influenced by large voids near the sensor. Thus, if the material is deep enough to be considered infinitely thick (29mm for commercial apparatus) then a large

sensor can be used and the properties will be less sensitive to heterogeneity and localised effects.

3.3.5.1 Ordinary plasterboard

The thermal properties of ordinary plasterboard have previously been obtained using the TPS technique by Park *et al.* (2010). The authors applied the technique at ambient temperatures and then used alternate means, namely DSC and a slug calorimeter, to derive the properties at elevated temperatures as opposed to using a furnace. The purpose of deriving the properties was to be able to model the performance of gypsum board in fire. The properties are summarised below in Table 3.6 to be used as a comparison for the properties of PCM plasterboard found in this chapter.

Table 3.6 - Thermal properties for ordinary plasterboard obtained using TPS for thermal conductivity, and DSC for specific heat capacity. Extracted from Park *et al.* (2010).

	With paper facing		**Without paper facing**	
	C_p	k	C_p	k
	$J \cdot g^{-1} \cdot K^{-1}$	$W \cdot m^{-1} \cdot K^{-1}$	$J \cdot g^{-1} \cdot K^{-1}$	$W \cdot m^{-1} \cdot K^{-1}$
Type C (USA)	1017	0.276	852	0.276
Type X (USA)	1089	0.258	947	0.252
Type F (Japan)	963	0.254	1034	0.238
Type R (Japan)	891	0.314	977	0.292

3.3.5.2 PCM plasterboard

Table 3.7 - Thermal properties for PCM plasterboard with varying amounts of microencapsulated PCM. Extracted from Karkri *et al.* (2015).

PCM content	**15°C, PCM in solid state**			**35°C, PCM in liquid state**		
-	C_p	$k^{\dagger}$	$\alpha^{\dagger}$	C_p	k^*	α^*
%	$J \cdot g^{-1} \cdot K^{-1}$	$W \cdot m^{-1} \cdot K^{-1}$	$m^2 \cdot s^{-1}$	$J \cdot g^{-1} \cdot K^{-1}$	$W \cdot m^{-1} \cdot K^{-1}$	$m^2 \cdot s^{-1}$
0	834.65	0.30	4.0	-	0.27	3.9
6.66	914.96	0.27	3.0	724.95	0.24	2.8
13.33	1047.45	0.17	2.3	772.51	0.14	2.2
35.71	1489.11	0.08	1.0	895.63	0.07	0.6

†Estimated from graph data in source.

Increasing the PCM content decreases the estimated thermal diffusivity, from $0.81 mm^2 \cdot s^{-1}$ at 0% PCM content to $0.52 mm^2 \cdot s^{-1}$ at 25% PCM content in concrete. This was obtained using the steady state guarded hot plate method (Haurie *et al.* 2014). A similar effect was noted by Karkri *et al.* (2015) for PCM plasterboard as summarised in Table 3.7. The authors noted that the thermal diffusivity decreased from $4.0 m^2 \cdot s^{-1}$ for ordinary plasterboard down to $1.0 m^2 \cdot s^{-1}$ for 35.71% PCM content. Similarly, the thermal conductivity was also decreased as the PCM content was decreased since the conductivity of the microcapsules is lower than gypsum. The specific heat was increased most notably in the solid state, but in the liquid state the changes were less significant. With respect to fire, the liquid properties are most relevant since this is

the state that the PCM will be in. The increase in specific heat capacity and density but decrease in thermal conductivity mean that the addition of PCMs will not definitely increase or decrease the thermal inertia. Instead, it will be dependent on the exact formulation of the board and needs to be evaluated on a case-by-case basis.

3.4 Experimental approach

The approach used for both TGA/DSC and TPS are outlined below. Some of the underlying assumptions and their implications are also discussed.

3.4.1Thermal analysis

3.4.1.1 Apparatus

All testing was carried out in a Mettler Toledo TGA/DSC 1 apparatus at the University of Edinburgh (Figure 3.5). This equipment is predominantly designed for TGA measurements but is also capable of recording heat flow for DSC. Measurements of TGA and DSC were recorded simultaneously using widely documented techniques (Sanders and Gallagher 2002, 2005).

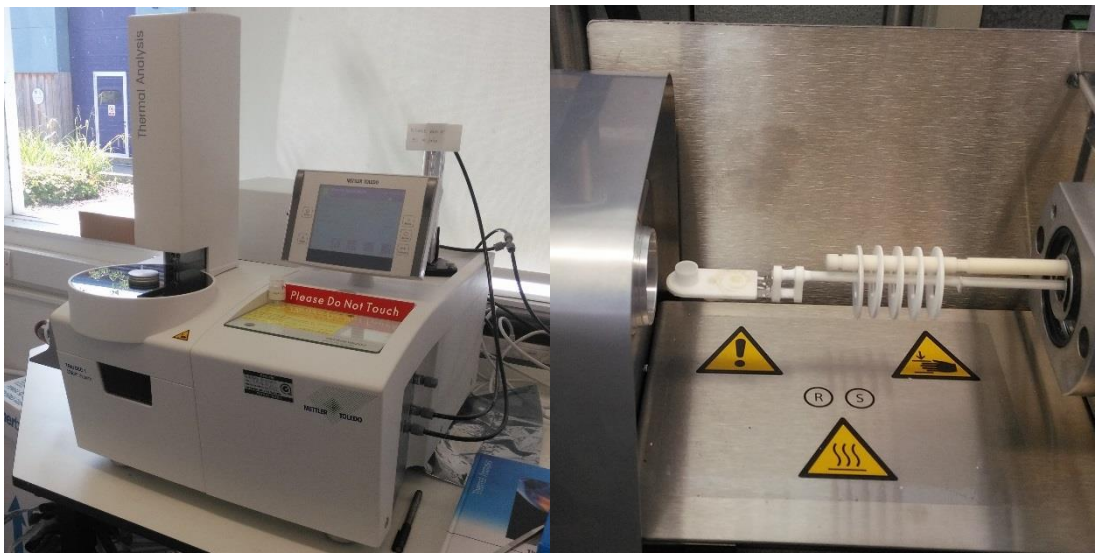

Figure 3.5 – Mettler Toledo TGA/DSC 1 at the University of Edinburgh. (a) Overall view of apparatus (b) view of weighing arm. The furnace is visible to the left of the photo, and the sample crucible is already placed on the arm.

3.4.1.2 Heating rates

All materials were tested at three heating rates which were 1°C·min^{-1}, 2.5°C·min^{-1} and 5°C·min^{-1}. These rates were chosen despite the fact heating rates in a fire are typically extremely high, with estimates of up to 100°C·min^{-1} (Witkowski *et al.* 2016). The decision was taken to instead use low heating rates to ensure no temperature gradients would be present within the sample, which is a key requirement for TGA (Gallagher 1998). Final tests were conducted at a heating rate of 20°C·min^{-1} up to 900°C to confirm that the general trends were still representative at higher heating rates.

3.4.1.3 Atmosphere

All tests were carried out in both air and nitrogen atmospheres to identify and evaluate the pyrolysis and oxidation reactions for each material. Gas flow was set to 50ml·min^{-1} in each case. DSC results were predominantly only available in air due to limitations with the apparatus.

3.4.1.4 Sample size

The sample mass for each material tested is given in Table 3.8. All samples had a minimum of six repetitions, with the exception of PCM hemp fibre at 1°C·min^{-1} which had two repetitions.

The mass of each sample was selected based on the minimum required to ensure sufficient resolution of the microbalance and to ensure that the signal to noise ratio was sufficiently low. This is often found to be the case with commercial materials, particularly those which are heterogeneous (Haines *et al.* 1998).

Table 3.8 – Summary of the average mass and standard deviations for each material.

Material	**Weight /mg**		
-	5°C·min^{-1}	2.5°C·min^{-1}	1°C·min^{-1}
PCM capsules	0.40±0.13	22.5±2.64	14.8±2.37
PCM plasterboard	9.59±1.81	12.2±5.27	10.59±4.65
Hemp shiv	0.67±0.17	1.56±0.30	1.33±0.22
PCM hemp fibre	-	5.38±2.83	5.25±4.39[†]

[†] Only in air

3.4.1.5 Specimen preparation

For all materials the specimens were prepared by cutting or placing a piece of material in the crucible. No materials were ground since this was found to damage the specimen and specific components were destroyed, thus removing the ability to evaluate their thermal degradation. For example, in PCM microcapsules some of the shell and paraffin wax were lost, which decreased the accuracy and certainty of the results.

For clarity, the specific preparation for each material is given below:

- PCM microcapsules – placed directly in crucible without tamping or grinding.
- PCM plasterboard – approximately cubic shaped samples were cut from the centre of the material using a clean knife. The bottom side was always flat to ensure good contact with the bottom of the crucible. Grinding or other methods of obtaining powder were not used because although similar results were obtained smaller yields of PCM were found. This suggests that some PCM was destroyed in the preparation process, and is not representative of the material. All specimens were taken from the centre.
- Hemp – an entire hemp shiv was placed in the crucible, ensuring good contact with the bottom of the crucible. Shivs of various dimensions and appearances were all

tested and the results averaged to ensure results are representative of the real material.

- HempPCM – shivs from the exterior of cast specimens were tested. Samples were visually inspected prior to testing to ensure good coverage of PCM and cement binder on the hemp fibre.

3.4.1.6 Crucibles

Alumina (*aluminium oxide*) crucibles with a volume of 70µl were used in all tests. No lids were used. Each individual heating rate and atmosphere was run using a different reference crucible. For each case, there was a minimum of one reference crucible per three samples and these were always run immediately prior to the samples. The heat flow and change in mass due to buoyancy are eliminated by subtracting the results of the reference crucible to obtain the sample behaviour.

Typically aluminium crucibles are used for pure DSC due to their very high thermal conductivities which ensure no thermal gradients. TGA and DSC results were recorded simultaneously and instead alumina crucibles were used since TGA was the primary goal of the experiments. This reduces the accuracy of the DSC results but they still provide a useful qualitative insight into the material.

3.4.2Transient Plane Source

The apparatus used was a Thermal Constants Analyser TPS 1500 (Figure 3.6) produced by Hot Disk AB (Gothenburg, Sweden). All experiments were performed at the University of Queensland. The determination of properties has been conducted in accordance with ISO 22007-2 (British Standards Institution 2015b).

The choice of sensor and the appropriate input power was first estimated then refined through testing (He 2005). A total of twenty three tests were conducted with four different Kapton material sensors ranging from 3.189 to 14.61mm radius.

Due to the solid to liquid phase transition of the paraffin wax at room temperature it was necessary to record values outside this range. Tests were conducted at 18°C when the wax was solid and then again at 26°C when the phase transition was complete and the wax was in liquid form. Between these two points the phase change occurred and the results were found not to be valid.

For liquid state tests the results are based on three repetitions using 3.189mm radius Kapton sensor and measurement times of 40 to 80 seconds. For solid state tests the results were based on four repetitions, half of which used a 3.189mm radius Kapton sensor, and the other half 9.868mm radius Kapton sensors.

The volumetric specific heat was calculated using the hot disk apparatus, and the density of specimens were measured separately using a load cell and callipers. Ideally the volumetric

specific heat should be measured using an alternative technique (He 2005), such as DSC, and then input into the TPS calculations to increase the accuracy of the measurements.

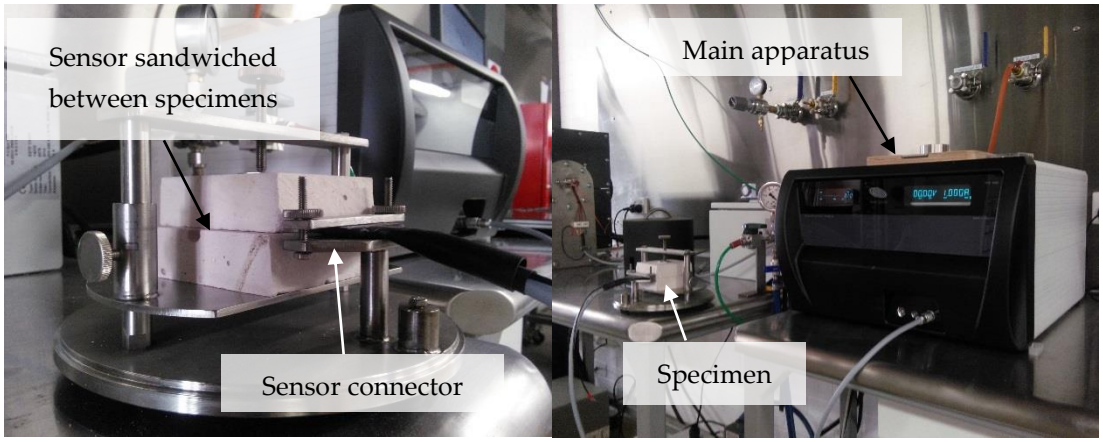

Figure 3.6 - Photographs of the Transient Plane Source apparatus at the University of Queensland, Australia. (a) PCM enhanced plasterboard with sensor in place (b) overview showing main apparatus with furnace in background.

3.5 TGA/DSC results and discussion

A complete analysis of all the materials – PCM microcapsules, PCM enhanced plasterboard, hemp shivs, and PCM enhanced hemp-lime – is presented. The thermal degradation steps in both nitrogen in air, as well material composition are given for each. For the sake of simplicity, values are quoted at 1°C·min^{-1} unless otherwise noted.

3.5.1PCM microcapsules

3.5.1.1 TGA

Figure 3.7 and Figure 3.8 show the TGA and DTG data respectively for PCM microcapsules in air and nitrogen. A four step thermal degradation process has been identified in air, and three steps in nitrogen. The first reaction between 114 and 189°C in air corresponds to the evaporation of free paraffin wax which was not properly encapsulated. This is also apparent in nitrogen, but has been lumped together with the second reaction since they overlap. This evaporation is due to inevitable imperfections in the manufacturing process where the paraffin wax is either not encapsulated, or the shell is damaged and the wax is able to escape. For a commercially obtained product the amount of free paraffin which is available is expected to be lower due to the higher quality manufacturing when compared to laboratory synthesised PCM. The loss of this wax corresponds to 18% of the total paraffin within the product. When the wax evaporates the temperature is not sufficiently high to combust, and instead the reaction is endothermic, relying on heat to convert the material from its liquid state to gaseous form.

In nitrogen, the second reaction from approximately 189 to 270°C corresponds to the endothermic evaporation of paraffin wax contained within capsules. It is hypothesised that

the capsule fails as the paraffin wax changes phase from liquid to gas, and rapidly expands in the process. This hypothesise is echoed in the literature (Fang *et al.* 2010, Zhang, Wang, *et al.* 2010, Zhang *et al.* 2011, Qiu *et al.* 2012, Asimakopoulou *et al.* 2015). In air, the paraffin wax is at sufficient temperature to autoignite upon exposure to the oxygen within the air atmosphere, and thus the mass loss is substantially more rapid (within the range 189 to 250°C). For both nitrogen and air this evaporation process represents the most rapid decomposition.

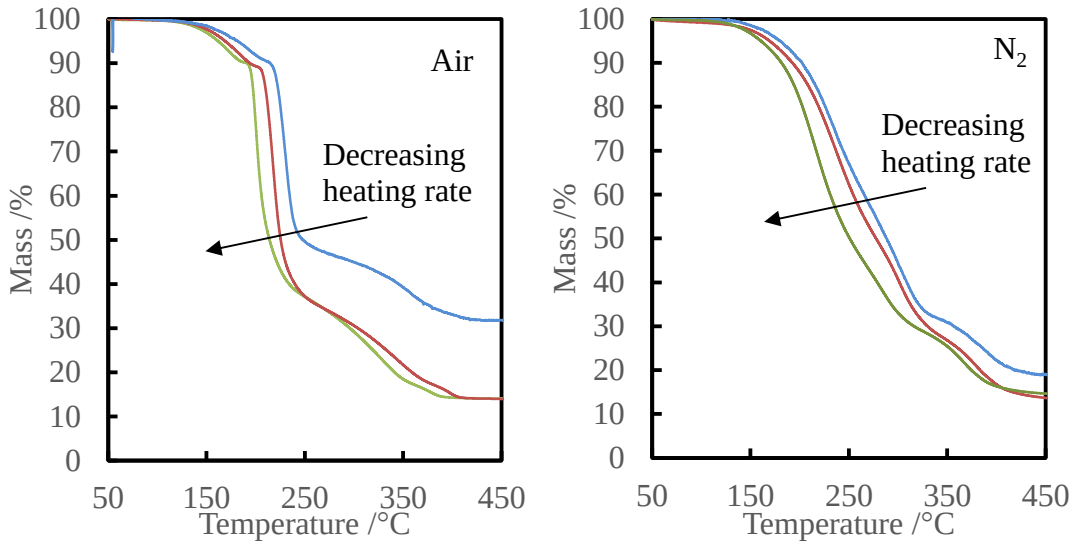

Figure 3.7 - TGA of PCM capsules in (a) air and (b) N_2. The blue, red and green lines correspond to heating rates of 5, 2.5 and 1°C·min^{-1} respectively where a minimum of three tests have been averaged. Maximum error is 0.93%, which is not visible. Note that at 5°C·min^{-1} smaller specimens were used.

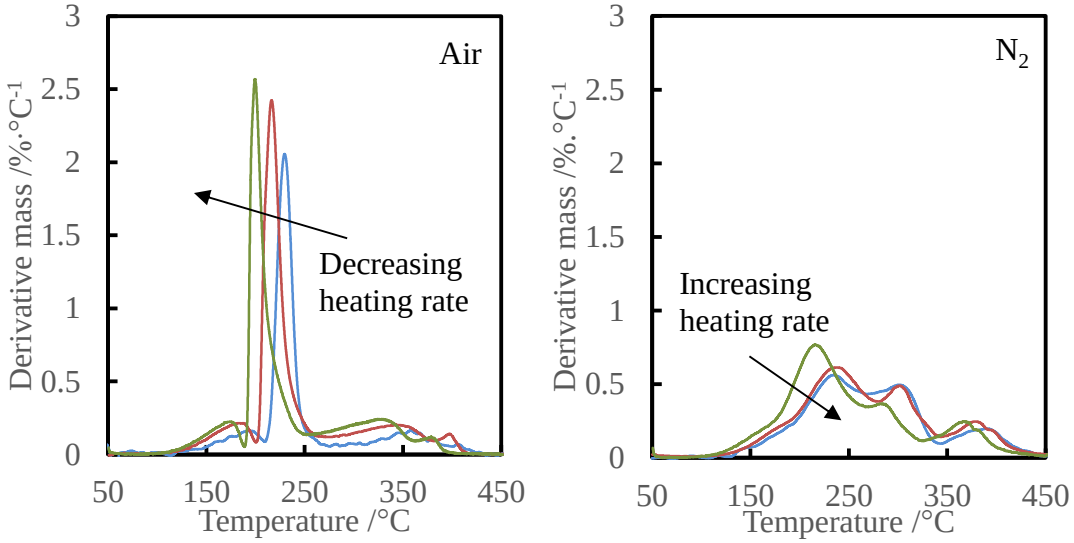

Figure 3.8 - DTG of PCM capsules in (a) air and (b) N_2. The blue, red and green lines correspond to heating rates of 5, 2.5 and 1°C·min^{-1} respectively where a minimum of three tests have been averaged. Maximum error is 0.93%, which is not visible. Note that at 5°C·min^{-1} smaller specimens were used.

The third and fourth reactions which occur at higher temperatures are attributed to the degradation of the acrylic polymer shell. This occurs in two separate steps in both nitrogen and air but the precise mechanisms are not known due to the lack of information on the composition of the shell. In both atmospheres comparatively similar mass is lost, but in air this occurs over a much longer and shallower range than in nitrogen (peak of 0.24%·°C^{-1} in air compared to 0.37%·°C^{-1}). The full temperature range of both steps in air is 254 to 400°C. A summary of all the reactions can be found in Table 3.9 and Table 3.10 for each respective atmosphere.

At the end of the test there was 14.3±0.2%, 13.78±0.39% and 31.82±13.8% mass remaining in air for respective heating rates of 1°C·min^{-1}, 2.5°C·min^{-1} and 5°C·min^{-1}. This was a combination of ash and inorganic remnants of the shell. In nitrogen there was 15.03±0.04%, 13.69±0.22%, 19.04±1.74% mass remaining for the same heating rates as above, which suggests that there was a minor char yield of up to 0.70% (at 1°C·min^{-1}), which oxidises in an air atmosphere. Whilst only accounting for a small amount of the material, this explains the change in colour of the shell when tested in nitrogen (black) compared to air (white).

Table 3.9 – Thermal degradation steps of PCM in air (50ml·min^{-1}) for three heating rates.

Reaction	**Heating rate**	**Onset**	**Peak**	**Endset**	**Peak magnitude**	**Mass lost**
-	°C·min^{-1}	°C	°C	°C	%·°C^{-1}	%
First	5	117.13 ±8.06	193.78 ±2.72	208.58 ±0.70	0.1838 ±0.0491	10.2 ±2.1
	2.5	122.91 ±3.69	187.34 ±3.90	200.64 ±1.16	0.1976 ±0.0330	10.3 ±0.7
	1	114.03 ±0.64	173.73 ±1.20	188.82 ±0.05	0.2255 ±0.0029	9.83 ±0.09
Second	5	208.58 ±0.70	229.86 ±0.23	283.05 ±6.81	2.1213 ±0.3181	44.6 ±7.8
	2.5	200.64 ±1.16	217.03 ±0.81	275.90 ±2.89	2.2693 ±0.6239	56.3 ±1.38
	1	188.82 ±0.05	199.37 ±0.32	254.39 ±2.21	2.5637 ±0.1687	53.6 ±0.3
Third	5	283.05 ±6.81	356.50 ±1.57	434.70 ±3.13	0.1815 ±0.0353	14.4 ±3.2
	2.5	275.90 ±2.89	339.23 ±12.90	380.27 ±1.28	0.1989 ±0.0150	16.3 ±0.7
	1	254.39 ±2.21	327.64 ±1.65	362.38 ±0.04	0.2423 ±0.0041	19.4 ±0.3
Fourth	2.5	380.27 ±1.28	399.04 ±1.95	429.73 ±0.03	0.1248 ±0.0394	3.43 ±0.45
	1	362.38 ±0.04	378.72 ±0.06	399.54 ±2.62	0.1193 ±0.0024	2.83 ±0.11

Remaining mass: 14.3±0.2% (1°C·min^{-1}), 13.78±0.39% (2.5°C·min^{-1}), and 31.82±13.8% (5°C·min^{-1}). All at 450°C.

Table 3.10 – Thermal degradation steps of PCM in nitrogen (50ml·min^{-1}) for three different heating rates.

Reaction	**Heating rate**	**Onset**	**Peak**	**Endset**	**Peak magnitude**	**Mass lost**
-	°C·min^{-1}	°C	°C	°C	%·°C^{-1}	%
First and second	5	139.22 ±3.53	233.50 ±0.85	272.00 ±4.30	0.5610 ±0.0164	42.74 ±2.96
	2.5	141.99 ±1.96	238.17 ±3.41	280.39 ±1.54	0.6156 ±0.0087	51.04 ±0.40
	1	133.82 ±1.50	216.50 ±1.68	269.57 ±2.22	0.7689 ±0.0024	56.79 ±0.80
Third	5	272.00 ±4.30	301.27 ±1.08	343.85 ±0.04	0.4962 ±0.0046	25.86 ±1.93
	2.5	280.39 ±1.54	301.75 ±0.45	343.50 ±0.98	0.4909 ±0.0118	21.23 ±0.21
	1	269.57 ±2.22	282.36 ±0.47	325.87 ±0.83	0.3675 ±0.0147	14.41 ±0.97
Fourth	5	343.85 ±0.04	389.60 ±3.61	441.29 ±2.08	0.2030 ±0.0072	12.35 ±0.55
	2.5	343.50 ±0.98	377.78 ±0.49	449.20 ±0.41	0.2464 ±0.0008	14.04 ±0.18
	1	325.87 ±0.83	367.50 ±0.07	429.90 ±3.54	0.2475 ±0.0021	13.77 ±0.25

Remaining mass: 15.03±0.04% (1°C·min^{-1}), 13.69±0.22% (2.5°C·min^{-1}), and 19.04±1.74% (5°C·min^{-1}). All at 450°C.

3.5.1.2 DSC

DSC data in Figure 3.9 confirms the existence of an exothermic oxidation peak at the same point as the evaporation of the paraffin wax (182 to 220°C, with a peak at 199°C). The free paraffin wax which has evaporated prior to this point does not generate energy, potentially because the temperature is not above the autoignition temperature of the wax, which is estimated to be in the region of 215°C to 235°C corresponding to hexadecane and octadecane respectively. Exothermic oxidation corresponding to the degradation of the shell occurs over a series of peaks between 225 and 400°C. The peak magnitude is substantially lower (0.5W·g^{-1} compared to 4.2W·g^{-1} for the wax) but because the reaction occurs over a much larger range this still represents a significant portion of energy.

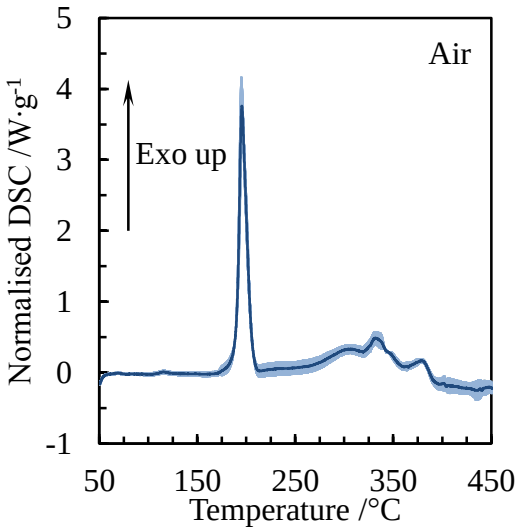

Figure 3.9 – Normalised DSC of PCM capsules in air at 1°C·min^{-1}. Positive values of the ordinate relate to exothermic reactions.

3.5.1.3 Material composition

The material composition, constructed from analysis of the TGA data, is given in Table 3.11 on a mass basis. The capsules contain approximately 65.0±1.2% paraffin wax by mass, and the remaining 35.0±1.1% accounts for the shell. This represents a significantly higher encapsulation ratio than Alkan *et al.* (2011) managed through lab synthesis of n-eicosane/PMMA, which was 30% wax. It is however relatively similar to the microcapsules contained within the commercial PCM plasterboard tested by Asimakopoulou *et al.* (2015). Their results indicated an encapsulation ratio of 58:42 for wax to shell. Thus, the microcapsules in this research agree well with the other commercially available PCMs which have been tested and have significantly higher encapsulation ratios than lab synthesised capsules due to the superior manufacturing methods.

Table 3.11 – Estimated composition of PCM capsules based on 1 and 2.5°C·min^{-1} heating rates.

Material	**Core**	**Shell**	
		Organic	Inorganic/ash
PCM capsules	65.0±1.2%	21.0±0.8%	14.0±0.3%

The pyrolysis temperature of the wax is in line with shells containing octadecane (Zhang and Wang 2009a, Zhang *et al.* 2011) and n-eicosane (Alkan *et al.* 2011). However, each PCM in the literature has different shell properties and this clearly has an effect on the temperature and conditions required for the paraffin wax to be able to escape. This is particularly true where the degradation of the shell overlaps with the pyrolysis of the wax. For this material the wax and shell pyrolysis processes are distinct, and no degradation of the shell occurs before the wax has finished pyrolysing.

The degradation of the shell occurs over a range similar to that found for PMMA as presented previously in
(Alkan *et al.* 2011). However, for the microcapsules in this research there was 14.0±0.3% mass remaining where PMMA is a non-charring material and has negligible amounts of mass remaining. Shells formed of SiO2 had large residual char amounts in the range of 19 to 36.2% (Fang *et al.* 2010, Zhang *et al.* 2011). The dehydration of silica found by Zhang *et al.* (2011) occurred over a similar range and had a peak with 2°C of the first degradation reaction found in this research. However, there was not the second reaction of the shell and thus the materials are different.

In summary, the core of the PCM microcapsule shows strong agreement with long chain paraffin waxes such as octadecane, hexadecane, and eicosane. Previously obtained information from the manufacturer indicated that the core is composed of a blend of hexadecane and octadecane which agrees well with the thermal analysis. The behaviour of the shell is similar to both PMMA and silica, but not identical to either. Its exact composition cannot be identified but the pyrolysis and oxidation reactions have been identified, which are the key component for interpreting flammability results. In addition, estimated encapsulation ratios have been found.

3.5.2PCM plasterboard

3.5.2.1 TGA

The combination of plasterboard, which has at least three degradation steps, and PCM capsules, which have up to four steps, results in a complex material degradation pathway. In air, there are three major steps, with an additional three steps which are less significant in terms of mass lost which have been summarised in Table 3.12 and Table 3.13. The major steps are the endothermic dehydration of the gypsum (assumed to be one step, approximately 82 to 130°C), the exothermic oxidation of the paraffin wax (190 to 222°C in air), and the decomposition of calcium carbonate (574 to 729°C). The minor steps are the leakage of paraffin wax (153 to 210°C at 5°C·min^{-1}), the degradation of the polymer shell (also assumed to be one step, 222 to 401°C), and an unknown decomposition which may be an additive in the gypsum (487 to 566°C at 5°C·min^{-1}).

The evaporation of the paraffin wax in nitrogen is over a larger range as was also seen in the PCM capsule TGA results previously. This may due to the fact that once the paraffin wax can escape the capsule it immediately reacts with oxygen, and the mass is more rapidly lost. In nitrogen, the process is pure evaporation. The gypsum degradation steps are the same in both nitrogen and air, illustrating the fact that these reactions are endothermic and do not require oxygen. As such, only the PCM accounts for exothermic heat release.

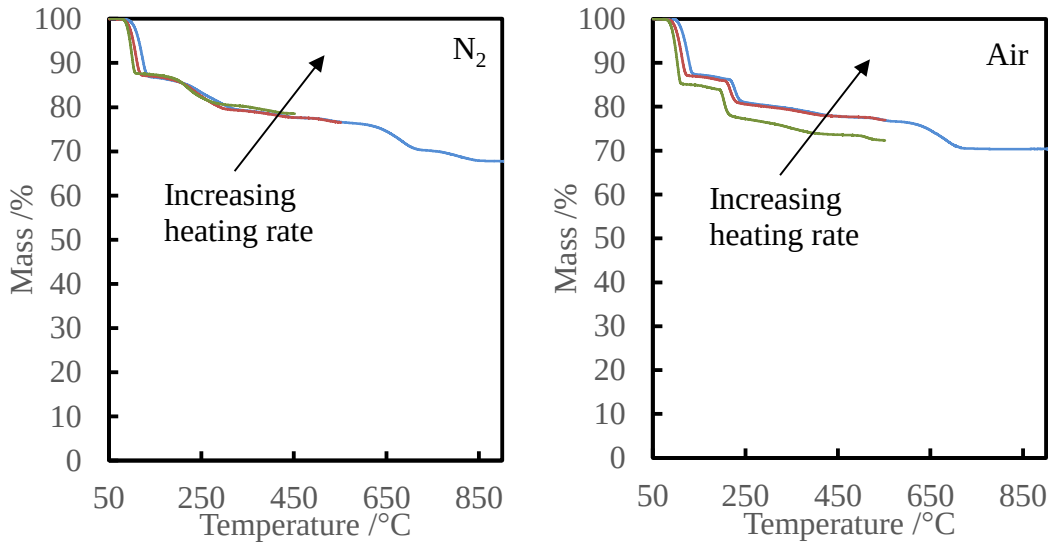

Figure 3.10 - Normalised TGA of PCM plasterboard (a) N_2 and (b) air. The blue, red and green lines correspond to heating rates of 5, 2.5 and 1°C·min^{-1} respectively where a minimum of three tests have been averaged.

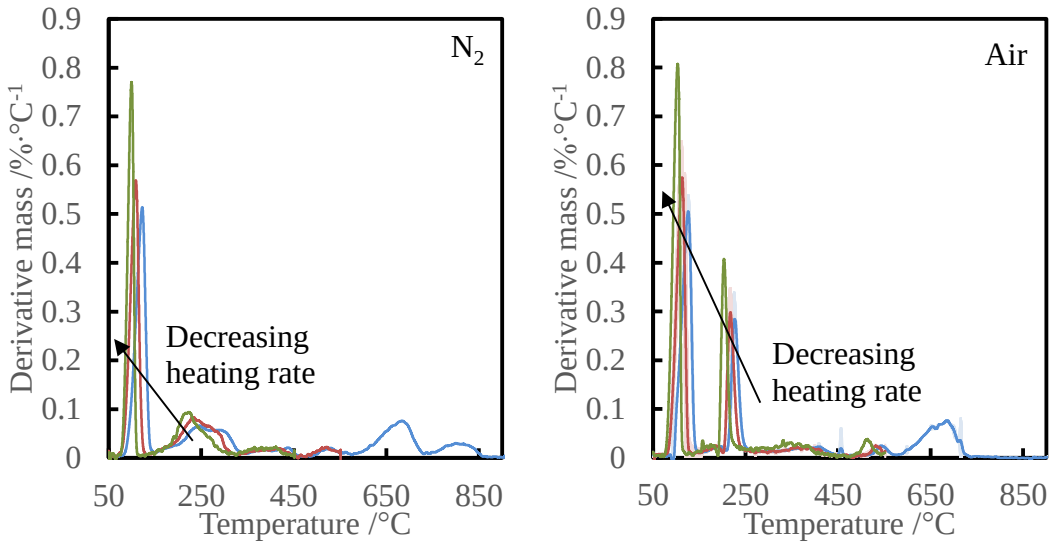

Figure 3.11 - DTG of PCM plasterboard in (a) N_2 and (b) air. The blue, red and green lines correspond to heating rates of 5, 2.5 and 1°C·min^{-1} respectively where a minimum of three tests have been averaged.

In nitrogen there is an additional step from 734 to 859°C (at 5°C·min^{-1}) which is not present in air. The existence of this step decreases the amount of mass remaining at the end of the experiment, and thus the residual mass is higher in air than in nitrogen. It is assumed that for one of the components the chemical pathways are different in air than in nitrogen. In air it is assumed that the component will combust at some point before 734°C and thus the material is consumed. In nitrogen the material there is no exothermic reaction and thus the component remains and is free to react at high temperatures. The PCM microcapsules were tested up to 900°C but had no mass loss beyond 450°C and can thus be ruled out as the cause. None of the existing plasterboard literature show this degradation step. However, the majority of the

plasterboard in the literature contains a paper facing where the plasterboard in this study does not, and instead has interwoven glass fibres. Whilst it cannot be certain, these interwoven glass fibres or another unspecified additive may be the source of the final degradation step in nitrogen.

Table 3.12 – Thermal degradation steps of PCM plasterboard in air (50ml·min^{-1}) for three different heating rates.

Reaction	**Heating rate**	**Onset**	**Peak**	**End**	**Peak magnitude**	**Mass lost**
-	°C·min^{-1}	°C	°C	°C	%·°C^{-1}	%
First	5	96.57 ±0.54	126.67 ±0.75	152.82 ±0.34	0.5273 ±0.0474	13.09 ±0.28
	2.5	88.09 ±0.30	114.06 ±2.86	129.68 ±7.04	0.6000 ±0.0410	12.97 ±0.04
	1	82.01 ±0.88	103.15 ±0.21	116.75 ±1.75	0.7983 ±0.4103	14.85 ±7.20
Second	5	152.82 ±0.34	191.83 ±0.34	210.26 ±1.00	0.0235 ±0.0025	1.00 ±0.07
Third	5	210.26 ±1.00	227.16 ±2.07	261.62 ±0.42	0.2938 ±0.0498	5.87 ±1.06
	2.5	202.95 ±0.36	217.15 ±0.08	238.11 ±0.69	0.3083 ±0.0175	5.15 ±0.12
	1	190.07 ±0.88	203.19 ±0.36	222.37 ±0.83	0.3987 ±0.2058	6.16 ±3.18
Fourth	5	297.74 ±22.13	394.85 ±24.09	449.782 ±3.83	0.0235 ±0.0041	2.37 ±0.41
	2.5	238.11 ±0.69	367.44 ±11.01	430.53 ±0.71	0.0250 ±0.0023	2.89 ±0.23
	1	222.37 ±0.83	340.04 ±12.23	401.44 ±1.26	0.3341 ±0.0178	3.88 ±1.70
Fifth	5	492.06 ±4.32	544.00 ±1.91	577.04 ±0.64	0.0256 ±0.0014	0.95 ±0.04
	2.5	514.77 ±0.79	531.72 ±2.63	*550+*	0.0260 ±0.0036	0.58 ±0.01
Sixth	5	577.04 ±0.64	685.58 ±0.74	724.50 ±1.48	0.0778 ±0.0031	5.92 ±0.08

Remaining mass: 73.94±12.46 (1°C·min^{-1}, 550°C), 76.97±0.22% (2.5°C·min^{-1}, 550°C), and 70.61±0.29% (6°C·min^{-1}, 900°C).

Table 3.13 – Thermal degradation steps of PCM enhanced plasterboard in nitrogen (50ml·min^{-1}) for three different heating rates.

Reaction	**Heating rate**	**Onset**	**Peak**	**End**	**Peak magnitude**	**Mass lost**
-	°C·min^{-1}	°C	°C	°C	%·°C^{-1}	%
First	5	93.13 ±2.41	123.06 ±3.07	149.81 ±3.63	0.5273 ±0.0617	13.28 ±0.07
	2.5	85.53 ±2.77	112.50 ±6.49	140.64 ±6.10	0.5458 ±0.0832	13.06 ±0.18
	1	82.03 ±0.93	101.67 ±4.15	130.05 ±2.69	0.7202 ±0.1060	12.65 ±0.36
Second	5	149.81 ±3.63	244.24 ±0.76	350.10 ±0.89	0.0665 ±0.0063	7.52 ±0.44
	2.5	140.64 ±6.10	232.37 ±0.99	330.43 ±1.77	0.0837 ±0.0004	7.79 ±0.07
	1	130.05 ±2.69	222.33 ±0.64	319.75 ±10.32	0.0974 ±0.0106	7.29 ±0.47
Third	5	350.10 ±0.89	437.16 ±1.39	471.94 ±12.79	0.0216 ±0.0009	1.65 ±0.11
	2.5	330.43 ±1.77	421.23 ±3.52	469.05 ±8.69	0.0203 ±0.0009	1.70 ±0.07
	1	319.75 ±10.32	379.33 ±12.82	443.32 ±8.50	0.0271 ±0.0072	1.79 ±0.47
Fourth	5	471.94 ±12.79	531.11 ±5.12	571.12 ±6.49	0.0213 ±0.0009	1.11 ±0.13
	2.5	469.05 ±8.69	519.08 ±2.31	551.17 ±0.30	0.0216 ±0.0026	1.03 ±0.10
Fifth	5	571.12 ±6.49	686.58 ±6.67	734.25 ±7.04	0.0774 ±0.0049	6.12 ±0.11
Sixth	5	734.25 ±7.04	816.85 ±17.18	858.55 ±7.21	0.0320 ±0.0035	2.40 ±0.39

Remaining mass: 78.27±0.57% (1°C·min^{-1}, 450°C), 76.42±0.21% (2.5°C·min^{-1}, 550°C), and 67.85±0.70% (5°C·min^{-1}, 900°C).

3.5.2.2 DSC

The DSC illustrates that the endothermic nature of the dehydration reactions from approximately 83 to 119°C, with a magnitude of –0.36±0.03 W·g^{-1} (Figure 3.12). DSC values are normalised to the total mass of the specimen. The resolution is not sufficient to be able to identify the two dehydration peaks individually, and instead they appear as a single lumped reaction. An exothermic peak is present for the degradation step which is associated with the oxidation of the paraffin wax between 189 and 221°C with a magnitude of 0.48±0.02 W·g^{-1}. Despite the fact the paraffin wax accounts for less of the total mass (5.51±0.59%) than water (13.01±0.19%) the magnitude of heat flow is greater. This shows that the energy released on a per mass basis for the paraffin wax is around 3.14 times more exothermic than the water is

endothermic. Thus, the dehydration effect of the water in the gypsum will be partially negated by the energy released by the PCM, thereby reducing its effectiveness as a fire resisting material when the temperature increases. At higher temperatures, above 250-300°C, the disadvantages of using alumina crucibles for DSC, which have relatively low thermal conductivity, as opposed to normal aluminium crucibles becomes apparent. Within this range it is not possible to identify endothermic or exothermic reactions from the baseline.

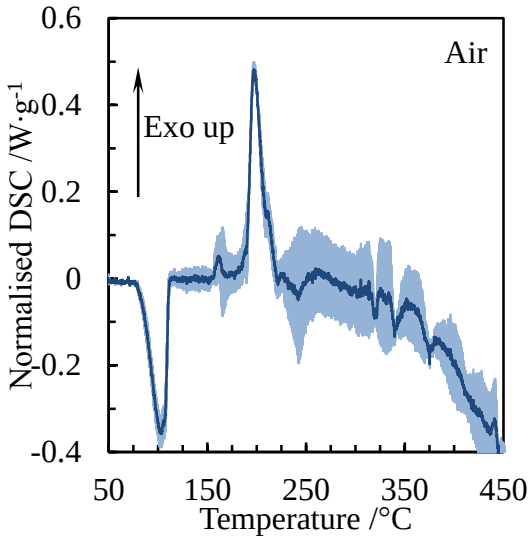

Figure 3.12 – Normalised DSC of PCM plasterboard at a heating rate of 1°C·min^{-1} in air. The shaded area indicates error between tests. Exothermic reactions yield positive ordinate results.

The exothermic oxidation of the paraffin wax agrees well between the microcapsules and the PCM plasterboard. Both have peaks at 199°C, although the endset for the exothermic reaction is earlier at 220°C compared to 254°C in DTG. This may partially be due to pyrolysis or thermal degradation of the shell between 220 and 254°C. A similar effect is noted in the degradation of the polymer shell, where both peaks fall within the error margin of the results. This suggests that the thermal stability of the plasterboard is not reduced by the inclusion of PCMs.

3.5.2.3 Material composition

The amount of water lost due to the dehydration reactions was 13.01±0.19%, compared to the oft quoted 21% for ordinary plasterboard (Wullschleger and Ghazi Wakili 2008) or 18% for one type of PCM plasterboard (Asimakopoulou *et al.* 2015). PCM plasterboard synthesised using dipping as opposed to microcapsules had a crystallised water content of 5.5% (Banu, Feldman, Haghighat, *et al.* 1998), but this technique is no longer used. The 38% reduction in water content compared to ordinary plasterboard will have a marked effect on the fire performance, which is reliant on the endothermic dehydration reactions to inhibit fire spread.

The total amount of PCM within the plasterboard is found to be 9.44±1.10%, of which 68.99±6.99% corresponds to the wax and 31.01±2.62% to the shell. This in-line with the previously calculated encapsulation ratio for the microcapsules which suggests the

formulation and wax content is similar when contained within plasterboard. Furthermore, loss of paraffin wax due to the breakage of shells is not excessive even when added into the plasterboard.

The residual mass of the material is 77.22±0.33%, which is a combination of the gypsum which can be rehydrated, and ash from the PCM. There may also be other additives remaining in the material which do not pyrolyse or combust. A summary of the estimated composition can be found in Table 3.14.

Table 3.14 – Estimated composition of PCM plasterboard based on all heating rates and environments.

Material	**Water**	**PCM**		**Gypsum, additives, ash**
		Core	Shell	
PCM plasterboard	13.01±0.19%	6.51±0.66%	2.93±0.55%	77.22±0.33%

The amount of PCM normalised to unit area is found to be 2.12kg·m^{-2} compared to 1.99kg·m^{-2} in the literature (Kolaitis *et al.* 2013). This is the method commonly employed in describing the loading of a PCM when designing for ambient conditions. Thus, the PCM plasterboard in this study shows a similar loading to the literature when expressed in this manner. However, because the thickness of the material is higher (25mm compared to 15.2mm) this means that the density of PCM is only 85kg·m^{-3} compared to 131kg·m^{-3} in the literature. As a result, this is expected to influence the fire performance in ways such as higher critical heat flux, longer ignition times, and lower heat release rates.

In other PCM literature the suggested loading for optimal energy savings is 3kg·m^{-2} (Lee *et al.* 2011). It can therefore be seen that the current material is lower than the maximum or optimal amount of PCM loadings that can be achieved. By being able to quantify the fire risks associated with PCMs it will be enable the safe usage of these materials which have higher loadings.

3.5.3Hemp fibre/shiv

3.5.3.1 TGA

In nitrogen hemp exhibits a one-step decomposition behaviour between 214 and 325°C with a drying reaction below 100°C (Figure 3.13a and Figure 3.14a). The main degradation step can be split into a total of three components of varying magnitude. The first part of the peak corresponds to the degradation of the hemicellulose with potential simultaneous degradation of pectins (first reaction). Identification of the two reactions cannot be achieved through DSC since the hemicellulose is significantly more exothermic than the pectin is endothermic. This also overlaps with the cellulose which represents the largest peak and the source of the majority of degradation (second reaction). Finally, a third reaction occurs over a wide range from 214 to above 450°C and overlaps with both hemicellulose and cellulose. This is attributed

to the decomposition of lignin (Brebu and Vasile 2010). Its peak magnitude is only 0.14%·°C^{-1} compared to the peak of cellulose which is 1.29%·°C^{-1}. Cellulose is therefore found to be the dominant component and thus the degradation is similar to that of pure cellulose in the literature (Kashiwagi and Nambu 1992).

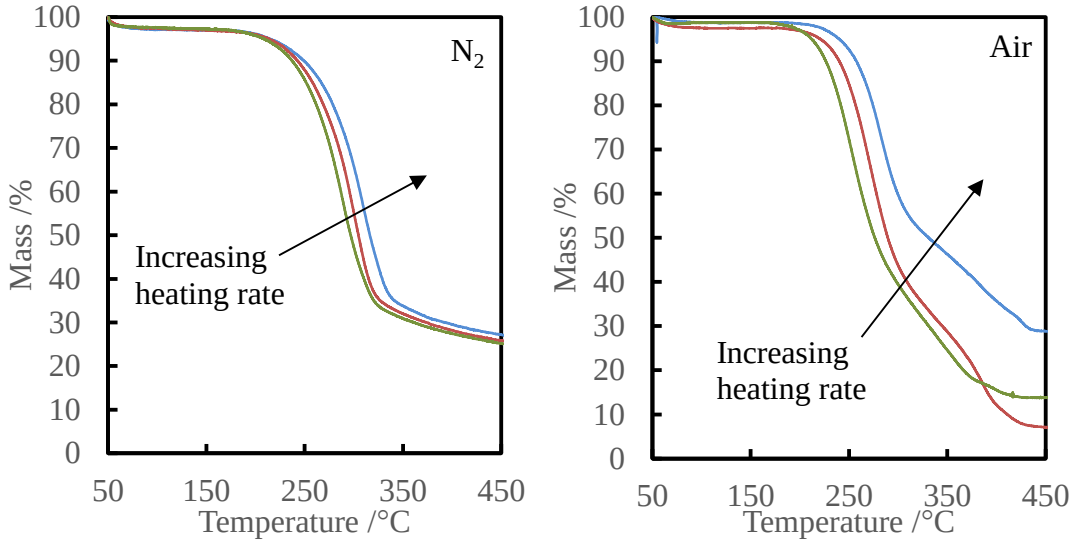

Figure 3.13 - TGA of a hemp shiv at in (a) N_2 and (b) air. The blue, red and green lines correspond to heating rates of 5, 2.5 and 1°C·min^{-1} respectively where a minimum of two tests have been averaged.

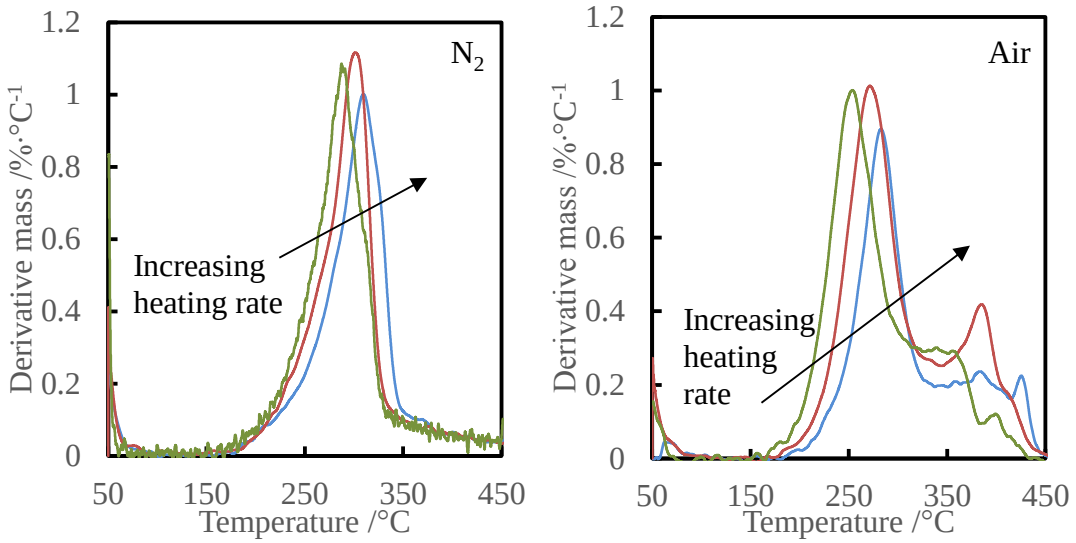

Figure 3.14 - DTG of hemp in (a) N_2 and (b) air. The blue, red and green lines correspond to heating rates of 5, 2.5 and 1°C·min^{-1} respectively where a minimum of two tests have been averaged.

In air additional steps are added for the oxidation of the chars (Figure 3.13b and Figure 3.14b). There are a total of three exothermic peaks: oxidation of the cellulose (201 to 253°C, first reaction), oxidation of the char (381 to 424, third reaction), and oxidation of lignin (253 to 381°C, second reaction). Note that the oxidation of cellulose overlaps with its pyrolysis

process, which was outlined above in nitrogen. The mass loss due to oxidation of hemicellulose and cellulose (75.9%) and oxidation of the char (3.7%) far outweigh the oxidation of lignin (maximum of 13.79±9.25%).

Pyrolysis and oxidation reactions of cellulose and other components overlap and thus it is difficult to distinguish the ranges they occur. In nitrogen the pyrolysis reactions can be correctly identified. However, in air the oxidation and pyrolysis will overlap and further testing must be conducted to identify the oxidation component. Thus, additional tests were carried out where samples were exposed to a nitrogen environment and then cooled whilst remaining in the apparatus. After a stabilisation period these samples were then again tested in an air environment to be able to correctly identify the oxidation reactions (Figure 3.15a).

The pyrolysis reactions have previously been described, and thus only the oxidation reactions will be discussed, which are shown in more detail in Figure 3.15b. The oxidation reactions in air vary for the two specimens due to the heterogeneity of the material. For one specimen, in black, the dominant component is lignin, and the oxidation is evident from 300 to 400°C. This matches the previously obtained peak value of 348°C, but provides more information on the temperature range of the reaction which previously overlapped with the pyrolysis of cellulose. In the other specimen, indicated in blue, the oxidation of char occurs from 350 to 440°C. An additional reaction in both cases occurs from 270 to 300-310°C.

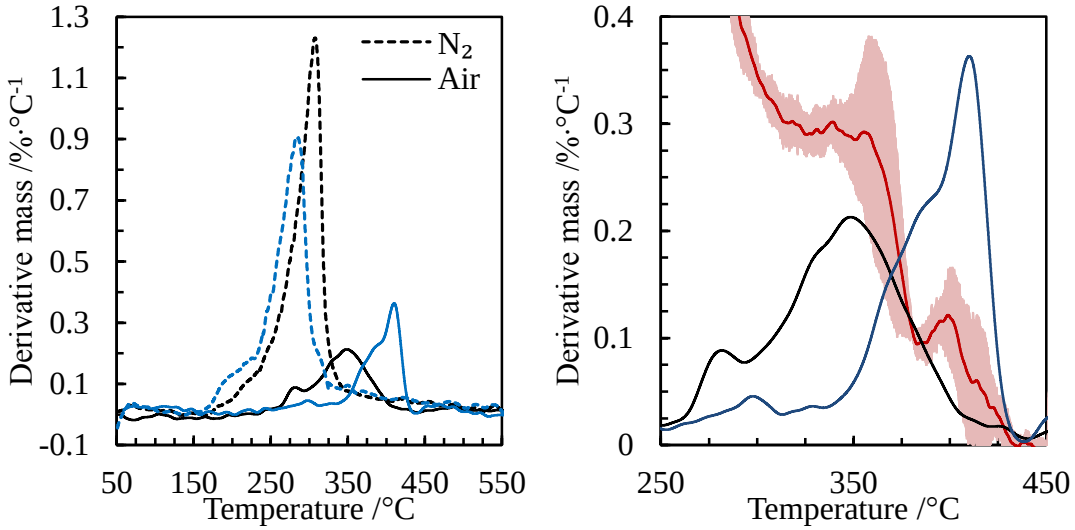

Figure 3.15 – (a) Two tests of a hemp shiv first run in a nitrogen atmosphere (at 5°C·min^{-1}), cooled, and then heating in an air atmosphere (at 1°C·min^{-1}) in blue and black, and (b) with results in air for the entire duration (red, with standard deviation for error).

Thus, it can be summarised that the pyrolysis reactions in hemp occur in a range of 214 to 325°C, with additional pyrolysis of lignin up to above 450°C. The oxidation reactions occur from 270 until 440°C.

Table 3.15 – Thermal degradation steps of hemp shiv in air (50ml·min^{-1}) for three different heating rates.

Reaction	**Heating rate**	**Onset**	**Peak**	**End**	**Peak magnitude**	**Mass lost**
-	°C·min^{-1}	°C	°C	°C	%·°C^{-1}	%
First	5	224.25 ±5.48	284.48 ±7.04	348.39 ±17.95	0.9167 ±0.1399	53.33 ±8.99
	2.5	213.12 ±4.86	271.15 ±3.83	361.19 ±29.04	1.0284 ±0.1127	76.19 ±15.40
	1	200.55 ±6.21	253.93 ±5.89	253.17 ±24.06	1.0568 ±0.0326	75.90 ±9.35
Second	5	348.39 ±17.95	383.91 ±20.98	412.40 ±7.35	0.2771 ±0.0641	13.52 ±0.15
	2.5	361.19 ±29.04	386.78 ±8.61	411.08 ±9.71	0.4749 ±0.0825	13.79 ±9.25
	1	253.17 ±24.06	344.14 ±14.11	381.22 ±7.78	0.3348 ±0.0353	6.55 ±8.72
Third	5	412.40 ±7.35	424.16 ±0.61	443.49 ±2.02	0.2080 ±0.0463	4.24 ±1.47
	2.5	411.08 ±9.71	409.19 ±2.78	440.95 ±10.72	0.1743 ±0.0124	2.85 ±2.41
	1	381.22 ±7.78	395.90 ±3.56	424.00 ±10.19	0.1361 ±0.0388	3.74 ±1.21

Remaining mass: 13.82±1.81% (1°C·min^{-1}), 7.17±4.46% (2.5°C·min^{-1}), and 28.90±9.43% (5°C·min^{-1}). All at 450°C.

Table 3.16 – Thermal degradation steps of hemp shiv in nitrogen (50ml·min^{-1}) for three different heating rates.

Reaction	**Heating rate**	**Onset**	**Peak**	**End**	**Peak magnitude**	**Mass lost**
-	°C·min^{-1}	°C	°C	°C	%·°C^{-1}	%
First and second	5	221.39 ±19.37	313.71 ±11.94	348.18 ±0.43	1.1851 ±0.0820	66.00 ±2.57
	2.5	222.48 ±6.86	302.66 ±8.96	333.16 ±4.24	1.3478 ±0.1494	66.14 ±4.38
	1	214.11 ±8.15	294.83 ±12.85	325.33 ±8.50	1.2890 ±0.0854	66.47 ±3.40
*Third**	*5*	-	*349.60 ±2.44*	*450+*	*0.1314 ±0.0283*	*8.06 ±2.29*
	2.5	-	*333.16 ±4.24*	*450+*	*0.1381 ±0.1989*	*7.94 ±0.39*
	1	-	*325.33 ±8.50*	*450+*	*0.1403 ±0.0055*	*8.29 ±0.52*

*Estimated since peak is hidden behind second reaction (cellulose)

Remaining mass: 25.24±2.99% (1°C·min^{-1}), 25.92±4.43% (2.5°C·min^{-1}), and 25.61±0.76% (5°C·min^{-1}). All at 450°C.

3.5.3.2 DSC

The DSC in air (Figure 3.16) illustrates the enthalpy of reaction for the hemp shiv. The oxidation of cellulose is evident between 246 and 353°C, and char oxidation between 405 and 433°C based on results by Kashiwagi and Nambu (1992). The highest peak, between 353 and 405°C, corresponds to the oxidation of lignin (Brebu and Vasile 2010). Lignin has the highest heat of combustion but has a maximum mass of 13.8% compared to cellulose which accounts for 79.64%. Approximate figures in the literature for the heats of combustion of the two components are 26.4kJ·g^{-1} for lignin and 17.6kJ·g^{-1} for cellulose (Lamprecht 1999). The energy released is therefore highly sensitive to the content of lignin. Where there are large amounts of lignin the amount of energy released will be much higher. Conversely, the lower heat of combustion for cellulose means that the quantity of cellulose has a smaller impact.

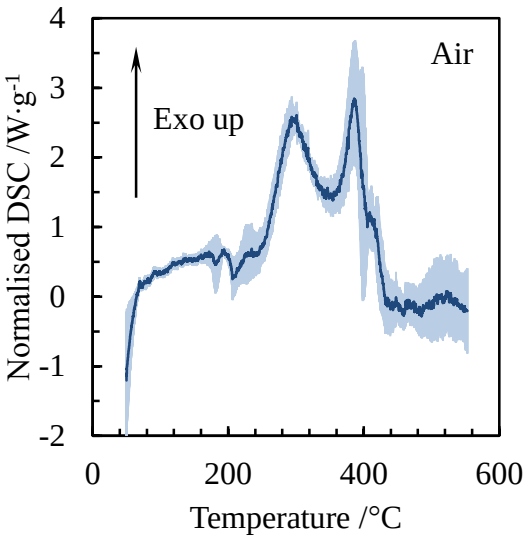

Figure 3.16 - DSC of a hemp fibre/shiv tested in air at a heating rate 2.5°C·min^{-1}. Average of three tests, where the shaded area indicates the standard deviation. Positive values of the ordinate relate to exothermic reactions.

The behaviour of the hemp shiv is in-line with both existing literature on other hemp materials (Kifani-Sahban *et al.* 1996, Mwaikambo and Ansell 2002, Ouajai and Shanks 2005, Yang *et al.* 2007, Rachini *et al.* 2009) and general cellulosic materials (Kashiwagi and Nambu 1992, Grønli *et al.* 2002, Yao *et al.* 2008, Brebu and Vasile 2010). Its behaviour can therefore be adequately characterised through the use of existing literature.

3.5.4PCM hemp-lime

The PCM hemp-lime material is composed of PCM microcapsules, hemp shivs, cement, and water. The mathematical addition of PCM microcapsules and hemp shivs DTG results are first provided since PCM hemp-lime as a completed material is highly heterogeneous and has a complex composition. This is then compared to the experimental results for a PCM hemp shiv as tested in the TGA/DSC. Results are presented at 2.5°C·min^{-1} unless otherwise noted.

3.5.4.1 TGA

The addition of DTG curves of hemp shivs and PCM microcapsules is given in Figure 3.17. This predicts that in nitrogen the reaction with the lowest temperature onset is the pyrolysis of the paraffin wax (134°C). This overlaps with pyrolysis of hemicellulose before the max rate of reactions is reached at 271°C due to the combined pyrolysis of cellulose, PCM shell material, and continued evaporation of paraffin wax. A final pyrolysis reaction is predicted from 380 to 430°C corresponding to the second pyrolysis reaction of the PCM shell.

In air the reactions are predicted to be highly distinct until 325°C. The evaporation of paraffin wax is predicted as the first reaction, followed by the sharp exothermic oxidation of the wax at 217°C. The oxidation of cellulose partially overlaps with this reaction as well as the degradation of the shell, and the predicted endset for all reactions is 450°C.

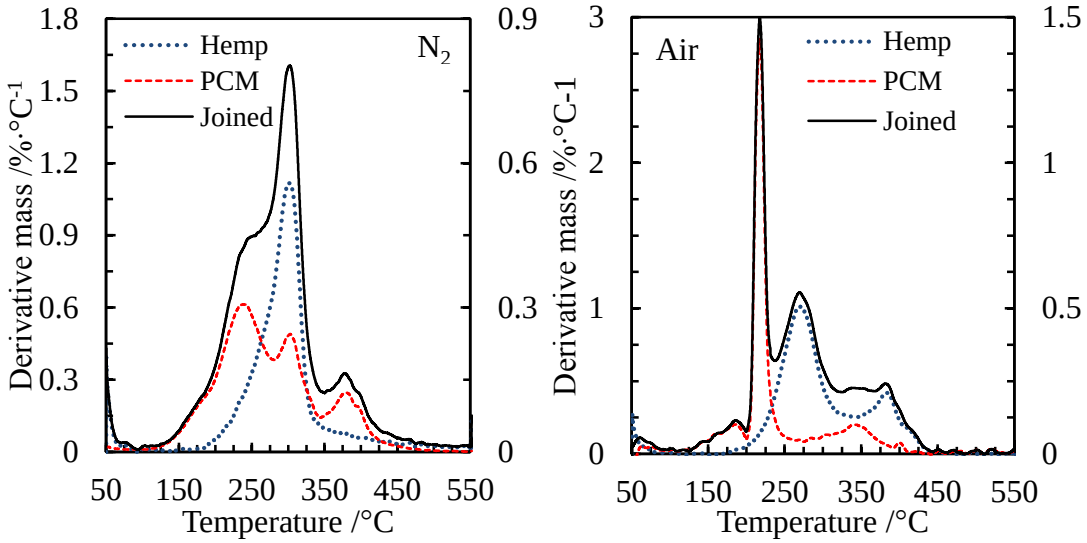

Figure 3.17 - Curves assembled from the PCM microcapsule and hemp shiv data. Blue dotted indicates hemp shiv DTG, red dashed indicates PCM microcapsules, and black solid is the mathematical addition of the two in (a) nitrogen and (b) air.

The actual TGA results for PCM hemp-lime is shown in Figure 3.18. A comparison of the DTG for both the actual and the predicted, or assembled, is then given in Figure 3.19. The actual results show that the pyrolysis behaviour has only two distinct reactions in nitrogen. The onset temperature of the first reaction is defined by the paraffin wax but it includes many components. This reaction comprises the wax evaporation process, and the pyrolysis of both cellulose and the PCM shell. The onset of this combined pyrolysis reaction was 147°C, which is significantly lower than the ordinary onset of cellulose pyrolysis which was found to be 222°C. The point corresponding to the maximum rate of decomposition was also found to decrease slightly from 303°C for cellulose down to 291°C. A second pyrolysis reaction corresponding to the subsequent pyrolysis of the shell remains clearly defined from 325 to 429°C. This matches the data obtained from the PCM microcapsules and there is no change in thermal stability. This reaction can therefore be adequately quantified through the TGA data

of the isolated capsules. The residual mass remains high at 69.80±8.75% due to the presence of the lime-cement binder which comprises a large amount of the total mass, and does not pyrolyse or degrade.

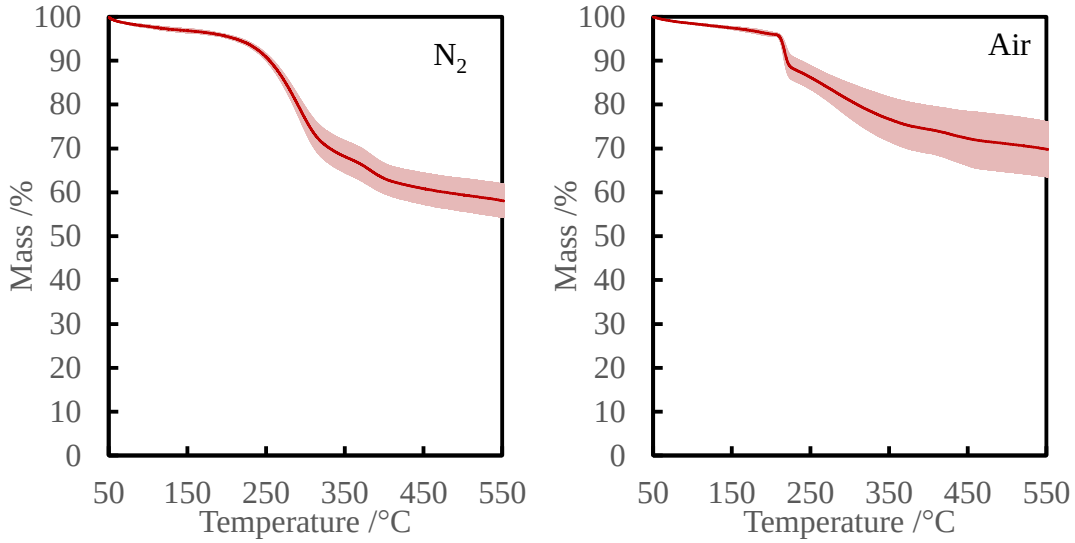

Figure 3.18 - Normalised TGA of a combined PCM and hemp shiv based on three repeats at 2.5°C·min^{-1} in (a) nitrogen and (b) air.

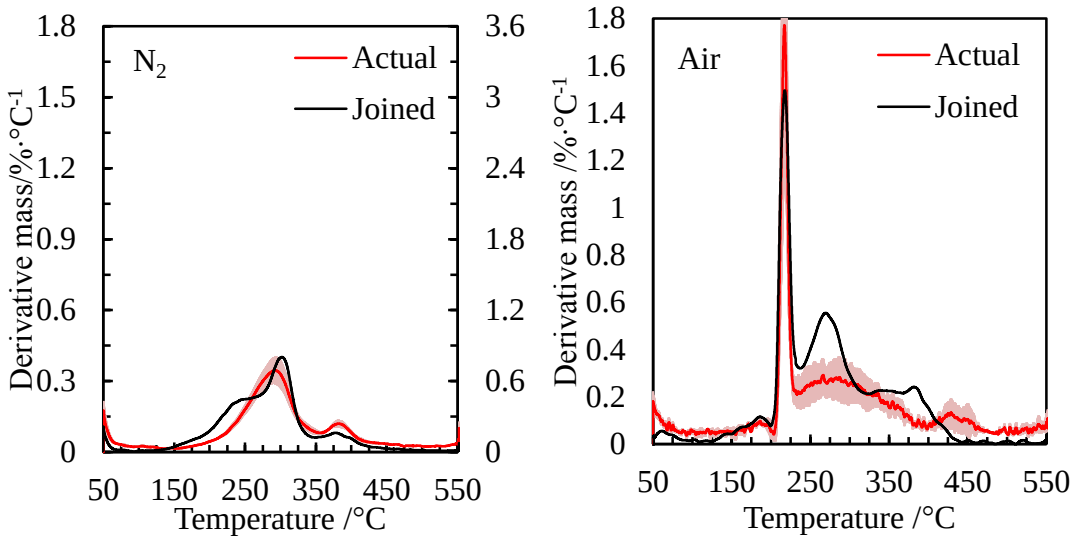

Figure 3.19 - Assembled (black) and experimental (red, with standard deviation in shading) derivative weights for PCM hemp-lime for a heating rate of 2.5°C·min^{-1} in (a) nitrogen (b) air.

In air, the initial oxidation reactions are dominated by the PCM. The evaporation of leaked wax and the exothermic oxidation both occur over the same range for the predicted and actual results. This confirms that the process of adding PCMs to hemp-lime was successful and that the capsules were not destroyed in the mixing process. Another major lumped reaction comprising of the oxidation of hemicellulose, cellulose, lignin, and both shell oxidations occurs from 235 to 398°C where 13.11±4.05% of the total mass was lost. The quantity of material lost is similar to that of the paraffin wax (13.26±3.42%) despite the differences in

magnitude and range. A final step corresponding to char oxidation occurred from 398 to 510°C, and the residual mass was 58.69±3.84%. The residual mass confirms that the remaining lime-cement binder does not oxidise in any significant manner, as the value is found to be similar to measurement in nitrogen. Differences are due to the heterogeneous nature of the material.

Table 3.17 – Thermal degradation steps of PCM hemp-lime shiv in air (50ml·min^{-1}) for two different heating rates.

Reaction	**Heating rate**	**Onset**	**Peak**	**End**	**Peak magnitude**	**Mass lost**
-	°C·min^{-1}	°C	°C	°C	%·°C^{-1}	%
First	2.5	120.00 ±18.46	184.36 ±1.38	203.51 ±0.16	0.0376 ±0.0059	4.18 ±0.52
	1	-	-	-	-	-
Second	2.5	203.51 ±0.16	217.51 ±1.03	235.61 ±2.89	0.7946 ±0.2576	9.08 ±2.90
	1	190.07 ±0.001	203.84 ±0.04	219.75 ±0.33	0.8796 ±0.0203	15.85 ±1.21
Third	2.5	235.61 ±2.89	284.36 ±2.64	398.23 ±0.15	0.1193 ±0.0475	13.11 ±4.05
	1	219.75 ±0.33	266.48 ±8.51	378.42 ±7.29	0.2370 ±0.0636	21.78 ±5.30
Fourth	2.5	398.23 ±0.15	426.77 ±2.98	510.09 ±0.001	0.0626 ±0.0244	3.84 ±1.28
	1	378.42 ±7.29	423.61 ±11.36	*450+*	0.1200 ±0.0738	4.53 ±2.84

Remaining mass: 57.83±9.35% (1°C·min^{-1}, 450°C), and 69.80±8.75% (2.5°C·min^{-1}, 550°C).

Table 3.18 – Thermal degradation steps of PCM hemp-lime shiv in nitrogen (50ml·min^{-1}) for a single heating rate.

Reaction	**Heating rate**	**Onset**	**Peak**	**End**	**Peak magnitude**	**Mass lost**
-	°C·min^{-1}	°C	°C	°C	%·°C^{-1}	%
First	2.5	147.46 ±13.27	291.32 ±2.68	354.02 ±4.46	0.3456 ±0.0568	32.21 ±3.90
Second	2.5	354.02 ±4.46	381.34 ±0.19	529.25 ±0.21	0.1202 ±0.0162	9.10 ±0.19

Remaining mass: 58.69±3.84% (2.5°C·min^{-1}, 550°C)

3.5.4.2 DSC

Exothermicity was recorded between the ranges of 199 and 388°C, and again between 426 and 493°C. The first oxidation reaction between 199 and 234°C agrees well with the DTG results, and thermal lag was not evident despite the increased specimen weight. Overlapping reactions between 234 and 388°C had two peaks where there was only a single lumped

reaction evident in TGA. The first peak at 315°C is expected to be predominantly due to the oxidation of cellulose, although this overlaps with the oxidation of the PCM shell material. The exothermic peak at 367°C is associated with the oxidation of lignin due to the large amount of heat released for the small amount of mass lost, which matches lignin's high heat of combustion. A final exothermic reaction was present between 429 and 493°C, which corresponds to the final char oxidation reaction.

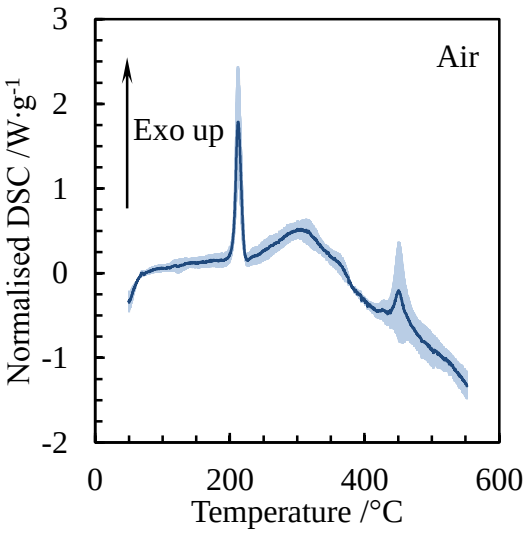

Figure 3.20 - DSC of a PCM hemp-lime shiv tested in air at a heating rate 2.5°C·min^{-1}. Average of three tests, where the shaded area indicates the standard deviation. Positive values of the ordinate relate to exothermic reactions.

The DSC results confirm that the oxidation of the paraffin wax forms the first exothermic reaction of the PCM hemp-lime shiv. This occurs at a lower temperature than the oxidation of cellulose, and is expected to increase the ignitability of PCM hemp-lime. Furthermore, the addition of the PCM increases the amount of energy released compared to ordinary hemp.

3.5.5 Application to bench-scale results

3.5.5.1 Hemp-lime with PCMs

Thermal analysis of the constituent components in PCM hemp-lime reveals the chemical reactions and processes, and the temperature ranges in which they occur. It is found that the major exothermic oxidation associated with the evaporation of the paraffin wax is at 199°C, which is lower than the oxidation of cellulose at 254°C. Thus, it is expected that the addition of PCMs into the matrix of hemp will decrease the ignition temperature, and hence the critical heat flux that will be obtained in bench-scale calorimetry.

Analysis of the PCM hemp-lime shiv showed that exothermic oxidation of the paraffin wax occurred over the same range as when the microcapsules were tested in isolation. The pyrolysis temperatures for the endothermic pyrolysis of cellulose and of the PCM shell were found to be lowered by the addition of the hemp. This suggests both that the addition of PCMs

will adversely affect the decomposition of the hemp, and that the degradation process may not be as straightforward as simply adding the degradation steps of the two materials. For oxidation reactions, the onset of the paraffin wax decreases the thermal stability of the hemp. Higher temperatures were found for the oxidation of cellulose and char, but these are offset by the decreased thermal stability and lower pyrolysis temperatures. The PCM hemp-lime results additionally illustrated that the composite material is more energetic than the individual components which will be reflected in bench-scale results.

3.5.5.2 PCM plasterboard

The thermal analysis reveals the chemical reactions which will be relevant to the flammability of the PCM plasterboard in bench-scale testing. The significant endothermic peaks attributed to the dehydration of gypsum in the temperature range of 82 to 117°C indicate that potential delay in the onset of ignition is possible since more energy is required to overcome these reactions and reach the temperature of the exothermic oxidation of paraffin wax. The approximate loading of PCM, as well as core to shell ratio has been obtained, which can be used to quantify the amount of fuel provided by the PCM in a building. This enables the quantifiable variation of PCM loading so that designers can achieve the optimal balance between potential energy savings and fire performance.

3.5.6Relevance of Arrhenius parameters

The Arrhenius equation (Arrhenius 1889) can be applied to TGA results in order to obtain the activation energy E_a, pre-exponential constant A, and order of reactions n for chemical reactions. There are a variety of well-established methods available to achieve this (Coats and Redfern 1964, Friedman 1964, Ozawa 1965, Flynn and Wall 1966). This has proved a popular method of describing the global kinetics for the use in fire modelling. In particular, the use of a genetic algorithm allows highly accurate results to be obtained (Rein *et al.* 2006). These methods potentially allow a significant of the underlying chemical reactions. However, this is not the objective of this work which instead focuses on enabling interpretation of bench-scale results.

3.6 TPS results and discussion

For TPS, the thermal transport properties for PCM enhanced plasterboard at ambient temperatures are presented and analysed. The properties (collated in Table 3.19) obtained agree well both with the values obtained by Park *et al.* (2010) for plasterboard as well as those obtained by Karkri *et al.* (2015) for PCM plasterboards. Despite the presence of PCMs, which have a lower thermal conductivity than gypsum, the thermal conductivity for the PCM plasterboard in this study is still higher than all the ones studied by Park *et al.* (2010). This suggests that where the PCM content is relatively low, which was previously calculated to be 9.44±1.10% using TGA, the thermal properties will be dominated more by the formulation of the gypsum and less by the presence of the PCM. Karkri *et al.* (2015) showed that once the PCM becomes a major component that it will have a marked effect on the thermal properties. Otherwise, the properties can broadly be modelled as plasterboard with additional specific heat.

When determining thermal properties for PCMs the core material should be in its liquid state. This is most relevant to the fire performance since it will never be in solid state at elevated temperatures. The values obtained in TPS for the liquid state were in good agreement with the literature, whilst the specific heat capacity in the solid state was significantly higher (2920±290J·kg^{-1}·K^{-1} compared to 1047.45J·kg^{-1}·K^{-1} for a PCM content of 13.33% (Karkri *et al.* 2015)). This suggests that the onset of the phase change may have initiated, despite the deviation in the recorded resistance being low.

Table 3.19 – Thermal properties obtained using Transient Plane Source for PCM plasterboard at 18°C (PCM in solid state) and 26°C (PCM in liquid state). Values were averaged over four tests for solid and three tests for liquid. In all cases the density was 900.08±4.25 kg·m^{-3}.

Parameter	**Units**	**Capsule state**	
		Solid	**Liquid**
Thermal conductivity, k	W·m^{-1}·K^{-1}	0.32±0.04	0.29±0.03
Thermal diffusivity, α	mm^2·s^{-1}	0.12±0.02	0.263±0.03
Volumetric heat capacity, c_v	MJ·m^{-3}·K^{-1}	2.63±0.26	1.12±0.11
Specific heat capacity, c_p	J·kg^{-1}·K^{-1}	2920±290	1240±120
Thermal inertia, $k\rho c$	J^2·s^{-1}·K^{-2}·m^{-4}	0.851±0.142	0.327±0.054
Root thermal inertia, $\sqrt{k\rho c}$	J·s$^{-1/2}$·K^{-1}·m^{-2}	0.920±0.075	0.570±0.048

Error margins are generally found to be around 10% over three or four specimens suggesting a high level of confidence, but this is a higher margin than TPS is capable of for other materials which is less than 5% (Gustafsson 1991). This is due to a balance between the inevitable thermal gradient present in the specimen due to its insulating properties, and the heterogeneity. Small sensors are suitable for overcoming the thermal gradient since they analyse a shallower depth where the gradient is less severe. However, the heterogeneity of the material – specifically localised air voids in in the case of gypsum – mean that the small sensor has relatively high error. For large sensors the probing depth is larger and thus the relative heterogeneity is overcome, but the temperature gradient is higher. Despite this, 10% can still be considered a relatively low error and TPS remains an attractive technique for determining the thermal transport properties at ambient temperatures.

3.7 Concluding remarks

In this chapter, the thermal degradation steps of each constituent material has been outlined, as well as the effect of adding components together. In addition, the thermal transport properties for PCM plasterboard at ambient conditions have been found.

- The pyrolysis and oxidation reactions have been identified for each material. The governing process of the PCM is the evaporation of the paraffin wax from the shell, whilst hemp is dominated by the pyrolysis of cellulose and lignin.
- The composition of each material is estimated. Hemp is found to match others in the literature, whilst the PCM is confirmed to have a paraffin wax core and an encapsulation rate of 65.0±1.2%.

- Identification of the mass of paraffin wax within the substrate provides a means to quantify the potential fuel load caused by the addition of PCMs.
- PCMs represent an energetic material which add a series of exothermic oxidation reactions to both plasterboard and hemp-lime which would not otherwise be present.
- The addition of PCMs into both plasterboard and hemp-lime is shown to have no influence on the thermal stability of the PCM. Thus, the paraffin wax still pyrolyses at relatively low temperatures regardless of the substrate material. In addition, this means data on the evaporation of paraffin wax is relevant to the end use material.
- The exothermic oxidation temperature of PCM microcapsules identified using DSC represents a useful insight into the potential ignition behaviour. It cannot be applied directly to bench-scale calorimetry due to the differing boundary conditions and assumptions delivers knowledge on the pyrolysis and oxidation reactions.
- The PCM loading of the commercial obtained plasterboard product was found to be lower than that recommended as optimal from the literature. This suggests compromised energy savings for fire performance which could be alleviated through quantification of the associated fire risk.
- Pyrolysis temperature of paraffin wax is lower than hemp and will affect the ignition behaviour in bench-scale calorimetry.
- The transient plane source technique was applied to PCM plasterboard and gave similar results to the literature when the wax in the capsules was in liquid state. The testing was only conducted at ambient temperatures due to the number of thermal degradation steps identified through TGA.

4 Characterisation of the smouldering risk of an innovative hemp-lime insulation material

4.1 Summary

Hemp-lime insulation is a cellulosic material used in low carbon construction due to its attractive sustainability credentials. The porous nature of this material means that smouldering reactions are the dominant combustion mode and thus it falls outside the scope of traditional standard fire testing methods for building materials. In this chapter, a new methodology to investigate the smouldering combustion of these materials in the widely available cone calorimeter is developed. This methodology permits the study of both downward opposed flow and upward forward flow smouldering regimes within the same setup without forced airflow. Key smouldering metrics including time to ignition, mass loss rate, spread rate, thermal evolution and gas emissions are all employed. In tandem with the previously conducted Thermogravimetric Analysis (TGA) results the material and its associated fire risks are characterised over a range of incident heat fluxes and conditions.

4.2 Introduction

Hemp-lime insulation has become an increasingly popular material in the built environment due to its sustainability and carbon sequestration. When exposed to heat the material is capable of sustaining both flaming and smouldering reactions. Heat is only able to penetrate through the material at low rates due to the insulating properties of the material. Because of this, the short residence time in flaming fires are not sufficient enough to represent a key fire risk as is the case in other traditional building materials. Instead, smouldering embodies the most significant risk. Little energy is required for ignition, and once initiated the smoulder can spread large distances undetected. Despite this, there is currently no standard fire test method specifically developed for smouldering. To enable designers to quantify the fire risk of this material requires the development of a bespoke testing framework.

The aim of this chapter is to develop a novel framework to enable holistic fire risk assessment of hemp-lime insulation. This will be achieved through the following objectives:

- Develop a cost effective, repeatable, and widely accessible method of studying smouldering combustion,
- Identify the key fire risks relating to hemp-lime insulation,
- Characterise the smouldering behaviour in a variety of conditions and understand their impact on the material performance.

4.3 Material synthesis

Bench-scale testing represents a cost effective method of assessing materials. The small scale of specimens requires the casting of hemp-lime material specifically for this purpose. The casting and curing processes which have been chosen are outlined below.

4.3.1 Component quantities

The final mix was a combination of the formulations discussed in *Section 2.2.2.2 Mix ratios* from Walker *et al.* (2014) and from the manufacturer. This mix comprised 1 part hemp shiv, 2 parts binder, and 3 parts water by weight. A series of trial casts varying the quantities of each component were run and the resulting material was found to be satisfactory in terms of strength, insulation properties, and workability. An illustration of the hemp shivs and fibres is given in Figure 4.1.

Figure 4.1 – Hemp shivs and fibres used in the casting process. Top left: woody pulp which makes up only a small portion, bottom left: the main shivs and fibres (cores) which make up the majority of the mass, right: general overview.

4.3.2 Mixing and synthesis process

The components were mixed using a Creteangle LE Pan Type Concrete Mixer with a maximum capacity of 0.04m³. This hemp manufacturer verified that this method was a suitable representation of the large-scale manufacturing methods used in industry. The entirety of the hemp and binder were added to the mixer and loosely combined. Water was then added in thirds and the resulting material was mixed until it was capable of roughly retaining its form. This typically took around five to ten minutes at most.

The mix was placed in 100mm cubes of formwork, ensuring good contact around the edges and corner to guarantee that a stable material was formed. The remaining volume was lightly

packed so that the resulting material has high porosity and thus low thermal conductivity. Furthermore, this reduces the amount of material required and hence the total cost, as would be desirable during the construction of a real building.

No thermocouples were placed during casting since it was found that the material was not sufficiently workable to be able to include the necessary instrumentation. These were instead added after the material was completed, as is discussed later in *Experimental approach* (Section 4.4).

The formwork was removed from the specimens after twenty four hours, and then left to cure in a conditioning room for six months at 21±4°C and 80±15% relative humidity.

4.3.3Final material

The resulting material had a density of 305±26kg·m^{-3}. Prior to testing, specimens were dried in an oven at 80°C for twenty four hours (Hadden 2011) and then removed one hour before testing. Regardless of the preparation time the one hour window was kept the same. The resulting material after the formwork was removed is shown in Figure 4.2.

Figure 4.2 – Rigid cast cube of completed hemp-lime insulation with dimensions 100 by 100 by 100mm.

4.4 Experimental approach

A test setup for the investigation of smouldering in the cone calorimeter (Babrauskas 1984, ASTM International 2014, British Standards Institution 2015a) was developed. Alterations to the standardised setup were made to accommodate the increased sample thickness and to modify the air flow conditions to allow smouldering combustion. An illustration of the modified experimental setup is given in Figure 4.3.

The standard cone calorimeter setup seals the side and bottom from air penetration to allow the analysis of one dimensional heat flow through a specimen. To be able to achieve suitable

flow conditions for smouldering, the bottom was instead unsealed. The sides remained closed with foil to prevent air ingress and ensure one directional smouldering propagation. The specimen was placed on a porous mesh (Figure 4.4a) which had a porosity lower than that of the specimen. This allowed buoyancy-induced air to enter at the bottom and diffuse upwards through the material to the reaction front. Hot post-combustion gases were able to exit the specimen through the top unsealed surface. The influence of such an apparatus on the flow through and around the specimen has been shown to have a negligible effect in a similar apparatus when studying wildland fuels (Schemel *et al.* 2008). The overall cone calorimeter apparatus is shown in Figure 4.4b.

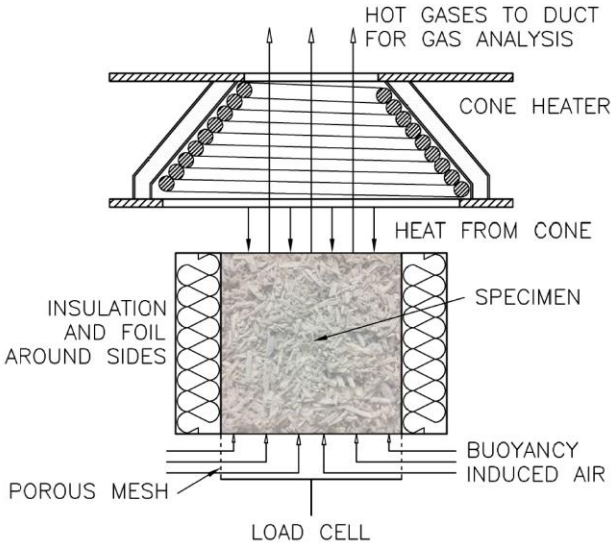

Figure 4.3 – Test setup in the cone calorimeter for investigating the smouldering combustion characteristics of hemp-lime insulation.

Insulation was used around the sides to reduce heat losses and ensure that a smoulder could be initiated and sustained. The effectiveness of the insulation over the long durations of these tests will diminish. However, it produces a repeatable boundary condition allowing for reproducible smouldering ignitions. The insulation used was 25mm of non-combustible stone wool. This stone wool was replaced every three tests to ensure consistent performance.

The top free surface of the specimen was positioned 25mm below the cone heater and no pilot ignitor was used. The addition of a pilot source would allow the investigation of flaming ignition in the same setup, if desired. Tests were undertaken in duplicate so that mass loss and temperature measurements could be recorded independently. Analysis of CO and CO_2 were used as a further independent measurement of the combustion processes.

For the temperature measurements, K-type thermocouples with 2.0mm diameter heads and Inconel sheathing were positioned at 10mm interval along the central axis. Holes were drilled with a 1.6mm drill bit since the material was too rigid to directly insert thermocouples, as previously mentioned in *Section 4.3 Material synthesis*. Casting with thermocouples in place was deemed unsuitable for the following reasons:

- the position of the thermocouple would not be known and would be difficult to verify post-test since the residue will have a high composition of ash and little remaining structural integrity;
- the hemp shivs are sufficiently large that filling the spacing between thermocouples is difficult. Thus, large air voids could be present around the position of the thermocouples and would not be representative;
- inserting the thermocouple prior to the testing allows the same set of thermocouples to be reused each test reducing the preparation time.

The first thermocouple was positioned 10mm beneath the surface. The brittle nature of the material prevented positioning closer to the surface. A broad estimation by Rein (2016) is that the minimum depth required to establish a smoulder is between 1 and 10cm. Thus, a thermocouple should not be required at any depth shallower than 1cm.

Figure 4.4 – (a) Porous sample holder used for testing (b) Cone calorimeter at the University of Edinburgh.

Due to the length of the tests, temperatures were recorded at 10s intervals. Two dataloggers were used; one for the thermocouples and one for all other measurements from the cone calorimeter. These were initialised at the same time, and a delay of 100s was added to generate baseline measurements for every test before the specimen was inserted.

The heat flux was measured prior to every test using a water-cooled Schmidt-Boelter gauge. The gauge was accurate to the larger of ±2.5kW·m^{-2} or ±10%. This was placed at the centre of the cone heater at a level equal to the top surface of the specimen.

4.4.1Gas analysis

Oxygen consumption was measured using a Servomex 540A Oxygen Analyser, whilst carbon dioxide and carbon monoxide were measured using a Siemens Ultramat 21P Gas Analyser. The fan speed was set to allow a constant extraction flow rate of 24 l·s^{-1} (0.024 m^3·s^{-1}). Samples

gases were pumped through a cold trap, air filters, and desiccant in the form of calcium sulphate.

Some issues were encountered with the use of calcium sulphate for extended periods which are not typically faced when studying flaming fuels using standardised methods. The slow propagating nature of smouldering combustion meant that tests took substantial amounts of time to complete, in the region of eight to ten hours. It was found that after approximately one to three hours the carbon dioxide and oxygen readings would deviate and no longer be accurate nor representative. This has previously only been documented by Hidalgo-Medina (2015). When the calcium sulphate is anhydrous it will absorb carbon dioxide and reduce the measured values. After an undetermined period the carbon dioxide is then released and artificially high values will be recorded. The timescales of these tests are sufficient that both the absorption and desorption of carbon dioxide yield erroneous results when studying smouldering combustion. As such, there is insufficient confidence in the CO_2 results and consequently they are not presented. The full reasons for these deviations in results are not completely understood at this time and would require further research outside the scope of this project to elucidate.

4.4.2Ignition criteria

In smouldering combustion the definition of time to ignition can prove difficult to define. In flaming, the ignition time is simply recorded as the delay until sustained flaming is observed for an arbitrary reference period (ASTM International 2014, British Standards Institution 2015a). Since smouldering is a flameless form of combustion, one strategy which can be employed is to instead measure the time to the onset of glowing combustion (Boonmee and Quintiere 2002). This however does not deal with the issue of in-depth ignition, where glowing ignition – should it even occur – will not be visible. At low heat fluxes there was no glowing ignition on the surface of the hemp-lime insulation and thus a visual observation method could not be used. If the Arrhenius parameters are known then the method can still be employed (Boonmee and Quintiere 2005) but in this case they have not been determined due to the difficulty in measuring extremely accurate values.

Both sets of tests, mass loss and temperature, recorded gas emissions and so this was deemed a suitable metric for measuring ignition delay. A substantial increase (10% of the peak, and a change in gradient) in carbon monoxide was used to mark the time to smouldering ignition. It is expected that for different configurations and scales the value of 10% will be different, and for these cases the key criterion is the inflection point. As such, this method records that ignition has occurred, and may not be as suitable in predicting the exact moment in which it occurs. Carbon monoxide was chosen over other gases because the resolution of the analyser at low concentrations is much higher, as well as previously described issues regarding calcium sulphate (*Section 4.4.1*). Both the oxygen and carbon dioxide analyser are intended to measure high concentrations during flaming, whilst the carbon monoxide analyser measures only the small amount of CO generated. To validate this method it was checked against the time to glowing ignition as observed on the surface. In all cases where glowing combustion was

observed the ignition times were found to be the near identical, and thus the results should be suitable for comparison with research which uses this method.

An illustration of this method is given in Figure 4.5 for two hemp-lime samples tested at 12kW·m^{-2}. The delay in the gas analyser is already taken into consideration and 0s represents the test start. Before the recorded ignition pyrolysis gases and charring are observed which are also reflected in the CO emissions. Additional tests at very low heat fluxes with long ignition times (>200 mins) also showed the same change in gradient of CO generated corresponding to the assumed smouldering ignition.

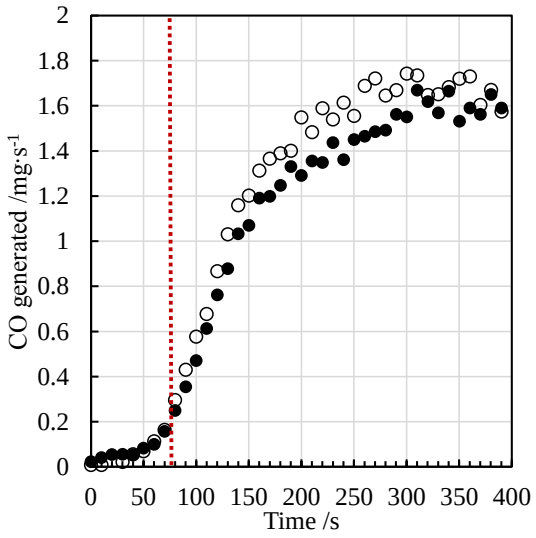

Figure 4.5 – Ignition criterion used in this research. The peak value is obtained, then the first timestep to exceed 10% is taken as the time to ignition (dotted line). Results for two samples of hemp-lime at 12kW·m^{-2} are displayed.

4.4.3Test duration

Various strategies to investigate the smouldering behaviour were evaluated since no standardised method currently exists. Firstly, introducing a heat shield to eliminate the influence of the cone part way through a test was considered. This would allow the sample to be partially heated and for a char layer to form, then permit the smoulder to propagate solely through the energy generated by the combustion reaction. The smoulder would be self-sustaining and in principle would follow the setups of Torero (1992), Pironi (2009), and Hadden (2011). However, the issue encountered with this approach is that by introducing an object between the cone and specimen the gases can no longer be collected in the hood. This means that there is no data on gas emissions after the specified time, which reduces the value of the test. Furthermore, gas emissions are used to verify that the behaviour between both mass loss and temperature tests is the same and without these measurements this validation cannot be performed. The shield which was used did not have a cooling system and thus would heat up after some period. The energy from the cone heater and the residual hot gases would heat up the shield and an uncharacterised amount of energy would be radiated to the sample, or the heat losses would otherwise be unquantifiable. The cone heater remained on and the sample was not removed until all recorded parameters had reached a steady state.

4.5 Results of representative test

The bespoke experimental setup employed in this research differs from other methods used to study smouldering in the literature and has not been used previously. Thus, tests for only a single heat flux, 8kW·m^{-2}, are presented to be able to clearly describe the smouldering propagation and the dynamics of the smouldering front. Afterwards, a detailed analysis and in-depth discussion over a range of conditions is given.

4.5.1 Smouldering ignition

Upon exposure to the radiant heat flux from the cone calorimeter the surface of the specimen will begin to heat up. At an incident flux above the critical value the material will reach its pyrolysis temperature and thermal degradation will occur thereby producing a carbon rich char. Exothermic oxidation of the char at or near the surface of the specimen releases additional energy to help initiate the smoulder process and, if the external heat flux is sufficient, allow sustained propagation. The ignition mechanisms can be inferred from the thermal analysis of the hemp previously conducted using TGA (Thermogravimetric Analysis) and DSC (Differential Scanning Calorimetry). Char is generated in an oxidative environment upon reaching the pyrolysis temperature. The thickness of the char increases and acts as an insulating layer reducing the heat losses from the reaction front. Oxygen contained within the air is readily available at the surface of the specimen to react with the char. At the critical value the char layer will be of sufficient thickness that the heat losses are less than the heat generated by the exothermic oxidation of the char. At this point a sustained downward opposed flow smoulder is initiated within the specimen.

The time to smouldering ignition was 270±10s at 8kW·m^{-2}. For the heat fluxes studied there was insufficient energy to initiate flaming combustion and thus the combustion reactions instead took place on the surface of the solid phase char.

4.5.2 Smouldering propagation regimes

Following ignition the established smoulder propagates downwards through the specimen under opposed flow conditions. As char is generated in an oxidative environment, the endothermic pyrolysis and exothermic oxidation planes overlap and cannot be easily distinguished from one another. Oxygen is induced by buoyancy from the bottom of the specimen and diffuses upward to the reaction zone. It reacts with the carbon rich char, releasing energy and producing post-combustion gases. These hot gases travel upward and escape from the top of the specimen, maintaining the temperature of the residual material. The energy released by the solid phase combustion reaction, in addition to the radiant heat provided by the cone, is sufficient to heat the virgin material upstream to the critical temperature, thus allowing the smoulder to be sustained. A schematic illustrating this propagation, which is termed Regime I, is shown in Figure 4.6a. The temperature evolution shows the propagation of this regime from five to 190 minutes before the reaction front reaches the bottom surface in Figure 4.7.

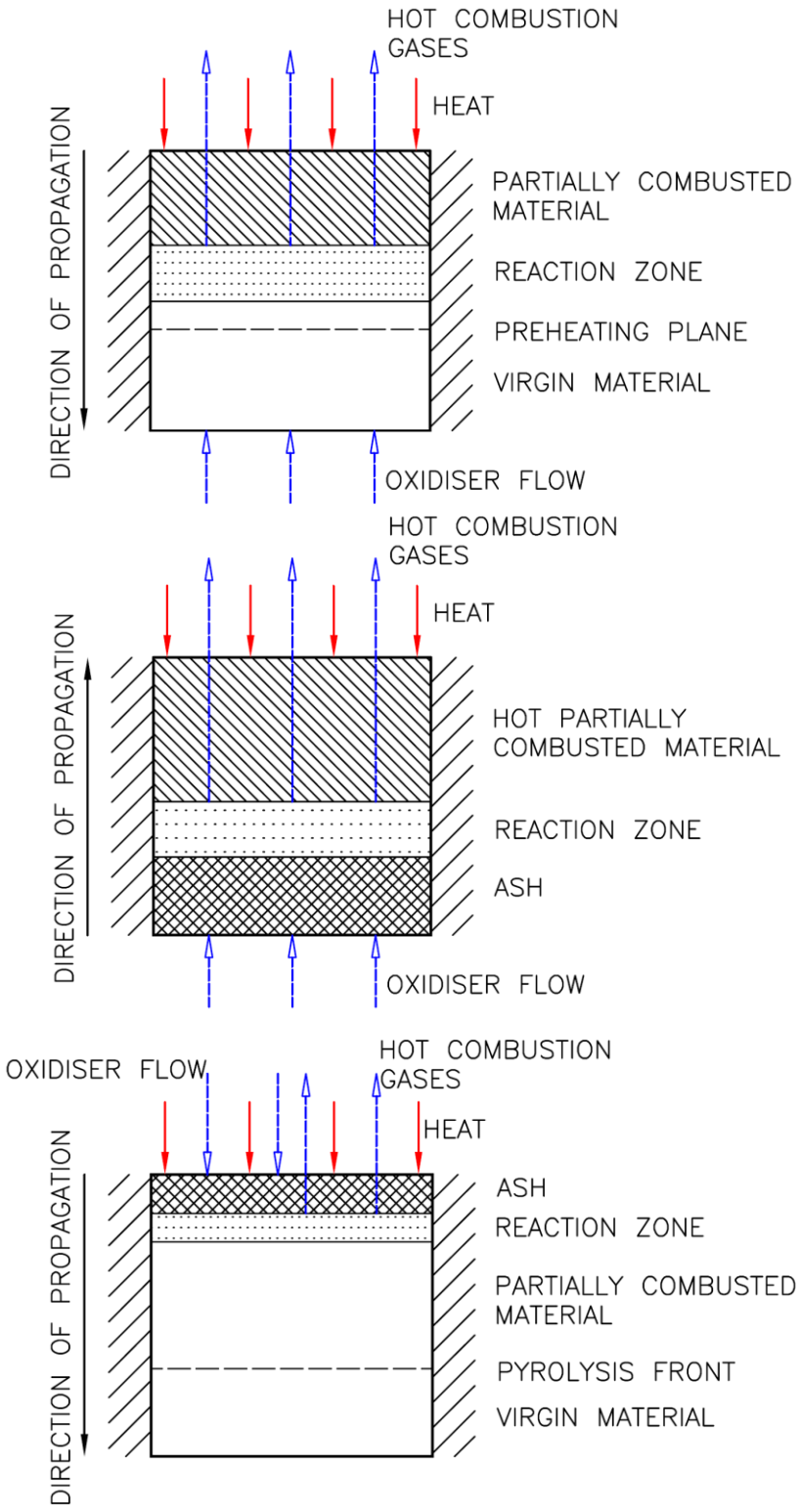

Figure 4.6 - Schematic displaying the various propagation modes of the smoulder. (a) Regime I, downward opposed flow conditions, (b) Regime II, upward forward flow conditions, and (c) Regime III, downward forward flow condition.

At some point the reaction front will reach the bottom surface of the specimen. The hot post-combustion gases and the radiant heat from the cone maintain the temperature of the specimen, which is composed mostly of partially combusted material, near the critical point. With these conditions a secondary ignition occurs at the bottom surface of the specimen, and propagates upwards (Regime II, Figure 4.6b). At an incident heat flux of 8kW·m^{-2} this secondary ignition occurs at around 325 mins, as seen in the bottommost thermocouple in Figure 4.7. Oxidiser remains available from the bottom of the specimen and travels upwards, thus resembling a forward flow smoulder. The material has already pyrolysed during the preceding Regime I and thus there is no pyrolysis front. Energy released from the exothermic oxidation of char is sufficient to raise the temperature above the critical point and allow the smoulder to propagate.

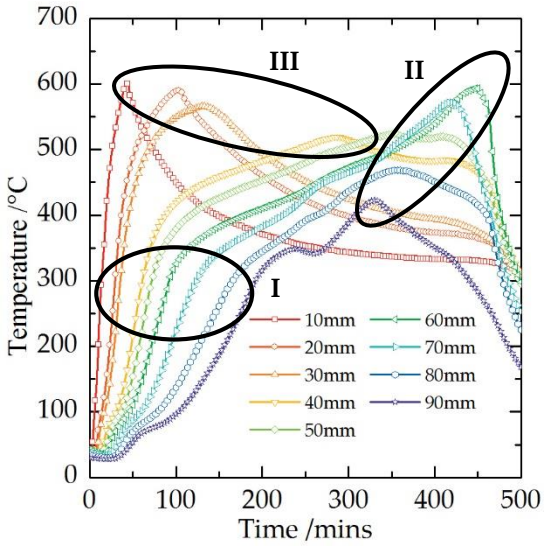

Figure 4.7 – Temperature evolution of hemp-lime insulation when exposed to 8kW·m^{-2}. Circled areas indicate (I) Regime I, downward opposed smoulder (II) Regime II, secondary ignition of upward forward smoulder, and (III) Regime III, downward forward smoulder.

The advancement of the Regime II upward smoulder can be inferred from the peak temperatures in progressive thermocouples. The temperature increases as the smoulder approaches a given point and reaches a peak as it passes through. Afterwards, the temperature drops but remains moderately high due to the continued exothermic oxidation still occurring elsewhere in the specimen. By 440 mins the smoulder reaches a depth of 60mm, but with little remaining combustible material there is insufficient fuel for the smoulder to sustain and thus it reaches extinction. Reactions cease and the temperatures rapidly drop to the baseline conducted from the radiant heat of the cone calorimeter.

The boundary conditions were set in such a way to promote a one-dimensional smoulder. Buoyancy induced air enters from the bottom, whilst hot post-combustion gases leave the specimen from the top surface. However, some air is still able to enter from the top surface and diffuse downwards to the pyrolysed material. The oxidiser reacts with still hot partially combusted material and a downward forward flow smoulder slowly propagates. This

propagation has been labelled Regime III (see Figure 4.6c). The location of this smoulder can be inferred from the peak temperatures in the thermocouples near the top surface of the specimen, as seen in Figure 4.7. The peak temperature of subsequent depths decreases in Regime III, and the smoulder velocity tends to decrease as it propagates in-depth and away from the radiant heat of the cone. Despite the high temperatures near the surface, this represents a weak smoulder that will not be able to sustain itself after a certain depth, and will eventually reach extinction (approximately 50mm at 350 mins, in this case)

4.5.3Mass loss

The mass loss measurements are used to further interrogate the smouldering behaviour of the hemp-lime insulation. The mass loss rate (MLR) rapidly reaches a wide peak of 1.4 $g \cdot s^{-1} \cdot m^{-2}$ on ignition, as is characteristic of a charring material (Spearpoint and Quintiere 2000), as can be seen in Figure 4.8. The mass loss begins to decrease from 15 mins, as it continues to do so for the remaining duration of the test. The majority of the total mass loss (73% by 200 mins) is during the downward opposed smoulder, Regime I, despite the low temperatures recorded. This is because the initial propagation includes the pyrolysis process, where the majority of mass is lost. The subsequent Regime II and Regime III smoulders are solely char oxidation reactions and thus the mass loss is lower.

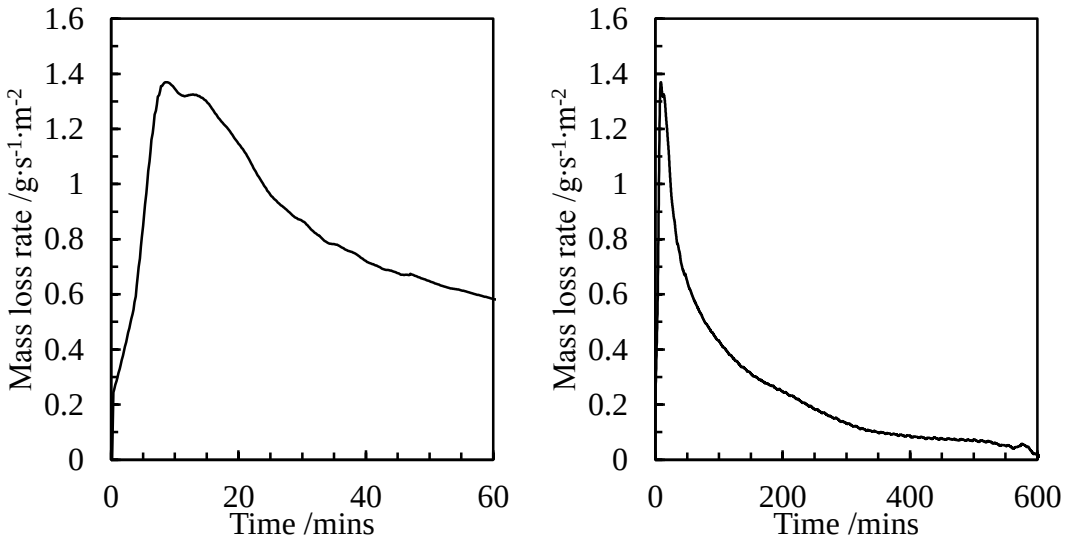

Figure 4.8 – Mass loss rate per unit area of hemp-lime insulation exposed to 8kW·m^{-2} showing (a) ignition and peak MLR (b) full duration of test.

A subtle drop in the MLR at 0.24 $g \cdot s^{-1} \cdot m^{-2}$ from 200 mins onwards signifies the end of Regime I and the transition to Regime II. This transition is more clearly identifiable at higher heat fluxes and the drop in MLR is more marked. By this point there is little remaining combustible material, which is reflected in the burning rate.

The rate of reactions and hence mass loss rate is highest when the heat losses are offset by the radiant heat of the cone calorimeter. The influence of the cone is weakened as the smoulder progresses downwards, and thus the burning rate also drops.

4.5.4 Gas emissions

The carbon monoxide yield holds a constant value around 0.082±0.003 $g \cdot g^{-1}$ during Regime I. This suggests a constant rate of combustion reactions and a clear regime which was not as evident in the mass loss measurements. The duration of this approximate plateau is from 30 to 235 mins (Figure 4.9). This matches almost exactly the thermal wave to reach the rear surface, as noted earlier in *Smouldering propagation regimes* (Section 4.5.2). After secondary ignition and the initiation of Regime II, the CO yield becomes erratic due to the very low MLR and CO emissions. In some of the tests the CO yield increases to a broad peak of 0.2 $g \cdot g^{-1}$ for the remaining propagation. This suggests that there in inadequate oxygen able to reach the reaction front, and thus an increased amount of CO as opposed to CO_2 is generated. Additionally, a greater amount of CO is generated by the exothermic oxidation of char than during either the endothermic pyrolysis or the oxidation of cellulose. However, the MLR and CO yield in this region are so low that there is little confidence in the results beyond 400 mins and thus the results cannot easily be interpreted at this incident heat flux.

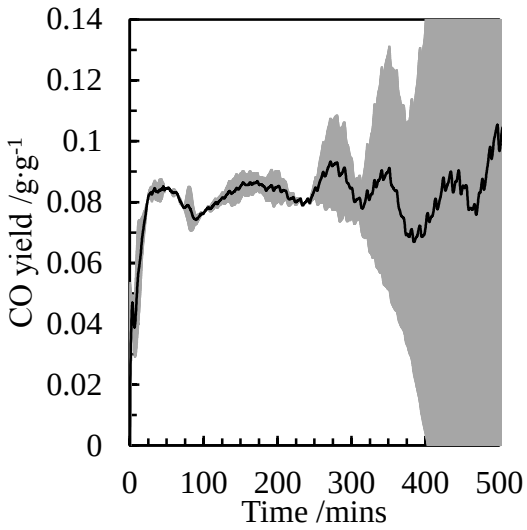

Figure 4.9 - CO yield of hemp-lime insulation for tests conducted at 8kW·m^{-2}. Results are truncated at 500 minutes since below this point the mass loss rate is too low to yield accurate values. Shaded area indicates standard deviation.

4.5.5 Visual evidence of residue

Specimens were left to cool and then a visual inspection was performed, as shown in Figure 4.10. A blackened char layer approximately 5mm thick exists at the top surface where the smoulder was not able to properly establish due to heat losses to the environment. This layer generally forms a shell around the entirely of the specimen, despite the radiant flux from above, and the insulation at the sides. The bottom 5mm of the specimen appears to be virgin and has not pyrolysed or combusted in the duration of the test. The comparatively cold ambient air is induced through this surface so the heat losses are highest, and thus a smoulder is not able to be sustained. This was previously seen in the thermal evolution where the secondary smoulder was only capable of igniting in-depth, and not at the bottom surface.

Figure 4.10 – Remains of hemp-lime insulation tested at 8kW·m^{-2}. (a) View of top surface (b) splice sawed through sample.

The vast majority of the material is ash, with little remaining integrity. This confirms that the specimen reached burnout, despite the various modes of propagation. Extinction is reached when Regime II and Regime III meet at the centre of the specimen, and all combustible material is consumed.

Upon disturbance the ashes will collapse, which makes visual inspection difficult. In a building this may have more serious repercussions. The collapse of material will reveal unexposed inner layers allowing the potential for a fire to spread more rapidly.

4.6 Discussion and analysis

The full results across all incident heat fluxes are discussed below, with additional analysis to rigorously interrogate the smouldering behaviour of hemp-lime insulation.

4.6.1Ignitability

The time to smouldering ignition and typical plot of $1/\sqrt{t_{ig}}$ used in the flaming ignition of solids is shown below in Figure 4.11. The classic ignition of solids theory (Torero 2008) is formulated for use with flaming, however, it was applied in this case to smouldering. The ignition theory considers an energy balance at the surface of the sample but due to in-depth ignition this is partially violated. Despite this, there was good agreement and the experiments appeared to follow the theory well. This theory has also previously been successfully applied to glowing and flaming ignition of wood by Boonmee and Quintiere (2002), and is also corroborated by Rein (2016).

The ignition theory is shown to have good agreement for the smouldering of hemp-lime over the range of heat fluxes studied. The smouldering ignition temperature derived from this theory, 341°C, is higher than the exothermic oxidation of the cellulose in the hemp as was discovered using the thermogravimetric analysis, which was found to have an onset at

200.55±6.21°C, and maximum decomposition rate at 253.93±5.89°C. The ignition properties of hemp-lime insulation are collated in Table 4.1.

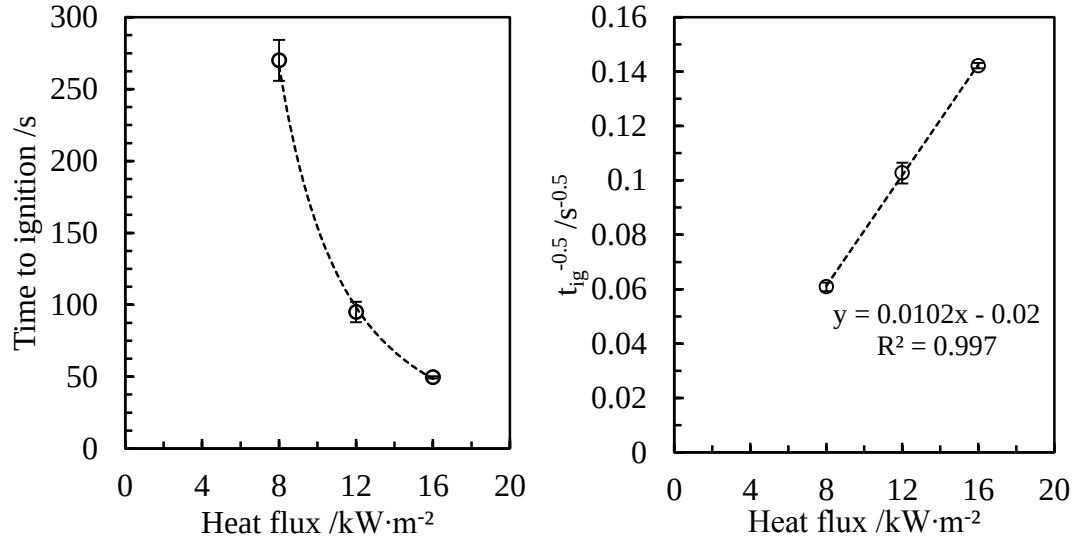

Figure 4.11 - (a) Time to smouldering ignition over a range of heat fluxes (b) $1/\sqrt{t_{ig}}$ according to ignition theory of solids. Error bars represent the standard deviation.

Table 4.1 – Summary of ignition properties in the cone calorimeter for hemp-lime.

Material	**Critical heat flux for smouldering ignition**	**Thermal inertia**	**Smouldering ignition temperature**
-	$kW \cdot m^{-2}$	$kJ^2 \cdot m^{-4} \cdot K^{-2} \cdot s^{-1}$	°C
Hemp-lime	8.0±2.5	0.119	341

The critical heat flux for smouldering ignition of hemp-lime insulation was found to be 8.0±2.5 $kW \cdot m^{-2}$. This is similar to 100mm foam specimens tested by Hadden *et al.* (2012) which had a critical heat flux of 8 to 9 $kW \cdot m^{-2}$. It is lower than common household items including PMMA, 11 $kW \cdot m^{-2}$, and wood, 12 $kW \cdot m^{-2}$ (Drysdale 1999), emphasising the ease of ignition.

Hemp-lime has a low thermal inertia characteristic of many insulation materials. Compounded with the lower temperature required for the onset of the endothermic pyrolysis of both hemicellulose and cellulose this represents a potential hazard. Low thermal inertia has long been associated with rapid ignition times, and rapid burning rates (Drysdale 1985). This is exacerbated when the key risk is smouldering which requires less energy than traditional flaming.

4.6.2Spread rate

Smouldering velocities can be used to interpret the different regimes and their relative importance. Each regime requires a different calculation method which can be extracted from the temperature history. For Regime I, the exothermic peak corresponding to the oxidation of cellulose, obtained using TGA, is used as the critical point. For both the Regime II and Regime

III smoulders the peak temperature is instead used. The calculated smoulder velocities are collated below in Table 4.2.

Table 4.2 – Average smoulder velocities (μm·s^{-1}) for various regimes and zones. Errors indicate standard deviation.

Smouldering regime	**Depth**	**Incident heat flux**	
-	mm	8 kW·m^{-2}	16 kW·m^{-2}
	10-50	15.9±8.4	16.9±11.4
Regime I	60-90	6.4±2.1	8.7±3.7
	10-90	11.7±7.8	13.2±10.0
Regime II	60-90	4.4±2.2	2.3±0.3
Regime III	10-50	3.3±1.9	6.2±6.2

The initial Regime I smoulder records the highest smoulder velocities throughout the depth of the material. This progresses rapidly downward through the specimen whilst the Regime III smoulder progresses at only a fraction of the rate. For 8kW·m^{-2}, the average velocity over the first 50mm is 15.9±8.4μm·s^{-1} for Regime I compared to 3.3±1.9μm·s^{-1} for Regime III in the same region (Figure 4.12). As the Regime I smoulder propagates downward away from the cone its velocity decreases, suggesting that the cone strongly influences the spread rate in this regime.

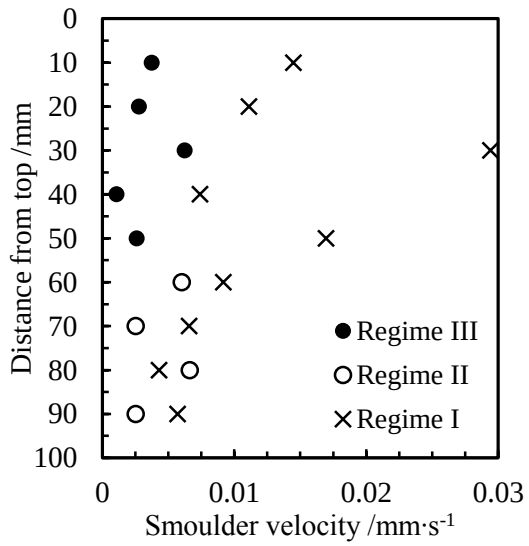

Figure 4.12 - Smoulder velocities for the various regimes at an incident heat flux of 8kW·m^{-2}.

The average smoulder velocity for the Regime II upward forward flow propagation is 4.4±2.2μm·s^{-1} which is around 33% faster than the Regime III smoulder at the top of the specimen. For the same region – the bottommost 40mm – the initial Regime I oxidation has an average velocity of 6.4±2.1μm·s^{-1}.

The presence of the cone calorimeter has the largest influence on the downward opposed Regime I smoulder. This is evident from the higher velocity measurements closer to the

surface, which then decrease as the distance from the cone increases. Despite this, increasing the incident heat flux does not clearly or substantially increase the smoulder velocities near the surface (Figure 4.13). This may be because the buoyancy-induced oxidiser flow does not diffuse rapidly enough to react with the char generated by the radiant heat flux. There is additional evidence for this in the bottom half of the specimen where the velocity is higher at a lower incident heat flux of 8kW·m^{-2} (4.4±2.2μm·s^{-1}) than at 16kW·m^{-2} (2.3±0.3μm·s^{-1}).

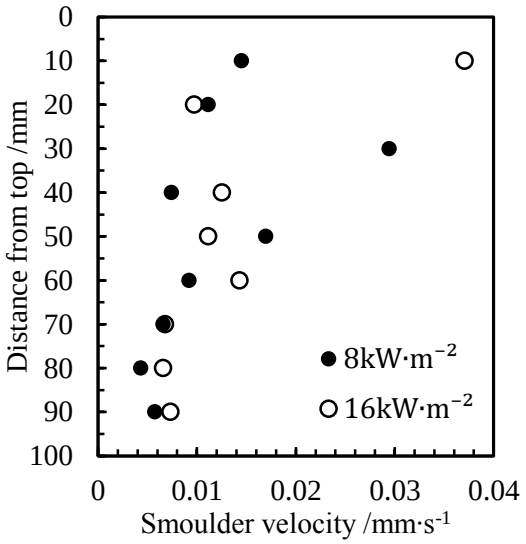

Figure 4.13 - Smouldering velocity of the Regime I downward opposed flow oxidation for two incident heat fluxes.

Regime II is the only smoulder where a slower velocity is recorded at a higher incident heat flux. The additional energy during Regime I from the cone may allow the smoulder to reach a higher temperature and react with a greater amount of lignin. This then leaves less combustible material remaining for the subsequent Regime II smoulder which allows the smoulder at the lower incident heat flux to propagate more rapidly.

The smouldering velocities measured are substantially lower than for other materials without forced oxidiser flow. Torero (1992) experimentally determined smoulder velocities for open-cell polyurethane foam materials of 60μm·s^{-1} for downward propagation, and 40μm·s^{-1} for upward propagation under buoyancy induced convection. The same author observed velocities up to 1.5mm·s^{-1} under forward forced flow conditions. Velocities for other materials and substances include 28 to 42μm·s^{-1} for a human faeces surrogate (Yermán *et al.* 2015), and 75 to 250μm·s^{-1} for peat under forced flow conditions (Pironi *et al.* 2009).

4.6.3Mass loss

As a charring material the mass loss rate three key parameters – time taken to reach peak (Figure 4.14a), peak magnitude (Figure 4.14b), and decay phase (Figure 4.15). Using a plot of incident heat flux against $1/\sqrt{t_{peak}}$ a strong linear relationship is shown. The peak mass loss rate is also shown to increase proportionally with the external heat flux provided by the cone. The

peak will be reached shortly after ignition when the smoulder is initiated near the surface and the heat losses are significantly reduced by the radiant flux from the cone.

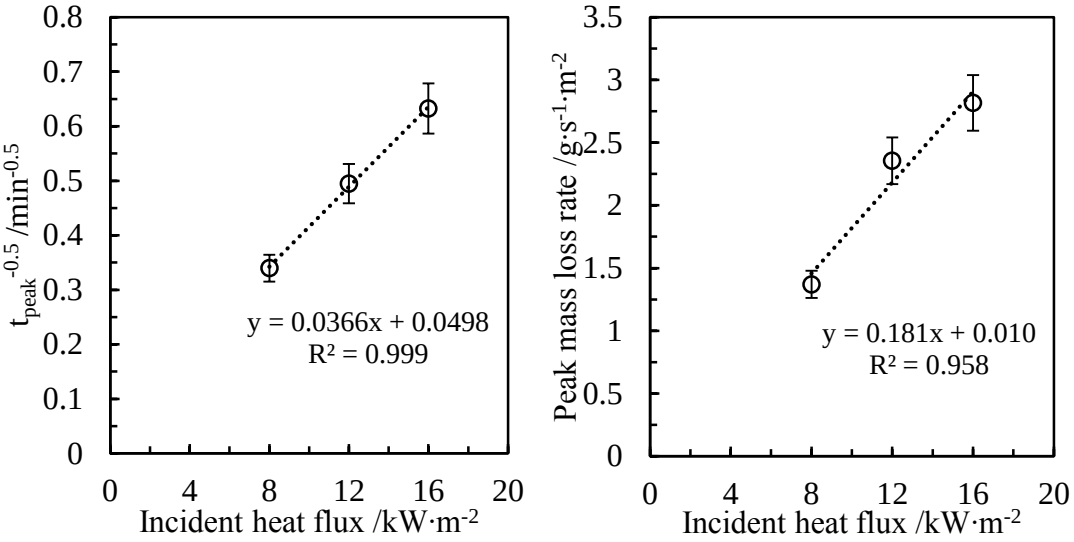

Figure 4.14 - (a) Peak mass loss rate, and (b) $1/\sqrt{t_{peak}}$ both as a function of incident heat flux. Standard deviation is calculated at 12kW·m^{-2} and extrapolated as error percentage to other incident heat fluxes.

The burning rate encapsulates a variety of processes including both endothermic pyrolysis and exothermic oxidation (Harmathy 1975). As specimens were oven dried, there are no dehydration reactions. An increased incident heat flux may initially increase the rate of pyrolysis, as will be reflected in the mass loss rate, but does not necessarily indicate an increased rate of combustion reactions. Increased oxidiser flow is required to be able to react with the increased amount of char generated. However, in this case the air is naturally induced by buoyancy and thus relatively limited. This explains why the mass loss rate increases with incident heat flux, but is not reflected in the previously calculated spread rates. In cases with forced oxidiser flow there may be sufficient oxygen to react with the char and the smoulder will propagate substantially faster.

Following on from the peak the mass loss rate will decrease until eventual extinction. After only five minutes of test initiation both the 16 and 12kW·m^{-2} specimens the MLR are near identical the entirety of this duration (Figure 4.15). For 8kW·m^{-2} this takes 14 mins until the same MLR is reached as the two other incident fluxes. After this time an insulating char layer forms which reduces heat and mass transfer from the cone. The smoulder then becomes more dependent on the energy generated through oxidation to drive the pyrolysis front forward. The presence of the cone, regardless of the heat flux, will reduce the heat losses at the top surface.

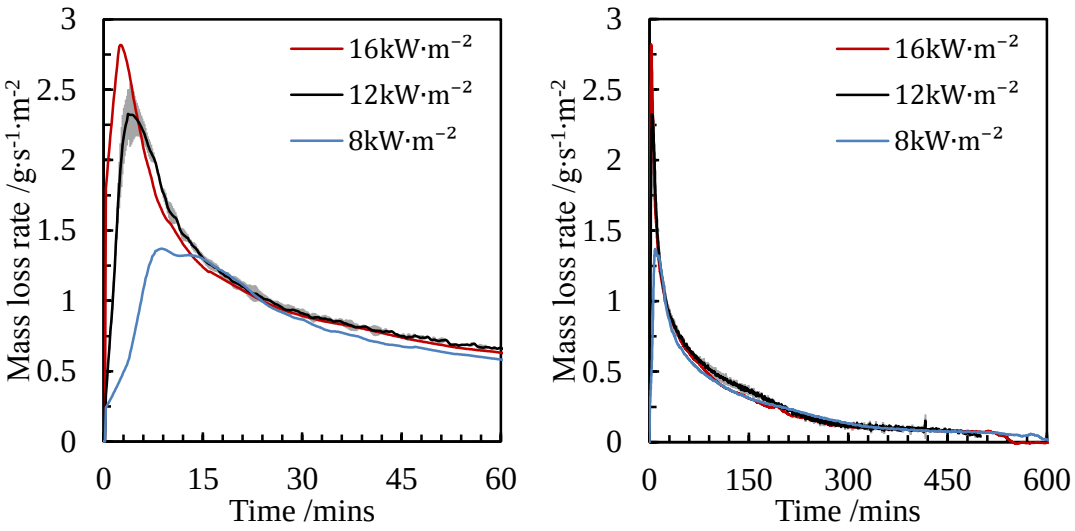

Figure 4.15 – (a) Mass loss rate of hemp-lime insulation specimens exposed to 8, 12 and 16kW·m^{-2} showing only the early period of the test and (b) peak mass loss rate as a function of incident heat flux. Error bars illustrating standard deviation are given for an incident heat flux of 12 kW·m^{-2}.

The total mass lost is relatively constant at 24.7±1.1% regardless of the level of incident heat flux exposure (Figure 4.16). Previous TGA experiments identified that hemp shivs and fibres lose 75% of their mass when heated in an oxidative environment, and the final 25% is composed of ash. Extrapolation of the total mass lost in these tests show that hemp accounts for 33% of the total mass. The final mix used during material synthesis was one part hemp to two parts hydraulic binder. This shows that the material tested in the cone reached complete burnout, otherwise the amount of mass lost during the test would be lower.

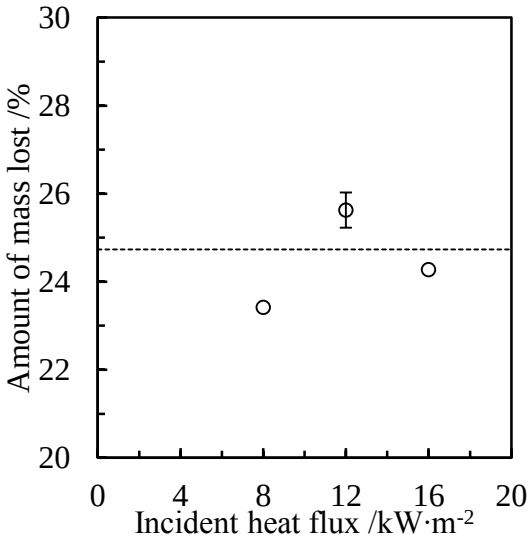

Figure 4.16 – Total amount of mass lost, where the average is indicated by a dashed line.

4.6.4 Thermal evolution

The temperature evolution as the smoulder propagates through the specimen for an incident heat flux of 8kW·m^{-2} is shown below in Figure 4.17. This has been split into two parts: the propagation downwards until secondary ignition at the bottom (Figure 4.17a), and the propagation upwards following the secondary ignition (Figure 4.17b). The two downward smouldering fronts can be identified from the profiles. The downward opposed flow smoulder (Regime I) propagates through the specimen and reaches the rear surface at around 180 mins. This smoulder is denoted by a profile reaching the oxidation temperature of cellulose in the range of 200 to 325°C (illustrated by the first shaded area in red in Figure 4.17). The downward forward flow smoulder (Regime III) can be seen in the profiles up to 130 mins in the top 30mm of the specimen, denoted by peak temperatures in the region of 567±4°C. In both instances the combusted material remains at a moderately high temperature due to both the hot post-combustion gases and the radiant heat provided by the cone.

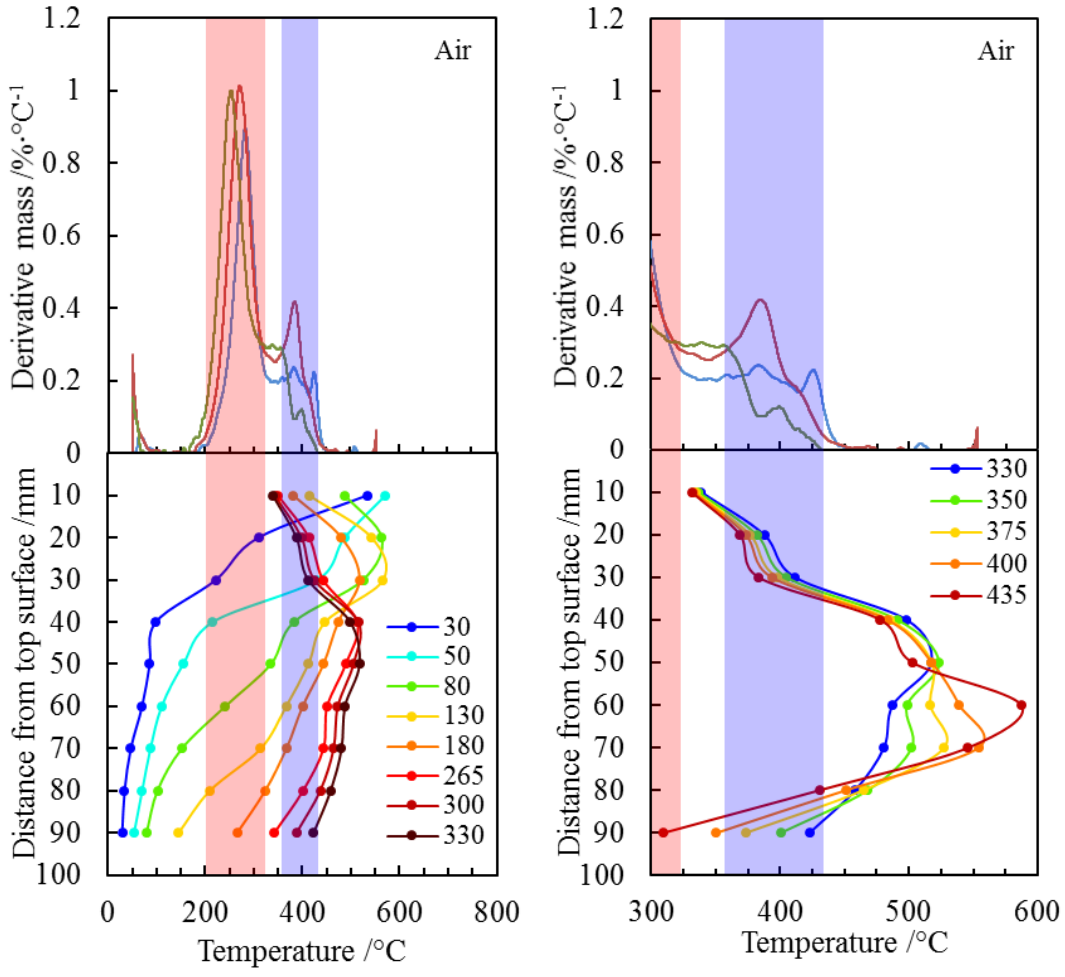

Figure 4.17 – TGA (top) and temperature depth-profiles (bottom) of hemp-lime insulation exposed to 8kW·m^{-2} during (a) Regime I, and (b) Regime II. Legends are in mins. Temperature-depth plots are non-linear piecewise fits.

The secondary ignition and subsequent upward forward flow smoulder (Regime II) are evident in Figure 4.17b. The smoulder is initiated in the area of 70 to 80mm and can be seen as it propagates upwards to 60mm. The progress of the smoulder can be identified from the increasingly large peak temperatures reached as the oxidation front propagates upwards. The environmental effects at 90mm are evident as the lack of a substantial char layer or insulation cause high heat losses. Furthermore, the ambient air entering the bottom surface will have a cooling effect. This causes the temperature to drop and a smoulder cannot be sustained in this region.

The second shaded area in blue represents the temperature required for char oxidation. This is reached during the Regime II smoulder, but the temperature during Regime I is too low. Thus, the initial downward smoulder represents a combination of the endothermic pyrolysis front generating char, and the exothermic oxidation of cellulose. The subsequent upward smoulder is then the exothermic oxidation of the char generated during Regime I. Regime III also represents the char oxidation of the material generated in the top part of the specimen in Regime I, but in the downward direction. Combustion of lignin occurs over a large range and will overlap with each of the other reactions.

The two main smoulders, Regime I and Regime II, show distinctly different behaviour. In the upward Regime II smoulder, the reaction front is thin but reaches significantly higher temperatures (560°C compared to only 325°C). Despite the high temperature combustion this represents a weak smoulder due to the narrow reaction zone. In contrast, the downward Regime I smoulder propagates more rapidly, has a thicker reaction front and lower temperatures. This is due to the greater quantities of fuel and carbon rich char available, and the lower temperature required for exothermic oxidation.

The thermal evolution and TGA degradation for an incident heat flux of 16kW·m^{-2} are displayed in Figure 4.18. The increased radiant flux at the surface allows a stronger ignition, and thus the pyrolysis and cellulose oxidation fronts are able to propagate more rapidly even outside the influence of the cone. After the reaction front reaches the bottom surface at 235 mins (Figure 4.18a) there is a lengthy delay before the secondary ignition to be initiated. This occurs within the period of 300 to 330mins and at a depth of around 80mm (Figure 4.18b). The heat losses between 90 and 100mm are still too significant for the smoulder to be capable of initiating close to the rear surface, and must instead still take place at depth.

The time to reach complete burnout, and thus extinction, are comparatively similar despite the change in incident heat flux. The initial Regime I propagation is more rapid at 16kW·m^{-2}, but there is a substantial delay in establishing the secondary ignition at the rear surface and hence the subsequent Regime II propagation is also delayed. This shows that the close proximity of Regime I to the cone calorimeter causes a large dependence on the incident heat flux but despite this will have a lessened effect on the time to secondary ignition. This illustrates that Regime I is assisted smouldering supported by the radiant heat from the cone, but Regime II is more akin to self-sustaining.

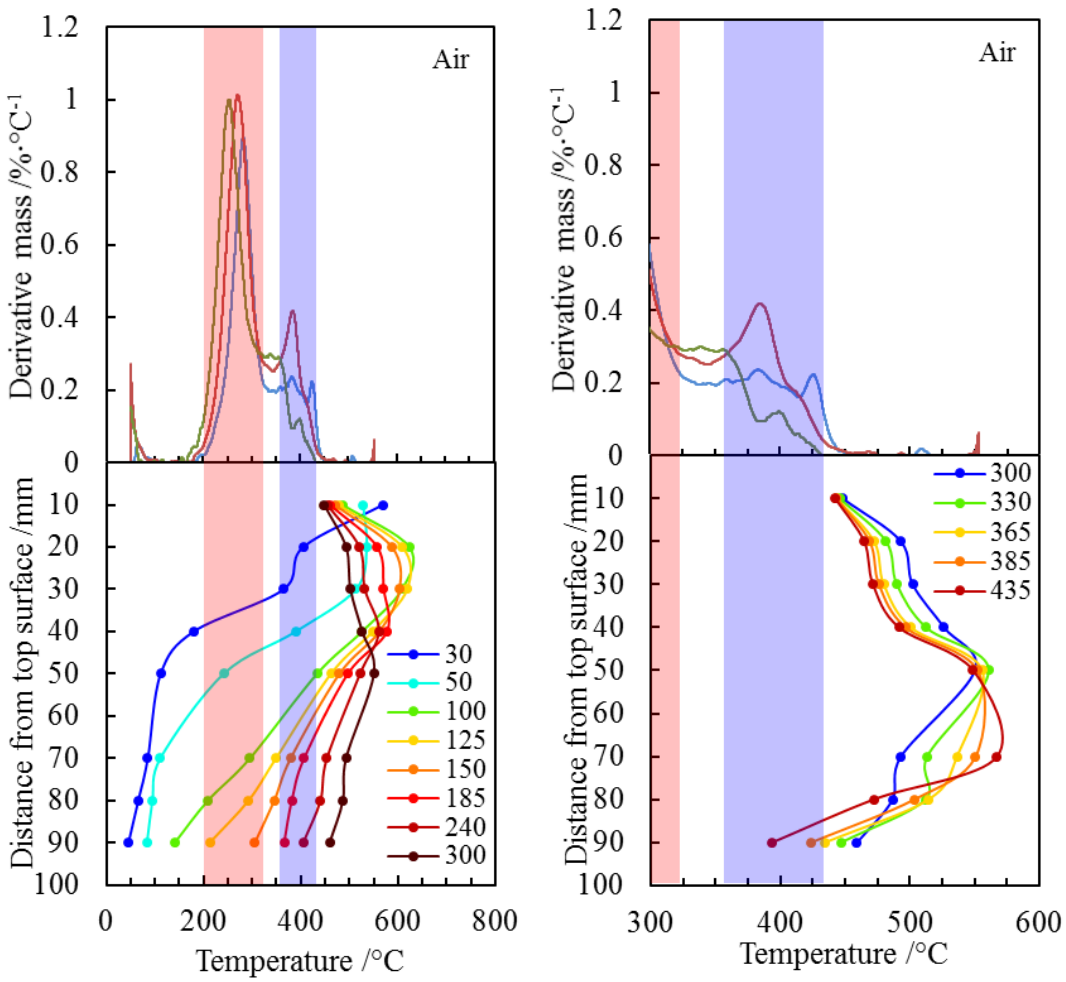

(a) (b)

Figure 4.18 – TGA (top) and temperature depth-profiles (bottom) of hemp-lime insulation exposed to 16kW·m^{-2} during (a) Regime I, and (b) Regime II. Legends are in minutes. Results at 60mm have been truncated due to instrumentation issues. Temperature-depth plots are non-linear piecewise fits.

Regime III experiences moderately higher temperatures (peaks of 620±3°C at 16kW·m^{-2} compared to 567±4°C at 8kW·m^{-2}) when exposed to higher heat flux from the cone due to the additional energy used to fuel the reactions. Despite this, its propagation rate remains relatively similar in both cases. A stronger smoulder is established at a higher heat flux and the reaction zone spans a larger zone. This helps reduce the heat losses which enhance the rate of reactions in Regime I.

4.6.5Gas emissions

The CO yield (Figure 4.19) for Regime I remains broadly constant and largely independent of heat flux. The deviation over the whole of the regime and across all heat fluxes is less than ±10%. The transition from Regime I to Regime II is noted by the end of the plateau. The CO yield of the char oxidation reaction is higher than the exothermic oxidation of cellulose

(Kashiwagi and Nambu 1992), which is reflected by an increase in CO yield as the smoulder ignites at the bottom and transitions to Regime II. The change in incident heat flux has some influence on this regime, but there is no proportional relationship.

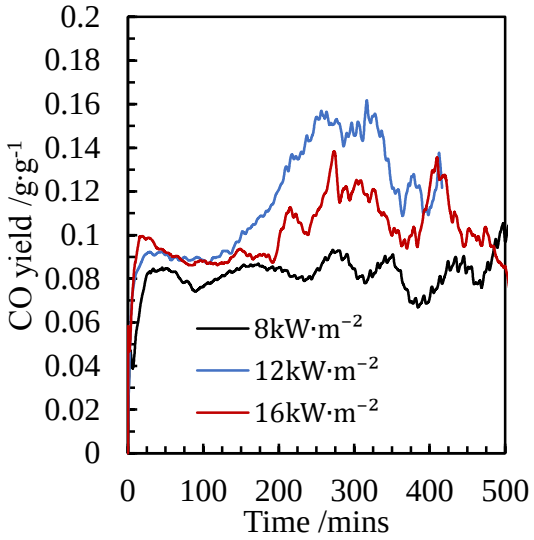

Figure 4.19 - CO yield over the duration of tests at an incident heat flux of 8, 12 and 16 kW·m^{-2}. Results are averaged from two tests each.

The char oxidation during Regime II represents the greater risk to human health due to its higher yield. This is despite the fact that the reaction front is shown to be relatively weak, and propagate at comparatively slow velocities. The yield in this regime is partially affected by the incident heat flux, where there is a 100% increase from 8 to 12kW·m^{-2}. The long duration of smouldering tests also means that the total CO released over the full duration will be a substantial risk when compared to traditional flaming materials.

4.6.6Dynamics of the smouldering front

The thermal evolution over time has previously shown higher temperatures at depth compared to the top surface adjacent to the cone. This confirms the presence of a smoulder and not simply the propagation of an endothermic pyrolysis front. Furthermore, in trial tests where the bottom was sealed and the smoulder was constrained to only Regime III conditions (downward forward flow) the smoulder was unable to sustain itself and led to extinction before reaching the bottom surface.

The smoulder in Regime II illustrates that hemp-lime insulation is capable of sustaining combustion reactions with little outside influence. Torero (1992) has noted for foam materials that ignition only occurs in a narrow range with very specific conditions. The ability of hemp-lime to ignite at low heat fluxes with no forced air flow, and no previously built up char layer, illustrate that it can ignite with relative ease. The propagation without forced air flow is slow, but can sustain when exposed to low radiant heat fluxes.

The potential for transition to flaming exists but is currently very poorly understood (Rein 2016) and would require additional study. As part of the current research some testing was done with a pilot in the cone and the potential for flaming was confirmed. However, due to its short residence times it was identified that smouldering is the most crucial fire risk relating to the design of buildings. Quantification of the smouldering behaviour provides the basis for mitigating the overall fire risk. The main scenario in which smouldering represents the largest risk is through this transition to flaming, but if the risk relating to smouldering is mitigated then this hazard can be effectively eliminated.

4.7 Concluding remarks

This chapter has explored the smouldering behaviour of a hemp-lime insulation material through the use of bench-scale calorimetry.

- An approach for evaluating key characteristics relating to the fire risk associated by hemp-lime insulation has been outlined. This method provides the basis for developing a novel framework to quantify their behaviour which is not currently possible with existing standard fire test methods.
- The time to smouldering ignition and critical heat flux for smouldering ignition reveal that hemp-lime insulation is a highly ignitable material. It may be prone to ignite when exposed to low energy sources for extended periods and propagate undetected.
- The ignition theory of solids was found to be applicable despite the fact that smouldering combustion was the dominant mode of reactions. Strong agreement was found for a range of low heat fluxes, allowing the determination of the thermal inertia and smouldering ignition temperature.
- A novel testing methodology was developed for the investigation of rigid smouldering materials in the cone calorimeter. Through this method it was possible to evaluate smouldering behaviour in both an opposed downward smoulder and an upward smoulder within the same test configuration.
- A method for identifying the smouldering ignition of materials was proposed based on CO emissions. This is capable of detecting ignition in-depth of the specimen, which is not possible using the existing glowing combustion visual observation criterion.
- The residual mass and TGA data were used to identify that the final composition of the material was one third ash, and two thirds hydraulic binder. This confirms that the specimen reached complete burnout and no combustible material remained by the end.
- The dependence of the smoulder behaviour on the incident heat flux has been ascertained by testing over a range of 8 to 16kW·m^{-2}. This found that the spread rate of the initial downward opposed oxidation was increased with incident heat flux, but the secondary smoulder initiated at the rear surface was largely independent.
- Ignition occurs within the depth of the material and requires a char layer to be built upon before a smoulder can be sustained. This was found at each heat flux, and at both the top and bottom surface. In the event of a fire, this increases the difficulty in identifying the initiation of smouldering combustion.

- CO yield remains constant during the endothermic pyrolysis and exothermic oxidation of cellulose, and is independent of the heat flux. However, higher rates are noted during the exothermic oxidation of char and this represents the greatest hazard to human health.

Some of the key numerical findings for this specific hemp-lime insulation material are summarised below in Table 4.3.

Table 4.3 – Summary of properties for hemp-lime insulation.

Parameter		**Material property**	
Critical heat flux ($kW \cdot m^{-2}$)		8.0±2.5	
Smouldering ignition temperature (°C)		341	
Apparent thermal inertia ($kJ^2 \cdot m^{-4} \cdot K^{-2} \cdot s^{-1}$)		0.119	
		Heat flux dependent	
		$8kW \cdot m^{-2}$	$16kW \cdot m^{-2}$
Time to ignition (s)		270±14	50±7
Spread rate ($\mu m \cdot s^{-1}$)	Downward opposed flow	11.7±7.8	13.2±10.0
	Upward forward flow	4.4±2.2	2.3±0.3
Peak mass loss rate ($g \cdot s^{-1} \cdot m^{-2}$)		1.37±0.11	2.82±0.22
Total mass lost (%)		23.4±1.1	24.3±1.1
Time to extinction (mins)		600	540
CO yield ($g \cdot g^{-1}$)	Regime I	0.082±0.003	0.091±0.004

5 Smouldering combustion of hemp-lime insulation containing microencapsulated Phase Change Materials

5.1 Summary

Microencapsulated phase change materials (PCMs) have been added to the previously characterised innovative construction material known as hemp-lime insulation. The combined behaviour provides a unique opportunity into understanding how the addition of PCMs can modify the behaviour of a combustible substrate. In this chapter, the fire risks associated with PCM enhanced hemp-lime insulation are quantified and the performance is compared with ordinary hemp-lime. The addition of PCMs is found to increase the heat of combustion, thereby increasing the temperature and rate of reactions, leading to more rapid burning rates. The ignition temperature is reduced due to the exothermic oxidation of paraffin wax occurring before the oxidation of cellulose. This lowers the critical heat flux from 8.0kW·m^{-2} to 3.0kW·m^{-2} and represents an increase in the ignitability. Furthermore, the lower ignition temperature and additional energy generation allows the ignition to occur closer to the surface where heat losses are higher. PCMs are shown to be a more energetic material which increase the strength of the reactions, as indicated in the width of the reaction fronts. The ignitability and energetic nature of PCMs are identified as the two most important fire risks associated with these materials.

5.2 Introduction

PCMs and hemp-lime insulation share similar goals in terms of sustainability and achieving energy savings. For this reason, the materials have been combined to quantify the change in fire risk associated with the addition of PCMs to a combustible substrate. The new material is evaluated using the same methodology in the cone calorimeter (ASTM International 2014, British Standards Institution 2015a) that was developed for hemp-lime insulation.

The aim of this chapter is to investigate the smouldering combustion behaviour of PCM enhanced hemp-lime insulation. This is achieved through the following objectives:

- Characterise the smouldering behaviour under a variety of conditions using previously established methodology;
- Compare the behaviour to ordinary hemp-lime insulation to quantify the change in fire risk;
- Highlight the key fire risks associated with the addition of PCMs.

5.3 Methodology

The method for synthesising material and the subsequent testing follow the same basis as testing for hemp-lime insulation, but with some additional modifications to accommodate the PCM.

5.3.1Material synthesis

The final composition of the mix was 16% hemp shivs, 28% lime binder, 42% water, and 13% microencapsulated PCM. This is approximately equal to 1 part hemp, 1 part PCM, 2 parts binder, and 3 parts water, but with slight alterations to ensure a workable mix was produced.

Figure 5.1 – Photographs of (a) raw microencapsulated PCMs which have a powder-like appearance and (b) completed cube of PCM enhanced hemp-lime insulation (100mm by 100m and 100mm tall).

5.3.2Experimental approach

The experimental approach is identical to the previous hemp-lime insulation testing methodology.

5.4 Results and discussion

A characterisation of the PCM enhanced hemp-lime insulation was performed using the same metrics as for hemp-lime. A comparison of both materials was conducted as part of the characterisation process, and the associated fire risks are highlighted. Extensive reference is made to the previous chapter and so it is strongly recommended that it should be read first.

5.4.1Ignitability

Upon exposure to the incident heat flux from the cone calorimeter the surface will begin to heat up. TGA previously identified that the lowest temperature exothermic reaction is the oxidation of evaporated paraffin wax which occurs at the autoignition temperature. This releases sufficient temperature to reach the exothermic oxidation of the cellulose contained in the hemp and initiate solid phase combustion reactions. Glowing combustion was evident at the surface of PCM enhanced hemp-lime insulation for both 8 and 16kW·m^{-2} (Figure 5.2).

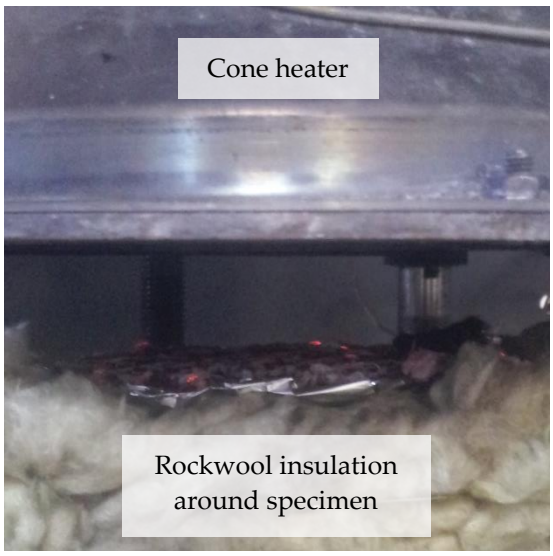

Figure 5.2 – Glowing embers observed during testing of PCM enhanced hemp-lime insulation at 16kW·m^{-2} at ignition.

The low autoignition temperature of the paraffin wax was sufficient to lower the time to ignition across all heat fluxes, as well as decrease the critical heat flux. This was due to the fact the temperature required to initiate the smoulder was lower and thus it can be reached more rapidly. In the case of the critical heat flux the difference in oxidation temperature between the PCM and the hemp was sufficient to decrease this from 8.0±2.5kW·m^{-2} down to 3.0±2.5kW·m^{-2}. The errors are based on the accuracy of the heat flux gauge, and are in agreement with literature on the measurement of low heat fluxes (Robertson and Ohlemiller 1995).

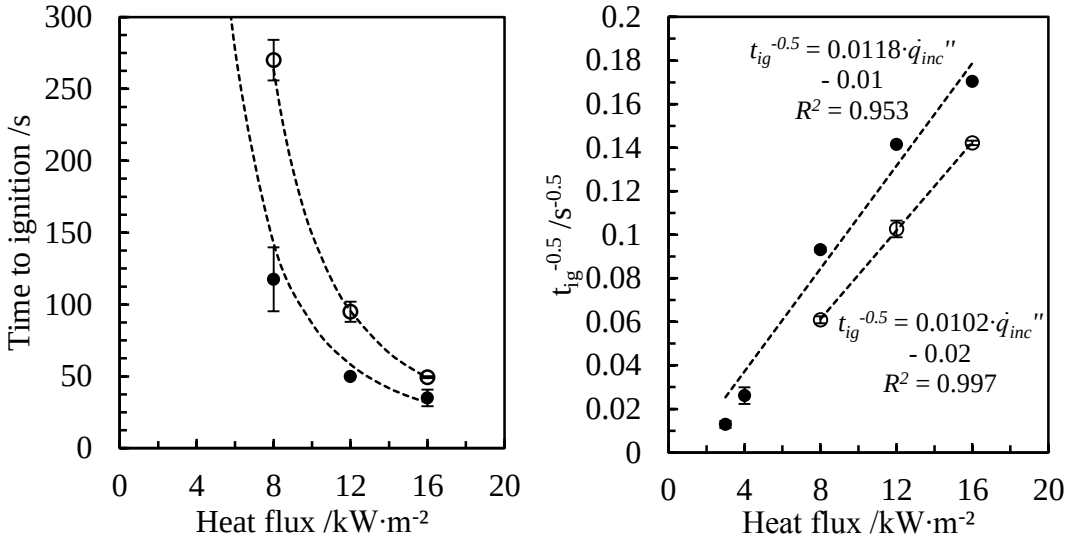

Figure 5.3 - (a) Time to ignition against incident heat flux and (b) incident heat flux, $\dot{q}_{inc}''$, against $1/\sqrt{t_{ig}}$ as used in the flaming ignition of solids theory. Hollow circles represent hemp-lime insulation, and black filled represent PCM hemp-lime.

The ignition mechanism is identified as the exothermic oxidation of paraffin wax, leading to the oxidation of cellulose. As the wax heats up and evaporates it expands and is able to escape the shell, then react with oxidiser. This agrees with analysis using a Scanning Electron Microscope (SEM) performed by Asimakopoulou *et al.* (2015).

The flaming ignition theory of solids (Torero 2016) still holds well for PCM enhanced hemp-lime insulation for smouldering combustion, as can be seen in a plot of incident heat flux against $1/\sqrt{t_{ig}}$ (Figure 5.3). A breakdown at very low heat fluxes where heat losses at the surface are overestimated is evident, as discussed in the literature (Mowrer 2005, Steinhaus 2010, Hidalgo-Medina 2015).

The properties derived from the ignition theory as well as the experimentally determined critical heat flux are collated in Table 5.1. An increase in the apparent thermal inertia is evident due to the addition of PCMs, which increase the specific heat capacity. This increases the time taken for the surface to heat up, however, the lower oxidation temperature of the PCM compared to the hemp still results in a lower ignition time.

Table 5.1 – Summary of ignition properties in the cone calorimeter for hemp-lime and PCM hemp-lime insulation.

Material	**Critical heat flux for smouldering ignition**	**Thermal inertia**	**Smouldering ignition temperature**
-	$kW \cdot m^{-2}$	$kJ^2 \cdot m^{-4} \cdot K^{-2} \cdot s^{-1}$	°C
Hemp-lime	8.0±2.5	0.119	341
PCM hemp-lime	3.0±2.5	0.353-0.625	141-181

The experimental determination of a representative value for the smouldering ignition temperature was attempted at the critical heat flux, $3kW \cdot m^{-2}$ (Figure 5.4). The surface temperature reached a value of 170°C by 165 mins. This is near the onset of the major exothermic oxidation and autoignition of the paraffin wax found in the TGA which was 188.82±0.05°C for a heating rate of $1°C \cdot min^{-1}$, with some evaporation of non-encapsulated wax prior to that point. The temperature then gradually increased over a period of ten minutes to 221°C at 175 mins before rapidly reaching 400°C, signifying ignition. These two increases are expected to represent the evaporation and oxidation of the paraffin wax, followed by the exothermic oxidation of cellulose sufficient to initiate a sustained smouldering front.

The addition of PCMs is shown to have drastic effect on the ignitability of hemp-lime insulation. The ignition time was lowered despite an increase in the apparent thermal inertia, owing to the lowered ignition temperature caused by the exothermic oxidation of the paraffin wax. This temperature is closely related to the autoignition of the paraffin wax contained with the PCM capsules.

The increased ignitability caused by the addition of PCMs represents a significant fire risk but can be mitigated through understanding the underlying mechanics, and quantification of the

condition. Designers can use this quantification of the fire risk to balance the potential energy savings from PCMs with the fire performance.

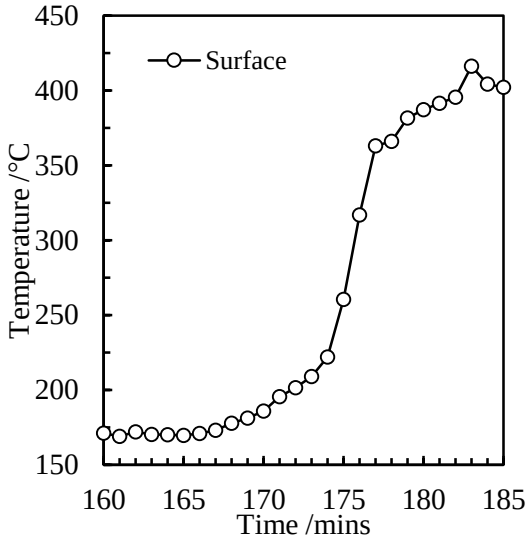

Figure 5.4 – Temperature increase recorded at approximate surface location for PCM hemp-lime insulation tested at 3kW·m^{-2}.

5.4.2Spread rate

The smouldering spread rates were calculated for the same three regimes identified in the previous chapter for both 8 and 16kW·m^{-2}. The calculation method remained the same for both Regime II (upward forward flow) and Regime III (downward forward flow) where the velocity was based on the time taken to reach the peak temperature in consecutive thermocouples. For Regime I, downward opposed flow, the exothermic oxidation of cellulose in the hemp shiv at 253.93°C for a heating rate of 1°C·min^{-1} in air was still used. This was because the testing of the PCM enhanced hemp-lime shiv showed good agreement to the isolated testing results, and the oxidation of the hemp marks the establishment of the smoulder as opposed to the exothermic oxidation of the paraffin wax.

The most rapid smouldering velocities were observed in the initial Regime I propagation in the bottom half of the specimen. Close to the top surface the spread rate remained largely independent of the incident heat flux. This shows that at this stage the rate of reactions were constrained by the diffusion rate of oxidiser from the bottom of the specimen. As the smoulder spread downwards a sufficient char layer was built up that at a higher incident heat flux the smoulder was able to propagate at an average rate of 32.3±19.0μm·s^{-1}.

Relatively constant smoulder spread rates were recorded in Regime II suggesting that the smouldering reactions were strong, despite their heterogeneity. As with Regime I, the smouldering in this regime was dependent on the initial heat flux despite the fact that it occurs far from the incident radiant heat.

Regime III had little influence on the overall behaviour of PCM hemp-lime insulation. It propagated at a relatively slow rate for both heat fluxes compared to the other regimes, and only propagated a small distance before the specimen reached burnout. This was partially due to the fact that the smouldering velocities in PCM hemp-lime insulation were more rapid than in ordinary hemp-lime, and thus the smouldering front was able to propagate downwards and back upwards further before meeting the Regime III smoulder at 30mm, and extinguishing due to lack of fuel.

An illustration of the spread rates as a function of depth is given in Figure 5.5, and the average velocities are collated in Table 5.2. More detailed analysis and comparison with ordinary hemp-lime insulation are given below.

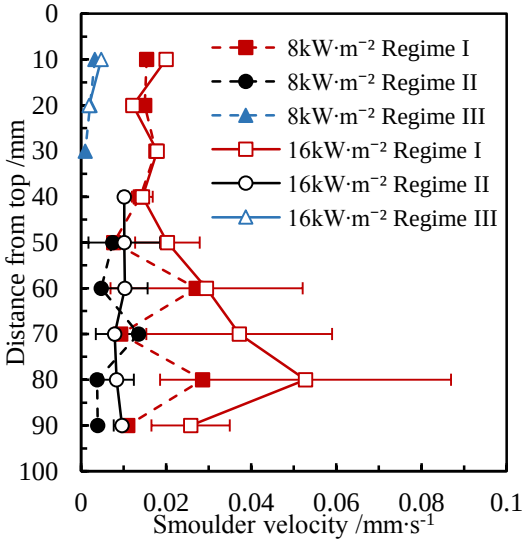

Figure 5.5 – Smoulder spread velocities for PCM hemp-lime insulation as a function of depth for two heat fluxes and each regime.

Table 5.2 – Average smoulder velocities (μm·s^{-1}) for various regimes and zones. Errors indicate the standard deviation.

Smouldering regime	**Depth**	**Incident heat flux**	
-	mm	8 kW·m^{-2}	16 kW·m^{-2}
	10-40	15.4±1.5	15.5±3.3
Regime I	50-90	16.7±10.2	32.3±19.0
	10-90	16.2±7.3	25.8±17.0
Regime II	40-90	6.7±4.1	9.4±3.6
Regime III	10-30	2.1±1.1	3.3±2.0

The behaviour in the Regime I downward opposed flow smoulder shows that PCMs can fundamentally change the behaviour of substrate materials. In ordinary hemp-lime insulation the Regime I behaviour up to a depth of 40mm was strongly affected by the incident heat flux from the cone, and the most rapid spread rates were recorded in this area (Figure 5.6). As the

smoulder approached the bottom (60 to 90mm) the spread rate dropped to 6.4±2.1μm·s^{-1} at 8kW·m^{-2}, or 8.7±3.7μm·s^{-1} at 16kW·m^{-2}. In PCM hemp-lime insulation the behaviour was instead the reverse. The propagation was initially diffusion limited near the cone and then as the reaction front spread to the bottom half of the specimen the smoulder accelerated before reaching the bottom surface.

The increase in spread rate is due to both the decreased ignition temperature, as discussed in the previous section, as well as the additional energy provided by the exothermic oxidation of the paraffin wax. This allows virgin material to be heated to the oxidation temperature of the paraffin wax, which quickly leads to the pyrolysis and oxidation of the cellulose.

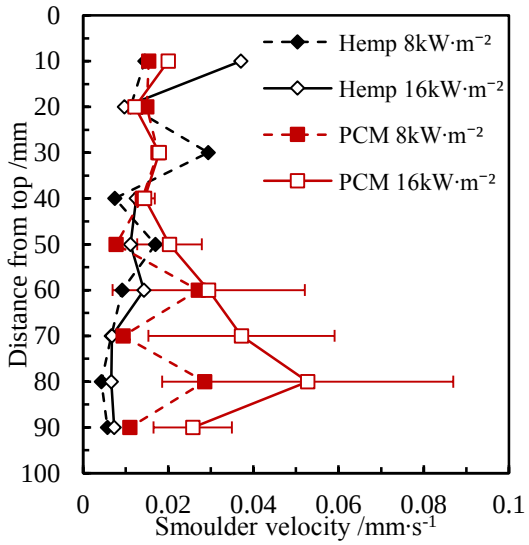

Figure 5.6 – Spread rate as a function of depth for both hemp-lime insulation (diamonds) and PCM hemp-lime (squares) for 8kW·m^{-2} (filled symbols) and 16kW·m^{-2} (hollow symbols) for Regime I.

Regime II represents a key area in characterising the smouldering behaviour since the assistance from the heat of the cone is diminished. The average smouldering velocity was increased from 4.4+2.2μm·s^{-1} (hemp-lime) to 6.7±4.1μm·s^{-1} (PCM hemp-lime) at 8 kW·m^{-2}, and from 2.3+0.3μm·s^{-1} to 9.4±3.6μm·s^{-1} at 16kW·m^{-2} (Figure 5.7). The paraffin wax evaporates at a relatively low temperature during Regime I yet despite this its effect is still evident in an increase of the smouldering velocity in Regime II. It is hypothesised that the greater energy released by the paraffin wax during Regime I permits and maintains higher temperatures in the specimen. This allows the energy from char oxidation to instead be used to fuel reactions instead of heating material upstream from the reaction front. The net result is increased temperatures and increased rate of reactions and hence increased smouldering velocity.

The smoulder was also able to propagate an additional 20mm further up through the specimen when PCMs were included. This was due to the more rapid velocity allowing the smoulder to spread further before meeting the downward Regime III smoulder and reaching

burnout. This represents an increase of 50% in the distance which the smoulder has propagated in this regime.

The increase in smouldering velocity due to the addition of PCMs highlights the change in fire risk, even away from the influence of the cone heater. A stronger smouldering front can be established at ignition which can propagate into areas where assistance is minimal and still maintain strong combustion reactions.

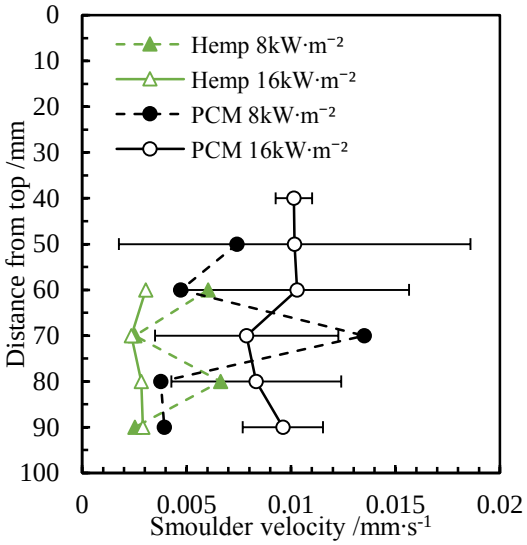

Figure 5.7 – Spread rate as a function of depth for both hemp-lime insulation (triangles) and PCM hemp-lime (circles) for 8kW·m^{-2} (filled symbols) and 16kW·m^{-2} (hollow symbols) for Regime II.

The smoulder velocities in Regime III were substantially lower than anywhere else. The low spread rates meant that the smoulder was only able to propagate 20 to 30mm before the specimen reached burnout (Figure 5.8), and in some instances no Regime III smoulder was observed.

The velocities were also slower than in ordinary hemp-lime insulation. The increased burning rate in Regime I and Regime II produce more post-combustion gases, which reduce the amount of oxidiser which can be induced through the top of the specimen. The preference is instead for buoyancy-induced cold air from the bottom which diffuses upward to the reaction front. This constrains the amount of oxygen able to react with the hot char, and thus the smoulder is of little consequence.

The low smouldering velocities and little proliferation mean that this regime does not represent a significant fire risk. The behaviour of PCM hemp-lime insulation is more adequately characterised in Regimes I and II. It is not expected that the smoulder would be capable of sustaining itself given that the environment is highly oxygen limited and the peak temperatures and velocities decrease as the smoulder propagates in-depth. As such, the regime represents a scenario which is not indicative of high risk scenarios in buildings.

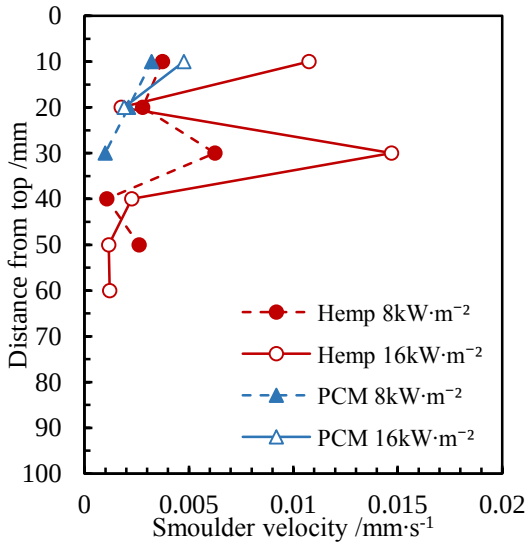

Figure 5.8 – Spread rate as a function of depth for both hemp-lime insulation (circles) and PCM hemp-lime (triangles) for 8kW·m^{-2} (filled symbols) and 16kW·m^{-2} (hollow symbols) for Regime III.

For PCM enhanced hemp-lime insulation the spread rates are most dramatically increased in the areas away from the cone, where its assistance is minimal. This is predominantly in the bottom 60mm of Regime I, and the entirety of Regime II. This highlights that PCMs will influence the areas which represent the greatest fire risk. The acceleration of the smouldering front as it propagates in-depth during Regime I highlights that the combustion is not at risk of extinction, and may be capable of sustaining itself outside the influence of the cone. Particularly with forced airflow this would represent the potential for a transition to flaming (Putzeys *et al.* 2008) would signify an important fire hazard.

5.4.3 Mass loss

The mass loss rate for PCM enhanced hemp-lime insulation shows a clear distinction between regimes as the initial reaction front reaches the rear surface (Figure 5.9). The mass loss rate for the three main heat fluxes studied – 8, 12, and 16kW·m^{-2} – remains the same following from the peak at ignition, as was the case with ordinary hemp-lime. Closer to the critical heat flux the time taken to reach this same stage was longer, in the order of 70 mins compared to 5 mins for 8kW·m^{-2}, and 2.5mins for 12kW·m^{-2} and 16kW·m^{-2}.

The difference in the behaviour of PCM hemp-lime and ordinary hemp-lime during Regime I (Figure 5.10a) can be clearly identified by an increase in the mass loss rate. The average mass loss rate at 15 mins was 1.94±0.06g·s^{-1}·m^{-2} for PCM hemp-lime compared to 1.29±0.03g·s^{-1}·m^{-2} for ordinary hemp-lime insulation. By the end of Regime I, at 100 mins, this had decreased to 0.86±0.12g·s^{-1}·m^{-2} for PCM enhanced hemp-lime and 0.45±0.03g·s^{-1}·m^{-2} for ordinary hemp-lime. This change of 0.63±0.10 to 0.41±0.15g·s^{-1}·m^{-2} for the respective time periods is attributed to the exothermic oxidation of the paraffin wax. In Regime II (Figure 5.10b) the change is significantly harder to distinguish which suggests there was less little effect from the PCM, which will have already evaporated and combusted.

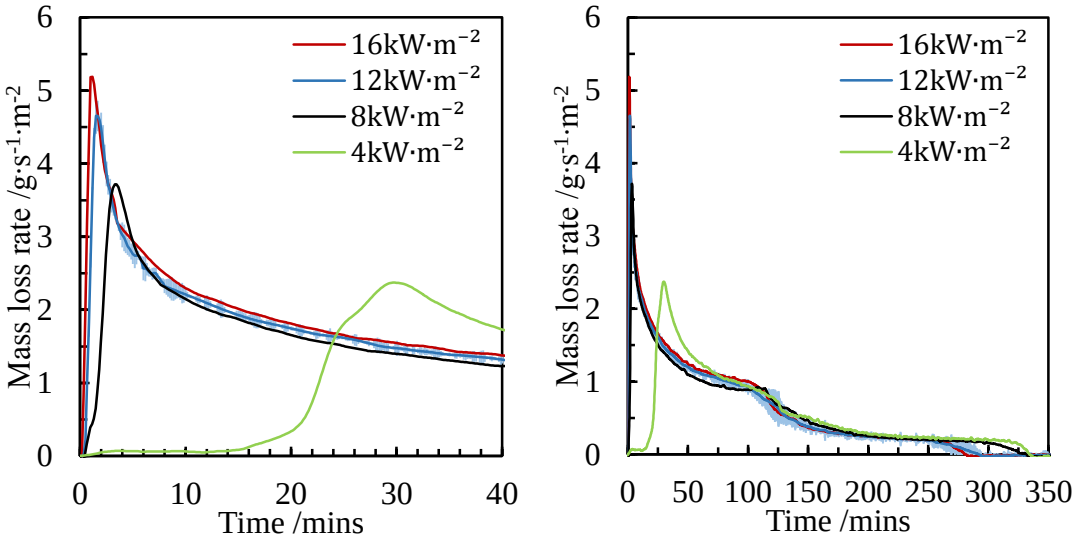

Figure 5.9 – Mass loss rate per unit area over time for four heat fluxes. Standard deviations are only shown on 12kW·m^{-2} for the sake of clarity. (a) Peak mass loss rate near ignition and (b) full duration of tests.

The time taken to reach peak mass loss rate (MLR) following ignition maintains a strong relationship when expressed as $1/\sqrt{t_{peak}}$ against incident heat flux (Figure 5.11a). The time to reach the peak is shorter across all the heat fluxes owing to the exothermic oxidation of the paraffin wax. The rate of reactions was faster and allowing the maximum rate of decomposition to be reached more rapidly.

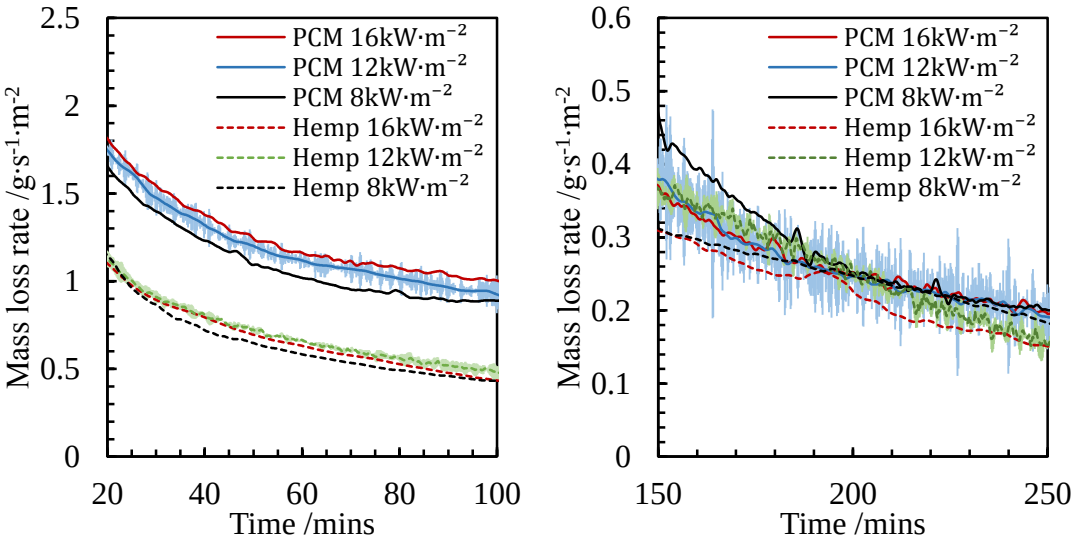

Figure 5.10 – Mass loss rate of both hemp-lime (dashed lines) and PCM hemp-lime (solid lines) during (a) Regime I, post-peak mass loss rate and (b) Regime II, prior to extinction. Standard deviations are shown on 12kW·m^{-2} tests.

Similarly, the peak mass loss rate follows a strong linear relationship with increasing incident heat flux (Figure 5.11b). Despite the fact that the quantity of PCM is relatively low, around 23% with water removed, it has a substantial effect on the peak MLR due to its high heat of combustion.

The mass loss rate shows that the contribution of PCMs to the smouldering behaviour of hemp-lime insulation is predominantly at ignition and in the initial propagation. A consistent increase in the burning rate was observed through the Regime I downward opposed oxidation, owing to the exothermic oxidation of the paraffin wax.

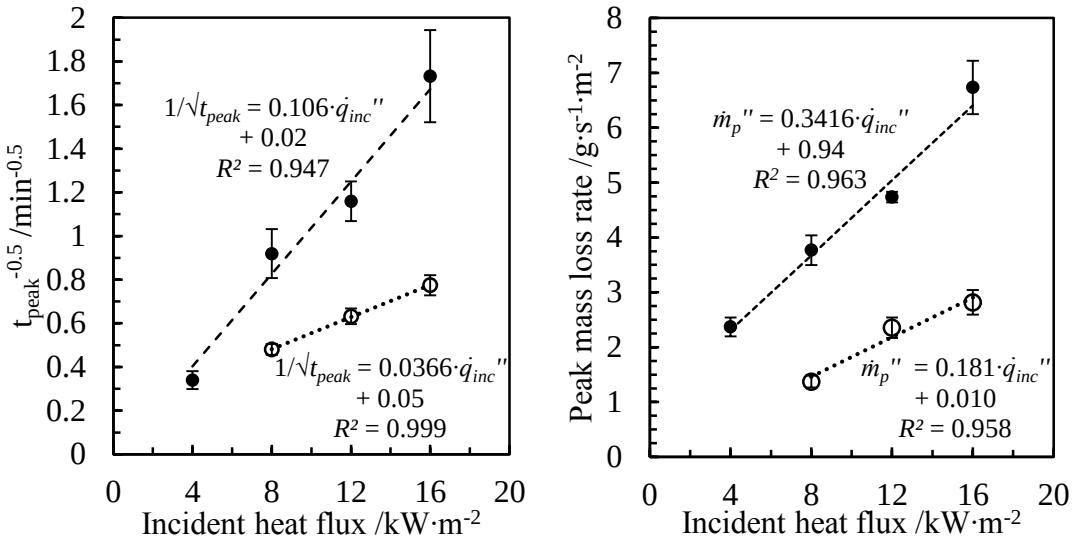

Figure 5.11 – (a) Incident heat flux against $1/\sqrt{t_{peak}}$ and (b) incident heat flux against peak mass loss rate for hemp-lime (hollow), and PCM hemp-lime (filled symbols).

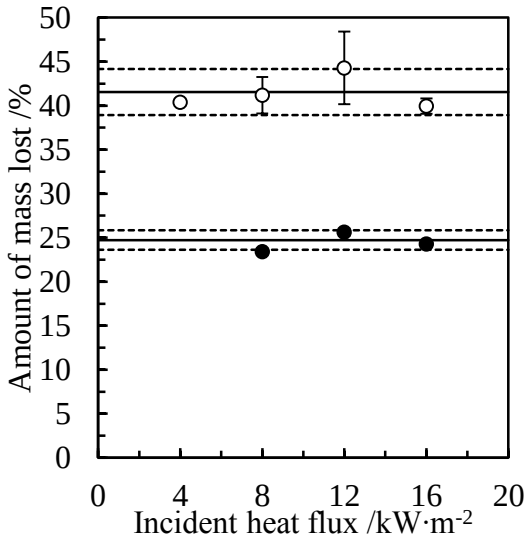

Figure 5.12 – Total amount of mass lost over test duration for both PCM hemp-lime (hollow symbols) and ordinary hemp-lime insulation (filled symbols). Solid lines illustrate the average over all tests, with standard deviation in dashed.

The average mass lost for PCM hemp-lime was 41.55±2.62% compared to 24.73±1.10% for ordinary hemp-lime insulation. The mass lost in the cone calorimeter agrees well with the previously performed thermogravimetric analysis. Based on the material synthesis, the theoretical total mass loss is calculated to be 42.7%. This shows that complete burnout occurred in each specimen regardless of the external radiant heat flux. The only difference is the time taken to reach this stage, and hence extinction. The change in total mass lost due to the addition of PCMs is purely attributed to their weight, and they are not able to cause additional degradation of the hemp.

5.4.4Thermal evolution

The different regimes can be clearly identified in the thermal evolution of PCM hemp-lime insulation, which is shown for 8kW·m^{-2} in Figure 5.13. The secondary ignition at the rear surface to initiate Regime II was significantly more rapid compared to ordinary hemp-lime, and occurred in the bottommost thermocouple at 90mm despite heat losses from the bottom surface. This again reached progressively higher peak temperatures as the smoulder propagated upwards through subsequent thermocouples, until reaching a peak temperature of 661°C. A strong and consistent smoulder was easily established, even at a relatively low heat flux.

The width of the peaks in Regime III illustrate the energetic nature of the PCMs. Where in ordinary hemp-lime insulation these appeared only as sharp peaks due to the reduced availability of fuel and narrow reaction front, instead a stronger smoulder was able to be established due to the contribution from the exothermic oxidation from the paraffin wax.

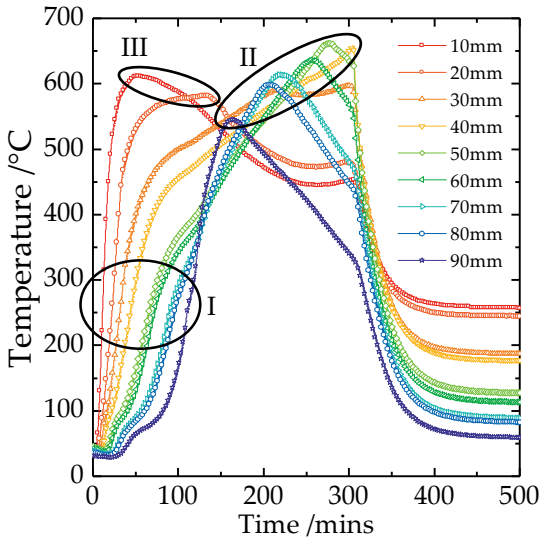

Figure 5.13 – Temperature evolution of PCM hemp-lime exposed to 8kW·m^{-2}. Circled areas represent Regime I (downward opposed flow), Regime II (upward forward flow), and Regime III (downward forward flow).

A more thorough interrogation of the thermal evolution can be performed using temperature as a function of depth, and interpreted using the previous TG analysis. This is shown in Figure

5.14 for 8kW·m^{-2}, and Figure 5.15 for 16kW·m^{-2}. Highlighted areas represent the major degradation steps of PCM hemp-lime insulation, which are provided for both the experimentally determined results as well as the added DTG of both hemp and PCMs.

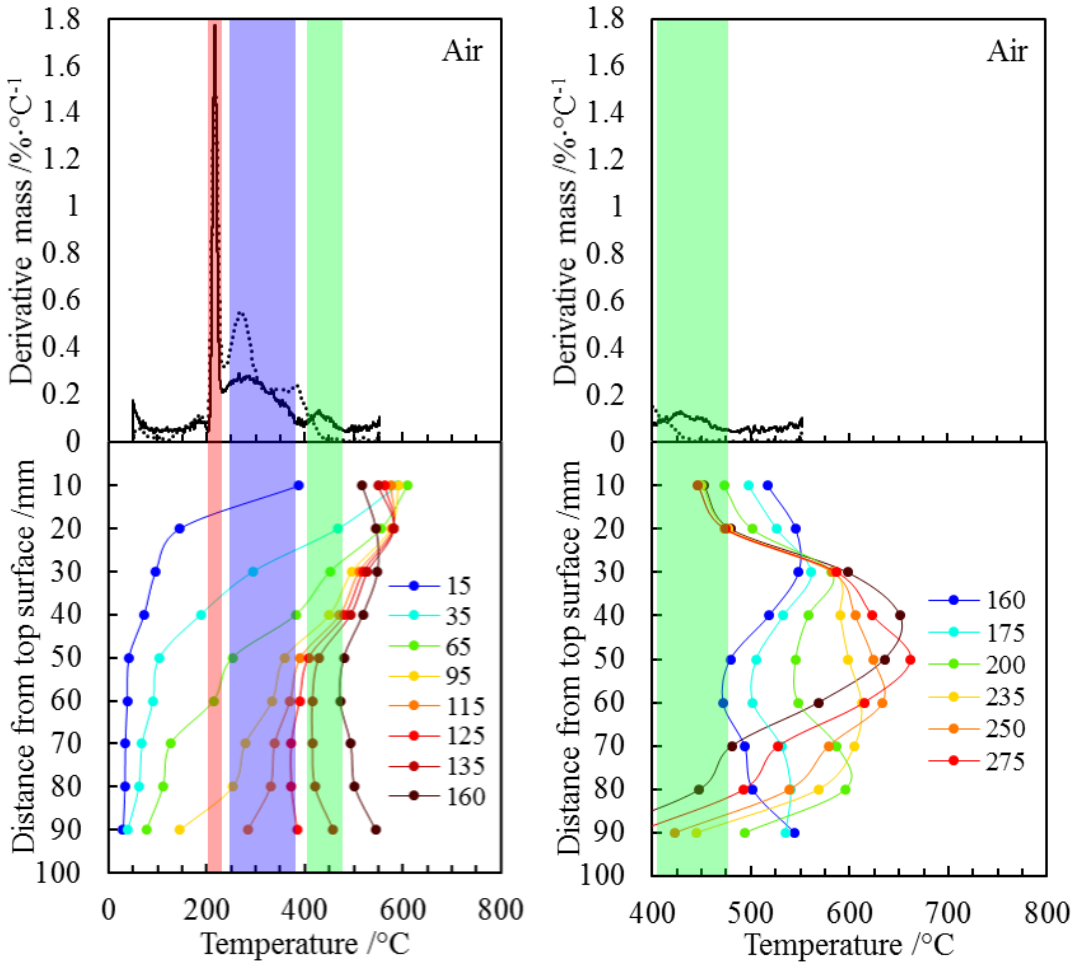

Figure 5.14 – DTG (top) and temperature-depth profiles (bottom) of Regime I (left) and Regime II (right) for PCM hemp-lime insulation 8kW·m^{-2}. Highlighted areas, starting from the lowest temperature, represent the oxidation of paraffin wax; oxidation of cellulose and PCM shell; and char oxidation.

The propagation of the oxidation front in Regime I is apparent as the temperatures reach the oxidation of paraffin wax, cellulose and shell material. Upon reaching the rear surface the secondary ignition was established quickly, as evident between 115 and 125 mins where the temperature at 90mm increased above the temperature at 80mm. Due to the heat losses from the bottom surface there was still a delay as the char oxidation occurred and the smoulder eventually began to propagate upwards between 160 and 175 mins, signifying Regime II. A strong smoulder was established from this secondary ignition, as evidenced by the width of the reaction front, high temperatures and constant velocity. This occurred at the bottommost thermocouple despite the heat losses to the environment due to its proximity to the surface. The propagation in Regime II is fuelled by the exothermic oxidation of the char. The energy

released by this reaction is substantial (Kashiwagi and Nambu 1992) and sufficient to allow the reaction front to sustain upwards.

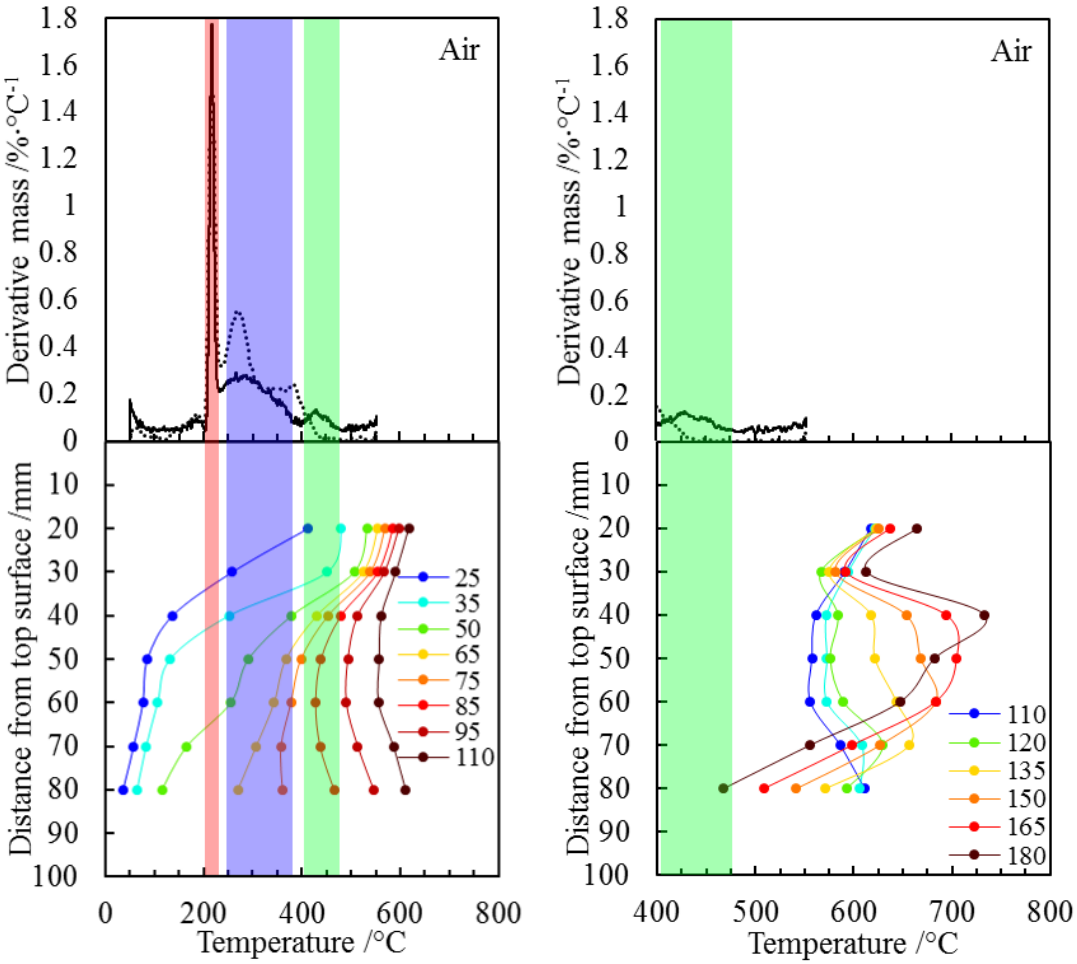

Figure 5.15 – DTG (top) and temperature-depth profiles (bottom) of Regime I (left) and Regime II (right) for PCM hemp-lime insulation at 16kW·m^{-2}. Highlighted areas, starting from the lowest temperature, represent the oxidation of paraffin wax; oxidation of cellulose and PCM shell; and char oxidation.

The time taken for the Regime I oxidation front is reduced when the incident heat flux is increased to 16kW·m^{-2} (Figure 5.15). A substantial increase occurs as the temperature passes the exothermic oxidation of paraffin wax (50 to 65 mins for rear face) which allows the exothermic oxidation point of cellulose to be rapidly reached between 65 and 75 mins. The rear surface then reaches a temperature higher than downstream, closer to the cone, providing additional evidence of smouldering combustion. The temperature continues to increase and an insulating layer is built up before a sustained smouldering reaction front can be established as the heat generated outweighs the heat lost. This is visible between 110 and 120 mins in Figure 5.15b as the smoulder begins to propagate upwards in Regime II. This rapidly propagates upwards to 40mm where the material reaches extinction in only 180 mins. The reaction front remains wide illustrating the energetic nature of PCMs.

The temperature of reactions at the higher heat flux are also increased, even in Regime II at the bottom of the specimen. The peak temperature recorded is 734°C at 16kW·m^{-2} compared to 661°C at 8kW·m^{-2}.

5.4.5 Gas emissions

The carbon monoxide yield was constant for the entirety of Regime I, and appears largely independent of the radiant heat flux (Figure 5.16a). During Regime II the yield increases owning to the additional CO generated by the char oxidation process (Kashiwagi and Nambu 1992). This shows some dependency on the external heat flux, but due to the fact that the mass loss rate drops to near zero the error becomes increasingly significant (Figure 5.16b).

The behaviour of the CO yield was similar to ordinary hemp-lime, despite the fact that PCM comprises a large component of the mass lost, and thus the resulting yield. Because PCMs account for around half of the mass lost yet the yield between PCM hemp-lime and ordinary hemp-lime remain similar, this suggests that their yields are also similar. However, because additional mass is lost during the smouldering of PCM hemp-lime this means that the absolute amount of CO generated will be significantly higher, proportional to the PCM content.

As with ordinary hemp-lime, the key fire risk relates to the char oxidation which has a higher yield than the exothermic oxidation of cellulose and paraffin wax. This risk was previously quantified for ordinary hemp-lime insulation, and the addition of PCM is found to increase the CO flux in absolute terms due to the greater amounts of mass lost. The increase in yield in Regime II, away from the original heat source, represents a key risk in buildings where smouldering may occur in-depth and undetected.

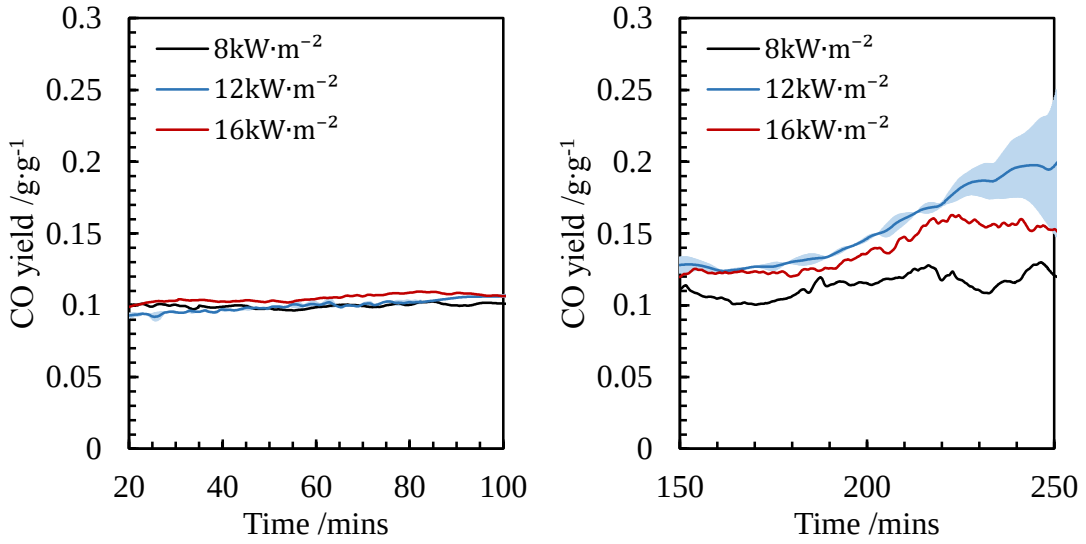

Figure 5.16 – CO yield of PCM hemp-lime for incident heat fluxes of 8, 12, and 16kW·m^{-2} shown in black, blue, red respectively for (a) Regime I and (b) Regime II. Standard deviation is only illustrated on 12kW·m^{-2} for the sake of clarity.

5.4.6 Visual observations

Visual inspection of the residue provides some additional understanding of the material. PCM hemp-lime` was found to lose significant portions of its integrity after the test due to the amount of mass lost. The surrounding foil and stonewool insulation provided sufficient restraint to maintain rigidity through the test, but specimens collapsed upon removal of the boundaries. This was more so true at 16kW·m^{-2} than at 8kW·m^{-2}, despite the fact the final masses were previously shown to be very similar. The cross-section of a partially collapsed specimen is shown in Figure 5.17. The specimen appears almost entirely composed of ash and residue material, with little to no virgin material remaining at the edges where the heat losses were highest.

Figure 5.17 – Remnants of a PCM hemp-lime specimen tested at 8kW·m^{-2}. Partial collapse of the sample occurred upon removal of the foil and insulation.

The remnants highlight that the greater amount of mass loss due to the addition of PCMs can result in reduced integrity after combustion. Fallout was already identified as a potential hazard for hemp-lime insulation, and this is exacerbated by the addition of PCMs. Quantification of this risk would require strength testing outside the scope of this work.

5.5 Concluding remarks

This chapter has investigated how the addition of phase change materials affects the behaviour of a hemp-lime substrate.

- The lower oxidation temperature of paraffin wax compared to cellulose means the ignition temperature is lower, and can be reached more rapidly than ordinary hemp-lime insulation. This also lowers the critical heat flux from 8.0kW·m^{-2} for ordinary hemp-lime down to 3.0kW·m^{-2} for PCM enhanced hemp-lime.
- The lower ignition temperature also causes more rapid smouldering propagation since less energy and less time are required to reach the critical temperature, allowing successive ignitions to occur more rapidly.

- The higher heat of combustion increases the temperature of reactions, thereby leading to a higher rate of reactions and hence a higher burning rate. This is reflected in both the mass loss and spread rates.
- The decrease in the ignition temperature in addition to the exothermic paraffin oxidation reactions allow the smoulder to ignite closer to the surface where heat losses are higher. This illustrates an increase in ignitability, and a decrease in the required char layer for ignition to occur.
- PCMs represent an energetic material which increase the amount of energy released by the specimen and allow stronger reactions to be established. This is reflected in the temperature-depth profiles which illustrate wider reaction fronts compared to ordinary hemp-lime insulation.
- The exothermic oxidation of paraffin wax only occurs during the initial downward opposed flow, Regime I, and is reflected in an increase in the mass loss rate throughout this regime.
- Spread rates near the cone calorimeter are largely independent of the incident heat flux, and thus in this area the smoulder is limited by the diffusion of oxygen to the reaction front. Forced airflow would be therefore have a large impact on the propagation rates.
- The total amount of mass lost is higher due to the PCM replacing non-combustible binder in the hemp-lime matrix. The specimens still reach burnout and thus the total mass lost will match the combined hemp and PCM content.
- The additional mass lost has repercussions for the integrity of the specimens. PCM hemp-lime specimens were found to lose their integrity after the boundary insulation was removed, where ordinary hemp-lime was capable of maintaining its form.
- The addition of PCMs causes a small increase in the carbon monoxide yield. Coupled with the higher mass loss rate however this represents a notable increase in the total amount of carbon monoxide generated. The highest rates were found deep in the specimens which in buildings would be difficult to reach.

Key numerical findings are summarised below in Table 5.3, and can also be compared to the previously obtained results for ordinary hemp-lime insulation in Table 4.3.

Table 5.3 – Summary of properties for PCM enhanced hemp-lime insulation.

Parameter		**Material property**	
Critical heat flux ($kW \cdot m^{-2}$)		3.0±2.5	
Smouldering ignition temperature (°C)		141-181	
Apparent thermal inertia ($kJ^2 \cdot m^{-4} \cdot K^{-2} \cdot s^{-1}$)		0.353-0.625	
		Heat flux dependent	
		$8kW \cdot m^{-2}$	$16kW \cdot m^{-2}$
Time to ignition (s)		118±22	35±6
Spread rate ($\mu m \cdot s^{-1}$)	Downward opposed flow	16.2±7.3	25.8±17.0
	Upward forward flow	6.7±4.1	9.4±3.6
Peak mass loss rate ($g \cdot s^{-1} \cdot m^{-2}$)		3.77±0.27	6.73±0.49
Total mass lost (%)		41.2±2.1	39.9±0.9
Time to extinction (mins)		330	280
CO yield ($g \cdot g^{-1}$)	Regime I	0.096±0.016	0.102±0.009

6 Flammability study of PCM plasterboard using bench-scale calorimetry

6.1 Summary

To understand the fire risk associated with phase change materials it is necessary to evaluate a commercially available end use product. Plasterboard containing microencapsulated paraffin wax is one of the most commonly used phase change material (PCM) product in the built environment at present. For this reason, a suitable PCM plasterboard product has been selected for study. A bench-scale characterisation of the material is undertaken as part of a holistic fire risk assessment. The critical heat flux, time to ignition, heat release rate, mass loss rate, temperature evolution, and gas emissions are all recorded for a range of heat fluxes for both horizontal and vertical orientations in the cone calorimeter. This produces the vital knowledge needed to understand the risks associated with, and the fire performance of, PCMs in the built environment. This information will be used as the input for the development of a performance-based fire framework to allow optimisation of energy savings with quantified fire performance, and enabling the usage of these materials in the built environment.

6.2 Introduction

The change in fire behaviour associated with the addition of PCMs through the use of a porous, combustible material has been covered in the previous chapter. In this chapter, analysis is performed on a commercially available product. Through a combination of literature review, interaction with manufacturers and contractors, and a market analysis a suitable product has been identified. This is gypsum board containing microencapsulated paraffin wax.

Standard fire tests (British Standards Institution 2009a, 2010d) have been carried out by individual product manufacturers to approve their usage in buildings. However, there has yet to be a holistic fire risk assessment of their behaviour in realistic fire conditions to allow predictive assessment of their fire performance.

6.3 PCM plasterboard product

The material used in this chapter is a commercial plasterboard containing PCM available on the market in 2014. No modifications were made to the material. The PCM contained within however is the same as was studied earlier to ensure that the results are comparable and can be used as part of the complete data analysis. This chapter focuses on the quantification of fire risk associated with commercially available end use products containing PCM.

A summary of the properties of the obtained PCM plasterboard can be found below in Table 6.1. The board is 25mm thick and has a density of 900.08 ± 21.68 kg·m^{-3}, as measured using a pair of callipers and a load cell, or 1000kg·m^{-3} according to the manufacturer. The thermal

conductivity and specific heat at ambient temperature are listed on the product data sheet as 0.27 $W \cdot m^{-1} \cdot K^{-1}$ and 28.3 $kJ \cdot m^{-2} \cdot K^{-1}$ respectively.

Table 6.1 – Summary of selected PCM plasterboard properties.

Product	**Thickness**	**Density**	**Thermal conductivity**	**Specific heat**
-	mm	$kg \cdot m^{-3}$	$W \cdot m^{-1} \cdot K^{-1}$	$kJ \cdot m^{-2} \cdot K^{-1}$
PCM plasterboard	25	900.08 ± 21.68[a]; or 1000[b]	0.27	28.3

[a] experimentally determined.

[b] from manufacturer.

6.4 Experimental approach

25mm thick PCM plasterboard was tested in a modified cone calorimeter (Babrauskas 1984, ASTM International 2014, British Standards Institution 2015a) setup, in both horizontal and vertical orientations. The experimental setup is illustrated in Figure 6.1. A 25mm thick aluminium block was placed at the back of the sample in order to quantify the heat losses (Reszka 2008, Carvel *et al.* 2011). The specimen was surrounded by 10mm thick ceramic paper in order to promote one-dimensional heat transfer. Ceramic paper was also used at the back of the aluminium block to insulate against heat losses.

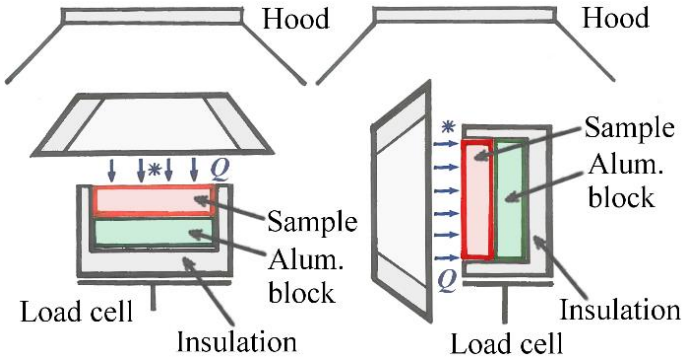

Figure 6.1 - Experimental setup for testing of PCM plasterboard in the cone calorimeter using both (a) horizontal and (b) vertical orientations. The asterisk (*) represents the position of the pilot ignition source.

The time to ignition, heat release rate (by oxygen consumption calorimetry (Janssens 1991)), mass loss rate, gas emissions and in-depth temperatures were all obtained. Separate tests were conducted for mass loss and temperature. Type K Inconel sheathed thermocouples with 2.0mm diameter were used. Three thermocouples were placed in the aluminium block at distances of 1mm, 12.5mm, and 24mm to confirm the assumptions inherent in the heat loss calculation.

6.4.1Pilot ignition source

The tests were conducted with a pilot source, which varied between the two orientations. In the horizontal orientation the ordinary spark ignitor was located 10mm above the centre of the specimen. The presence of the spark provides the necessary energy to ignite a sufficiently mixed concentration of flammable gases above the critical value (Drysdale 1999).

A study on the impact of the pilot ignition source in both horizontal and vertical was conducted previously by Shields *et al.* (1993). This evaluated the time to ignition using both a spark igniter, which is the typical pilot source in the cone calorimeter, as well as a pilot flame, as is used in the Fire Propagation Apparatus. This was investigated for three cellulosic materials; chipboard, softwood, and plywood for heat fluxes between 20 and 70kW·m^{-2}. This found that the pilot flame caused shorter times to ignition for both orientations. This was due to the radiation from the flame source (Janssens 2002) which was sufficient to reduce the time to ignition.

The method of introducing a pilot flame source in the vertical orientation is similar to one used for igniting foams in the vertical orientation elsewhere (Galaska *et al.* 2014). The authors did not quantity the differences using this method and found it repeatable, but not ideal. They instead suggested a methane pilot which could be mechanically moved into position. The ignition results in this chapter echo this suggestion, but it was not employed due to the fact that manufacturing time was relatively long compared to a moderately small benefit since there were no plans to reuse this method in future.

The spark igniter was not used in the vertical orientation because its position did not intercept the pyrolysis gases. The igniter was positioned outside the upward convective flow of gases which rise above the specimen due to buoyancy. In these instances, and where the heat flux was sufficiently high, the specimen instead autoignited at the surface. Thus, it was not representative of piloted ignition.

6.4.2Choice of insulation

The choice of insulation material requires it to be of lower thermal conductivity than the sample. In the case of testing highly insulating materials there is potential that the specimen will have lower thermal conductivity. To avoid this, ceramic fibre paper is used as the insulation material. The thermal conductivity of these fibres varies with temperature from 0.06 to 0.14W·m^{-1}·K^{-1} in the range of 260 to 816°C. The thermal conductivity of the completed PCM plasterboard is not known, however, from the thermal analysis it is known that only 9.44±1.10% of the total weight is PCM. Thermal conductivity of PCMs are 0.1505 to 0.3964W·m^{-1}·K^{-1} for n-octadecane with tetraethoxysilane shells (Zhang, Wang, *et al.* 2010), 0.15W·m^{-1}·K^{-1} (solid) for pure octadecane (Abhat 1983), 0.24W·m^{-1}·K^{-1} for unspecified paraffin wax, (Ettouney *et al.* 2005), and 0.128 to 0.163W·m^{-1}·K^{-1} for PCM gypsum wallboard (Lee *et al.* 2007). The thermal conductivity of plasterboard was explored in the literature review, and found to be in the range of 0.1 up to 1.10W·m^{-1}·K^{-1} at high temperatures for Type X board (Mehaffey *et al.*

1994, Bénichou and Sultan 2005, Park *et al.* 2010). The determination of thermal transport properties performed in this thesis using the hot disk apparatus found values at ambient temperature of 0.29±0.03W·m^{-1}·K^{-1}. A comparison of all the above values clearly shows that the thermal conductivity of the PCM plasterboard is higher than the surrounding ceramic fibre paper, and thus the assumption remains complete.

6.4.3 Choice of orientation

The horizontal orientation is the preferred setup and recommended for use in standardised testing. Despite potentially unrealistic to the end use for materials such as wall linings, this orientation allows testing of materials which are prone to melt, drip, or deform upon exposure to elevated temperatures. In this respect the vertical orientation gives unrepresentative results and thus is only recommended for research purposes (Babrauskas 1984, Babrauskas and Parker 1987). However, the boundary conditions in the vertical orientation, especially the convective boundary layer which dictates the convective heat transfer at the surface, are more repeatable when compared to the horizontal orientation (Reszka 2008, Tsai 2009). Thus, for the research purposes the vertical orientation may be considered preferential where the materials do not melt or suffer any of the above limitations. This may be particularly evident in the cases where the material is a wall lining or otherwise the end use is in the vertical orientation. For these reasons, both orientations are used for the testing of PCM plasterboard.

6.5 Results of representative test

The results of a single representative test are given in the following section. An intermediary imposed heat flux, 50kW·m^{-2}, was chosen to give an explanation of the general fire behaviour of the PCM plasterboard in the testing series. Then, a more detailed analysis and discussion involving other imposed heat fluxes is then given in the following section, *6.6 Discussion and analysis*.

Results are generally given over twelve minutes, although longer durations are used wherever needed. The figure of twelve minutes was calculated by adding an arbitrary period of two minutes to the longest duration of flaming, which was experimentally determined to be ten minutes. The additional two minutes were to ensure that there was sufficient time for all gases to travel through the sampling line and to the analyser before measurements were stopped.

6.5.1 Pyrolysis and ignition

Upon exposure to the imposed heat flux of 50kW·m^{-2} the surface of the specimen begins to heat up. The dehydration reactions of the gypsum are rapidly reached after 10s owing to the low temperatures required and water vapour is released. At higher temperatures the material will reach the pyrolysis temperature of the PCM and an increasing amount of pyrolysis gases will be generated. Immediately before ignition a large amount of gases were visually observed. Upon reaching the boiling point of the paraffin wax this will vaporise and escape the shells, transport through the plasterboard matrix to the free surface and mix with the air above the sample to form a flammable mixture. Flaming ignition will occur upon reaching the lower flammability limit in the region of the spark ignitor (Figure 6.2).

Figure 6.2 – Photograph of PCM plasterboard exposed to 80kW·m^{-2} for illustrative purposes.

6.5.2Mass loss rate

The mass loss rate (MLR) provides the means to evaluate the burning behaviour of PCM plasterboard. The MLR over time for specimens exposed to 50kW·m^{-2} is shown below in Figure 6.3. Dehydration reactions and generation of pyrolysis gases are evident in the mass loss rate prior to ignition. This climbs to 4.08±0.16 g·s^{-1}·m^{-2} in 11 seconds and plateaus for a further 8s. The burning rate climbs to a peak of 7.01±0.65g·s^{-1}·m^{-2} at approximately 40s (8s after ignition) and then decays over the remaining duration of the experiments. This is similar behaviour to charring solids. The thermal wave penetrates through the depth of the specimen but the pyrolysis rate decreases. The result is that the rate of pyrolysis decreases to the point where a flame can no longer be sustained.

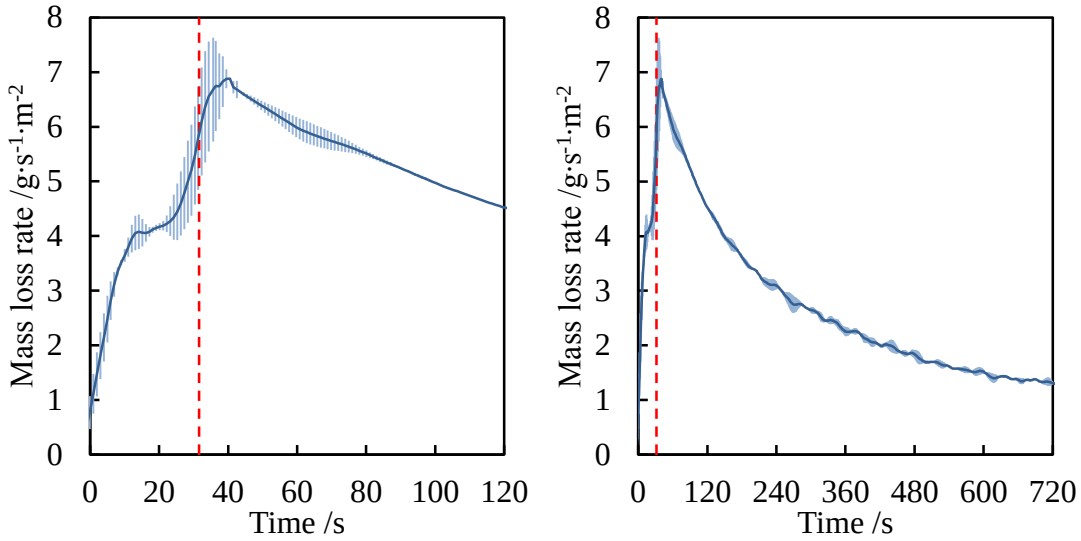

Figure 6.3 – Mass loss rate of specimen exposed to 50kW·m^{-2} in the horizontal orientation for (a) around ignition (31.6±3.3s); (b) full 12 minute duration. Time to ignition is marked in a red dashed line, and error indicates standard deviation.

This decrease in the rate of reactions is evident in the decrease of the mass loss rate. However, it is not clearly distinguishable when flaming ends. After extinction a base rate of pyrolysis and thermal decomposition of the gypsum continues, due to pyrolysis and dehydration,

despite the lack of flaming combustion. In this case the baseline mass loss rate after extinction is found to be 1.77±0.05g·s^{-1}·m^{-2}.

6.5.3Heat release rate

The heat release rate (HRR) as per the oxygen consumption approach (Janssens 1991) surges to a peak value of 81.2±13.6kW·m^{-2} at 51.5±1.4s after ignition. During pyrolysis there is no oxygen consumption observed. The HRR decays until extinction, as was the case with MLR, but the time of flameout cannot be easily deciphered. Following extinction a small amount of oxygen was still depleted, corresponding to a heat release rate of 12.31±1.87kW·m^{-2}, signifying continued combustion reactions despite no visible flaming. Specimens were always removed whilst the gas analysers were running to ensure that this was not an artefact of the experiment or due to an inaccurate calibration. Given the porous nature of the material this therefore represents slow smouldering combustion reactions propagating downward through the specimen.

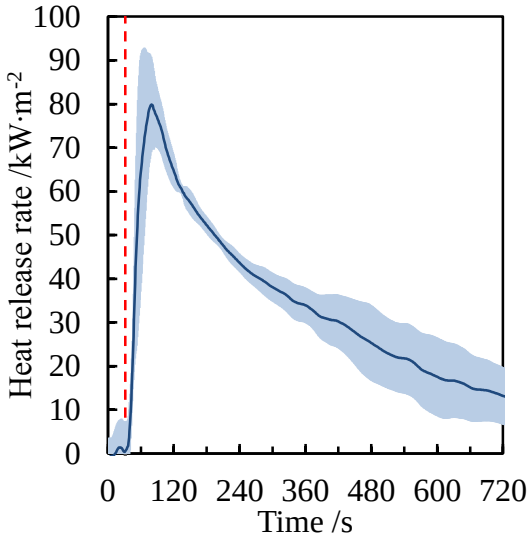

Figure 6.4 - Heat release rate per unit area over time of PCM plasterboard exposed to 50kW·m^{-2} in the horizontal orientation. Red dashed line indicates ignition, and the shaded area indicates standard deviation.

6.5.4Heat of combustion

The heat of combustion has been calculated as a function of time for the given heat flux (Figure 6.5). The data was corrected to account for the delay in the oxygen analyser. A steady state value of 14.6±2.6kJ·g^{-1} is observed from 80 to 450s, which broadly corresponds to the visually observed period of flaming. As the combustion mode transitions to smouldering the heat of combustion drops to 10.8±1.8kJ·g^{-1} for a further 400s before dropping near the termination of the experiment. Thus, the heat of combustion for flaming is approximately 35% higher than the heat of combustion during smouldering. For the full recorded duration the effective heat of combustion was found to be 12.4±2.4kJ·g^{-1}. Thus, it can be seen that the energy released

during pyrolysis and smouldering has a large effect on the effective heat of combustion, and lowers the value from the steady state value measured during flaming.

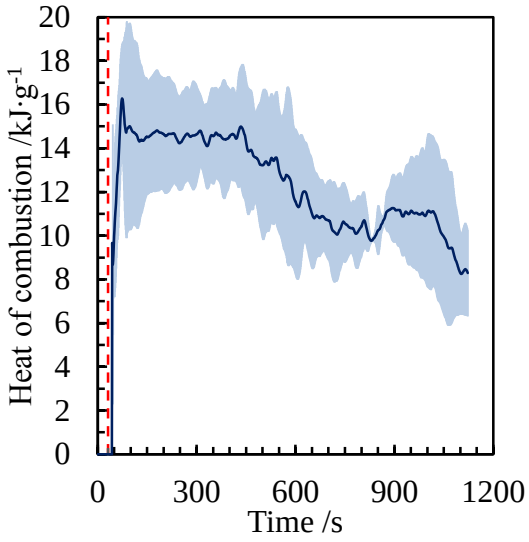

Figure 6.5 – Heat of combustion as a function of time for tests at 50kW·m^{-2} in the horizontal orientation. The red dashed line indicates ignition.

6.5.5Gas emissions

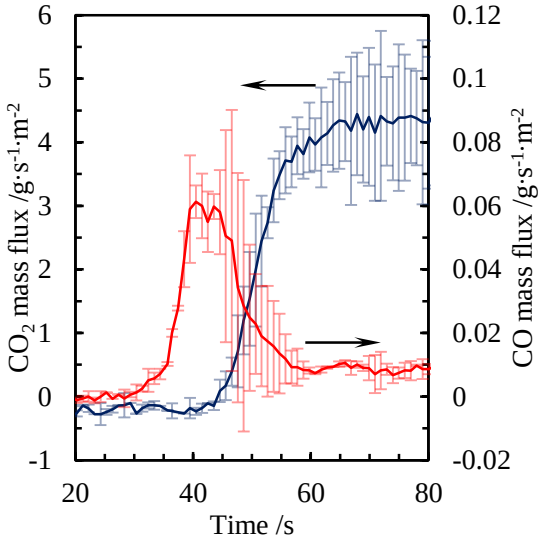

Figure 6.6 - CO flux and CO_2 flux at the start of the test for 50kW·m^{-2} in the horizontal orientation.

Data from the start of the test has been highlighted in Figure 6.6 to further enlighten the behaviour at ignition. The surge in carbon monoxide flux corresponds to the generation of a significant amount of pyrolysis gases prior to ignition (0.061±0.009g·s^{-1}·m^{-2} peak), as was previously noted in *Section 6.5.1 Pyrolysis and ignition*. Following ignition, the CO_2 flux starts to rise to its peak value as the burning rate increases and there is adequate oxygen to react with the pyrolysis gases. A peak of 4.44±1.09g·s^{-1}·m^{-2} is observed 39 seconds after ignition. An

apparent short steady state exists following ignition between 60 and 100s where both CO_2 and CO mass fluxes are constant at 4.30±0.97g·s^{-1}·m^{-2} and 0.0085±0.0016g·s^{-1}·m^{-2} respectively.

Typical carbon dioxide and carbon monoxide mass fluxes for the full duration of the experiment are given in Figure 6.7. Following on from the aforementioned apparent steady state, the intensity of the flaming combustion decreases and the CO mass flux progressively increases, reaching a peak of 0.102±0.013g·s^{-1}·m^{-2} after 540s. This is consistent with observations of charring solids which have shown that as the burning rate decreases and the efficiency of the combustion decreases, the more CO that is generated (Tewarson 1980).

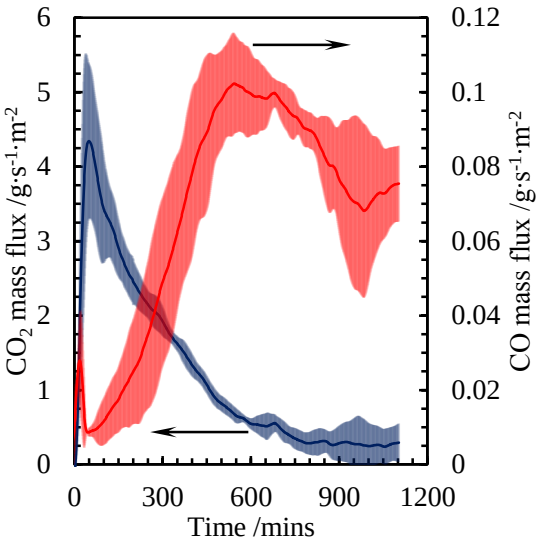

Figure 6.7 – Carbon dioxide flux per unit area (blue, primary ordinate) and carbon monoxide flux per unit area (red, secondary ordinate) for PCM plasterboard at 50kW·m^{-2} in the horizontal orientation.

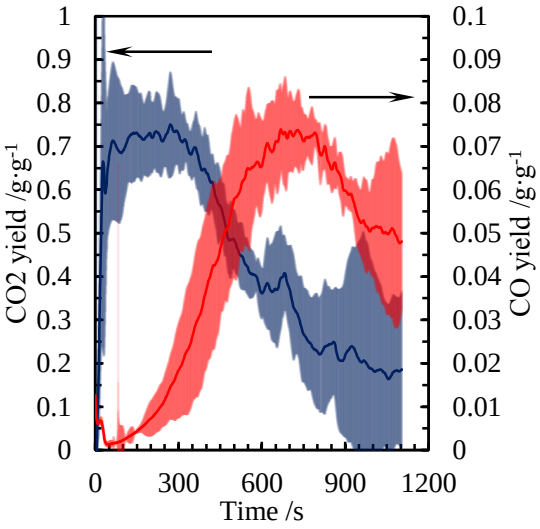

Figure 6.8 – CO_2 yield (primary ordinate) and CO yield (secondary ordinate) for 50kW·m^{-2} in the horizontal orientation. Shaded areas indicate standard deviation.

As was evident from the HRR data, there may be some pyrolysis and combustion that continues after flaming, and thus the CO flux does not return to zero. Furthermore, the decomposition of the gypsum continues and pyrolysis gases will continue to be generated until the thermal wave reaches the rear face, or the temperature drops below the pyrolysis temperature.

Different regimes of burning can be identified between the CO_2 and CO yields (Figure 6.8). The periods of these are similar to the periods of constant heat of combustion noted in Figure 6.5. The CO_2 yield holds a constant value of $0.72\pm0.11 g \cdot g^{-1}$ for the duration of flaming. After this period the CO_2 yield decreases as the CO yield increases. This is indicative of the transition from flaming combustion to smouldering combustion as the pyrolysis front penetrates the depth of the specimen.

6.5.6 In-depth temperatures

The temperature evolution provides the means to be able to probe the thermal response of the material, and track the propagation of the thermal wave as it progresses downward through the specimen. These are provided both as a function of time, and of depth for a series of time steps.

6.5.6.1 Temperature time series

The in-depth temperature profile of a specimen is shown below in Figure 6.9. Ranges of temperatures corresponding to the major reactions observed from Thermogravimetric Analysis (TGA) obtained in the thesis previously are marked. It can be seen that even though flaming lasts a short time compared to the total test length (5mins compared to 180) the thermal wave continues to penetrate through the specimen long after flaming has ended. The contribution of radiation from the flame increases the temperature through the depth of specimen, the topmost thermocouple reaching a peak temperature of 622°C compared to the residual temperature of 521°C, despite the short period of flaming. This can be seen by tracking the peak temperatures experienced at each of the depths. The specimen eventually reaches a steady state after 180 mins and will have different levels of thermal degradation through the depth of the specimen arising due to the time history of temperature at each location.

The first zone (I) represents the combined endothermic dehydration reactions where energy is absorbed and the gypsum is degraded. This can be seen in the temperature profiles as the rate of temperature increase is reduced due to energy absorption by the endothermic process. This is most notable at the deepest thermocouple within the specimen due to the lower levels of heat conducted, but the effect is still evident near the exposed surface.

The expected pyrolysis temperature (II) is based on the TGA results of the PCM plasterboard. The full analysis was previously given in the thermal degradation framework chapter. The temperature for pyrolysis is given as a range of 190 to 222°C. Testing at $50 kW \cdot m^{-2}$ shows that the thermal waves penetrates through the specimen and exceeds the expected pyrolysis

temperature for at least 20mm, and the remaining 5mm enters the range. The use of an aluminium block at the rear increases the heat losses and thus the temperature at the rear face is lower than it would be if there was insulation. It is expected that no paraffin wax remains at the end of the test and that in similar conditions in a real fire the entirety of the PCM loading would be capable of contributing to the fire load.

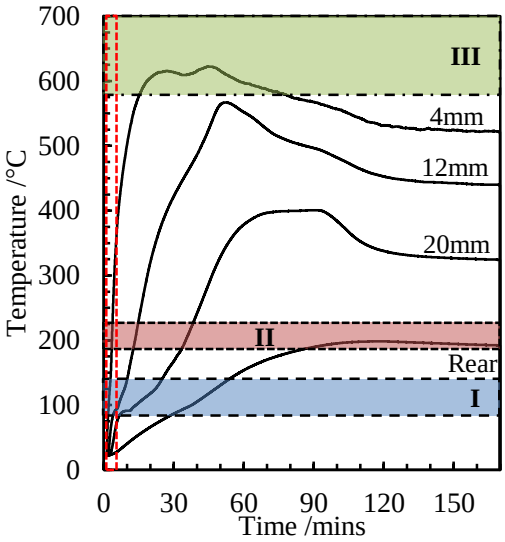

Figure 6.9 – Temperature profiles of a representative specimen exposed to 50kW·m^{-2} in the horizontal orientation. Shaded areas indicate (I) overlapping dehydration reactions of gypsum (II) oxidation of PCM (III) decomposition of calcium carbonate. Vertical red dashed lines indicate the period of flaming.

There is some additional thermal degradation to be expected in the region between areas II and III (not explicitly marked). This would be due to the pyrolysis of the acrylic polymer within which the paraffin wax is contained, as well as additional reactions of the gypsum or any additives such as glass fibres. These are believed to play a lesser role compared to the other thermal degradation steps. This is due to the fact that much of the available gypsum literatures lists little to no decomposition in this range. For PCMs, the magnitude of the exothermic reaction of the paraffin wax far exceeds that of the polymer shell, as was previously quantified in this thesis using TGA.

The final range considered is the decomposition of the calcium carbonate (III). The endothermic decomposition is only experienced when the temperature reaches 575 to 725°C. These temperatures are only recorded near the surface for high heat fluxes (greater than 50kW·m^{-2}).

6.5.6.2 Temperature depth profiles

Temperature-depth profiles at various timesteps are provided to aid in understanding the propagation of the thermal wave through the specimen (Figure 6.10). The observations at each timesteps selected is given in Table 6.2**.** This shows that the depth of penetration of the 190°C

isotherm is approximately 18mm. Steady state temperature distribution is obtained after 180 mins.

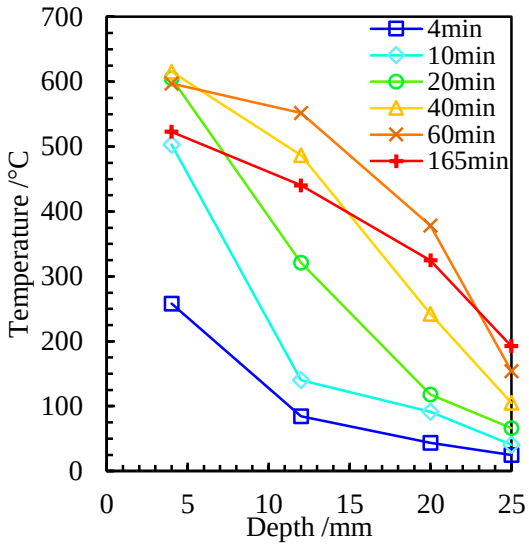

Figure 6.10 – In-depth temperature profile at various steps of sample exposed to 50kW·m^{-2} in the vertical orientation. Note that the period between each timestep is not constant.

Table 6.2 – Selection of timesteps for temperature depth profile.

Timestep (mins)	Point of interest
4	Flaming is well established
10	Flameout
20	4mm deep into specimen reaches peak temperature
40	12mm deep into specimen approaches peak temperature
60	20mm deep into specimen reaches peak plateau
165	Steady state values at end of test

6.5.7 Visual observations

On ignition a luminous flame forms above the specimen, with the intermittent region stretching into and above the cone heater. The flame height was observed to correspond to the recorded mass loss and heat release rates for the majority of the period during flaming. This transitions into a lean, blue flame corresponding to the drop in heat of combustion and CO_2 yield.

As a char layer forms and the thermal wave penetrates deeper into the specimen the pyrolysis rate of volatiles decreases. Eventually this rate drops to the point that the surface temperature is close to the firepoint. Sustained flashes are observed on the surface for the duration of the test, suggesting the temperature may lie between the flashpoint and firepoint. Traditionally these concepts are applied to liquid fuels but there has been success in applying them also to solid fuels (Rasbash 1975, Rasbash *et al.* 1986, Drysdale and Thomson 1989). The duration between flashes of burning increases as the pyrolysis rate and flame temperature continue to

decrease. The flashes are sustained, despite no pilot ignition source, until eventually extinction occurs and the pyrolysis gases are not in sufficient concentration to reach the lower flammability testing. Supplementary testing reintroduced the pilot source after extinction and confirmed that the mixture was not flammable.

The initial colour of the PCM plasterboard is a light pink colour, as is typically seen on "fire" rated gypsum board materials (Figure 6.11a). Once a specimen is inserted into the test chamber it can be difficult to decipher accurately its shade due to the light radiation from the cone heater. Nonetheless, it is clear that once ignition occurs the surface turns to a black colour which will remain for the duration of flaming. This is due to the charring of the PCM capsules, which was evident when tested using TGA in a nitrogen environment. Upon extinction the shade turns to white, marking the completion of oxidation and combustion, evident in the testing of PCM microcapsules in an air environment where the char can subsequently oxidise. Some yellow discolouration is noted in places owing to different levels of thermal degradation. It is hypothesised that this is associated with the decarbonation of calcium carbonate which occurs at high temperatures (above 575°C) and does not appear uniformly across the surface. An incident heat flux of 50kW·m^{-2} is generally too low for this degradation is to be clearly identifiable, but is more visible in later analysis at higher incident heat fluxes (Figure 6.21).

Figure 6.11 – Specimen prior to testing (left) and surface of specimen exposed to 50kW·m^{-2} (right).

Once a test is stopped the specimen is left in the chamber to ensure all the necessary data is collected. It is then removed and allowed to cool. Vapour is emitted from the specimen and cracking of the surface begins to occur once removed from the hot chamber (Figure 6.11b). The cracks are limited to the surface of the material do not extend through the depth of the specimen, and are not sufficient to cause failure of the material. This is due to the glass fibres which are present throughout, which are capable of reducing the tensile stresses that cause cracking.

6.6 Discussion and analysis

A series of experiments were conducted on specimens with imposed heat fluxes of 20kW·m^{-2} up to 100kW·m^{-2}. Particular focus was given to heat fluxes of 20, 50 and 70kW·m^{-2} to ensure the repeatability and reliability of the results. Separate experiments were conducted to allow analysis of both mass loss and thermal profiles. The configuration of the cone heater was considered a variable and experiments were performed in both the horizontal and vertical orientation. This provides a quantification of behaviour of this material in a wide range of fire conditions for use as part of a performance-based fire framework. The properties are discussed in more detail in the subsequent section, and a summary is given in the later in Table 6.4.

6.6.1Ignition

The time to ignition and a plot of $\dot{q}_{inc}''$ vs. $1/\sqrt{t_{ig}}$ are given in Figure 6.12. Good agreement is shown with the ignition theory of solids (Torero 2016) across the range of heat fluxes studied. The endothermic dehydration reactions of the gypsum mean that even at high heat fluxes the time to ignition are considerable, for example, 18±1s at 70kW·m^{-2}. This is similar to some paper-faced plasterboard (Carpenter and Janssens 2005, Asimakopoulou *et al.* 2015) despite the differences in material formulation.

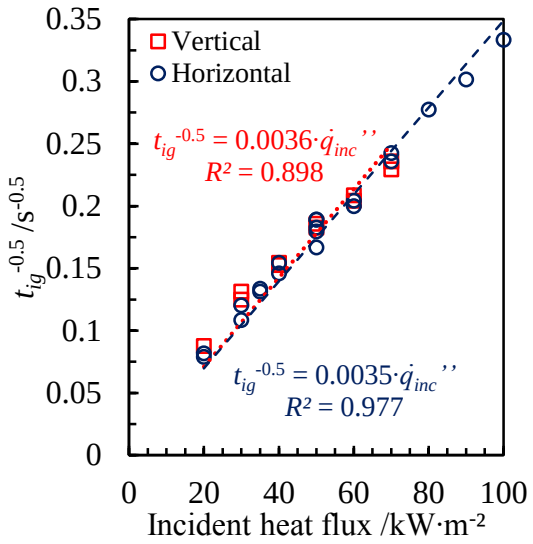

Figure 6.12 – $\dot{q}_{inc}''$ vs. $1/\sqrt{t_{ig}}$ plot from ignition theory of solids. Blue circles represent experiments in the horizontal orientation, whilst red squares represent the vertical orientation.

6.6.1.1 Critical heat flux

The critical heat flux has been determined to be 17.5±2.5kW·m^{-2} in both the horizontal and vertical orientations. This was established experimentally by decreasing the heat flux until no ignition occurred within 10 minutes.

6.6.1.2 Ignition temperature and thermal inertia

The ignition temperature has been found by applying the experimentally determined critical heat flux to the flaming ignition theory of solids, previously given in the *Literature review* chapter. This gives a value of 403°C for data from both orientations, based on a total heat coefficient of 45W·m^{-2}·K^{-1} (Torero 2016).

Using a regression analysis and the assumption that the material is thermally thick a lumped apparent thermal inertia is found to be 0.695 kW^2·s·m^{-4}·K^{-2} for the horizontal. Given that the critical heat flux is not absolute, the range of values for thermal inertia are 0.517 to 0.920 kW^2·s·m^{-4}·K^{-2}. Using the same method, the vertical orientation yields a value of 0.686 kW^2·s·m^{-4}·K^{-2}, with a range of 0.510 to 0.908 kW^2·s·m^{-4}·K^{-2}.

A variation between the two orientations is not unexpected since the ignition theory applied in this manner is not a material property. It is susceptible to environment effects, particularly the convective heat losses. Despite this, very similar values of thermal inertia were found owing to the near identical ignition times over the range of imposed heat fluxes.

The thermal inertia and ignition temperature summarised in Table 6.3, which can be compared with values of other common building materials covered in the *Literature review* chapter. The thermal inertia appears to be higher than other types of plasterboard, but due to large error margins and differences in the calculation method it is not possible to quantify the difference. PCMs have a higher specific heat, thus resulting in a higher thermal inertia for PCM enhanced plasterboard compared to than ordinary plasterboard. The ignition temperature is higher than many of the other materials, whilst lower than paper-faced fire resistant and wallpaper-faced gypsum plasterboards. This suggests that in terms of risk mitigation the propensity for ignition is not a severe issue.

Table 6.3 – Summary of ignition temperature and thermal inertia of the PCM plasterboard in this study.

Material	**Ignition temperature**	**Thermal inertia**	**Critical heat flux**
-	°C	kW^2·s·m^{-4}·K^{-2}	kW·m^{-2}
PCM plasterboard (H)	403; 353-464	0.695; 0.517-0.920	17.5±2.5
PCM plasterboard (V)	403; 353-464	0.686; 0.510-0.908	17.5±2.5

6.6.1.3 Effect of orientation

The time to ignition is found to be almost identical between the horizontal (spark pilot) and vertical (pilot flame): 30.6±3.3s in the horizontal compared to 29.5±0.7s in the vertical, both at 50kW·m^{-2}. Previous research has characterised the difference between orientations during ignition across a variety of materials and found similar results (Shields *et al.* 1993). This shows that for changes in orientation the PCM plasterboard behaves similarly to classic materials and is sufficiently addressed by existing literature.

6.6.2Mass loss rate

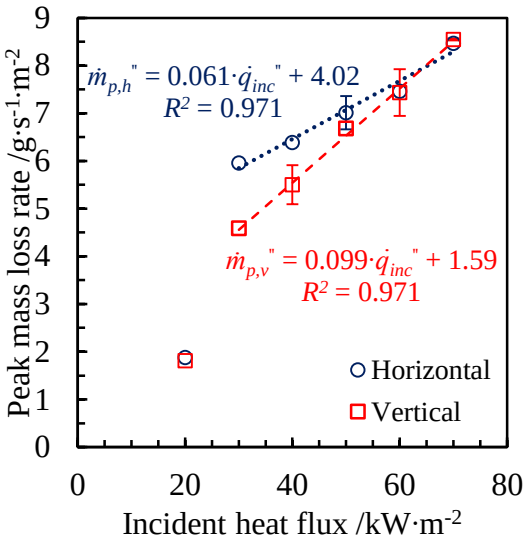

Figure 6.13 – Peak mass loss rate as a function of incident heat flux for both horizontal (blue circles, dotted) and vertical (red squares, dashed) orientations.

The peak mass loss rate across a wide range of heat fluxes for both vertical and horizontal orientations is given in Figure 6.13. A linear trend exists between these two variables at heat fluxes above the critical (20kW·m^{-2}) for both orientations. The relationship is strong without significant deviation across the range of fluxes showing that material behaves well and provides repeatable mass loss rate. The significant deviation of peak mass loss rate from the trend at the critical value suggests that the flaming is not able to properly establish and reach its peak value. Because flaming does not fully establish the convective heat transfer effects are not as dominant in the vertical orientation, thereby yielding an identical peak MLR to the horizontal. At higher heat fluxes where sustained flaming is achieved for a reasonable period then there is a notable difference between horizontal and vertical.

At low heat fluxes the horizontal orientation gives a high MLR. As noted above, the major difference between horizontal and vertical orientations is the dominant heat transfer mode. In the vertical this shows that convective heat losses are reducing the rate at which the material is burning. In the horizontal there are less losses and thus the MLR is higher. As the heat flux from the cone is increased the radiative component becomes more dominant and the convective component, and hence the effect of orientation, becomes less noticeable. At the highest heat flux studied there is little to discern between the orientations for the peak MLR. The full MLR over time for each orientation and heat flux are given in Figure 6.14.

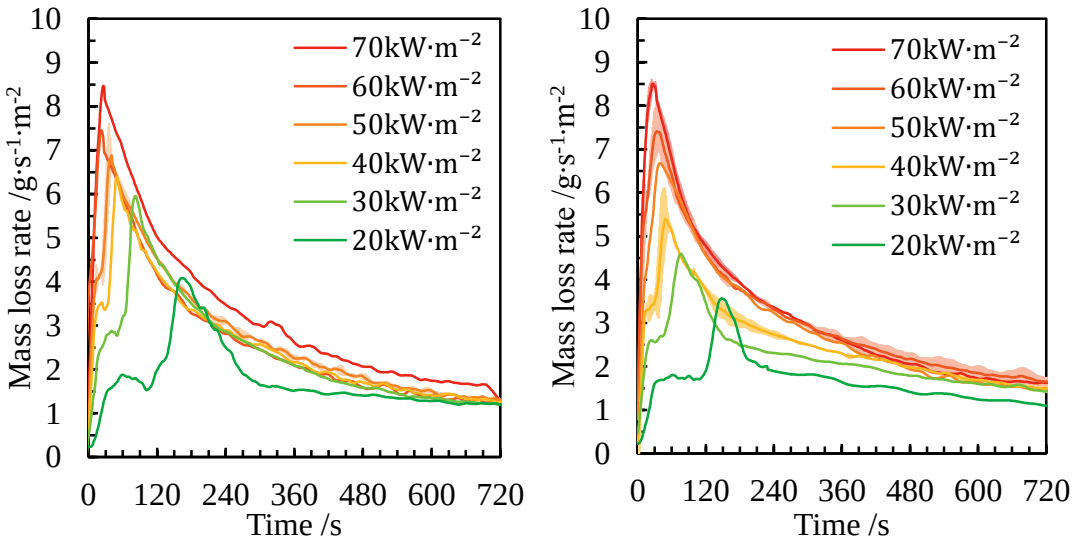

Figure 6.14 – Mass loss rate of (a) horizontal (error bars on 50kW·m^{-2}), and (b) vertical orientations (error bars on 70, 60 and 40kW·m^{-2}). Standard deviation is used as the error, indicated by shaded areas.

6.6.3Total mass lost

The total mass loss after 12 minutes has been recorded for each heat flux in both horizontal and vertical orientations (Figure 6.15). There is not a significant amount of difference in the total mass lost between the two orientations despite the differences in peak MLR throughout the tests. This suggests that the overall MLR is more similar and that the same amount of material is still consumed over time regardless of the peak value.

There is a linear increase with the incident heat flux, although at the critical flux (20kW·m^{-2}) there is less mass lost than would be expected with this relationship. In this instance is it noted that significant vapours generation was visually observed however these were insufficient to sustain flaming.

The total mass lost will give an upper bound limit on the amount of PCM which has pyrolysed and combusted. However, since the endothermic dehydration reactions produce water, this will mean that this is an overly conservative estimate of the quantity of flammable vapours which may potentially be contributed to a fire. The significant amount of mass remaining following the end of flaming confirms that the material behaves as a charring solid.

Other techniques, including Thermogravimetric Analysis (TGA), are employed to identify the amount of mass lost due to each individual components, as well as the material properties. These were previously employed in the thermal degradation framework chapter to obtain accurate properties and provide more knowledge on the fundamental thermal characteristics of PCMs.

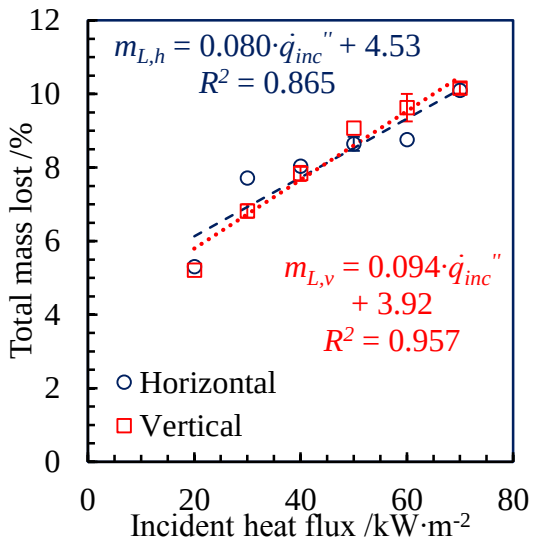

Figure 6.15 – Percentage of mass lost after 720 seconds for horizontal (blue circles, dashed trendline) and vertical (red squares, dotted trendline) orientations.

6.6.4Heat release rate

The heat release rate per unit area calculated using oxygen consumption calorimetry (Janssens 1991) is shown in Figure 6.16. The trend throughout the test follows similarly to the mass loss rate, suggesting a relatively constant value of the effective heat of combustion and the completeness of combustion during flaming, as was noted in Figure 6.5.

Despite good agreement with the ignition theory the peak HRR does not follow a strong trend (Figure 6.17). Clearly the tendency is that peak HRR increases with imposed heat flux, as would be expected. However, across smaller ranges of heat fluxes the error margin is large enough that the resultant peak HRR is not distinguishable between the fluxes. It might therefore be considered that there is a relatively weak relationship between the flammability and incident heat flux, with very high heat fluxes required for a notable increase in the resultant HRR. This is because at high heat fluxes there was strong ignition and a consistent flame with a temperature far exceeding the firepoint was established and sustained. Robust, repeatable trends were noted in the time to ignition, peak MLR, total heat released, and the total mass lost. The weak trend in HRR can be partially put down to the sensitivity of the parameter to environmental conditions for a material which behaves similarly to charring solids.

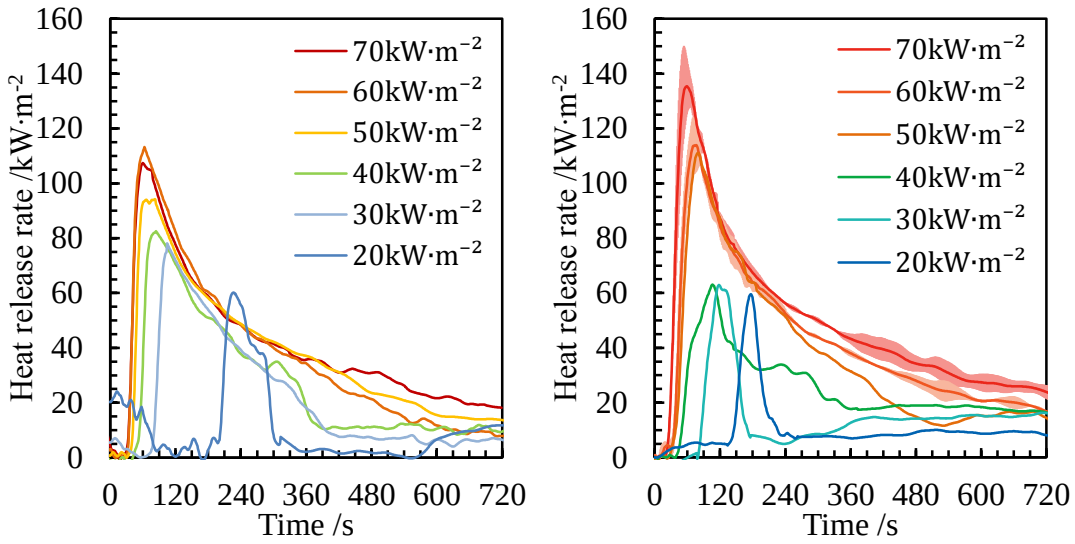

Figure 6.16 – Heat release rate per unit area for (a) horizontal and (b) vertical, showing standard deviation on incident heat fluxes of 60 and 70kW·m^{-2}.

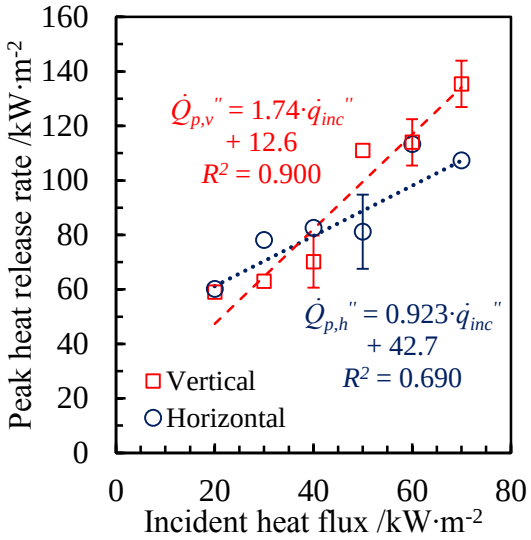

Figure 6.17 – Peak heat release rate of PCM plasterboard in horizontal (blue circles) and vertical (red squares). Standard deviation represents error.

6.6.5 Effective heat of combustion

The heat of combustion has been provided both as a peak value and as an average. The peak is obtained as an average over five seconds, whilst the average, termed the effective heat of combustion, is calculated from ignition until 12 minutes after the start of the test.

The effective heat of combustion increases with incident heat flux and shows a similar trend in both horizontal and vertical orientations (Figure 6.18a). This encompasses the entire duration of burning and provides a more realistic information on the amount of energy produced, which is not reflected in the peak values.

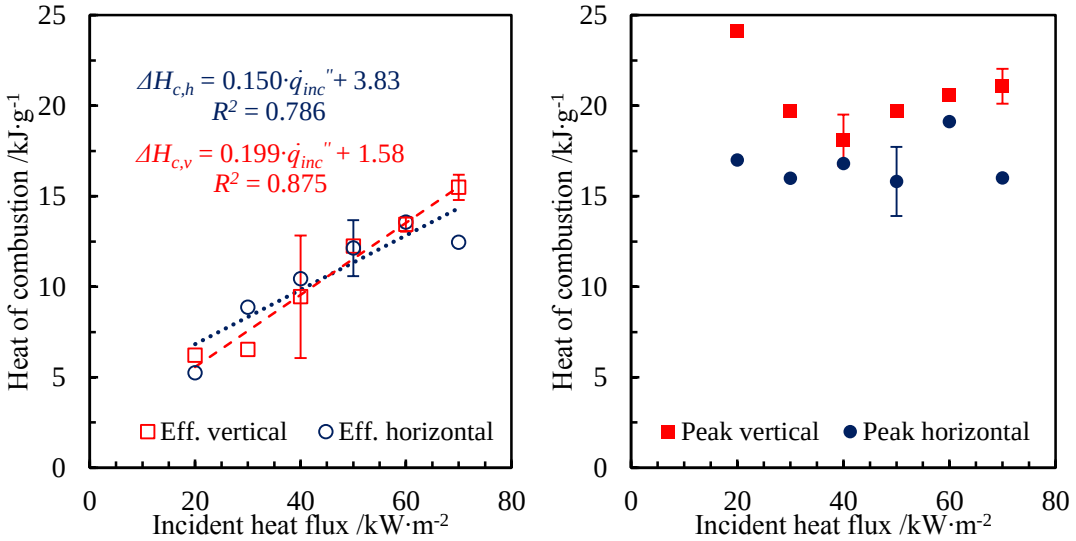

Figure 6.18 – Effective heat of combustion (left, hollow symbols) and peak heat of combustion (right, filled symbols) as a function of incident heat flux for horizontal (blue circles) and vertical (red squares) orientations.

The average peak heat of combustion for the vertical orientation is 20.34±1.91kJ·g^{-1}, and 16.64±1.42kJ·g^{-1} for the horizontal orientation (Figure 6.18b). This differences is due to the flame being able to radiate more heat back to the specimen in the vertical orientation, and thus release more energy for the same amount of mass lost. Despite only a very short flaming period at 20kW·m^{-2}, estimated to be 111s from the heat release rate, the heat of combustion is very high. This corresponds to a short period of efficient combustion during which a lean blue flame was observed at the surface.

The error margins at high heat fluxes are significantly reduced, particularly for the vertical orientation. This is due to the fact that a stronger and more stable flame can be established where at low heat fluxes the temperature lies closer to the flash and firepoints. The boundary layer in the vertical orientation provides more consistent results and more repeatable boundary conditions, as noted in the literature (Reszka 2008).

6.6.6 Gas emissions

Gas emissions in the form of CO_2 and CO yields provide more information on the combustion, and potential transition from flaming to smouldering (Figure 6.19). The peak CO_2 yield values range from 0.7 to 0.9g·g^{-1} during flaming, then immediately drop upon extinction. For low heat fluxes, 20 to 40kW·m^{-2}, the yield drops to near zero levels following flameout which suggests there is not sufficient energy to sustain smouldering combustion beneath the surface. The peak is narrower indicating that the period of constant burning is shorter compared to the higher heat fluxes, namely 50 to 70kW·m^{-2}.

The CO yields predominantly provide information on pyrolysis and the transition to smouldering. For the central range of heat fluxes, 30 to 60kW·m^{-2}, the CO yields are comparable. However, the yield is lower in the two extreme cases of 20 and 70kW·m^{-2}, most likely for differing reasons. In the case of the low heat flux there is insufficient radiation to penetrate the depth of the specimen and generate high levels of carbon monoxide nor be able to initiate a smoulder. This suggests mass is being lost due to the dehydration reactions, but there is insufficient energy to sustain substantial combustion reactions. In the case of the highest heat flux there is flaming for the majority of the test and there will be a preference for CO_2 to be generated over CO as the combustion remains efficient. This is typical of flaming combustion when compared to smouldering (Rein 2009). By the test end there will be flameout and the CO yield will eventually start to increase. Because of the delay in flaming ending it does not reach as high a level as the other heat fluxes before the experiments were terminated.

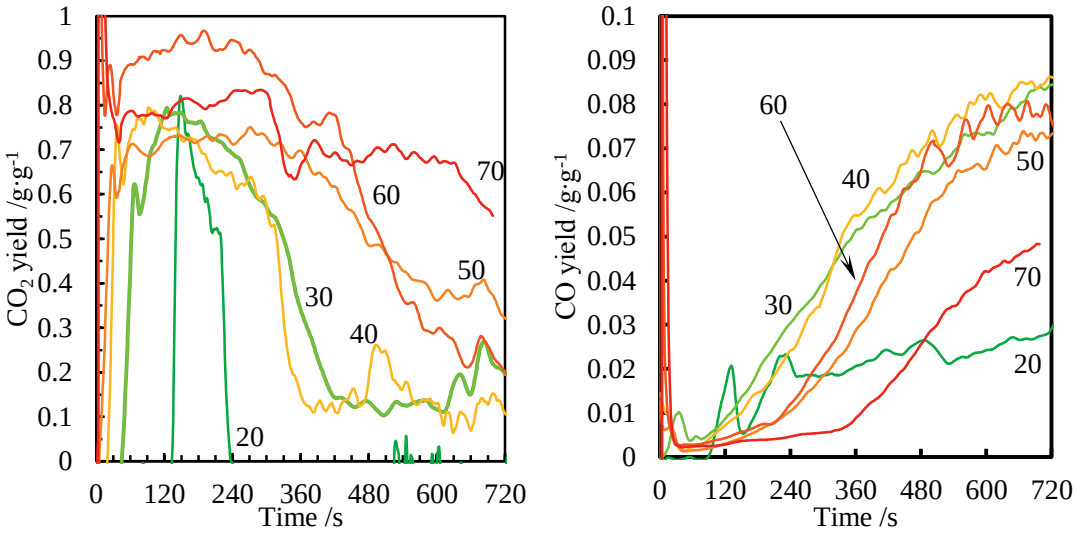

Figure 6.19 – Yields in the horizontal orientation across a variety of heat fluxes, labelled in kW·m^{-2}, for (a) carbon dioxide (b) carbon monoxide.

For the remaining heat fluxes there appears to be a balance between the energy required to penetrate the specimen and sustain some level of smouldering, and in the length of the flaming where the period of efficient combustion persists.

Overall, the CO yields are very low compared to the CO_2 thus representing a very low CO/CO_2 ratio throughout the duration of the testing. Even the peak values which take the length of the test to achieve are only a maximum of 0.085g.g^{-1}, which is lower than the CO_2 yields throughout the duration of tests at all heat fluxes, which are a bare minimum of 0.10g·g^{-1}. The peak CO_2 yield is around 10 times higher for incident heat fluxes of 30 to 60kW·m^{-2}. This shows that whilst combustion is occurring that the reactions are extremely efficient.

6.6.7Thermal penetration

Temperature-depth profiles are used as a measurement of the extent of thermal penetration, which are given in Figure 6.20 for heat fluxes of 35 and 20kW·m^{-2}. For the case of 35kW·m^{-2} the

thermocouple closest to the surface reaches the exothermic oxidation temperature of the paraffin wax by four mins. This would be after flaming had ended and thus much of the evaporation of the material is after extinction. By 20mins the depth to which the pyrolysis front has reached is 21mm, which means that most of the material would already have evaporated and been able to react with oxidiser if there was sufficient concentration and a pilot. For the case of 20kW·m^{-2}, close to the critical heat flux, the time taken for the thermocouple closest to the surface to reach the exothermic oxidation temperature is in the region of 10 to 14mins. This is long after flaming has ended, which only lasts 111s at this heat flux for the horizontal orientation. By 20 mins the closest surface measurement has only reached 375°C, and the pyrolysis front will have reached 13mm.

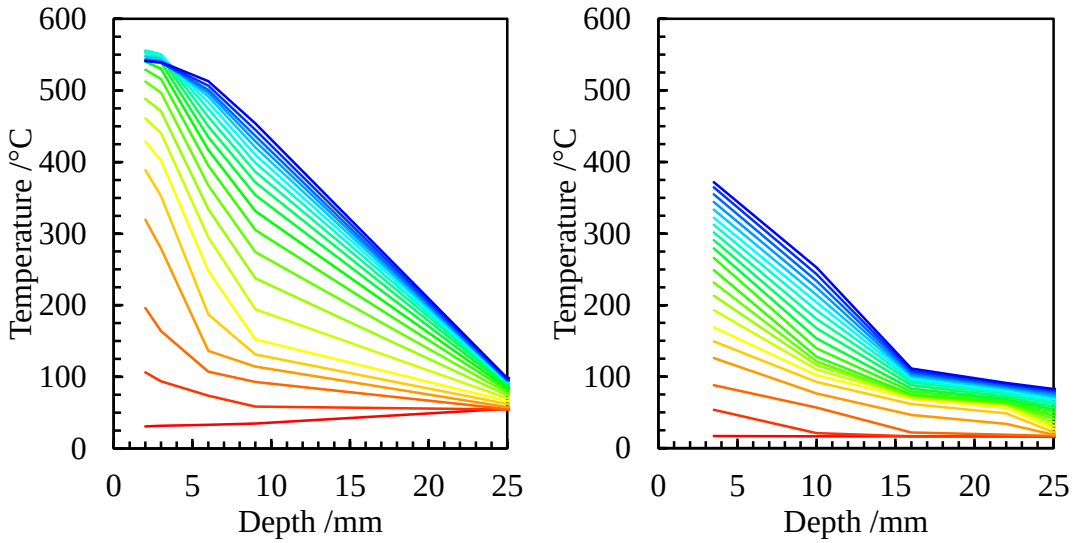

Figure 6.20 - Thermal penetration for both (a) 35kW·m^{-2} and (b) 20kW·m^{-2}. Timesteps are at 2 min intervals, up to a total of 20 mins and both plots are linear piecewise fits.

Despite the short residence time and the comparatively low heat flux this still represents around half of the paraffin wax contained within the material, and would represent significant contribution to a compartment. The temperature evolution provides the means to evaluate the quantity of fuel which can be contributed to a compartment, which may combust if in sufficient concentration and with either a pilot source, or sufficient energy to autoignite.

6.6.8 Visual observations

The darkened surface which is visible throughout the duration of the experiments is partially evident in testing at 20kW·m^{-2} where oxidation has not completed before extinction (Figure 6.21a). This is even more evident in the vertical orientation where more energy from the flame is radiated to top of the specimen due to buoyancy, and thus more oxidation occurs and the surface is lightened. Localised extinction occurs at the bottom once the amount of pyrolysis gases is no longer above the lower flammability limit, and spreads upwards until global extinction occurs. Extensive cracking occurs despite the lower surface temperature compared to other heat fluxes.

Light
brown/grey
surface

Figure 6.21 – Photographs of specimens exposed to (a) 20kW·m^{-2} (vertical orientation) and (b) 70kW·m^{-2} (horizontal orientation).

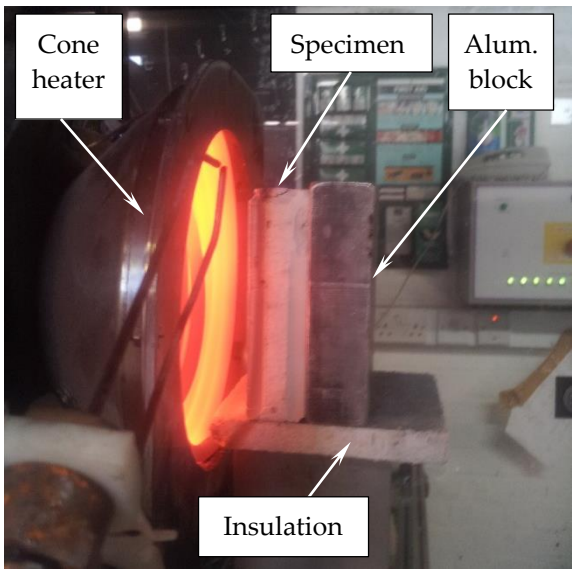

Figure 6.22 – Photograph of a specimen in the vertical orientation after flaming has ended, and with side insulation removed. For illustrative purposes only.

Experiments at 70kW·m^{-2} illustrate the yellow discolouration evident only at higher heat fluxes (Figure 6.21b). This may therefore correspond to a high temperature thermal degradation step. As was noted under the visual observations in the *Results of representative test* section it is hypothesised that this may be due to the decomposition of calcium carbonate, which was the highest temperature reaction noted in TGA. No such colour change is reported in the gypsum literature.

Supplementary testing with the side insulation removed is shown below in Figure 6.22. From right to left the following can be observed: aluminium block forming rear boundary condition, white virgin material, some brown preheating ahead of the black char layer, and finally pink/purple combusted material. The characteristic shape due to the boundary layer in the vertical orientation is evident in the side profile of the specimen, where less heat from the flame is radiated back to the bottom of the specimen compared to the top. The pilot source is not illustrated.

6.6.9 Definition of flaming

For heat fluxes close to the critical heat flux, including 20kW·m^{-2} in the horizontal orientation, the identification of the onset of flaming is associated with a decrease in the oxygen concentration in the exhaust duct and the generation of carbon monoxide and carbon dioxide. Only an extremely small blue/purple flame of approximately 1mm in height is visible on the surface. The low luminosity of the flame and the comparatively thin layer in which combustion reactions occur means that visual identification alone cannot be used to identify the onset of flaming.

6.6.10 Comparison with ordinary plasterboard

Flammability properties of paper-faced plasterboard were previously collated in the *Literature review* chapter to provide a baseline to compare the fire performance of the PCM plasterboard. The test conditions between cases are similar but not necessarily identical. It should be noted in particular that the work carried out in the current study had an aluminium block at the rear surface, which acts as a heat sink. Otherwise, most tests were conducted following the standard cone calorimeter procedure (ASTM International 2014, British Standards Institution 2015a) and should give more or less representative and repeatable results.

Figure 6.23a shows the comparative ignition characteristics of PCM plasterboard compared to ordinary plasterboard. This figure also illustrates the wide range of ignition behaviour for materials assigned to generic term of "gypsum plasterboard". It can be generally seen that the PCM performs neither favourably or unfavourably when compared to plasterboard. For example, at 50kW·m^{-2} the ignition time of PCM plasterboard was 31.6±3.3s while paper-faced plasterboards were within the range of 13 to 72s, or 41.3±26.4s if expressed as an average with standard deviation. From ignition properties it was noted that the thermal inertia of PCM plasterboard is higher, but clearly the ignition temperature is sufficiently low compared to ordinary plasterboard that the time to ignition is lower when compared to the average. Nonetheless, this does not represent a significant fire risk but the ignitability can clearly be properly quantified when tested across a range of heat fluxes.

Similar conclusions can be drawn when evaluating the peak HRR against the literature (Figure 6.23b). The peak HRR at 50kW·m^{-2} for PCM plasterboard was 81.2±13.6kW·m^{-2} compared to a range of 47.6 to 113.14kW·m^{-2} for paper-faced plasterboard, or 74.5±27.4kW·m^{-2}. It can be seen that these values are similar, and that there is a large variance in the paper-faced plasterboard results. It should be emphasised that the PCM plasterboard studied does not have paper-facing and if it did it is expected that this would increase the peak HRR and cause a notable change.

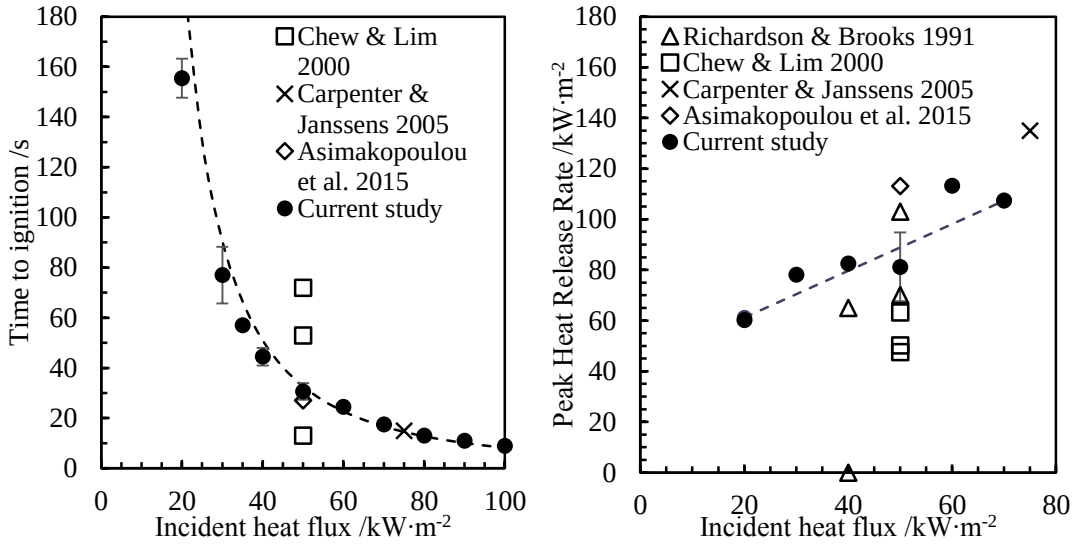

Figure 6.23 – Comparison of paper-faced plasterboard from the literature to PCM plasterboard in this study for (a) time to ignition and (b) peak HRR. Contains data from Richardson and Brooks (1991), Chew and Lim (2000), Carpenter and Janssens (2005), and Asimakopoulou *et al.* (2015).

The total heat released, shown in Figure 6.24, presents the largest difference between PCM enhanced and paper-faced plasterboards. Using this flammability metric, the PCM forms an upper envelope around both ordinary and fire resistant types of gypsum plasterboard. At all imposed heat fluxes the PCM released more total energy when compared to a variety of plasterboard materials. Thus, the PCM does not produce higher peak performances but over a sustained period there will be a contribution to the compartment fuel load resulting from the PCM. The magnitude of this greater contribution depends partially on the specific board in which the PCM is compared to and can be up to six times greater. This corroborates with the observations in *Chapter 5* which quantified the energetic nature of PCMs when added into the matrix of other materials.

The total possible energy released by a paper-faced lining can be quantified if the thickness, or weight, and heat of combustion are known. The British Standards allow a maximum weight of 320g·m^{-2} to attain a B rating (British Standards Institution 2009c) as part of the European standard fire classification system (British Standards Institution 2009a). The heat of combustion of the paper facing can be approximated by using the value for pure cellulose, although this will be overly conservative. Jessup and Prosen (1950) list the heat of combustion of pure cellulose as 17.5MJ·kg^{-1}, which results in the maximum amount of energy which can be released by a B rated paper-faced plasterboard as 5.6MJ·m^{-2}. Additionally, Mowrer (2004) tested a gypsum board with 220g·m^{-2} of paper, which would achieve A2 in the European classification system. At 50kW·m^{-2} this released a total energy of 1.6MJ·m^{-2}, which results in an effective heat of combustion 7.2MJ·kg^{-1}. This confirms that using pure cellulose to represent the paper facing is conservative, and that the heat of combustion of the paper is significantly less than that of the PCM. This, combined with the long flaming durations of PCM plasterboard, results in the much greater quantities of energy released.

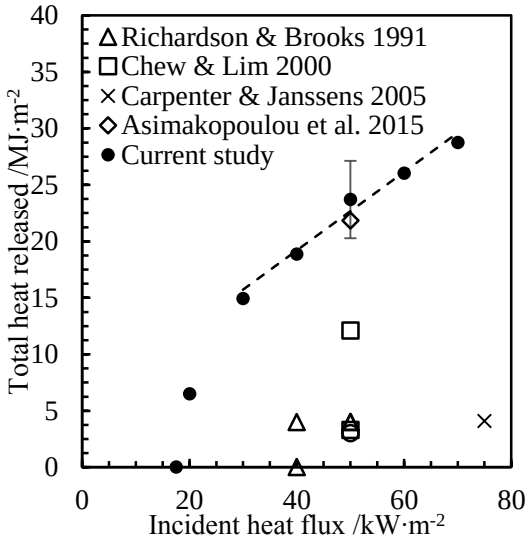

Figure 6.24 – Total energy released for PCM plasterboard and paper-faced plasterboards. Contains data from Richardson and Brooks (1991), Chew and Lim (2000), Carpenter and Janssens (2005), and Asimakopoulou *et al.* (2015).

6.6.11 Comparison to previous testing of PCM plasterboard

The comparison to plasterboard can be extended to the few studies available on PCM plasterboard also. Two different studies which evaluated the flammability of PCM enhanced plasterboard were discussed in the *Literature review* chapter. Research by Banu *et al.* (1998) used a 12.5mm thick material synthesised in a laboratory with both immersion and dipping encapsulation techniques. Asimakopoulou *et al.* (2015) studied a commercially available 12.5mm thick board containing microcapsules, similar to the current study. However, the board in this chapter is instead 25mm thick and has a different level of PCM loading by weight. It should also be noted that both of the referenced studies contain combustible paper facings, which are not present for the material in this thesis. The effect of the paper facing has already shown to be comparable to the addition of PCM for both time to ignition and peak HRR.

For the parameters studied the closest agreement is found in the time to ignition. This is similar at 50kW·m^{-2} in the horizontal orientation for both this study, 31.6±3.3s, and the study by Banu *et al.* (1998), at 33±1s. This is likely due to the similar thermal inertias of the materials, which is dominated by the plasterboard. It is assumed that the ignition temperature of these materials is similar. This is logical given that only a certain set of paraffin waxes can be used to achieve the desired melting point of the PCM for room temperature, and these will have comparable boiling and firepoints. The time to ignition in the study by Asimakopoulou *et al.* (2015) is higher, 41s at 50kW·m^{-2}, which may be due to the fact that the exothermic oxidation of the PCM was found to be higher using TGA. This would lead to a higher ignition temperatures and hence longer time to ignition, assuming that the thermal inertia remains similar. The effect of the paper facing on the time to ignition is minimal. The TGA study in this thesis conveniently included cellulose contained within hemp, and identified that the primary exothermic oxidation of paraffin wax occurs at a lower temperature than the

exothermic oxidation of cellulose. This was also confirmed in the previous two chapters testing the ignitability and flammability of the cellulosic hemp-lime material. This confirms that the paraffin wax is the primary component in the ignition of PCM enhanced plasterboards, and not the paper facing.

The heat release rate is often given as the key metric in determining material flammability (Babrauskas and Peacock 1992, Biteau 2009). In the current study the peak HRR is only 45% of the value found by Asimakopoulou *et al.* (2015), and 48% of the value found by Banu *et al.* (1998). Considering that the paraffin wax content is only 54% of the value found by Asimakopoulou *et al.* (2015), this suggests that there may be a linear relationship between paraffin wax content and peak HRR. More data with different quantities of PCMs contained in plasterboards would be required to confirm this. Indeed, the PCM plasterboard in Banu *et al.* (1998) has a 250% higher paraffin wax content yet the peak HRR is not proportionally higher, at 170.75±12.66kW·m^{-2}, and is in fact lower when compared to Asimakopoulou *et al.* (2015), which was 181.38kW·m^{-2}.

The total heat released (27% compared to Asimakopoulou *et al.* (2015), 39% compared to Banu *et al.* (1998)) and the total mass lost (20% of Asimakopoulou *et al.* (2015), 24% of Banu *et al.* (1998)) are far below the values expected given the paraffin wax content. This may be because the lower wax content reduces the amount of pyrolysis gases which can be produced, and hence brings the flammable gas mixture closer to the lower flammability limit. This also brings the flame temperature closer to the flash and firepoints of the material. The effect of the dehydration reactions also has greater significance where less pyrolysis gases are generated and less heat is released. These reactions were previously shown by TGA to have magnitudes of –0.36±0.03W·g^{-1} for endothermic dehydration and 0.48±0.02W·g^{-1} for exothermic oxidation of the paraffin wax. This, in addition to heat losses, may be sufficient to quench the combustion. Furthermore, both PCM enhanced plasterboards in the literature had paper facings which will increase the total amount of energy released. The paper facing could act as a wick (Faraday 1861) which would allow the paraffin wax to burn more effectively but would further study would be required to investigate this. The amount that the paper facing will contribute has been quantified for ordinary plasterboard in the previous section, and remains a small portion compared to the energy released by the PCM.

6.6.12 Effect of sample orientation

For each of the properties investigated in this chapter the difference due to the orientation has been discussed. Generally, there has not been significant difference between the two orientations. Past research (Tsai 2009) has indicated strong trends which can be observed between the two orientations, and generally note that the vertical gives greater repeatability. For this research there is generally not found to be a definitively higher level of repeatability or consistency from either orientation for mass loss rate, heat release rate, or gas emissions. The results of heat release rate in the vertical orientation at low heat fluxes where only a weak flame was established had large errors and poor trends. The trend between incident heat flux and peak HRR was also relatively weak in the horizontal orientation, but was still more clearly

defined. In the case of time to ignition the vertical orientation yielded results with a much smaller standard deviation across all heat fluxes. The usage of a pilot flame in the vertical instead of the spark igniter used in the horizontal may also have an effect on these results.

Given that there is no melting or dripping for this material the vertical orientation remains a suitable possibility. It is recommended that when tests are carried out on these materials that they should never solely be conducted in the vertical orientation, since this limits the amount of comparison and the correlations that can be used. The greater repeatability in the times to ignition would suggest that the vertical orientation is preferable where research is concerned, and should continue to be used.

6.6.13 Optimisation techniques

The knowledge generated through this study allows the optimisation of energy savings against quantified fire performance. In terms of thermal penetration the designer can select an appropriate critical temperature for the rear facing of the PCM lining. This may for example correspond to the point at which pyrolysis gasses are generated by the layers behind the PCM plasterboard. The knowledge from this research can then be used to limit the amount of thermal penetration through the wall and ensure that this critical temperature is not exceeded. Alternatively, it may identify the need to reduce the incident heat flux that will be resultant upon the wall, so that the thermal penetration will be reduced through this way.

The PCM board in this research behaves similar to a charring material. Harmathy (1979) identified the fire behaviour for compartments containing charring and non-charring materials, as well as a combination of the two. It was found that in compartments either completely or predominantly containing charring materials would be highly dependent on the fuel load. Only small amounts of ventilation were required to achieve peak pyrolysis rates even during early stages of a fully developed fire, and additional ventilation beyond this point had little to no effect. Thus, designers should consider the mass loss rate and heat release rate per unit area which PCMs will potentially contribute to a fire. The high surface area of these materials means that there is the potential for a significant increase in the amount of fuel available in a compartment.

These different measures should be checked against the energy savings that can be attained through the usage of PCMs. This then allows a balance of the amount of energy that can be saved through the incorporation of PCMs to be balanced with their quantified fire performance. The designer can set specific goals and ensure that these are met, whilst still achieving high levels of energy saving. Furthermore, design in this manner ensures that the material is properly understood and the fire risk associated with these materials can be mitigated.

6.7 Concluding remarks

The work on this chapter has investigated the fire behaviour of an end use PCM plasterboard product already implemented in the built environment. The conclusions are as follows:

- PCM plasterboard acts in a manner which is not consistent with the materials studied in the middle to late 20th century when many of the existing fire safety frameworks were developed.
- The fire risk associated with a material representative of PCMs currently used in the built environment was quantified in a range of conditions to evaluate its performance in realistic fire conditions.
- Upon exposure to the imposed radiant heat flux the temperature reaches the endothermic dehydration reactions. Eventually the temperature reaches the vaporisation point of the paraffin wax, allowing it to escape from its shell and react with the air.
- The highly endothermic dehydration reactions of the gypsum substrate cause a lengthy delay in ignition even at very high heat fluxes (18±0.5s at 70kW·m^{-2} in both horizontal and vertical orientations).
- The critical heat flux was experimentally determined to be 17.5±2.5kW·m^{-2} in both horizontal and vertical orientations. The use of a spark igniter in the vertical orientation may increase the critical heat flux by a small amount (up to 20% in the literature).
- The PCM plasterboard behaves similarly to a charring material and thus charring models are applicable to describe its behaviour. The MLR and HRR reach a peak shortly after ignition, and then decay as a char layer forms. The thickness of the material does not decrease during burning, and significant mass remains at the end of the tests.
- The heat release rate per unit area has been provided as a function of imposed incident heat flux. This allows a simplified method to evaluate the behaviour of this material in realistic fire conditions.
- The thermal penetration as a function of heat flux was provided as a method to characterise the behaviour of the material. This allows understanding of the amount of material which will be involved and contribute to a fire.
- A surge in carbon monoxide corresponding to the generation of a significant amount of pyrolysis gases prior to ignition is evident. The CO generation remains very low during flaming, but increases as the thermal wave penetrates through the specimen.
- Oxygen depletion is evident even after flaming has ended, suggesting that combustion reactions continue as the thermal wave propagates through the depth of the material. This is particularly evident at high heat fluxes, but at lower heat fluxes there appears to be insufficient energy to establish and sustain a smoulder.
- The lower exothermic oxidation of paraffin wax compared to the exothermic oxidation of cellulosic paper reduces the ignition temperature. Despite a higher thermal inertia, the time to ignition for PCM plasterboard is lower compared to most ordinary and fire rated gypsum boards.
- When compared to ordinary plasterboard both the time to ignition and the peak HRR were similar for PCM plasterboard. However, large differences were noted in the total energy released due to the longer incident times of flaming, as well as the high heat

of combustion of paraffin wax compared to paper. This confirms the energetic nature of PCMs.

- The total energy released represents the contribution to fuel load due to PCM plasterboard, and can be quantified using the methodology set out in this chapter. The amount of energy released is related to the quantity of paraffin wax, which will be pertinent to designers seeking potential energy savings.

Some of the key numerical results for this specific PCM plasterboard have been summarised below in Table 6.4.

Table 6.4 – Summary of flammability properties of PCM plasterboard tested in the cone calorimeter.

Parameter	**Horizontal**			**Vertical**		
Incident heat flux ($kW \cdot m^{-2}$)	20	50	70	20	50	70
Peak heat release rate† ($kW \cdot m^{-2}$)	60.2	81.2±13.6	107	59.4	111	135±8.5
Total energy released ($MJ \cdot m^{-2}$)	6.5	23.7±3.4	28.8	7.3	25.4	35.3±1.3
Peak mass loss rate† ($g \cdot s^{-1} \cdot m^{-2}$)	1.88	7.01±0.65	8.47	1.81	6.68	8.56±0.02
Residual mass (%)	94.7	91.4±0.2	89.9	94.8	91.0	89.8±0.1
Time to ignition (s)	150	31.6±3.3	18	130	29.5	18.5±0.7
Time to flameout (s)	235	315	335	207	373	505
Effective heat of combustion ($kJ \cdot g^{-1}$)	5.25	12.1±1.2	12.5	6.22	12.3	15.5±0.7

†Peak values are averaged over five seconds.

7 Intermediate-scale standard fire testing of PCM plasterboard

7.1 Summary

Testing at intermediate-scale is necessary to confirm that the bench-scale flammability results are applicable to realistic fire conditions on a larger scale. For this purpose, two series of testing using standardised intermediate-scale apparatuses have been conducted. The first is LIFT (ISO 5658, British Standards Institution 2006) to investigate flame spread as a key component to fire growth. The second in Single Burning Item (BS 13823, British Standards Institution 2010) which analyses the impact of a localised fire on wall linings in a corner configuration. These tests were conducted using additional temperature measurements so that the performance of the material can be assessed in these conditions and to allow comparison to the flammability assessment in the previous chapter. Otherwise, the tests were carried out as per the standardised procedure referenced above. It was found that the micro- and bench-scale results were a useful tool in interpreting the intermediate-scale test results. In LIFT (Lateral Ignition and Flame spread Test), there was found to be minimal fire risk associated with this specific PCM plasterboard. For SBI (Single Burning Item), the energy contribution from the PCM was relatively low and thus it achieved a B classification, which is the same as other plasterboard materials. However, the test method was not able to quantify the differences from ordinary plasterboard which were found in flammability study.

7.2 Introduction

LIFT and SBI represent two fundamental tests in the 'reaction to fire' series. The tests are capable of representing full-scale behaviour more readily than the cone calorimeter, but without having to conduct large-scale experiments which are both costly and time consuming.

ISO 5658 LIFT (Lateral Ignition and Flame spread Test) allows characterisation of the propensity of a material to sustain flame spread when exposed to an external heat flux. Through analysis based on Quintiere (1981) the minimum heat flux for spread and flame spread parameter can be calculated, in addition to the same flammability metrics which can be found in the cone calorimeter. Samples which are 800mm long are exposed to a radiant panel which provides a heat flux distribution with a peak incident flux of 50kW·m^{-2} near the panel, and eventually decays to zero near the far end. Materials are ignited at one side, and the spread of the flame front is measured to determine the above parameters.

The ISO 13823 SBI test (Single Burning Item) was designed with the explicit goal of representing the ISO 9705 room corner test (British Standards Institution 1993) on a smaller and more affordable scale (van Mierlo and Sette 2005). It provides a method of analysing how wall linings react to a fire exposure from a 30kW gas burner. Wall linings which are 1.5m high are placed in a corner configuration which is exposed to the burner for 20 mins. A specially designed parameter, FIGRA, takes into consideration the magnitude and rate of heat release is used to classify materials (Sundström 2007). The test method allows the interrogation of a

variety of parameters including the propensity for lateral or upward flame spread, the heat release rate per unit area on a larger scale, heat feedback, interactions between perpendicular walls, and the potential for breach or failure of the element. Many of these properties are not possible to investigate using bench-scale apparatus, and are only evident on larger scales.

The aims of this chapter are to: investigate the applicability of the bench-scale results on a larger scale; quantify the fire performance of this material in the standard test; and interpret the results obtained from the standard tests using flammability data.

7.3 Literature review

The ability to understand how a material will behave in a full-scale fire scenario is critical to understanding its fire performance and the resulting risks (Torero 2013). A key parameter of each of these tests, both LIFT and SBI, is flame spread. In the LIFT apparatus, this is apparent where the lateral opposed flow flame spread is directly measured. In SBI the connection is less obvious. However, one of the critical parameters is the flame height and HRR caused by upward flame spread on the walls. Driven by buoyancy, this flame spread is more akin to concurrent flow conditions (Quintiere *et al.* 1986). The upward flame spread in SBI is correlated to the ISO corner room test in which the impingement of flames on the ceiling is generally associated with flashover in prediction models, for example, Karlsson (1993), Kokkala *et al.* (1993), and Hakkarainen (2001).

7.3.1Flame spread

Flame spread is one of the key factors governing the growth phase of a fire (Drysdale 1999). In this section, a brief theoretical background to opposed flame spread is presented before discussing the development and practical means of measuring flame spread.

7.3.1.1 Opposed flow flame spread

Opposed flow flame spread is a fundamental topic in the field of fire science and has been the focus of an abundance of research for the past decades. As such, there are a wide variety of approaches, mainly based on the seminal work by de Ris (1969), which each have different assumptions, applications, and complexities. The work in this chapter generally follows the empirical approach developed by Quintiere and Harkleroad (1985), although some of the fundamental and theoretical implications are also discussed. The focus is on opposed flow flame spread since this is the most relevant case for downward or lateral flame spread with no forced flow conditions.

Flame spread is usually defined as the movement of a flame across a surface (Wichman 1992). Radiation from the flame, and to some extent convection, heat fuel ahead of the flame front to the pyrolysis temperature. Once the flow of pyrolysis gases is sufficiently high the flame will act as a pilot and will be able to spread forwards. Heat, in the form of radiation and convection, are transferred from the flame to the solid downstream and maintain the generation of pyrolysis gases, and thus the flame is sustained. There will also be some conduction from the decomposition layer to the fuel ahead which increases the rate at which the virgin material

will reach the pyrolysis temperature. A schematic illustrating these processes by Fernandez-Pello (1984) is shown in Figure 7.1.

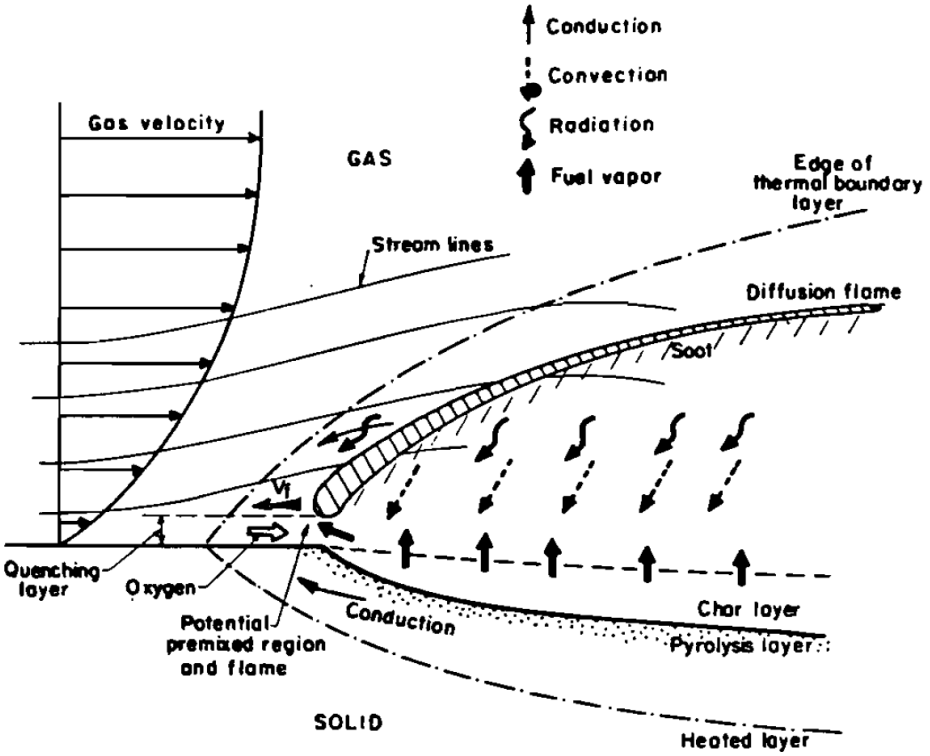

Figure 7.1 – Processes in opposed flow flame spread. Extracted from Fernandez-Pello (1984).

For the case of charring solids the mechanism of flame spread is more complex. Additional decomposition processes are involved, and the build-up of an insulating char layer inhibits heat transfer to the solid. Di Blasi (1994) also noted that the contribution of conduction from the decomposition layer forms a significant portion of the total energy transferred to the virgin material upstream, and may be up to 50% in the case of wood.

Flame spread has also been the subject of study for liquid fuels, where the propensity for spread is partially described by the flash and firepoints of the liquid. The flammability study in the previous chapter identified both that (i) the concepts of flash and firepoint were useful in describing the ignition behaviour of PCMs, despite being solids, and (ii) that PCMs contain a liquid fuel within a material which behaves similarly to charring solids. A comprehensive review by Glassman and Dryer (1981) stated that for paraffins greater than C_9 there was a pulsing blue flame in front of the main luminous yellow flame. This blue flame was termed a precursor flame, pulsing flame, or oscillatory flame. It was hypothesised that the reason for this premixed flame was due to the fact that the gas mixture upstream was not stabilised, and that the rate of consumption was faster than the rate of generation (Akita 1973). It was found that this occurred in materials where there was a wide range between the flash and firepoint, as it was not repeated in experiments with n-butanol where these points are significantly closer. Glassman, in comments to Akita (1973), concluded that the reason this occurred was because the preheating was not sufficient, and that the flame spread was a gas phase controlled premixed process. The relevance of this to PCMs is that the core is often a long

chain paraffin wax, around C_{16} to C_{18}, and as a charring-like material preheating will be inhibited by the formation of a char layer which limits the generation of pyrolysis gases. Thus, there is the potential for a precursor or pulsing flame ahead of the main diffusion flame front. The flammability study in the cone calorimeter previously identified the presence of a lean blue premixed flame which flashed frequently across the surface. Furthermore, it was found that there was a large gap between the flash and firepoint.

7.3.1.2 Experimental determination

The capability to quantify the ability of a material to spread flame became highly desirable in the mid to late 20th century, and many research laboratories devised apparatus capable of describing this property (Quintiere 1981). However, the results from these were entirely apparatus-dependent and consequently a single standardised apparatus applicable to the majority of materials was required to consistently determine key fire growth parameters. The LIFT (Lateral Ignition and Flamespread Test) apparatus was developed by Quintiere *et al.* (1983) to achieve this goal, and was later accepted as both an ASTM standard, ASTM 1321 (ASTM International 2013b), and as an international standard, ISO 5658 (British Standards Institution 2006).

The purpose of the LIFT apparatus is to be able to describe the bulk processes without requiring knowledge on the chemical kinetics and other complicated mechanisms (Quintiere *et al.* 1983). This is valid for instances where the rate of chemical reactions is far more rapid than the time taken for the conduction of heat through the solid, which is the case for flaming combustion. The theory is based on the heating of a thermally thick inert solid to the ignition temperature. PCM plasterboard was shown to be thermally thick from the thermal evolution of samples in the cone calorimeter. The inert solids assumption was found to be adequate for the ignition theory of solids since good agreement was found. For radiative terms a black body is assumed.

A radiant panel is offset at a distance of 125mm and an angle of 15° from the leading edge of an 800mm long sample, as shown in Figure 7.2. This configuration yields an incident heat flux which varies along the length of the specimen. During the development of the apparatus, the distribution was based on the incident heat flux measured at a point 50mm from the leading edge of the sample. The heat flux at this location was selected to be approximately 5 to 10kW·m^{-2} above the critical (ASTM International 2013b), which would be derived from other appropriate means. These means include the cone calorimeter (Babrauskas 1984); the LIFT apparatus itself could be reconfigured so that the radiant panel is parallel; or in modern times the Fire Propagation Apparatus can also be used (ASTM International 2013c). The heat flux was controlled by varying the gas flow to the radiant panel, which could typically operate in the range of 15 to 70kW·m^{-2}. Ignition would be achieved using a pilot flame introduced 50mm from the leading edge, and a period of preheating could be added if desired. As the remainder of the specimen would be below the critical heat flux for ignition, the flame spread could be investigated (Quintiere and Harkleroad 1985). In the standardised methods of ASTM 1321 and ISO 5658 (British Standards Institution 2006, ASTM International 2013b) the incident heat flux

is instead normalised to be 50.5±0.5kW·m^{-2}, which is far higher than the critical heat flux of most materials. The flame spread then only becomes of particular interest as the pyrolysis front progresses to the region of the sample where the incident heat flux is below the critical flux. Beyond this point the critical heat flux for flame spread can be determined.

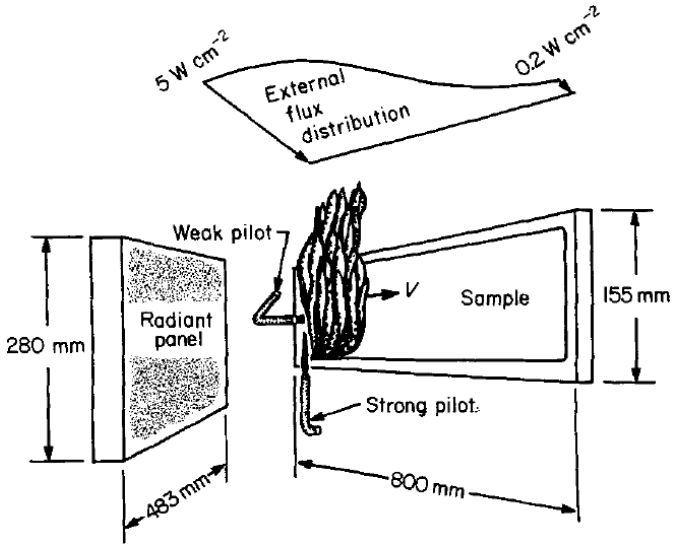

Figure 7.2 – Initial proposal for LIFT configuration. Note that in ISO 5658 the weak pilot is not used. Extracted from Quintiere (1981).

7.3.1.3 Derivation of parameters

One of the key properties used to evaluate lateral flame spread as part of the standardised LIFT test is CFE (Critical Heat Flux at Extinguishment). This refers to the point in which flames do not spread beyond at the time the test is stopped. The corresponding heat flux from the calibration is then used and this is listed as CFE. Other terminology used in the literature includes critical heat flux for flame spread, $\dot{q}_{0,s}''$ (Quintiere 1981). This differs slightly from the critical heat flux for ignition which was discussed in the bench-scale calorimetry chapters. The critical flux for ignition defines the amount of energy required to sustain a flame for a given heat flux, whilst the critical spread flux, or CFE, refers to the amount of energy required to sustain flaming aided by an external radiant heat flux.

The final term used in the standardised testing is the average heat of burning. This is obtained by multiplying the time taken to reach a specified distance by the incident heat flux at that location. This is then averaged for all the locations and given as a single value.

Two of the critical parameters derived from the flame spread test are the rate coefficient (or flame spread modulus), *C*, and flame spread parameter, *Φ*. These are empirical parameters which are determined in LIFT. The flame spread modulus, *C*, is defined as (Quintiere 1981, Quintiere *et al.* 1983):

$$C = \frac{1}{\dot{q}_f'' \cdot \sqrt{a \cdot \delta_f}}$$

and;

$$a = \frac{{h_t}^2}{k \cdot \rho \cdot c_p}$$

Which then allows calculation of the flame spread parameter (Quintiere 2006):

$$\Phi = \frac{k \cdot \rho \cdot c_p}{{h_t}^2 \cdot C^2}$$

Where the product $k \cdot \rho \cdot c_p$ is the thermal inertia ($kW^2 \cdot m^{-4} \cdot K^{-2} \cdot s$), h_t is the total heat transfer coefficient ($kW \cdot m^{-2} \cdot K^{-1}$), $\dot{q}_f''$ is the heat transfer from the flame ($kW \cdot m^{-2}$), and δ_f is the flame heat transfer length. The flame spread modulus, *C*, can be obtained experimentally by taking the gradient of incident heat flux against $1/\sqrt{V_f}$, where V_f is the flame spread velocity ($mm \cdot s^{-1}$).

7.3.1.4 Plasterboard results

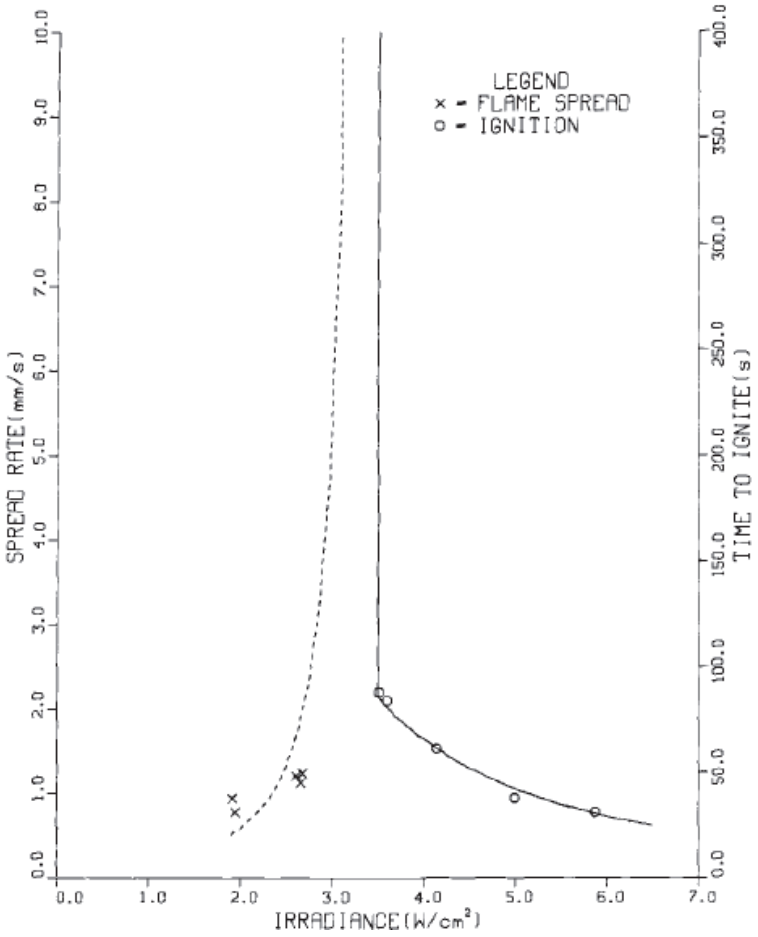

Figure 7.3 – Flame spread rate and time to ignition as a function of incident heat flux for a paper faced gypsum board (12.7mm thick). Extracted from Quintiere and Harkleroad (1985).

Quintiere and Harkleroad (1985) studied a variety of materials using the LIFT apparatus. This included paper faced gypsum board (shown in Figure 7.3), fire resistant gypsum board, and wallpaper faced gypsum board which had flame spread parameters of 14.44, 9.25, and

$0.79 kW^2 \cdot m^{-3}$, respectively. It should be noted that for some materials – epoxy fiberite (aircraft panel), fire resistant plywood, and polystyrene – the authors were unable calculate flame spread.

7.3.2 Single Burning Item

The ISO 13823 SBI test (British Standards Institution 2010d) forms an integral part of the European classification framework for products, ISO 13501 (British Standards Institution 2009a). This test method is used to classify products based on their predicted performance in the ISO 9705 room corner test (British Standards Institution 1993). From this, an appropriate lettered classification is given which will determine how a product can be used in a building. Consequently, it is an extremely important test in the development of new products.

7.3.2.1 Development of the test method

Wall linings and similar materials play a significant role in the development of a compartment fire (Drysdale 1999). A short time to flashover has been strongly associated with loss of life and greatest damages in buildings fires. Some statistics to support this are available in the UK (Department for Communities and Local Government 2012), but these can often be difficult to interpret accurately. Nonetheless, avoiding flashover, or maximising the time to flashover, has been identified as a key mechanism to reduce fire casualties and losses.

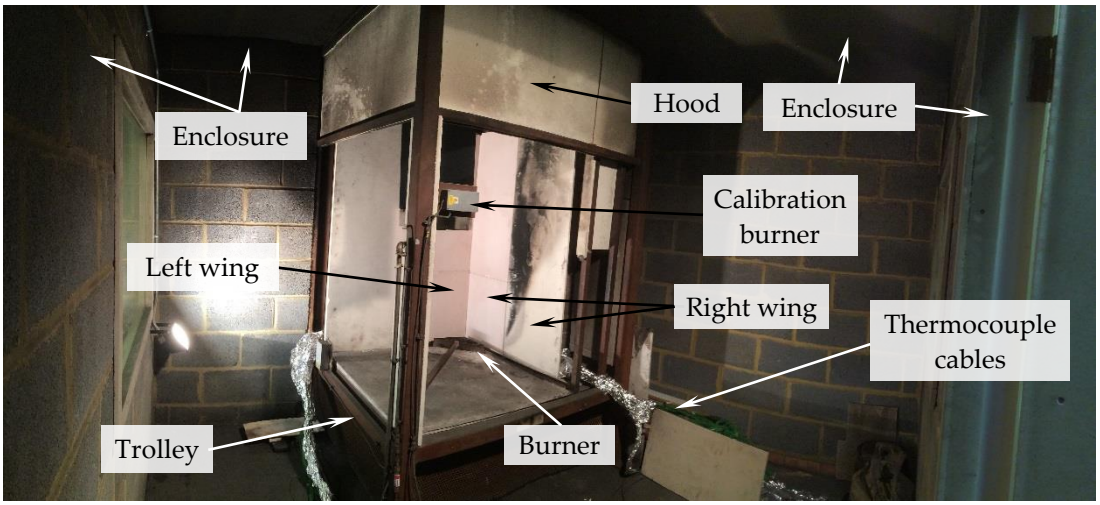

Figure 7.4 – General overview of the SBI setup. The apparatus is positioned on a trolley within a room, and under a hood. Thermocouple extension cables emerge from the left and right sides of the trolley, and are covered in aluminium foil.

Since the time to flashover cannot be adequately predicted by scale up of material flammability, a harmonised test method capable of adequately classifying materials was required to allow them to be ranked based on their contribution to fire growth. This lead to the development of the ISO room corner test, which is described in detail later, and subsequently the SBI test. The purpose of SBI is to provide a method of classifying materials without the need to perform costly and time consuming full-scale ISO room corner tests. The

performance of a material in SBI results in a Euroclass rating (British Standards Institution 2009a).

The fire exposure in SBI is a 30kW triangular propane burner placed in the corner formed by a short wing, which is 0.5m wide and 1.5m tall, and a long wing, 1.0m wide and 1.5m (Figure 7.4). The extra width of the long wing is to facilitate lateral flame spread along the surface of the exposed specimen. Oxygen consumption, and carbon monoxide and dioxide generation are all measured in the hood above which collects the smoke and post-combustion gases. The purpose of the surrounding enclosure is to reduce the influence of convective flow effects.

7.3.2.2 Classification

The classification of products in the SBI test is achieved through the use of the FIGRA (FIre Growth RAte) parameter, which was developed by Sundström (2007). This parameter is calculated by dividing the peak HRR (W) by the time taken to reach this peak (s). This parameter, measured in $W \cdot s^{-1}$, describes the fire growth associated with a material or product. When obtained from SBI, it is generally notated as FIGRA(SBI) since different test methods will yield slightly different values. This is often stated to be the key parameter which affects both the propensity and time taken for flashover in the ISO room corner test (Sundström 2007).

Products tested in SBI will have their FIGRA(SBI) value checked against limits and then given an appropriate classification. The class limits were determined during the development of SBI, and is based on the 30 materials tested in a round robin at nine laboratories. A summary of the classification system connected to SBI is given in Table Table 7.1.

Table 7.1 – SBI limits for European classification system. Note that to achieve a certain classification other tests must be conducted, which is particularly evident for A2.

Class†	**FIGRA(SBI) limit**	**Predicted ISO room behaviour**
-	$W \cdot s^{-1}$	-
A2/B	≤120	No flashover
C	≤250	Flashover at 300kW exposure
D	≤750	Flashover after 2 minutes of 100kW
E	≤750	Flashover before 2 minutes of 100kW

SBI was able to correctly predict the outcome of the ISO room corner test in 26 out of the 30 products tested as part of the first round robin (Messerschmidt *et al.* 1999). Furthermore, FIGRA was found to be an accurate representation for 90% of materials during its development (Sundström 2007).

For four products, the results from SBI did not correlate well with the ISO room test: cables, pipes, polycarbonate, and polystyrene sandwich panels. For cables, pipes and other similar products it was agreed that these materials were not intended as wall linings and an alternate, more appropriate, method was developed (Sundström and Axelsson 2002). For the other two it was identified that the ISO room corner test would need to be performed to obtain

representative results (Johansson and Van Hees 2000), but no alternate solution was provided and these materials can still be tested and certified in SBI.

The reason that these final two materials were not adequately characterised by SBI was that large-scale mechanical phenomena may not be observed in the intermediate-scale environment. An analysis of the sandwich panel tests found that the fire exposure and the exposed area were not sufficient to adequately capture the failure mechanism of the panels (Messerschmidt 2008). Only in the full-scale was it evident that the panels would buckle and expose their combustible core, which would contribute to the fire load of the compartment and flashover would be observed. None of these effects were observed in SBI, which highlights some of its limitations. Nonetheless, it is expected that SBI will provide good understanding of PCM plasterboard since the behaviour of ordinary plasterboard can generally be scaled well.

7.3.2.3 Fire exposure

Quantification of the incident heat flux in SBI is necessary to allow comparison with the flammability measurements. Zhang *et al.* (2008) measured the heat flux in the SBI test arrangement using an array of steel plate heat flux gauges. The gauges were 35mm wide, 35mm long and 3.2mm thick. They were surrounded by unspecified insulation except for the surface which was left exposed. The surface was painted with carbon black so that the absorptivity could be assumed to be 1.0. The heat flux measurements from the plates were compared against a Gardon gauge in the cone calorimeter across a range of heat fluxes to validate their results.

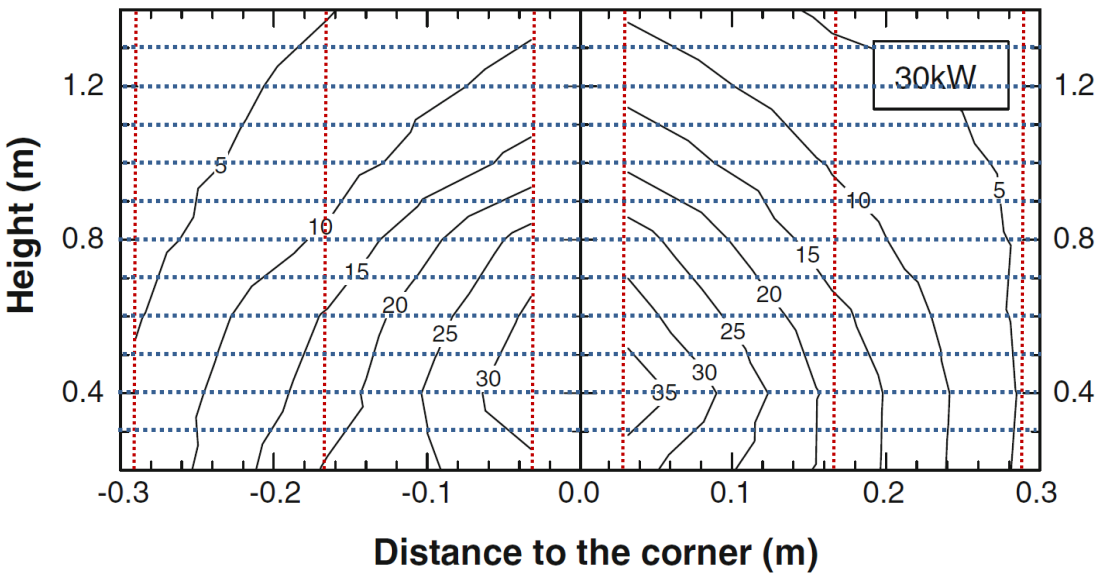

Figure 7.5 - Heat flux measurements from steel plates in SBI setup with a 30kW burner. Estimated error in the heat flux is ±15% when compared to Gardon gauges. Base diagram extracted from Zhang *et al.* (2008), with dotted overlay added where the intersections indicate the positions of the steel plates.

These steel plates were positioned on both wings at 200mm vertical spacing, and then 32.5, 165 and 290mm laterally from the corner, resulting in 42 measurement points. Two Gardon gauges were also used, with one on the short wing at a height of 400mm and 165mm laterally from the corner, and the other on the long wing at a height of 800mm and also 165mm laterally from the corner. This was to validate the measurements of the steel plates, and to obtain an error value. The average error for both gauges in three burner outputs (30, 45 and 60kW) was found to be 15%. However, in the case of the 30kW burner the steel plates significantly overestimated the heat flux, and the average deviation for this case was 48%.

The resulting heat flux distribution for a 30kW burner is displayed in Figure 7.5. It can be seen that the peak exposure measured by the steel plates is in the order of 30 to 35kW·m^{-2} in the corner below 500mm. This is in agreement with previous work which estimated the heat flux to be 40kW·m^{-2} in this area (Messerschmidt *et al.* 1999). Kokkala *et al.* (1993) report figures of 40kW·m^{-2} for an area of approximately 30×10^{-3}m^2 behind the burner.

The orders of magnitude for these heat fluxes match broadly with that of a small fire, such as a waste bin fire, which are typically reported as having heat fluxes from 25 to 50kW·m^{-2} (Babrauskas 1995). However, it should also be noted that for real fires the accumulation of an increasingly hot gas layer will increase the incident heat flux on ceiling and wall surfaces, and slightly higher figures would be expected that than listed above.

The burner in the ISO room corner test is set to higher heat release rates of 100 and 300kW·m^{-2}, as discussed below. Some information is available on the possible incident radiant heat fluxes to the walls in the corner from these burner levels. The range of 40-60kW·m^{-2} is given for the duration of the 100kW, and 60-80kW·m^{-2} is given for the 300kW (Quintiere 2006). The manner in which these heat fluxes were determined is not listed. Nevertheless, the values in the ISO room corner test can be seen to be quite significantly higher compared to the estimated values from the SBI exposure.

7.3.2.4 Plasterboard results

During the development of SBI there were a number of products tested to both ensure its robustness as well as provide the limits for a classification system. A number of these materials contained plasterboard in some manner or another, and these have been highlighted in Table 7.2. Some of the plasterboard results were used to define the class limits, notably the painted and ordinary plasterboard were used for the A2/B FIGRA(SBI) limits. However, two of the plasterboard products also caused flashover in the ISO room corner test due to their linings. As a result, these were placed into the C and D classes.

Based on the results of PCM plasterboard in the cone calorimeter, it is anticipated that this product will achieve the B class, as noted on its product sheet. This is due to the fact that the SBI test is heavily influenced by peak HRR but not the total energy released. As was shown in the previous chapter, the peak HRR of PCM plasterboard closely matches a wide variety of ordinary and fire rated gypsum plasterboard products. Hakkarainen and Kokkala (2001)

developed a simple model which agrees with this conclusion. Other gypsum plasterboards such as those with wallpaper or textiles covers (Chew and Lim 2000), oil-based paint (Mowrer 2004), or PVC and thick paper as was tested in the SBI round robin, have higher peak HRR and rapid ignition times. For example, peak HRR for oil-based paint increased from 117.25±10.08 for zero layers, to 256±25.09kW for eight layers when exposed to 50kW·m^{-2} (Mowrer 2004). This results in a high FIGRA parameter, and a poor classification rating, such as C or D.

Table 7.2 - FIGRA results of ISO room corner and SBI from the first round robin during the development of SBI. Reproduced from SP report 1998:20 (Hakkarainen *et al.* 1998).

Product	**FIGRA(RC)**	**FIGRA(SBI)**	**Euroclass**
-	kW·s^{-1}	W·s^{-1*}	-
Painted plasterboard	0.11	59	A2
Plasterboard on polystyrene	0.13	44	B
Plasterboard/FR PUR foam core	0.13	36	B
Plasterboard	0.15	56	A2
Paper wall covering on plasterboard	0.62	191	C
PVC wall carpet on plasterboard	1.04	350	D

*The source lists the units as kW·s^{-1} but this is assumed to be a mistake and has therefore been corrected to W·s^{-1}.

7.3.3ISO room corner test

The key full-scale test in the reaction to fire framework for surface linings is the ISO 9705 room corner test (British Standards Institution 1993). It should be noted that this test has not been carried out as part of this research, but knowledge of the test will assist in interpreting the results from SBI.

The ISO room corner test is designed to simulate a fire in a room. The aim of the test is to measure the propensity for surface lining materials on both ceilings and walls to spread flame from one compartment to another. This fire spread is characterised through the compartment reaching flashover. Furthermore, the possibility of igniting other items in the room is measured through a heat flux meter at ground level.

The test features a small room with dimensions 2.4m wide, 3.6m long and 2.4m high (Figure 7.6). A doorway is represented by an opening situated in one of the short sides of the room. In a corner opposite is a square propane burner which provides the fire exposure for the test. This is initially set to a constant output of 100kW for 10 minutes, before being increased to a constant output of 300kW for a further 10 minutes. If flashover occurs then the time is recorded and the test is stopped, if not, the test is stopped after 20 minutes have elapsed. Gases are collected from a hood outside the doorway of the room, and the heat release rate is calculated based on oxygen consumption calorimetry principles.

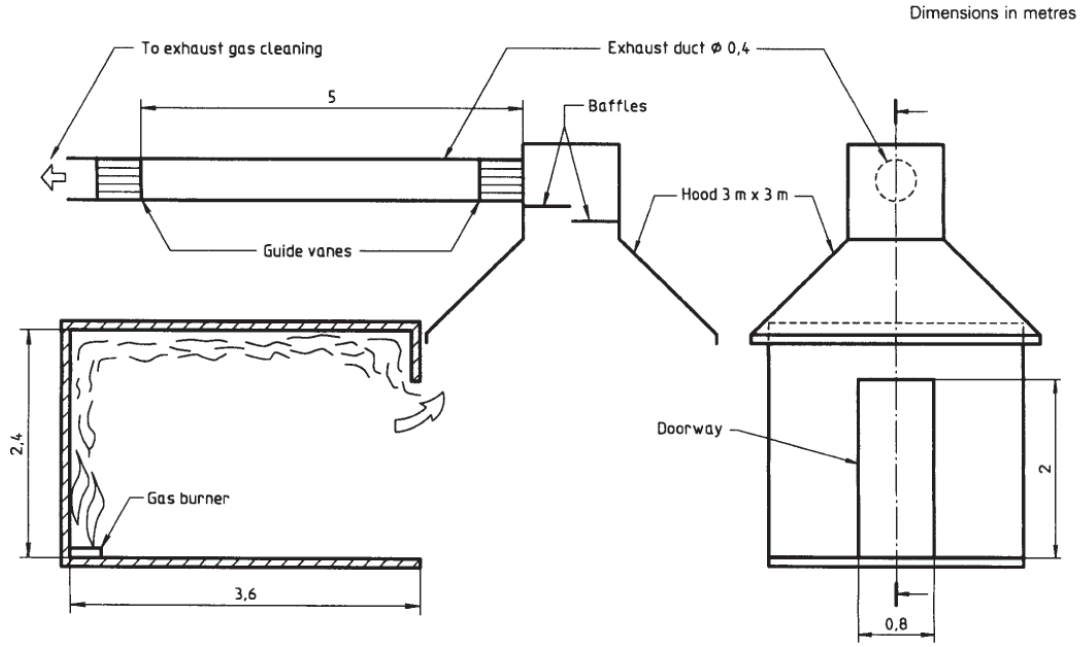

Figure 7.6 – General arrangement of the ISO 9705 room corner test. Extracted from British Standards Institution (1993).

One of the key differences between SBI and the room corner test is that the latter has a ceiling, whilst the former does not. This means that in SBI it is not possible for a smoke layer to build up as post-combustion gases are instead immediately extracted by the hood above. Therefore, in the room corner test there is additional contribution from the smoke layer which is not captured by SBI.

7.4 Methodology for intermediate-scale testing

The LIFT and SBI tests were carried out at the facilities of the BRE Group (Watford, UK) according to the standards, ISO 5658 and ISO 13823 (British Standards Institution 2006, 2010d) respectively, subject to some minor modifications as discussed.

7.4.1Flame spread – LIFT

The LIFT test was, unless otherwise noted, carried out according to ISO 5658 (British Standards Institution 2006). Modifications were made to allow additional measurements of temperature and video recordings to be made without, as far as possible, affecting the behaviour of the material or the outcome of the test. A general overview of the apparatus is given below in Figure 7.7.

Temperature measurements were made at six positions along the centreline of the specimen. The incident heat fluxes at these respective positions are given in Table 7.3. For each position four thermocouples were placed at depths of 3mm, 6mm, 12mm, and 24mm from the surface. Each thermocouple was located within a 15mm diameter circle on the surface to allow offsetting of the thermocouple positions and minimise interference in the measurements. The six positions are noted in Figure 7.8, which were adopted for tests one and two. For test three,

having evaluated the results, the positions were moved closer to the leading edge and consequently in the zone subject to higher heat fluxes. In all cases, the sample was ignited by a strong luminous pilot flame which extended from the bottom of the sample to the top, and was positioned 5mm from the edge.

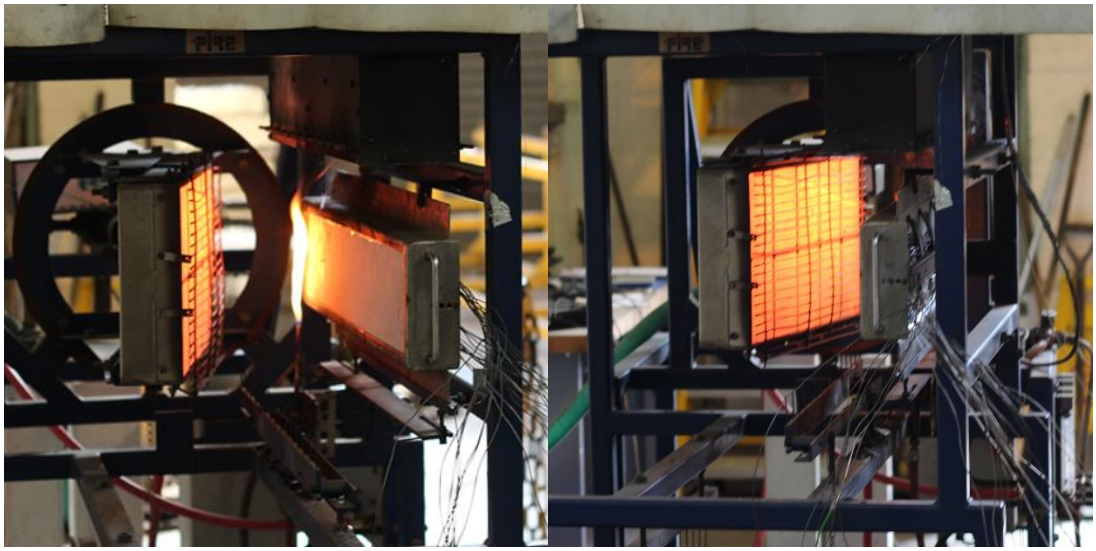

Figure 7.7 – (a) General overview of apparatus during operation (b) view of radiant panel, with instrumentation emerging from the back of the sample.

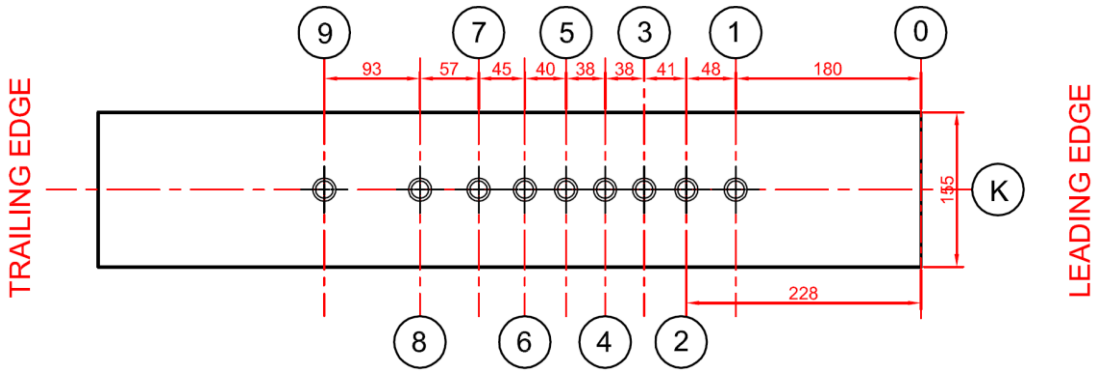

Figure 7.8 - Overview and thermocouple positioning in LIFT tests. Dimensions in millimetres unless otherwise noted. The pilot flame and radiant panel would be positioned at the right of the diagram.

Table 7.3 – Incident heat flux on thermocouple locations in $kW \cdot m^{-2}$ for set distances in mm. Six locations, K4-9, were used in tests one and two. and K1-6 in test three.

Location	**K1**	**K2**	**K3**	**K4**	**K5**	**K6**	**K7**	**K8**	**K9**
Distance	180	228	269	307	345	385	430	487	580
Test 1 & 2				29.96	24.94	19.96	15.00	10.01	5.02
Test 3	44.97	40.02	34.97	29.96	24.94	19.96			

7.4.1.1 Test duration

The test length according to the standard procedure was determined as follows:

1. If there was no ignition after 10 minutes, the test was stopped and CFE was assumed to be 50kW·m^{-2}.
2. Where there was flaming and this ended, the test was stopped 10 minutes after extinction.
3. If the flame front did not progress outside the initial area after 30 minutes then the test was stopped.

As part of the goal is to characterise the performance of the PCM plasterboard in the apparatus it was deemed necessary to modify these conditions in one of the tests. Thus, for the first two tests the above conditions were followed and (2) was found to be the stoppage criterion. For the final test it was instead terminated after a total of 60 minutes had elapsed, and a steady state was reached in the topmost thermocouples, 3mm from the surface, at all locations.

7.4.1.2 Pilot location

The LIFT apparatus was initially proposed by Quintiere (1981) and then subsequently refined over the next years (Quintiere *et al.* 1983, Quintiere and Harkleroad 1985), before becoming an ASTM standard (ASTM International 2013b). In these developments the position of the pilot location was improved.

The initial location was at the bottom of the specimen pointing to the top of the sample. The flame height was approximately equal to the length of the specimen, and was described as a strong pilot. This was the method adopted by the ISO standard (British Standards Institution 2006) and is shown in Figure 7.9a.

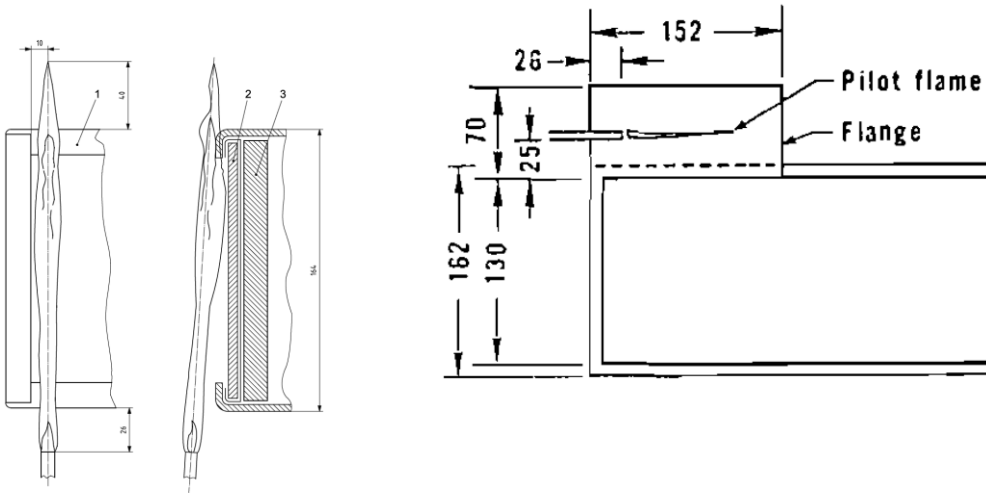

Figure 7.9 – Pilot location for (a) ISO 5658 standard, at the bottom of the specimen and parallel to leading edge, and (b) ASTM 1321, positioned at the top of the specimen and perpendicular to the leading edge. Extracted from British Standards Institution (2006) and Quintiere *et al.* (1983) respectively.

The subsequent location chosen by Quintiere *et al.* (1983) was above the specimen, perpendicular to the leading edge and penetrating the boundary layer of hot pyrolysis gases (Figure 7.9b). A number of different pilot flame locations were evaluated to obtain the optimal location, whereby the pilot had the least influence and there was the highest repeatability. The importance of the pilot on ignition was previously quantified in work by Simms (1963). The decision for the new pilot flame location was based on the fact that it did not radiate flame to the fuel, only to the hot gas mixture above the specimen, and it was found to be consistent with no abnormal behaviour. The location chosen is conceptually similar to the spark ignitor in the vertical orientation of the cone calorimeter (Babrauskas 1984) where ignition occurs at the highest concentration of flammable gases. The modified pilot flame location was then adopted in the development of the ASTM standard (ASTM International 2013b).

The pilot location in the previous chapter in the cone calorimeter conceptually reflects the ASTM position, where the pilot intercepts the hot boundary layer. The LIFT testing in this chapter was done according to the ISO standard where the pilot is instead at the bottom, and thus the implications of the different locations are discussed in the results.

7.4.2Single Burning Item – SBI

Due to the modifications the tests are not certified. A recommended rating is given by the sponsor but this cannot be used in any official capacity, and may not be representative of a non-modified standard fire test.

7.4.2.1 General setup and modifications

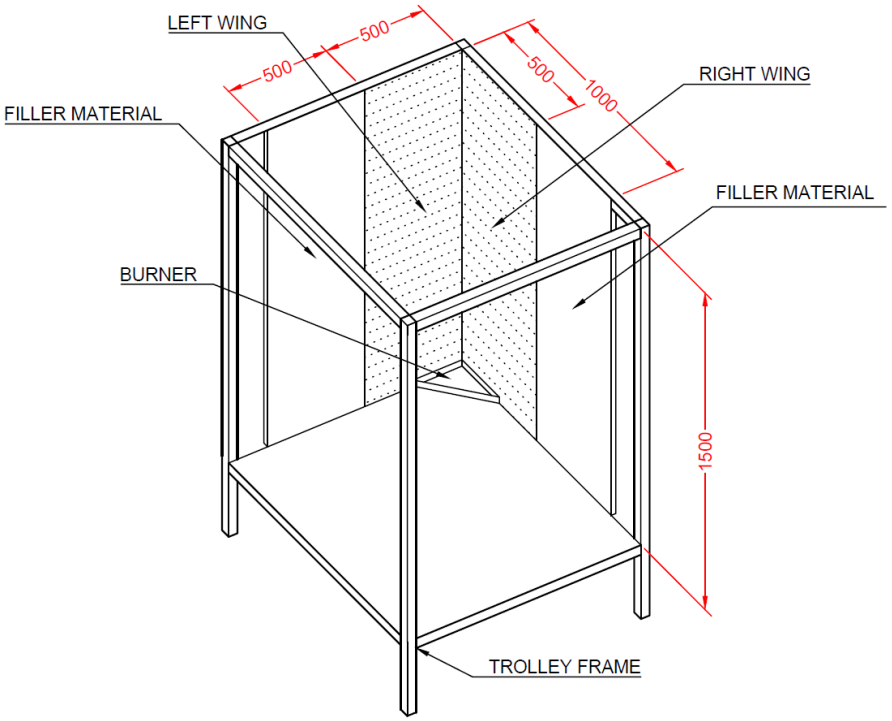

Figure 7.10 – Schematic of the SBI test setup. Dimensions are in millimetres.

The entire surface area of the PCM plasterboard was exposed to the burner. The horizontal tongue and groove joint was positioned 500mm from the bottom on both wings, and no vertical joint was used. Behind the board was a 20mm air gap and then 12.5mm thick calcium silicate board with a density of 870kg·m^{-3}. To create the air gap small pieces of calcium silicate were used as spacers around the corners of each panel.

Two sheets of the PCM plasterboard material with dimensions 0.5m wide by 1.5m tall are placed in the corner of a room. Typically the corner is formed of a long wing and a short wing of lengths 1.0m and 0.5m respectively. This was reduced to 0.5m for both wings to reduce the amount of material required, which is illustrated in Figure 7.10. The removal of 0.5m of material is not expected to have an effect on the result of the test since the flames often do not spread beyond 0.5m within the timeframe for materials with limited flammability, which includes PCM plasterboard. A total of two tests were carried out to assess the reproducibility of the results.

7.4.2.2 Thermocouple placement

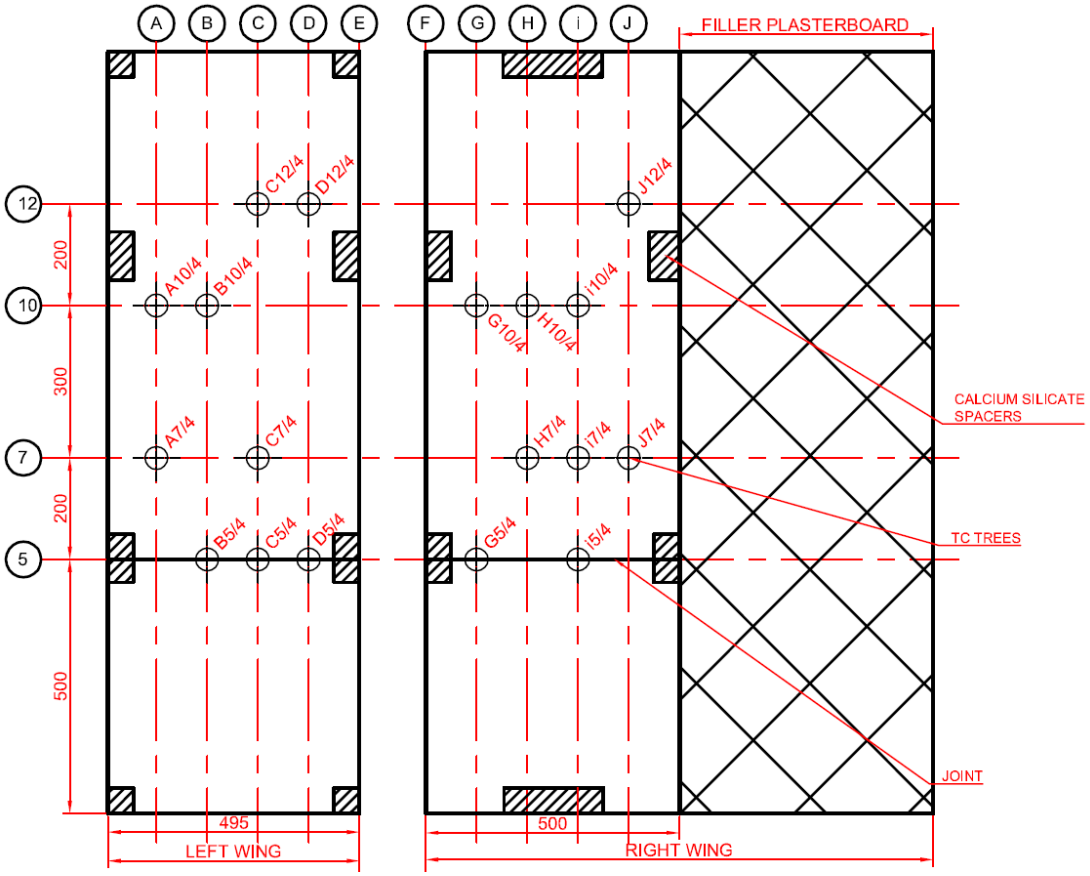

Figure 7.11 - Position of thermocouples in both SBI tests. All dimensions in millimetres. The notation "/4" signifies four thermocouples at a given location.

The distribution of thermocouples is illustrated in Figure 7.11. For each position there were four thermocouples placed at depths of 3mm, 6mm, 12mm, and 24mm from the exposed surface. These were positioned 7.5mm radially from a centre point. K-type thermocouples of

2.0mm diameter with Inconel sheathing were used in all cases. Many of the thermocouples have been placed in areas near the critical heat flux to aid in characterising the flame growth away from the burner.

7.5 Results and discussion

The standardised results, interpretation of behaviour, and analysis of results are all discussed in this section. These have been divided into sections for both SBI and LIFT. Generally the standardised results are stated, then the actual performance of the material is characterised before finally discussing the implications and effectiveness.

7.5.1Flame spread

The critical heat flux for flame spread, flame spread parameter, visual observations, and thermal evolution are all discussed for this specific PCM plasterboard tested in LIFT, over three repetitions.

7.5.1.1 Standard testing results

The results as per the standard test and calculation methods are given in Table 7.4. The two key quantities are the critical flux at extinguishment (CFE) which was found to be 29.06kW·m^{-2}, and the average heat sustained for burning which is 4.00MJ·m^{-2}.

Table 7.4 – Results obtained as according to the standardised procedure.

Criteria	Specimen			
	1	2	3	Average
Heat for ignition (MJ·m^{-2})	2.97	3.25	3.67	3.30
Critical flux at extinguishment (kW·m^{-2})	24.94	37.31	24.94	29.06
Average heat sustained for burning (MJ·m^{-2})	5.41	3.11	3.49	4.00
Total heat release (MJ)	0.24	0.03	0.27	0.18
Peak heat release (kW)	1.39	0.68	1.31	1.13

7.5.1.2 General observations

Visual observations form an important aspect of the LIFT test, since these are used to track the propagation of the flame front. An illustration of the pyrolysis and oxidation processes is given below in Figure 7.12. The established flame front was weak and can generally be discerned by tracking the blackened areas propagating along the length of the specimen, for example, 250-325mm at 7 mins, and 325-425mm at 14 mins. The area preceding this, closer to the leading edge and the pilot flame, correspond to the completion of oxidation, and hence extinction. Upstream the virgin material is heated to the pyrolysis temperature and volatile gases are generated until the weak flame front arrives.

A weak diffusion flame front was established near the leading edge where the heat flux is at its highest, around 50±0.5kW·m^{-2}. Beyond this point the flame front took the form of a lean blue flame which rapidly pulsed across the surface, and proved difficult to measure. The nature of the pilot conditions, as discussed later, resulted in autoignition of the material as

opposed to piloted ignition. This caused only a weak flame front to be established, which did not radiate sufficient heat to the sample to generate an adequate flow of pyrolysis gases. The pulsing blue flame was discussed earlier for long chain paraffin pool fires in the *Literature review*, as well as the flammability study in the cone calorimeter.

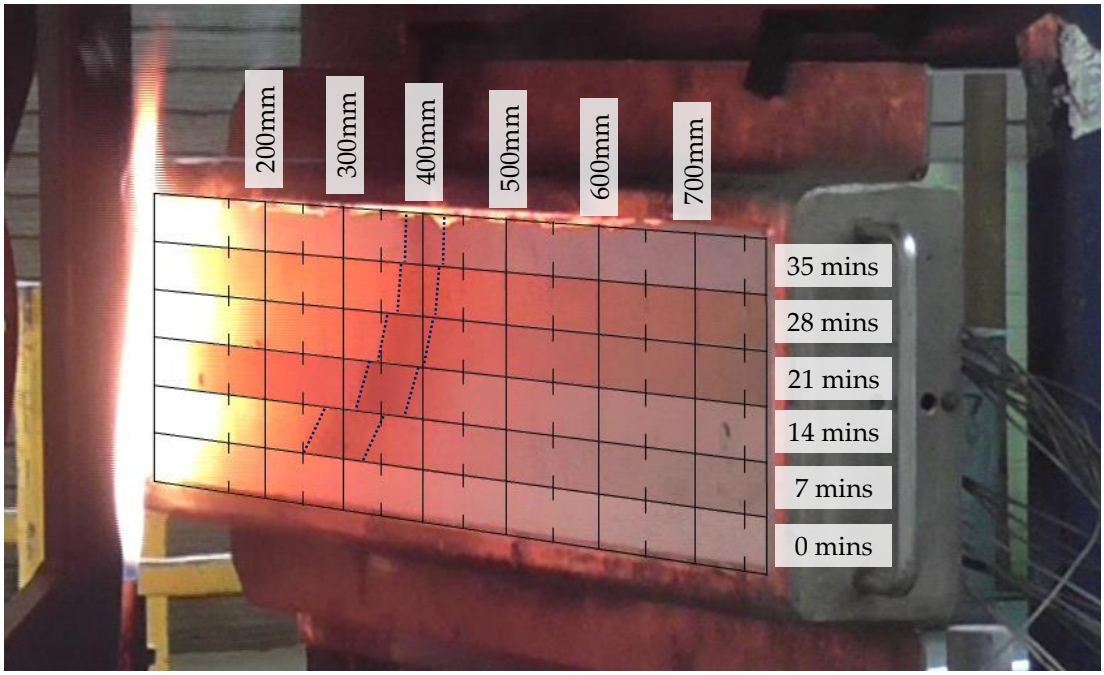

Figure 7.12 – Various time intervals of the third test. The approximate reaction zone based on discolouration is highlighted with blue dotted lines for each time step. Note that the bright area on the left side (<200mm) is a reflection of the pilot flame.

7.5.1.2.1 Flaming above sample

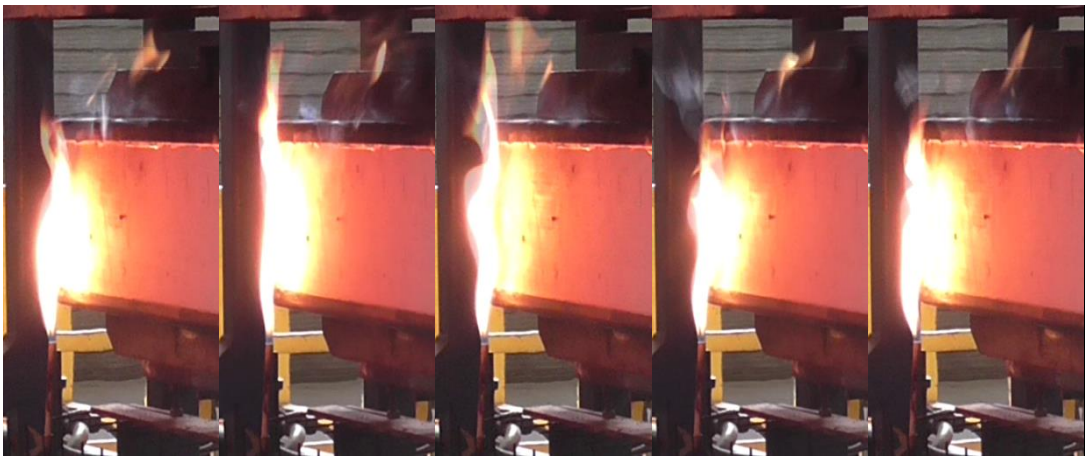

Figure 7.13 - Flaming visible above sample at 1 minute and 15 seconds in test 3. The furthest extent of the flame is estimated to be 225mm. The time between each image is approximately 25ms.

Before ignition of the surface there was some luminous flaming evident above the top of the sample (Figure 7.13). Small flames were present throughout the duration of the test, and

remained after extinction of the main pulsing on the surface of the sample. In some instances, the flame above the sample was observed to ignite pulses from the surface.

7.5.1.2.2 Secondary ignition

In test 3, after 34 minutes pyrolysis gases from the bottom of the sample ignited and a continuous diffusion flame was established. This covered the height of the sample for up to 10 minutes and extended to a maximum of approximately 200mm (Figure 7.14e), before beginning to recede. The progression of the flame was extremely slow due to the rate in which gases were able to escape from the bottom. Furthermore, the gases were generated at a depth in the sample where the heat absorbed was significantly lower. This secondary flaming is not valid for many of the theoretical considerations of the flame spread test as were discussed in the *Literature review*. However, it does confirm that the material is capable of sustaining a diffusion flame if the right conditions are met. In this case, the flow of pyrolysis gases is low since they must escape through the bottom surface, but the hot surface of the material maintains a high temperature to minimise heat losses from the flame.

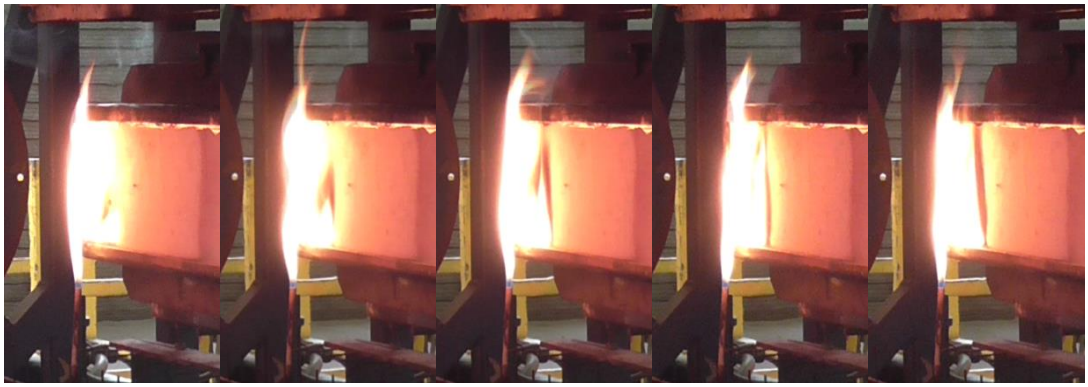

Figure 7.14 - Ignition of pyrolysis gases at the bottom of the sample in test 3 at, in minutes and seconds, (a) 36:23 (b) 40:48 (c) 43:06 (d) 44:06 (e) 46:09.

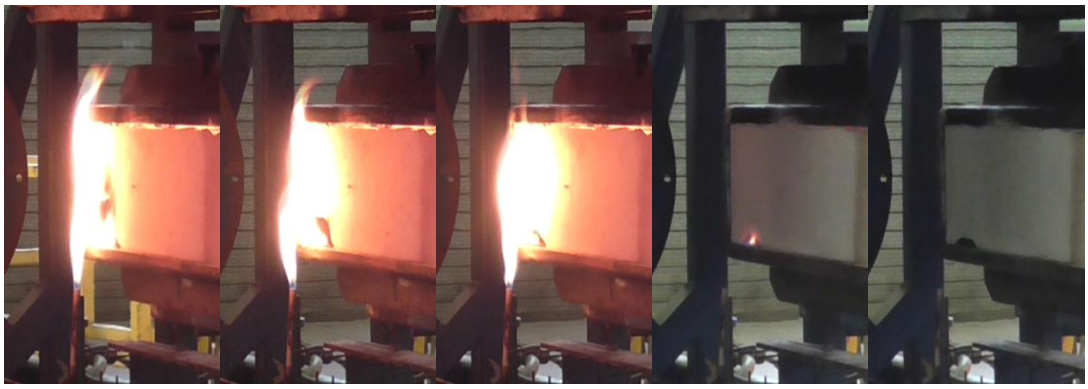

Figure 7.15 - Ignition of pyrolysis gases at the bottom of the sample in test 3 at, in minutes and seconds, (a) 53:43 (b) 56:25 (c) 59:36 (d) 00:05 after test end (e) 01:58 after test end.

The flaming was still present at the time the test was stopped but was only around 15mm tall (Figure 7.15d). This extinguished after just under two minutes and a small blackened area remaining (Figure 7.15e).

7.5.1.3 Temperature profiles

Temperatures were measured to help understand the fire behaviour of the PCM plasterboard in LIFT. The temperature profile along the distance of the material at a depth of 3mm highlights the areas of greatest interest (Figure 7.16). Higher temperatures are recorded across incident heat fluxes of 30 to 45kW·m^{-2} after which there is a notable drop and plateau. At 45kW·m^{-2} there should be well established flaming based on the flammability study in the cone calorimeter, whilst between 20 and 30kW·m^{-2} extinction occurred.

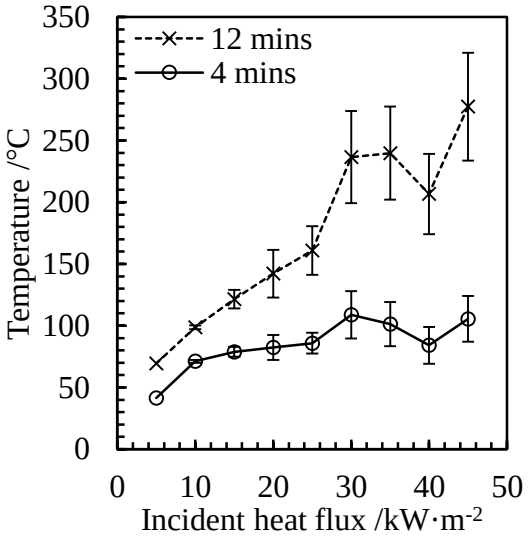

Figure 7.16 – Temperature at 3mm across the distance of the sample, indicated by the incident heat flux. For 5-30kW·m^{-2}, results are averaged from three tests and standard deviation is displayed. For 35-45kW·m^{-2}, the results are only from test 3 and the error from 30kW·m^{-2} is taken and applied as a percentage.

7.5.1.3.1 Key locations

The temperature depth profiles for the key locations identified above are presented. Extinction was previously identified between 29.96 and 24.95kW·m^{-2} from visual observations and gives insight into the extent of the flame spread. For profiles at 29.96kW·m^{-2} (Figure 7.17a), the temperature near the surface is seen to rise more rapidly during flaming (up to two mins). This is also noted by the more significant temperature increase between 3mm and 6mm, which is smaller in the case of 24.95kW·m^{-2} since there was no flaming (Figure 7.17b). The radiation from the flame was insufficient to maintain adequate flow of pyrolysis vapours and thus extinction occurred. The temperature at 3mm for the two respective heat fluxes at flameout, 4 mins, were 109 and 86°C. At the lowest common heat flux measured in all the tests, 19.96kW·m^{-2} (Figure 7.18), the temperature was 82°C. In all cases the thermal wave had already managed to penetrate the back surface, noted by a temperature increase at 24mm.

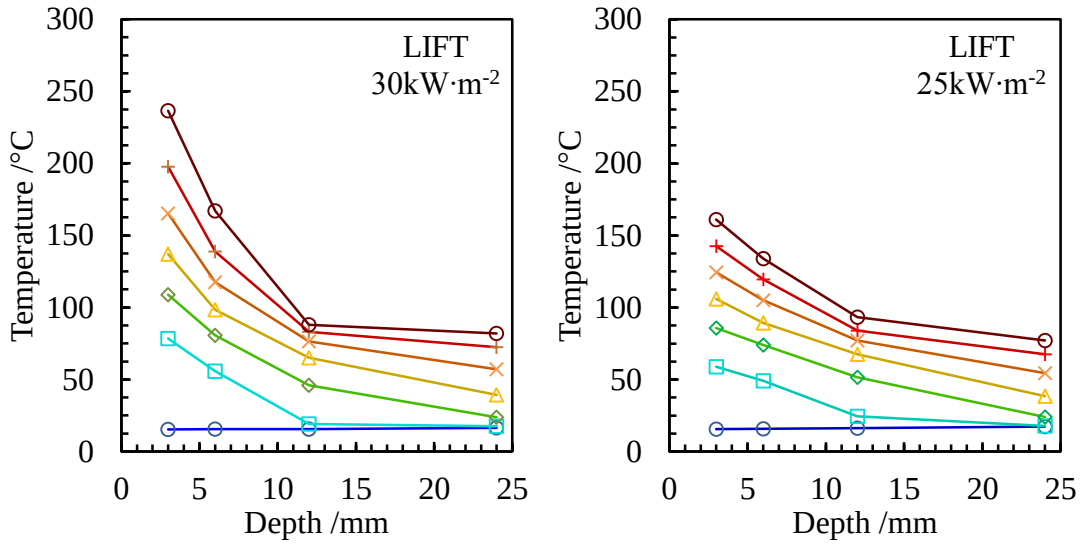

Figure 7.17 – Temperature depth profiles at distances corresponding to (a) 29.96kW·m^{-2} and (b) 24.95kW·m^{-2}. Timesteps are at 2min intervals up to 12mins. Data are averaged from three tests.

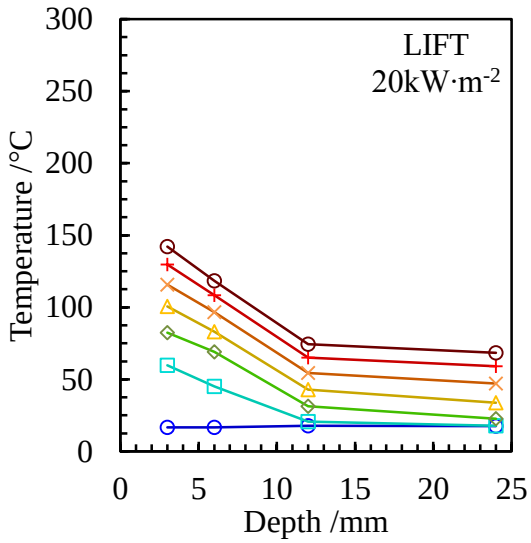

Figure 7.18 - Temperature depth profiles at a distance corresponding to 19.96kW·m^{-2}. Timesteps are at 2min intervals up to 12mins. Data are averaged from three tests.

7.5.1.3.2 Comparison with cone calorimeter data

The temperature-depth profiles have been compared with those obtained previously in the cone calorimeter. It is found that for corresponding heat fluxes the temperatures are significantly higher in the cone calorimeter compared to LIFT. For example, for the case of 45-50kW·m^{-2} the temperature 3mm deep at 12 mins is 550°C in the cone compared to 275°C. This is heavily affected by the fact that a strong luminous flame was not established, and thus is not able to radiate and convect heat downwards. The temperature profiles also illustrate that within 2 mins there are already sufficient deviations between the apparatus (Figure 7.19, top).

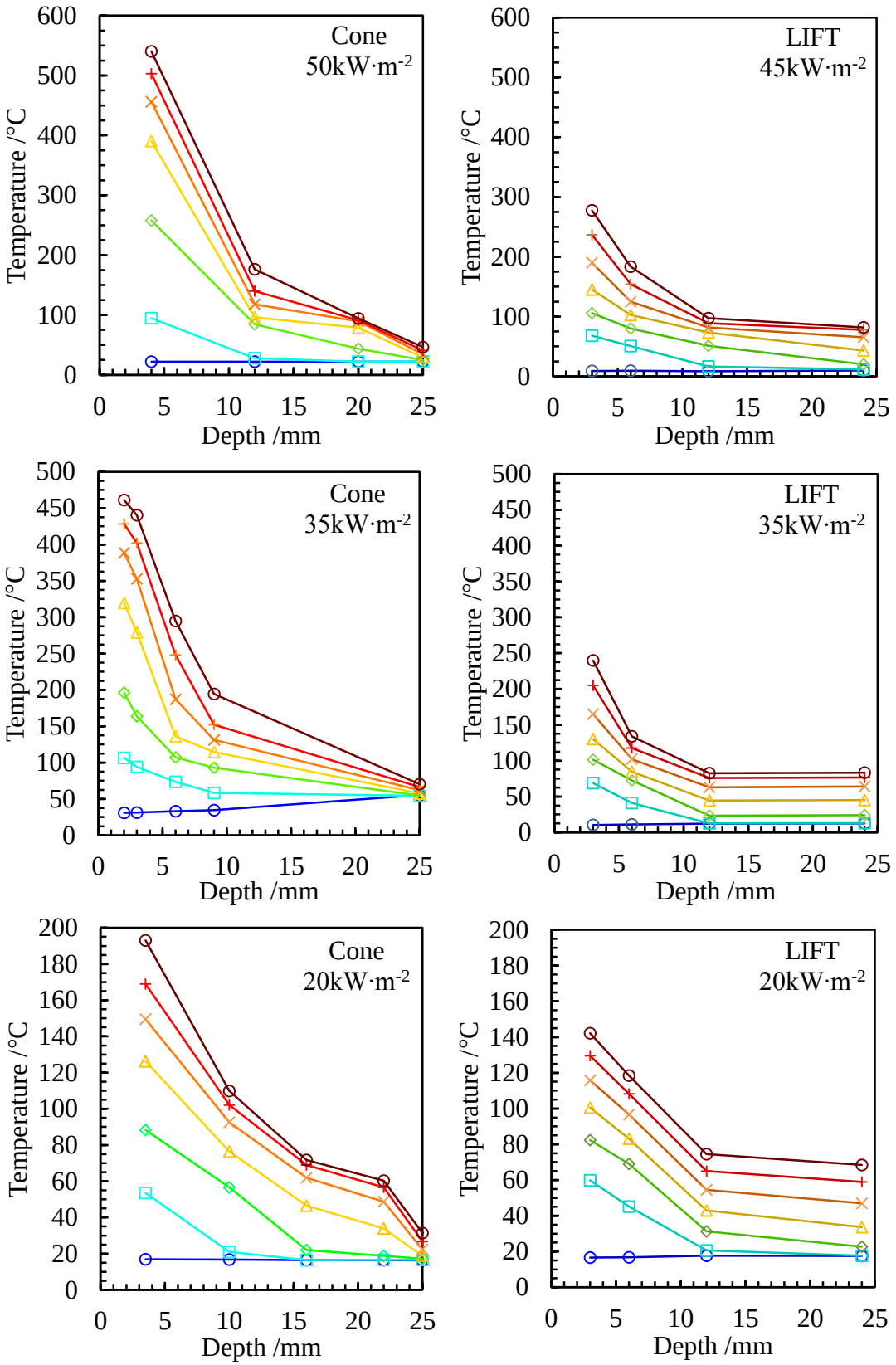

Figure 7.19 - Temperature-depth profiles for cone (left) and LIFT (right) for heat fluxes from, top to bottom, 45-50, 35, and 20kW·m^{-2}. Timesteps every 2 mins.

For the case of 35kW·m^{-2} the change in the rate of temperature increase near the surface is evident at 2 to 4 mins. Where in the cone calorimeter there is a rapid increase and sustained flaming occurs, in LIFT the rate of temperature increase is only moderate as a weak flame front is established at the surface. Due to the short duration of flaming, even after 12 mins the temperature does not rise to those reached in the cone calorimeter (Figure 7.19, middle).

Finally, near the critical heat flux for ignition, at 20kW·m^{-2}, similar temperature profiles are recorded for the first 4 mins in both the cone calorimeter and LIFT (Figure 7.19, bottom). The time to ignition was previously found to be at 140±14s and thus it is expected that the results in this period are similar. The rate of temperature increase between 3mm and 6mm for LIFT is not significantly different unlike each of the other results, which suggests there is less radiation from the flame owing to weaker spread. The charring nature of the material likely contributes to the weak flame spread. This is due to the fact that by the time the flame front arrives, part of the fuel will have already pyrolysed and an insulating char layer will reduce the rate at which heat can conduct through the sample, and thus the pyrolysis rate is reduced.

7.5.1.4 Application of flame spread theory

The time at which the flame front crossed specified points was recorded, and used to calculate the flame spread rate. However, for much of the length of the sample the spread appeared in the form of pulsing combustion owing to the fact that the temperature lay between the flash and firepoint. The time taken for the pulsing flame front to reach a location has been used for the flame spread calculations.

A comparison of both the flame spread velocity and the time to ignition, obtained from the cone calorimeter, illustrate the weak flame spread at low heat fluxes (Figure 7.20). There is an overlap between the flame spread velocity and the time to ignition above the critical heat flux, due to the fact that a weak flame front was established. Furthermore, as a charring material PCM plasterboard cannot easily be preheated to aid the spread rate above the critical heat flux. Despite this, the velocity remains broadly similar to the values obtained by Quintiere *et al.* (1983) which were around 1.0mm·s^{-1} at 20kW·m^{-2}, to 1.2mm·s^{-1} at 30kW·m^{-2}.

Based on the flame spread of the flashing combustion, the flame spread modulus, C, is found to be 28.1(mm·s)$^{3/2}$·J^{-1}. This is far lower than other materials, even ordinary plasterboard. The thermal inertia and ignition temperature obtained in the cone calorimeter yield a flame spread parameter of 500kW^{2}·m^{-3}. This value is 30 to 600 times higher than the values for gypsum boards in the literature by (Quintiere and Harkleroad 1985). The flame spread rate as a function of incident heat flux is shown in Figure 7.21.

In their analysis of plasterboard (Figure 7.3), Quintiere *et al.* (1983) adopted a slightly different method to obtain a suitable value for the flame spread rate. This involved fitting the flame spread coefficient directly to the critical heat flux found in flammability testing. This results in a poor fit, but still provides a value. This was also attempted for PCM plasterboard but the

flame spread parameter was still significantly higher. From this, it is concluded that there is not significant flame spread for this specific PCM plasterboard.

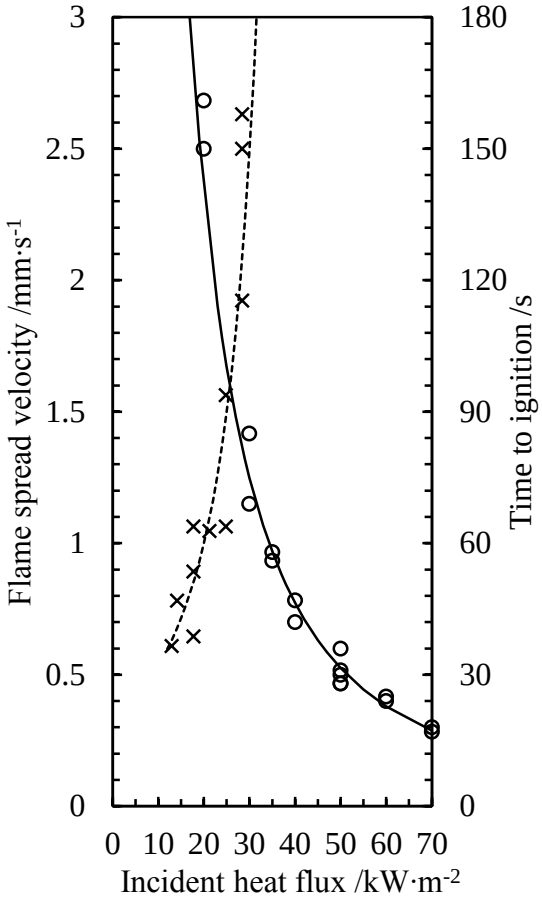

Figure 7.20 – Time to ignition (obtained from the cone calorimeter, circles) and flame spread velocity (crosses) as a function of incident heat flux.

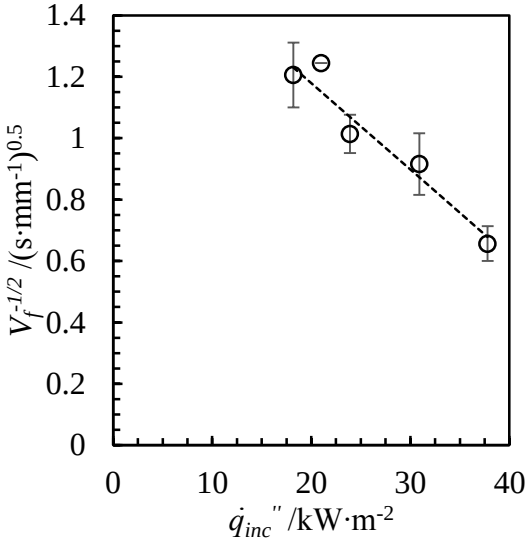

Figure 7.21 - Flame spread rate against the incident heat flux along the distance of the specimen for PCM plasterboard. Three tests are averaged, and the standard deviation is displayed as the error.

7.5.1.5 Minimum heat flux for spread

The minimum heat flux for flame spread may be determined in a number of ways due to the ambiguous manner in which the flame front propagated. According to the standardised procedure, the furthest extent which the flame front propagates is recorded and the corresponding heat flux is used. The average value was 29.06±7.14kW·m^{-2} over three tests. Alternatively, the apparent length over which pulsing flaming may also be used. The figure for this was 22.39±2.50kW·m^{-2} and is listed here as the critical flux for spread (flashing). The minimum heat flux for pyrolysis estimated from analysis of the discolouration of the samples is 14.50±1.01kW·m^{-2}.

The minimum temperature for flame spread can be determined by considering a heat balance at the surface of a material (Quintiere 1981, Torero 2016). Assuming a total heat coefficient of 42W·m^{-2}·K^{-1} (Quintiere *et al.* 1983) the values for flame spread, spread (flashing), and pyrolysis are found to be 712, 553, and 365°C respectively. These results are summarised in Table 7.5.

Table 7.5 – Summary of LIFT flame spread results for PCM plasterboard.

Combustion mode	**Critical heat flux**	**Ignition temperature**
-	kW·m^{-2}	°C
Flaming	29.06±7.14	712
Flashing	22.39±2.50	553
Pyrolysis	14.50±1.01	365

7.5.1.6 Effect of the pilot flame

As previously noted, the pilot flame location varies between ASTM 1321 and ISO 5658. The placement of the pilot at the bottom of the specimen in the ISO standard may have caused issues with properly igniting the sample. If the pilot flame lies outwith the laminar boundary layer then piloted ignition will no longer occur as there is not sufficient flammable vapours outside this region. Instead only autoignition will be possible, which requires more energy. For example, piloted ignition of redwood has a critical heat flux of 3 to 12kW·m^{-2} (Spearpoint and Quintiere 2001), whilst the critical heat flux for autoignition is 35 to 37kW·m^{-2} (Boonmee and Quintiere 2002). For PCM plasterboard, autoignition was observed at 50kW·m^{-2} in the cone calorimeter in this thesis. It is therefore concluded that in this case autoignition occurred at the leading edge. The long time to ignition and the charring nature of the material mean that many of the pyrolysis vapours of fuel close to the surface were already depleted, and only a weak flame front was established. The use of the pilot flame above the specimen, as in ASTM 1321 and the vertical orientation cone calorimeter studies, would be expected to give better results.

7.5.1.7 Validity of theory

Flame spread models are based on the theory that a combination of energy from the external heat flux and from the flame will heat up material ahead of the flame front, and additionally there will be some influence of conduction through the solid (Fernández-Pello and Williams

1977). Once the temperature reaches the pyrolysis temperature, flammable vapours will be generated and mix with the air until a critical point is achieved and ignition occurs. The critical point is usually considered to be the lower flammability limit of the pyrolysis vapours in the vicinity of the pilot. In many cases the radiation from the flame is sufficient to ensure the supply of flammable pyrolysis vapours and consistent flaming will be present (de Ris 1969). However, in some cases the temperature will lie between the pyrolysis and ignition temperatures and constant burning is not achieved. This could be considered to be above the flashpoint, but below the firepoint. In this instance flammable vapours will constantly be produced and a pilot will be available to ignite them, but there is insufficient energy from the flame and other sources to be able to generate the pyrolysis gases at a sufficient rate.

Consequently, we can ascertain that the majority of the PCM plasterboard lay between the critical heat flux for the flashpoint and firepoint. This may be due to the similarity of its behaviour to a charring material. Upon reaching an elevated temperature a 'char' is generated which helps insulate material in-depth from the external radiation, and hence limits the flow of pyrolysis gases that can be generated. Furthermore, this allows the finite amount of volatile vapours to escape before the flame front reaches an area, hence preventing flame spread.

7.5.1.8 Post-test analysis

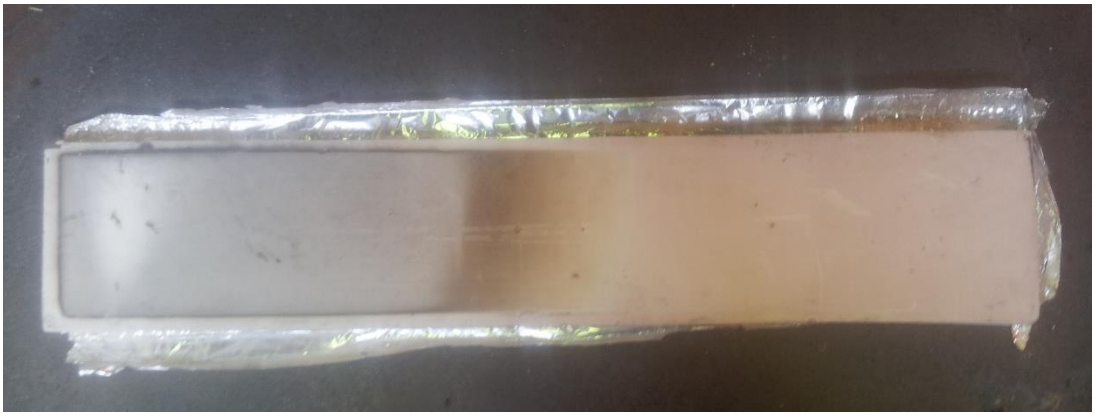

Figure 7.22 - Overview of sample 1 after testing.

The residual samples from test 1 and 2 are shown in Figure 7.22 and Figure 7.23 respectively. The areas and extent of degradation match closely despite the different values obtained for the standardised test results. The grey area extends to approximately 330mm (26.90kW·m^{-2}), the dark brown to around 375mm (21.16kW·m^{-2}), and no degradation is evident beyond 415mm (16.56kW·m^{-2}). The orientation of the degradation front is sloped slightly towards the top of the specimen due to buoyancy. This extends approximately 10mm forward at the top and 10mm backwards at the bottom when compared to the centreline.

Figure 7.23 - Sample 2 following testing for approximately 12 minutes of thermal exposure.

7.5.2Single Burning Item

Two tests were successfully conducted according to ISO 13823 (British Standards Institution 2010d). Visually, there appeared to be little contribution from the PCM to the flame. However, this requires quantification which can be achieved using the thermal profiles, and checked against the measured heat release rate measured by oxygen consumption calorimetry. An illustration of the SBI setup before, during and after for one of the tests is given in Figure 7.24.

Figure 7.24 - SBI test setup: (a) Burners and PCM plasterboard in corner with joint visible (b) main burner during test (c) bottom section after testing.

7.5.2.1 Standard testing results

The results of the SBI fire test for two specimens are shown in Table 7.6. Based on the results, the material would obtain an indicative classification of B according to BS ISO 13501 (British Standards Institution 2009a). This is the same official classification listed by the manufacturer and compares with other similar PCM plasterboards. Full details can be found in the *Literature review* chapter.

When compared with other plasterboards which were tested as part of the SBI development round robin (Table 7.2) the material similarly achieved a B classification, although its FIGRA(SBI) is slightly higher. Some of the plasterboard products however achieved C and D due to combustible facings such as thick paper, PVC, or wallpaper. Compared to these materials therefore, the PCM plasterboard has an improved FIGRA(SBI). This suggests that the use of this PCM plasterboard would increase the heat released in the compartment but not sufficiently to cause flashover. It is not possible to estimate the additional energy the product will contribute to a fire from the standardised SBI results alone. However, it can be estimated based on the predicted pyrolysed area based on thermal evolution, and then calculated using the heat of combustion, mass loss rate and heat release rate obtained in the flammability study.

Table 7.6 - Results of two standardised SBI tests on PCM plasterboard.

Parameter	Test		
	1	2	Average
$FIGRA_{0.2MJ}$ ($W \cdot s^{-1}$)	64.1	82.7	73.2±13.2
$FIGRA_{0.4MJ}$ ($W \cdot s^{-1}$)	63.2	81.2	72.2±12.7
SMOGRA ($m^2 \cdot s^{-2}$)	0.0	0.0	0.0±0.0
THR_{600s} (MJ)	3.3	4.6	4.0±0.9
TSP_{600s} (m^2)	34.1	18.0	26.1±11.4

7.5.2.2 Heat release rate and FIGRA

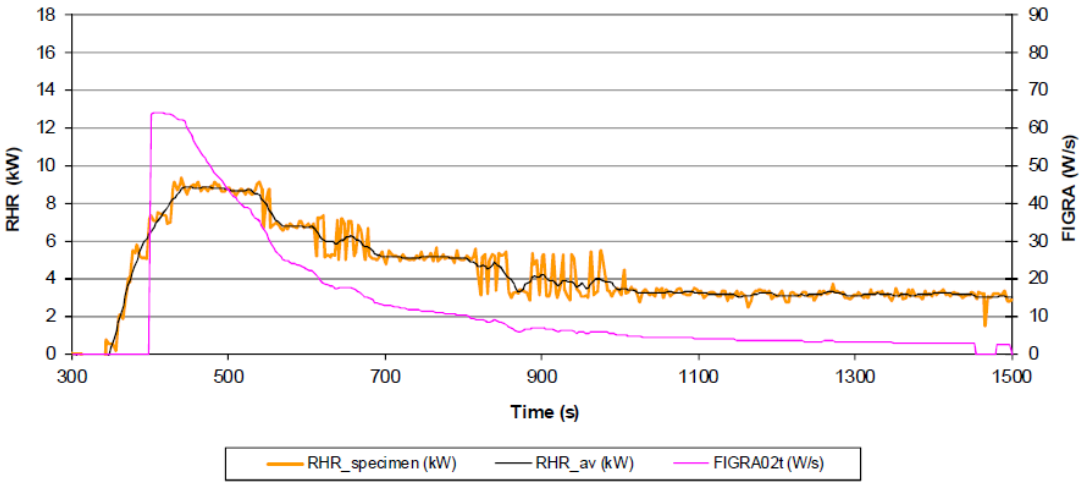

Figure 7.25 - HRR and FIGRA for SBI test 1.

In the case of test one there was approximately a 50s delay before an increase in the HRR (Figure 7.25). Note that test was started at 300s, and prior to this point the calibration was performed. In the second test the time delay until the increase in HRR was reduced to approximately 30-40s (Figure 7.26). These correspond to the ignition delay times obtained previously in the cone calorimeter for 35kW·m^{-2}, and 40-50kW·m^{-2} respectively. The peak HRR of 10.5±1.5kW is then reached approximately 150s after starting. As with a charring material, the HRR decays after reaching the peak to an asymptotical value of 4±1kW after around 600s. The reason that the HRR does not return to zero is that pyrolysis and smouldering combustion

processes continue after there is little flaming. This is evident from the temperature results which show the thermal wave continuing to propagate after the peak period of flaming. This is the same as was found in the cone calorimeter.

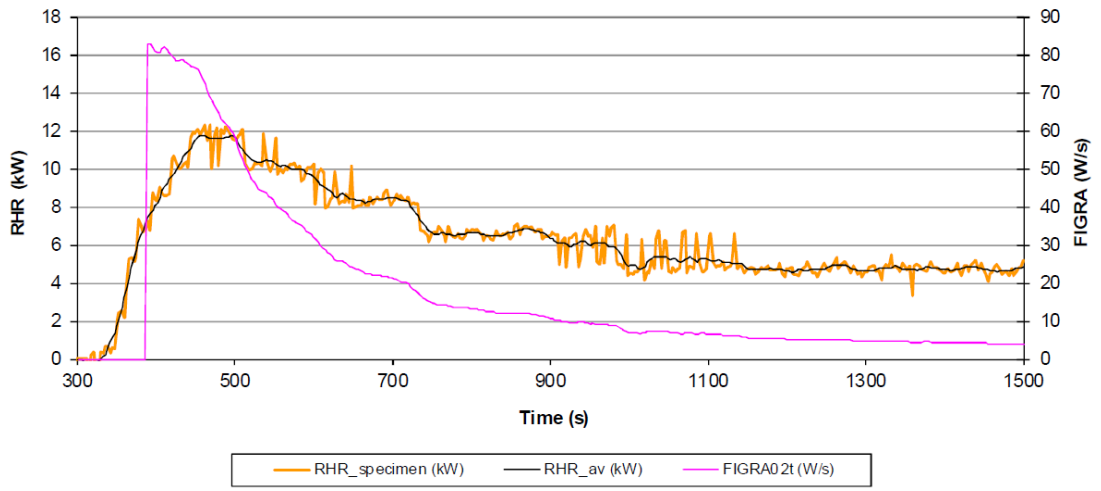

Figure 7.26 - HRR and FIGRA for SBI test 2.

7.5.2.3 Temperature distribution

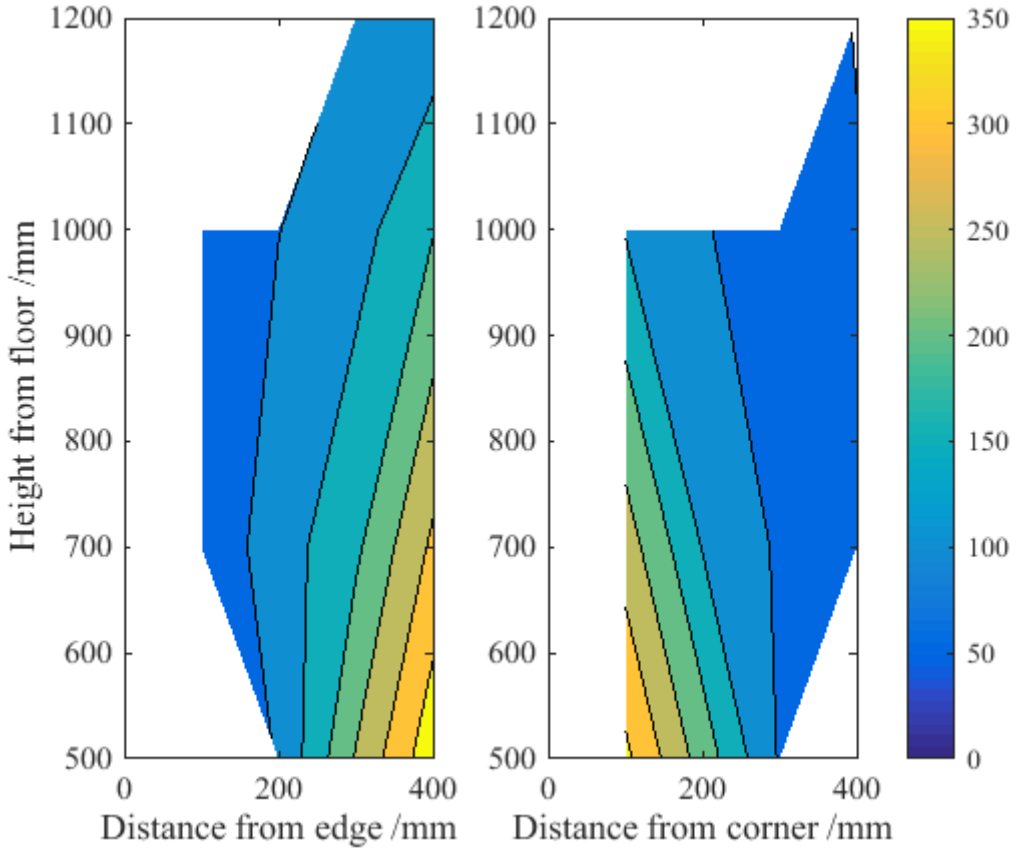

Figure 7.27 - Temperature distribution of (a) left wing and (b) right wing. Readings are taken from thermocouples which are 3mm below the surface, and are averaged between the two tests. Linear interpolation is used between TC locations.

The temperature distribution illustrates that the fire exposure from the burner is highly focussed on the corner area (Figure 7.27). Outside of this area there is little absorbed heat flux and no lateral spread is evident. Some vertical flame spread is expected to have occurred, the extent of which is discussed later.

By considering the endothermic pyrolysis and exothermic oxidation processes identified previously using thermogravimetric analysis it is possible to estimate the amount of PCM which has contributed. These processes were previously found to occur in the range of 190.07±0.88 to 222.37±0.83°C, with a maximum decomposition rate at 203.19±0.36°C. For the area above a height of 500mm, which encapsulates all the thermocouple locations, this leads to a pyrolysis area of $220\times10^{-3}m^2$. The temperature is assumed to be constant from the corner to the first thermocouples, which are 100mm away laterally. In addition, it is assumed that the temperature is constant from a height of 500mm down to the ground. Both these are a reasonable if not overly conservative estimates based on the heat flux readings of Zhang *et al.* (2008). The latter adds a further $175\times10^{-3}m^2$, bringing the total area pyrolysed to $395\times10^{-3}m^2$.

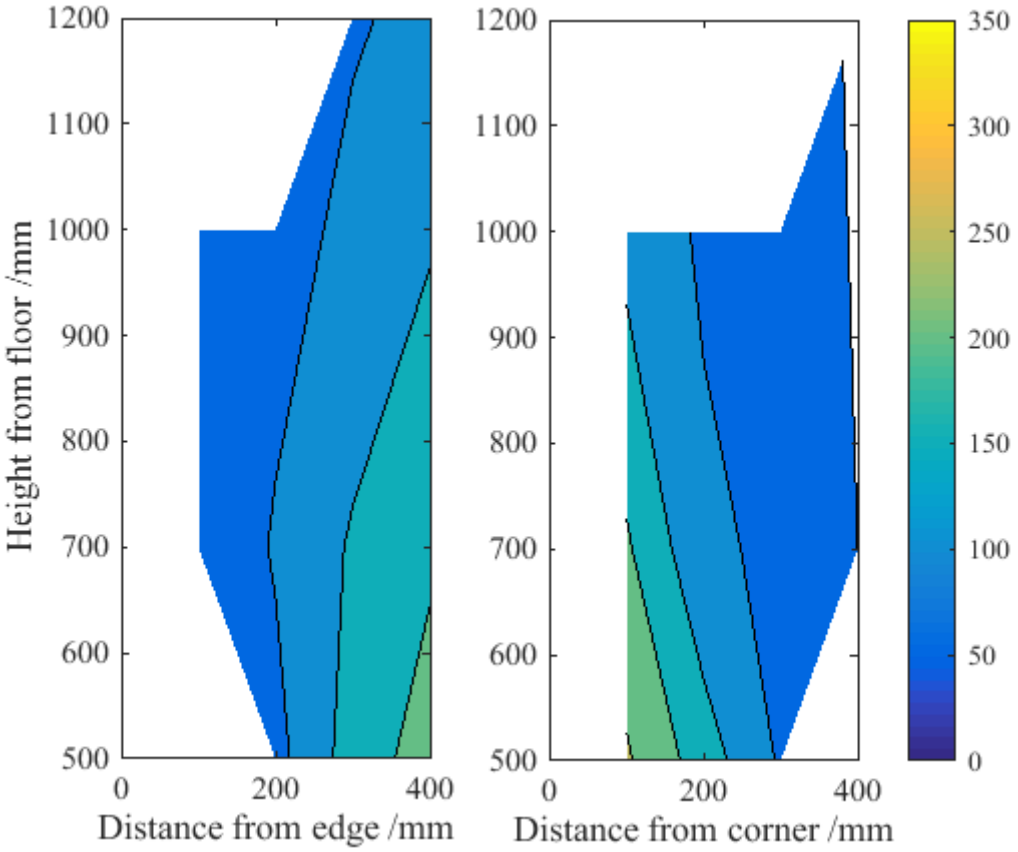

Figure 7.28 - Temperature distribution of (a) left wing and (b) right wing. Readings are taken from thermocouples which are 6mm below the surface, and are averaged between the two tests. Linear interpolation is used between TC locations.

Areas in which the thermal wave has reached the pyrolysis temperature of the paraffin wax at a depth of 6mm represent those which will have had established flaming at the surface,

based on the cone calorimeter results. The distribution across the wings for 6mm is shown in Figure 7.28.

The area above the pyrolysis point at this depth matches heat fluxes of at least 15-20kW·m^{-2} based on Zhang *et al.* (2008). This suggests that the results from the cone calorimeter may be adequate in predicting the area which will pyrolyse in SBI in conjunction with the measured heat fluxes. The distribution however is mainly focused near the burner, illustrating the lack of an accelerating spread which may lead to flashover. As noted in the *Literature Review* within this chapter, SBI does not include a ceiling and thus the contribution from the smoke layer is not taken into consideration. In either the room corner test or a realistic environment, this would radiate additional heat. For the case of PCM plasterboard, this may establish stronger flaming capable of releasing significantly more energy to the compartment.

7.5.2.4 Thermal evolution

The thermal evolution at the positions with the highest measured fire exposure is shown in Figure 7.29. The location of these thermocouples was 500mm above the floor and 100mm from the corner (refer back to Figure 7.11 for locations). Using the thermogravimetric data, it is found that approximately 10.5±1.1mm (or 42±4% of the total thickness) of the material at this location pyrolysed by the end of the 20 min test. If the test duration were extended, it is expected that the thermal wave would continue to propagate through the thickness of the material and generate pyrolysis gases for the remaining 58±4% of material. Thus, a fire exposure longer than 20 mins would contribute greater fuel loading to a compartment.

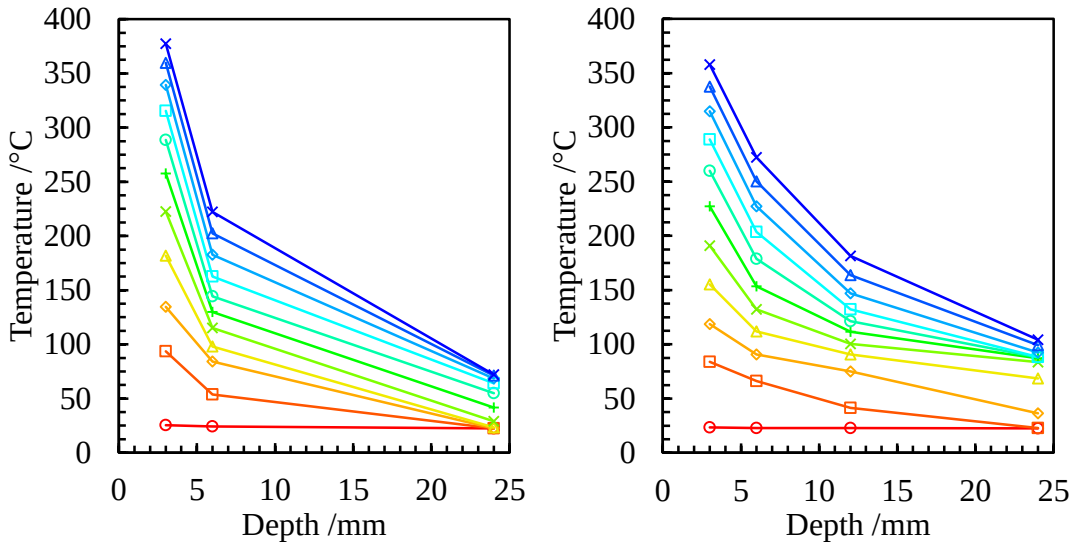

Figure 7.29 - Temperature evolution averaged for two tests at (a) D5 (b) G5. Timesteps are every 120 seconds for the full 20 minute duration of the test. The thermocouple at 12mm in D5 was non-operational from the start of the test.

By three minutes into the test the thermal wave was able to reach the back of the board. Furthermore, the temperature increase through this period is at its highest, and corresponds to the peak HRR (Figure 7.25 and Figure 7.26).

Other locations containing thermocouples which were exposed to the highest levels of radiant heat flux were at C5 and C7, which were 200mm from the corner of the short wing, and at heights of 500 and 700mm respectively. The top 3mm of both these locations reaches the 203.19±0.36°C threshold for pyrolysis and oxidation of the PCM by 18 minutes into the test. This shows the potential for flaming and the combustion of volatiles long after the peak, and that this may continue as the material continues to heat up.

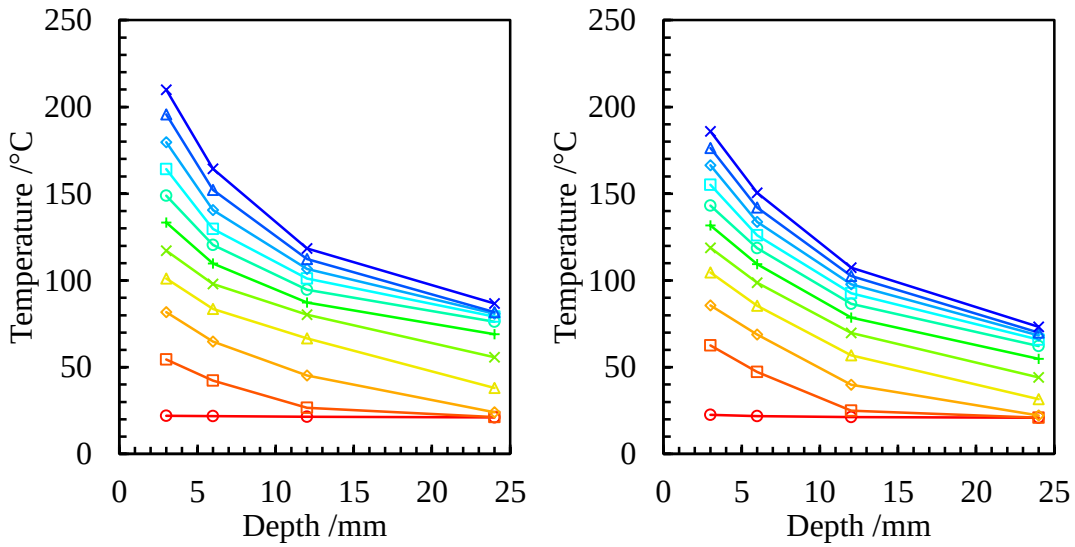

Figure 7.30 - Thermal evolution at (a) C5 (b) C7. Timesteps are every 120 seconds up to 20 minutes, and temperatures are averaged over the two tests.

7.5.2.4.1 Upward spread

Evidence of upward spread is evident where a location a greater distance from the burner – and hence exposed to a lower heat flux – measures a higher temperature than a location closer to the burner. This was observed at heights of 500mm and 700mm for the first 8 mins of both tests, on both wings (Figure 7.31). It is concluded that after this period the flame extinguished due to the build-up of a char layer decreasing the amount of pyrolysis gases generated, and thus the gas mixture dropping below the lower flammability limit. From this point until the end of the test, the lower location, which was exposed to the higher heat flux from the burner, increased in temperature more rapidly.

No lateral flame spread was evident from the temperature measurements in any of the SBI tests. This is to be expected given that this parameter was already explicitly investigated in LIFT, and this material was found to have little propensity for lateral flame spread. In addition, has been identified that the conditions in SBI are not well suited to lateral flame spread for most materials (Messerschmidt 2008). Thus, if the material is not found to promote flame spread in LIFT then it is highly unlikely to occur in SBI.

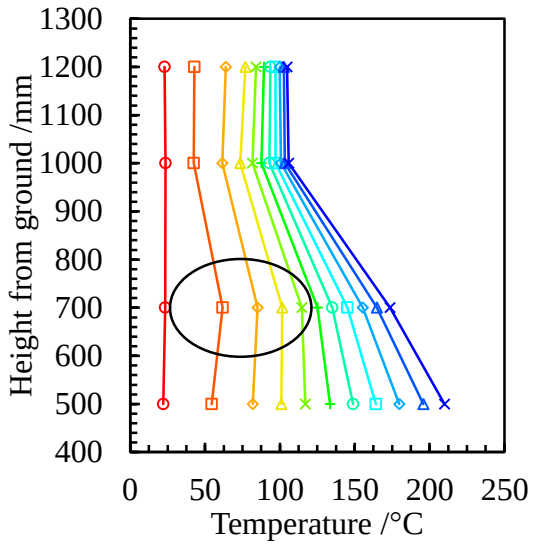

Figure 7.31 - Contribution from PCM plasterboard to upward flame spread, marked in circled area. Thermocouples are positioned 200mm from the corner (gridlines C and H), and readings from both wings and both tests are averaged. Measurements are every 2mins.

7.5.2.5 Visual observations

For both samples and on both wings clear cracks emerged during testing. The crack in the left wing of test 2 (Figure 7.32a) emerged 185mm above the bottom exposed surface, with a length of 210mm. In the right wing (Figure 7.32b) the horizontal crack was 50mm lower, and crossed through a crack near vertical in orientation. It should be noted that no thermocouples were in this area, and that the board was restrained to the supporting calcium silicate board on all the corners.

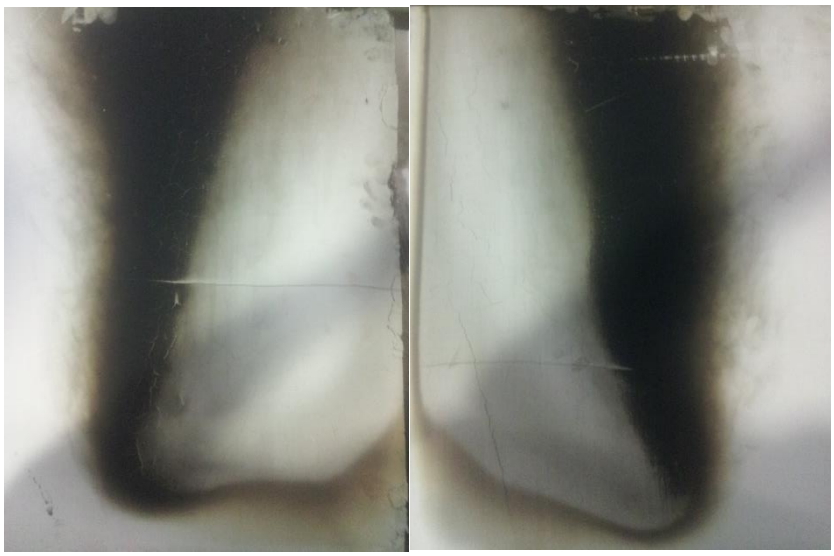

Figure 7.32 - Photos taken after test 2 of (a) left wing, bottom section and (b) right wing, bottom section.

Aside from the large cracks formed and visible during testing, other minor crack patterns were observed. Across the main burning area a pattern of minor horizontal and vertical cracks was present (Figure 7.33a). This is very similar to those observed in the cone calorimeter testing after specimens were removed. This cracking extended up to the pyrolysed area and beyond this point there is no general cracking (Figure 7.33b). There was no failure of the material, but the SBI was able to show that on a larger-scale there is a greater quantity of cracking with this material. Large-scale mechanical effects were shown to be a limitation of SBI previously (Messerschmidt 2008), and thus it is not an effective tool in evaluation the full-scale behaviour of either a fire in a room, or the ISO room corner test.

Figure 7.33 - Some crack patterns from the bottom section of the short wing, test 2 (a) general crack pattern across main burning area (b) cracking desists outside main area of burning.

7.6 Concluding remarks

The following conclusions are made on the intermediate-scale standard fire testing. They have been separated for both flame spread and single burning item.

7.6.1Flame spread

- Over three tests, the standardised results were obtained for spread of flame. These were a critical flux of extinguishment of 29.06kW·m^{-2}, and an average heat for sustained burning of 4.00MJ·m^{-2}.
- The positioning of the pilot flame at the bottom of the specimen extending upwards was found not to be adequate to ignite the flammable gas mixture, even at 50.5±0.5kW·m^{-2}. Instead, autoignition occurred after a delay.
- Due to the ignition conditions, there was little to no strong diffusion flame front established. A transient blue front with consistent flashing or pulsing upstream was observed for around three minutes before extinction occurred.
- The pulsing combustion is hypothesised to be a lean premixed flame front which arises because fuel is consumed faster than it can be generated. This is due to the

charring rate of the material inhibiting the pyrolysis rate, which is slower than the rate of reactions in the gas phase. This effect has been previously noted for long chain paraffins (>C_9) in liquid fires.

- The thermal evolution confirms the lack of radiative and convective flame transfer from the flame to the fuel which was present in the cone calorimeter. This reduces the amount of heat absorbed by the specimen and decreases the pyrolysis rate further, which severely inhibits flame spread.
- The ignition of pyrolysis gases at the bottom of the sample in test 3 confirm that the material is capable of sustaining a strong diffusion flam, as in the cone calorimeter. Thus, it is expected that with an appropriate pilot source that a strong flame front could be established from the start of the test.
- The use of ASTM 1321 instead of ISO 5658 to study flame spread is highly recommended. The cone calorimeter should be used to verify that the incident flux in LIFT is sufficiently high that the specimen will ignite and a strong flame front will be established.
- Overall, flame spread is not believed to be a major hazard for this specific PCM plasterboard. Based on testing on the cone calorimeter, it is believed that even in ASTM 1321 the flame front would not easily be able to propagate. This is due to the small radiative and convective components of the weak flame at the critical heat flux, and the charring nature of the material inhibiting pyrolysis.

Key numerical findings outside of the standardised results are outlined below in Table 7.7.

Table 7.7 – Summary of all flame spread properties for PCM plasterboard.

Parameter		**Value**
Flame spread modulus $(mm \cdot s)^{3/2} \cdot J^{-1}$		28.1
Flame spread parameter $(kW^2 \cdot m^{-3})$		500
Minimum heat flux for spread $(kW \cdot m^{-2})$	Flaming	29.06±7.14
	Flashing	22.39±2.50
	Pyrolysis	14.50±1.01
Ignition temperature (°C)	Flaming	712
	Flashing	553
	Pyrolysis	365

7.6.2 Single burning item

- FIGRA(SBI) was found to be 73.2±13.2$W \cdot s^{-1}$ over two tests thereby suggesting this product to be well within the limits of Euroclass B. SMOGRA was 0.0$m^2 \cdot s^{-2}$ for both tests.
- The fire exposure has been partially characterised by using the in-depth thermal evolution of the PCM plasterboard. The heat flux appears to broadly agree with values put forth by previously by Messerschmidt *et al.* (1999) and Zhang *et al.* (2008).
- Only limited vertical flame spread was identified. This was due to the relatively weak fire exposure, and the charring nature of the material. Based on the cone calorimeter

results, a more severe fire exposure would cause different results since the PCMs would have significantly greater contribution.

- The energy generated and thermal evolution are in line with values found in the cone calorimeter. This confirms the scalability of the flammability study up to an intermediate-scale.
- Large cracks formed during heating in both SBI tests located approximately 150 to 200mm from the bottom, and up to 210mm in length. Otherwise, cracking appears to occur during cooling, as was the case in the cone calorimeter tests. The limited nature of the cracking is expected to be due to the glass fibres interwoven into the matrix of the material, and there is not expected to be failure of the material.
- PCM plasterboard has a different value of FIGRA(SBI) than ordinary gypsum plasterboard, and also different from the various lined plasterboards. Thus it is justified to evaluate the performance of this material using bespoke methods.
- SBI assigns the same classification to ordinary plasterboard and PCM plasterboard but cannot identify the associated fire risks. The flammability study identified that the materials behaved differently, and quantified the fire risk associated with PCM plasterboard.

8 Novel linking frameworks

8.1 Summary

The work in this thesis has provided the platform to develop a novel framework capable of assessing and quantifying the fire performance of phase change materials (PCMs) and hemp-lime insulation. In this chapter, the methodology to link knowledge from each of the chapters is outlined. This provides future researchers and designers with an effective method of characterising the behaviour of PCMs and hemp-lime insulation for use in realistic fire conditions. Optimised energy savings can be achieved whilst still ensuring quantifiable fire performance. Fire risks specific to PCMs and hemp-lime are identified so that designers can employ adequate mitigation strategies specific to the design. A suitable methodology for characterising the smouldering risk associated with porous materials is outlined. There is currently no test method for smouldering and this represents the first characterisation and quantification of the potential fire risks associated with hemp-lime materials in the built environment.

8.2 Motivation

The PCM plasterboard which was studied in this thesis was found to achieve a *B* rating according to the European classification system, BS ISO 13501 (British Standards Institution 2009a). This is the same rating which ordinary plasterboard achieves but the FIGRA(SBI), FIre Growth RAte, was shown to be different for the two materials. This rating is based on the BS ISO 13823 Single Burning Item (British Standards Institution 2010d) test which is used to classify materials. The behaviour of the PCM enhanced plasterboard is shown to be different from the behaviour of the ordinary plasterboard in bench-scale testing and this is not reflected in the rating provided by the Euroclass system. The flammability study in the cone calorimeter testing identified a greater fire risk that was not reflected in either LIFT or SBI. Recommendations were made in *Chapter 7* to run the flame spread according to ASTM 1321 (ASTM International 2013b) as opposed to ISO 5658 (British Standards Institution 2006).

Given that PCM plasterboard and ordinary plasterboard behave differently it is necessary to quantify the fire risks and characterise the behaviour of PCMs applicable to realistic fire conditions. The framework outlined in this thesis provides the means to achieve this. The existing standard fire test methods provide a means for classifying and comparing similar materials but do not deliver knowledge on how they perform in the event of a real fire. Through this understanding it is possible to attain an optimised building design and empower the designer to make decisions based on the quantified fire performance.

Hemp-lime insulation is an innovative building material which currently represents an unquantified fire risk. Due to its porous cellulosic matrix the dominant mode of combustion is smouldering for which there is currently no standard fire test method. There is also no way to characterise its behaviour and these materials have yet to be tested in a way which is

meaningful to their potential risks. The framework in this thesis provides a simple and cost-effective method to evaluate the fire risks associated with these materials to enable their usage in buildings.

8.3 Outline of fire risks

The methodology of the novel frameworks are outlined for both materials, and categorised according to the different fire risks which have been identified. Designers can adopt risk mitigation strategies for each of these key fire risks, and produce a design with both optimised energy savings and quantified fire performance.

8.3.1Ignitability

Ignition represents one of the most fundamental fire risks to these materials since it is the precursor to each of the other risks. If the risks associated with ignition can be mitigated, then the other risks become a non-factor. For both PCMs, which have a low exothermic oxidation temperature, and hemp-lime insulation, which requires little energy to sustain a smoulder, the ignitability represents a significant hazard that must be quantified.

Ignitability can either be evaluated at a surface exposed to an incident heat flux, or as in-depth pyrolysis due to heat transfer through another material within a wall assembly. For incident heat fluxes, using the flaming ignition theory of solids (Torero 2008) there was shown to be strong agreement for PCMs and the materials behaved well. This provides both the critical heat flux, the time to ignition as a function of incident heat flux, as well as the ignition temperature and apparent thermal inertia which can be derived from the above theory. The critical heat flux can be evaluated against suitable fire exposures by the designer, such as those found in the literature (Babrauskas 1995, Quintiere 2006). A range of 25 to 45 $kW \cdot m^{-2}$ was given for the incident heat flux from an upwards travelling flame to a vertical surface, such as a wall lining. Thus, critical heat fluxes below these values could generally be associated with low and quantified ignitability.

For hemp-lime insulation, a suitable method for detecting in-depth ignition was developed. This empirical method was based on carbon monoxide exceeding a 10% threshold which was found to coincide with the onset of glowing ignition at high heat fluxes for energetic materials. At low heat fluxes, the mass loss rate and thermal evolution confirmed the time to ignition. A more fundamental method, although more difficult to implement, has previously been outlined by Boonmee and Quintiere (2005) which is also suitable for use. The ignition theory for solids was also found to hold, and which allowed determination of the smouldering ignition temperature and apparent thermal inertia of the material.

In some cases the material will be concealed behind a barrier and thus an incident heat flux is not immediately useful in determining the ignitability. For these instances, a thermal degradation framework was outlined using thermogravimetric analysis (TGA). This allows the determination of endothermic pyrolysis and exothermic oxidation reactions which can be used to quantify the behaviour of the materials. Given the high ignitability, these values could

be used to ensure that the temperature reached within a wall assembly does not reach the pyrolysis temperature obtained using TGA, and thus there is not either contribution to the fuel load of a compartment, nor the initiation of smouldering reactions concealed deep within a wall assembly. The associated fire risk in this instance may be modified by either adjusting the properties of the protective material, for example, reducing the thermal inertia or increasing its thickness, or by modifying the pyrolysis behaviour of the material. This could potentially be achieved through the addition of flame retardants to increase the pyrolysis temperature and hence either avoid ignition or increase the time so that a building can be safely evacuated. In the case of PCMs, an alternate core material with a higher boiling point, and hence evaporation and pyrolysis temperature, may wish to be considered.

The risk of ignition is intrinsically linked to each of the other risks. If the material does not ignite, then it is not capable of spreading. For fully developed fires the risk of ignition is unavoidable if no protective layer is used, since the incident heat fluxes in a post-flashover fire are typically in the region of 150 to 200kW·m^{-2} (Babrauskas 1995) and thus far higher than any typical critical heat fluxes. This also matches figures found in the Cardington tests, where intensities of 200kW·m^{-2} and beyond were found (Jowsey 2006).

Thus, the risk can be quantified by obtaining the critical heat flux as well as the time to ignition for the appropriate heat fluxes. These can then be evaluated against the heat exposure specified by the designer to evaluate the fire risk associated with these materials. If ignition occurs then the potential for fire growth must be considered.

8.3.2Fire growth

Where ignition is found to occur the greatest risk is that PCMs will facilitate fire growth and cause a response disproportionate to the original source. This is typically evaluated in the propensity to cause flashover in a compartment fire. Both the potential to cause flashover as well as the time taken to reach this stage are often checked. For hemp-lime insulation fire growth can be evaluated using smoulder propagation velocities. Where a smoulder is capable of sustaining there will be the potential for growth from the initial ignition source.

Flame spread is a key parameter in determining the potential for fire growth, and the possibility of flashover. For this it is necessary to understand the rate at which a given burning area will expand, commonly as a function of the heat release rate of the material and time. Furthermore, data on the ignition characteristics of the material are required to be able to describe the spread rate since this will determine the rate at which the flame front of the expanding burning area can propagate. Models of varying complexities which apply these principals are readily available (Magnusson and Sundström 1985, Mowrer and Williamson 1991, Karlsson 1993).

The PCM enhanced plasterboard that was studied was found to behave similarly to a charring material when tested in the cone calorimeter. Thus, fire models for use with charring materials

are suitable for use with these materials, for example, Spearpoint and Quintiere (2000) and Delichatsios *et al.* (2003).

Thus, the ignition properties can first be evaluated as per the previous section. If ignition is found to occur then the propensity for flashover may need to be evaluated. This can be done using flammability properties determined from the cone calorimeter or LIFT apparatus appropriate to the fire exposure imposed by the designer. If the model incorporates flame spread properties then this may be obtained using ASTM 1321 (ASTM International 2013b).

Smouldering propagation velocities for hemp-lime insulation and other porous materials can be calculated using in-depth temperature measurements in the setup devised in the cone calorimeter. A range of heat fluxes can be used to establish different smouldering fronts. This setup allows the study of both downward opposed flow and upward forward flow away from the influence of the radiant heat from the cone heater. Designers may wish to modify the properties of the material if the smoulder is found to accelerate once a smoulder is established. These properties could include increasing the density to decrease permeability and hence oxygen diffusion, reduce the amount of fuel, or increase the critical temperature for smouldering which will inhibit spread. Alternatively, appropriate protection materials may be needed to prevent the smoulder from being able to spread large distances and transition to flaming. As in the previous case, it may also be necessary to ensure that ignition does not occur if the risks associated with fire growth cannot be adequately mitigated.

8.3.3Fire spread

In cases where a fire will be established, such as flashover in a compartment, it is necessary to evaluate the contribution from PCMs. Based on the concept of convective fire spread by Harmathy (1976) this can be used to prevent the fire from spreading away from the origin to elsewhere in a building. For hemp-lime insulation, the unique nature of smouldering means that fire spread can be evaluated through the previous fire risks of ignitability and fire growth.

The flammability study in the cone calorimeter provides sufficient means to be able to quantify the potential contribution of PCMs to the fuel load in a compartment. This also requires knowledge of the pyrolysis and oxidation reactions, which can be found from the thermal degradation framework in the TGA. In-depth thermal measurements can be used to quantify both the area and depth of material which is pyrolysed based on the temperatures for these processes identified using TGA. The flammability study in the cone calorimeter then provides the means to quantify the amount of energy released when exposed to a given heat source. Testing in the SBI showed that this methodology was effective when increased to an intermediate-scale, and the results were in good agreement. This therefore provides the simple and effective means to evaluate the contribution of PCMs to a fire.

8.4 Summary of novel fire frameworks

The frameworks in this thesis have been outlined for both PCMs and hemp-lime insulation. The process is described succinctly below, with one risk illustrated graphically in Figure 8.1.

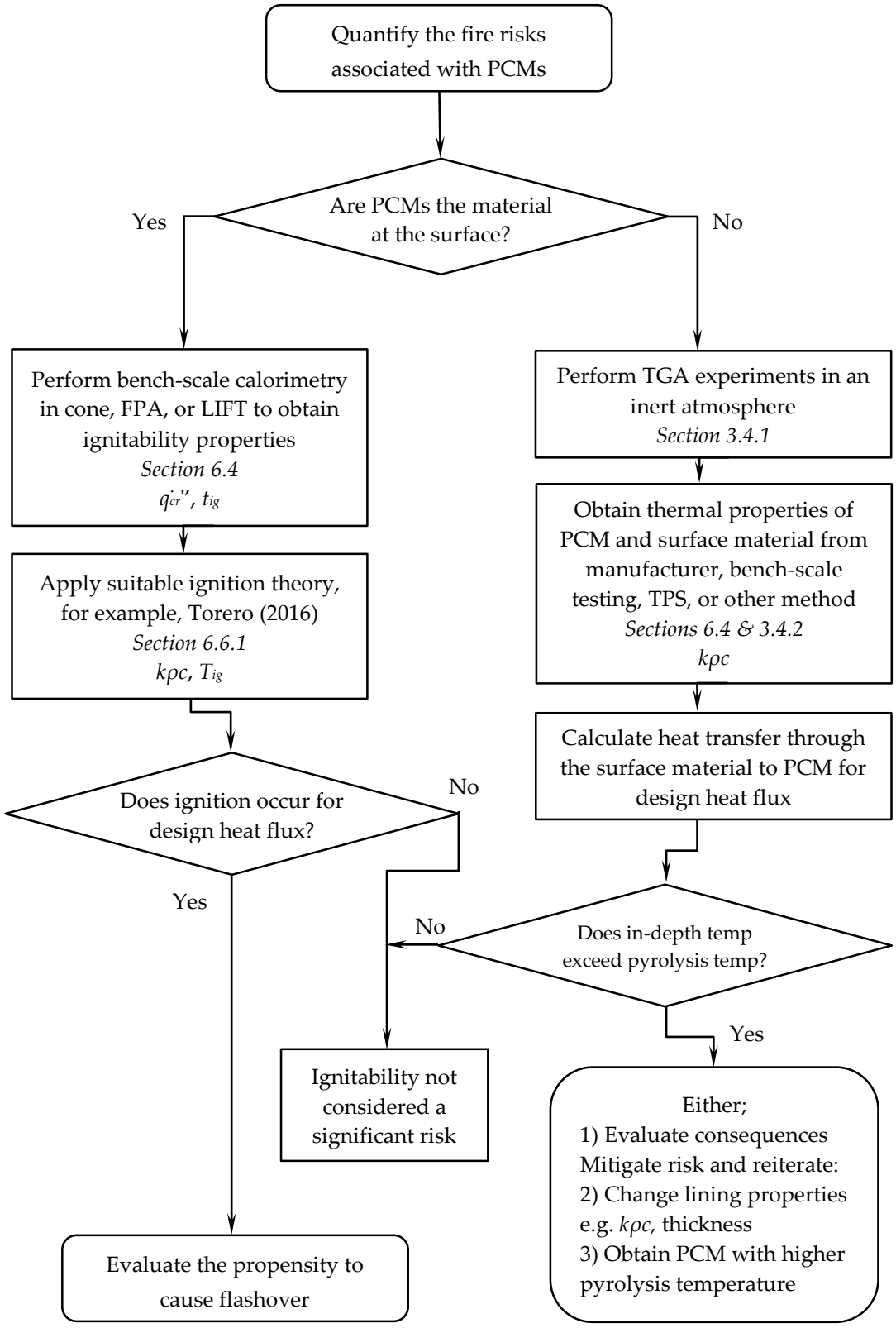

Figure 8.1 – An example of the process for checking the ignitability risk of PCMs

8.4.1Phase change materials

1. Check risk of ignition using critical heat flux and time to ignition from the cone calorimeter for the design fire exposure. For PCMs contained at a depth, evaluate with pyrolysis temperatures from TGA instead.
2. If ignition will occur, then evaluate flame spread and check for the propensity to cause flashover. These are determined using ASTM 1321 LIFT for flame spread, and the cone calorimeter can be used to determine the properties for use in appropriate charring models.
3. If flashover will be reached then the contribution from PCMs should be checked. The flammability study in the cone calorimeter can be matched with the thermal degradation framework from TGA to calculate the amount of material which will be pyrolysed, and how much energy will be released as a result.

8.4.2Hemp-lime insulation

1. Evaluate ignitability using carbon monoxide emissions in the cone calorimeter for a range of incident heat fluxes. Endothermic pyrolysis and exothermic oxidation temperatures can be found in the TGA to ensure no ignition when the material is contained within a wall assembly.
2. If ignition is found to occur, assess the ability to establish a self-sustaining smoulder through the propagation rates in the smouldering methodology developed in the cone calorimeter.

8.5 Concluding remarks

The conclusions relating to the linking framework are as follows:

- Frameworks for both PCM plasterboard and hemp-lime insulation have been outlined using the research contained within this thesis. These provide the means to quantify the fire performance of the materials, which can be balanced by designers with their potential energy savings.
- For both materials, ignitability represents the most important risk and should be the main focus of designers. Some mitigation strategies are outlined, but these can be decided by the designer having quantified the fire risk associated with the material.
- Ignitability, fire growth, and fire spread are identified as the relevant fire risks for PCMs, whilst ignitability and fire growth are identified for hemp-lime insulation.
- Various models can be employed based on the results obtained from the frameworks. These include prediction of flashover for the flammability study, or the behaviour of charring materials for PCM plasterboard. At present, models for predicting smouldering require additional work.

9 Conclusions and further work

In each chapter specific concluding remarks were noted for the body of work covered. In this section, the most important conclusions are collated in addition to some general conclusions for the research as a whole. Finally, suggestions for suitable avenues of further work are given.

9.1 Conclusions

- Phase change materials currently represent an unquantified fire risk which cannot adequately be evaluated using the existing standard fire test methods. This thesis has developed a novel framework to quantify the fire performance of future PCMs to enable designers to implement them within the built environment.
- The addition of PCMs to a substrate material may not affect its classification as part of the existing standard fire testing system but the materials behave fundamentally differently. For this reason it is necessary to quantify the behaviour and ensure that the fire performance can be understood.
- Thermogravimetric Analysis (TGA) was found to be a suitable method to characterise the endothermic pyrolysis and exothermic oxidation reactions. This informs on the ignitability of the material and can be used to identify the effect that the PCM will have on a substrate material.
- Transient Plane Source (TPS) was found as a valid method for obtaining key thermal transport properties. With PCMs the apparatus must be carefully operated to ensure that the phase change at room temperature is avoided. When coupled with a furnace the apparatus is capable of delivering these properties at elevated temperatures for use in more accurate heat transfer or ignition models.
- The behaviour of the PCMs in fire was characterised. It was found that the paraffin wax blend within the capsules evaporates and is able to break free from the polymer acrylic shell. Upon exposure to oxygen the PCM vapours then combust and release substantial amounts of energy.
- PCM plasterboard behaves similar to a charring material and can be treated as such. Thus, its fire behaviour within a compartment can be predicted using an appropriate model as part of a goal driven design.
- At low incident heat fluxes, the fuel consumption rate is faster than the pyrolysis generation rate. This is due to the charring nature of PCM plasterboard, and the rapid rate of reactions in the gas phase. This results in a lean blue premixed flame which pulses across the surface. In flame spread, this front preceded the main diffusion flame front.
- The LIFT apparatus can only be used to evaluate flame spread where the heat flux is sufficiently high that a strong flame front can be established. For PCMs, which have comparatively high critical heat fluxes, the behaviour should first be evaluated in the cone calorimeter before bespoke testing is done in LIFT using an appropriate reference heat flux.

- The cone calorimeter was found to be a viable test apparatus for evaluating smouldering combustion on a bench-scale. This was achieved through the use of a porous specimen holder which allowed the study of a one-dimensional heat transfer problem.
- The smouldering behaviour of hemp-lime insulation was quantified using this methodology. It provides a means to characterise the material which is not currently possible as there are no standard fire test methods applicable to smouldering materials.
- The addition of PCMs to a porous, combustible substrate was shown to increase the ignitability by decreasing the critical heat flux and time to ignition. This was caused by the lower exothermic temperature of the microencapsulated PCM compared to the hemp, thereby lowering the ignition temperature.
- The heat of combustion was increased by the presence of the PCM which thereby increased temperature and the rate of reactions as reflected in the mass loss rate. This caused a more rapid propagation of the smouldering front in both downward opposed and upward forward regimes.
- The Single Burning Item test was not able to evaluate the differences in fire behaviour between plasterboard and PCM plasterboard. The test was found not to be sufficient to characterise more than a small burning item and the duration was insufficient to cause extensive pyrolysis. It is therefore recommended that to quantify the fire performance of PCMs that the novel framework outlined in this thesis is followed.

9.2 Further work

This thesis represents the first in-depth characterisation of PCMs and hemp-lime insulation and as such there are many ripe opportunities for continuing the study. These include:

- The development of a fire model capable of predicting the behaviour of PCMs based on the experimental data that was generated. This was deliberately performed in a wide range of fire conditions so that it would be of use to future researchers.
- The evaluation of other types of organic PCMs so that designers can more readily choose the most appropriate type for their building. Other types include sheets of macroencapsulated PCMs, and various shape stabilised PCMs.
- Testing of a wall assembly to evaluate whether pyrolysis vapours are capable of diffusing through the wall and spreading fire to a compartment away from the origin. This would be coupled with methods to mitigate this fire risk and prevent the spread of fire.
- The behaviour of PCMs may be highly relevant within fire resistance testing. This thesis has focused on the reaction to fire framework but there are still opportunities to evaluate how the addition of PCMs may affect the fire resistance of the substrate.
- Extension of the risk assessment of hemp-lime insulation to other bio-based materials which are becoming increasingly common. An investigation of the transition to flaming may also be highly pertinent.

10 References

Abhat, A., 1983. Low temperature latent heat thermal energy storage: Heat storage materials. *Solar Energy*, 30 (4), 313–332.

Ahmed, M., Meade, O., and Medina, M.A., 2010. Reducing heat transfer across the insulated walls of refrigerated truck trailers by the application of phase change materials. *Energy Conversion and Management*, 51 (3), 383–392.

Akita, K., 1973. Some problems of flame spread along a liquid surface. *Symposium (International) on Combustion*, 14 (1), 1075–1083.

Alaru, M., Kukk, L., Olt, J., Menind, A., Lauk, R., Vollmer, E., and Astover, A., 2011. Lignin content and briquette quality of different fibre hemp plant types and energy sunflower. *Field Crops Research*, 124 (3), 332–339.

Alkan, C. and Sari, A., 2008. Fatty acid/poly(methyl methacrylate) (PMMA) blends as form-stable phase change materials for latent heat thermal energy storage. *Solar Energy*, 82 (2), 118–124.

Alkan, C., Sari, A., and Karaipekli, A., 2011. Preparation, thermal properties and thermal reliability of microencapsulated n-eicosane as novel phase change material for thermal energy storage. *Energy Conversion and Management*, 52 (1), 687–692.

Antal, M.J.J. and Varhegyi, G., 1995. Cellulose Pyrolysis Kinetics: The Current State of Knowledge. *Industrial & Engineering Chemistry Research*, 34 (3), 703–717.

Arnaud, L. and Gourlay, E., 2012. Experimental study of parameters influencing mechanical properties of hemp concretes. *Construction and Building Materials*, 28 (1), 50–56.

Arrhenius, S., 1889. Über die Reaktionngeschwindigkeit bei des Inversion von Rohrzucker durch Säuren. *Zeit. Phys. Chem.*, 4, 226.

Asimakopoulou, E.K., Kolaitis, D.I., and Founti, M.A., 2015. Fire safety aspects of PCM-enhanced gypsum plasterboards: An experimental and numerical investigation. *Fire Safety Journal*, 72, 50–58.

ASTM International, 1998. *D3806-98 Standard Test Method of Small-Scale Evaluation of Fire-Retardant Paints (2-Foot Tunnel Method)*.

ASTM International, 2013a. E2257-13a Standard Test Method for Room Fire Test of Wall and Ceiling Materials and Assemblies.

ASTM International, 2013b. E1321-13: Standard Test Method for Determining Material Ignition and Flame Spread Properties.

ASTM International, 2013c. ASTM E2058-13a Standard Test Methods for Measurement of Material Flammability Using a Fire Propagation Apparatus (FPA).

ASTM International, 2014. E1354-14: Standard Test Method for Heat and Visible Smoke Release Rates for Materials and Products Using an Oxygen Consumption Calorimeter.

Babrauskas, V., 1984. Development of the cone calorimeter—a bench-scale heat release rate apparatus based on oxygen consumption. *Fire and Materials*, 8 (2), 81–95.

Babrauskas, V., 1995. Specimen heat fluxes for bench-scale heat release rate testing. *Fire and Materials*, 19 (6), 243–252.

Babrauskas, V. and Parker, W., 1987. Ignitability measurements with the cone calorimeter. *Fire and Materials*, 11 (1), 31–43.

Babrauskas, V. and Peacock, R.D., 1992. Heat release rate: The single most important variable in fire hazard. *Fire Safety Journal*, 18 (3), 255–272.

Baetens, R., Jelle, B.P., and Gustavsen, A., 2010. Phase change materials for building applications: A state-of-the-art review. *Energy and Buildings*, 42 (9), 1361–1368.

Banu, D., Feldman, D., Haghighat, F., Paris, J., and Hawes, D., 1998. Energy-storing wallboard:

flammability tests. *Journal of Materials in Civil Engineering*, 10 (2), 98–105.

Banu, D., Feldman, D., and Hawes, D., 1998. Evaluation of thermal storage as latent heat in phase change material wallboard by differential scanning calorimetry and large scale thermal testing. *Thermochimica acta*, 317 (1), 39–45.

Bénichou, N. and Sultan, M. a., 2005. Thermal properties of lightweight-framed construction components at elevated temperatures. *Fire and Materials*, 29 (3), 165–179.

Bevan, R. and Woolley, T., 2008. *Hemp lime construction: A guide to building with hemp lime composites*. Bracknell, UK: IHS BRE Press.

Bisby, L., Gales, J., and Maluk, C., 2013. A contemporary review of large-scale non-standard structural fire testing. *Fire Science Reviews*, 2 (1), 1–27.

Biteau, H., 2009. Thermal and chemical behaviour of an energetic material and a heat release rate issue. University of Edinburgh. PhD thesis.

Di Blasi, C., 1994. Processes of flames spreading over the surface of charring fuels: Effects of the solid thickness. *Combustion and Flame*, 97 (2), 225–239.

Boh, B. and Šumiga, B., 2008. Microencapsulation technology and its applications in building construction materials. *RMZ – Materials and Geoenvironment*, 55 (3), 329–344.

Boonmee, N. and Quintiere, J.G., 2002. Glowing and flaming autoignition of wood. *Proceedings of the Combustion Institute*, 29 (1), 289–296.

Boonmee, N. and Quintiere, J.G., 2005. Glowing ignition of wood: The onset of surface combustion. *Proceedings of the Combustion Institute*, 30 (1), 2303–2310.

Braga, S.L., Milón Guzmán, J.J., and Jiménez Pacheco, H.G., 2009. A study of cooling rate of the supercooled water inside of cylindrical capsules. *International Journal of Refrigeration*, 32 (5), 953–959.

Brebu, M. and Vasile, C., 2010. Thermal degradation of lignin—a review. *Cellulose Chemistry & Technology*, 44 (9), 353–363.

British Standards Institution, 1987a. BS 476-21:1987 Fire tests on building materials and structures — Part 21: Methods for determination of the fire resistance of loadbearing elements of construction.

British Standards Institution, 1987b. BS 476-22:1987 Fire tests on building materials and structures—Part 22: Method for determination of the fire resistance of non-loadbearing elements of construction.

British Standards Institution, 1993. *BS 476-33/ISO 9705 Fire tests on building materials and structures - Part 33: Full-scale room test for surface products*. British Standards Institution.

British Standards Institution, 2006. *BS ISO 5658-2:2006 Reaction to fire tests -- Spread of flame -- Part 2: Lateral spread on building and transport products in vertical configuration*.

British Standards Institution, 2009a. *BS EN 13501-1:2007+A1:2009 Fire classification of construction products and building elements — Part 1: Classification using data from reaction to fire tests*. Brussels.

British Standards Institution, 2009b. *BS EN 13501-2:2007+A1:2009 Fire classification of construction products and building elements — Part 2: Classification using data from fire resistance tests, excluding ventilation services*. Brussels.

British Standards Institution, 2009c. BS EN 520:2004+A1:2009 Gypsum plasterboards — Definitions, requirements and test methods.

British Standards Institution, 2010a. *BS EN ISO 1182:2010 Reaction to fire tests for products — Non- combustibility test*. Brussels.

British Standards Institution, 2010b. *BS EN ISO 1716:2010 Reaction to fire tests for products — Determination of the gross heat of combustion (calorific value)*. Brussels.

British Standards Institution, 2010c. *BS EN ISO 11925-2:2010 Reaction to fire tests — Ignitability of products subjected to direct impingement of flame Part 2: Single-flame source test*. Brussels.

British Standards Institution, 2010d. *BS EN ISO 13823. Reaction to fire tests for building products — Building products excluding floorings exposed to the thermal attack by a single burning item*. British Standards Institution, London, UK.

British Standards Institution, 2015a. *BS ISO 5660-1:2015. Reaction-to-fire tests — Heat release, smoke production and mass loss rate. Part 1 : Heat release rate (cone calorimeter method) and smoke production rate (dynamic measurement)*. Brussels.

British Standards Institution, 2015b. *BS ISO 22007-2: Plastics — Determination of thermal conductivity and thermal diffusivity — Part 2: Transient plane heat source (hot disc) method*. London, UK.

Burhenne, L., Messmer, J., Aicher, T., and Laborie, M.-P., 2013. The effect of the biomass components lignin, cellulose and hemicellulose on TGA and fixed bed pyrolysis. *Journal of Analytical and Applied Pyrolysis*, 101, 177–184.

Cabeza, L.F., Castell, A., Barreneche, C., de Gracia, A., and Fernández, A.I., 2011. Materials used as PCM in thermal energy storage in buildings: A review. *Renewable and Sustainable Energy Reviews*, 15 (3), 1675–1695.

Cai, Y., Hu, Y., Song, L., Kong, Q., Yang, R., Zhang, Y., Chen, Z., and Fan, W., 2007. Preparation and flammability of high density polyethylene/paraffin/organophilic montmorillonite hybrids as a form stable phase change material. *Energy Conversion and Management*, 48 (2), 462–469.

Cai, Y., Hu, Y., Song, L., Tang, Y., Yang, R., Zhang, Y., Chen, Z., and Fan, W., 2006. Flammability and thermal properties of high density polyethylene/paraffin hybrid as a form-stable phase change material. *Journal of Applied Polymer Science*, 99 (4), 1320–1327.

Cai, Y., Song, L., He, Q., Yang, D., and Hu, Y., 2008. Preparation, thermal and flammability properties of a novel form-stable phase change materials based on high density polyethylene/poly(ethylene-co-vinyl acetate)/organophilic montmorillonite nanocomposites/paraffin compounds. *Energy Conversion and Management*, 49 (8), 2055–2062.

Cai, Y., Wei, Q., Huang, F., and Gao, W., 2008. Preparation and properties studies of halogen-free flame retardant form-stable phase change materials based on paraffin/high density polyethylene composites. *Applied Energy*, 85 (8), 765–775.

Cai, Y., Wei, Q., Huang, F., Lin, S., Chen, F., and Gao, W., 2009. Thermal stability, latent heat and flame retardant properties of the thermal energy storage phase change materials based on paraffin/high density polyethylene composites. *Renewable Energy*, 34 (10), 2117–2123.

Carpenter, K. and Janssens, M., 2005. Using heat release rate to assess combustibility of building products in the Cone Calorimeter. *Fire Technology*, 41 (2), 79–92.

Carvel, R., Steinhaus, T., Rein, G., and Torero, J.L., 2011. Determination of the flammability properties of polymeric materials: A novel method. *Polymer Degradation and Stability*, 96 (3), 314–319.

Chern, C.S., 2006. Emulsion polymerization mechanisms and kinetics. *Progress in Polymer Science*, 31 (5), 443–486.

Chew, M. and Lim, S.M., 2000. The Impact of Wall Linings on Fire Hazard. *International Journal on Architectural Science*, 1 (2), 96–107.

Coats, A.W. and Redfern, J.P., 1964. Kinetic Parameters from Thermogravimetric Data. *Nature*, 201 (4914), 68–69.

Colinart, T., Glouannec, P., and Chauvelon, P., 2012. Influence of the setting process and the formulation on the drying of hemp concrete. *Construction and Building Materials*, 30, 372–380.

Delichatsios, M., Paroz, B., and Bhargava, A., 2003. Flammability properties for charring

materials. *Fire Safety Journal*, 38 (3), 219–228.

Department for Communities and Local Government, 2006. *Code for Sustainable Homes - A step-change in sustainable home building practice*. Wetherby, UK.

Department for Communities and Local Government, 2012. *The impact of European fire test and classification standards on wallpaper and similar decorative linings*. London, UK: Department for Communities and Local Government.

Drysdale, D., 1999. *An introduction to fire dynamics*. 2nd Ed. Chichester, United Kingdom: John Wiley & Sons.

Drysdale, D.D., 1985. Fundamentals of the Fire Behaviour of Cellular Polymers. *Cellular Polymers*, 4 (6), 405–419.

Drysdale, D.D. and Thomson, H.E., 1989. Flammability of plastics II: Critical mass flux at the firepoint. *Fire Safety Journal*, 14 (3), 179–188.

van Ekeren, P.J., 1998. Chapter 2 Thermodynamic Background to Thermal Analysis and Calorimetry. *Handbook of Thermal Analysis and Calorimetry*, 1, 75–145.

Elfordy, S., Lucas, F., Tancret, F., Scudeller, Y., and Goudet, L., 2008. Mechanical and thermal properties of lime and hemp concrete ('hempcrete') manufactured by a projection process. *Construction and Building Materials*, 22 (10), 2116–2123.

Elizabeth II, 1971. *Misuse of Drugs Act Chapter 38*. United Kingdom.

EN Standards: *See British Standards Institution.*

Entrop, A., Brouwers, H.J.H., and Reinders, A.H.M.E., 2011. Experimental research on the use of micro-encapsulated Phase Change Materials to store solar energy in concrete floors and to save energy in Dutch houses. *Solar Energy*, 85 (5), 1007–1020.

Ettouney, H., El-Dessouky, H., and Al-Ali, A., 2005. Heat Transfer During Phase Change of Paraffin Wax Stored in Spherical Shells. *Journal of Solar Energy Engineering*, 127 (3), 357.

European Parliament, 2010. Directive 2010/31/EU of the European Parliament and of the Council of 19 May 2010 on the energy performance of buildings. *Official Journal of the European Union*, 13–35.

Fang, G., Chen, Z., and Li, H., 2010. Synthesis and properties of microencapsulated paraffin composites with SiO2 shell as thermal energy storage materials. *Chemical Engineering Journal*, 163 (1-2), 154–159.

Faraday, M., 1861. The Chemical History of a Candle. *In*: W. Crookes, ed. *A course of lectures delivered before a juvenile audience at the Royal Institution*. London, UK: Chatto & Windus.

Farid, M.M., Khudhair, A.M., Razack, S.A.K., and Al-Hallaj, S., 2004. A review on phase change energy storage: materials and applications. *Energy Conversion and Management*, 45 (9-10), 1597–1615.

Fernández-Pello, A. and Williams, F.A., 1977. A theory of laminar flame spread over flat surfaces of solid combustibles. *Combustion and Flame*, 28, 251–277.

Fernandez-Pello, A.C., 1984. Flame Spread Modeling. *Combustion Science and Technology*, 39 (1-6), 119–134.

Flynn, J.H. and Wall, L.A., 1966. A quick, direct method for the tetermination of activation energy from thermogravimetric data. *Journal of Polymer Science Part B: Polymer Letters*, 4 (5), 323–328.

Fraser, F.M. and Prosen, E.J., 1955. Heats of combustion of liquid n-hexadecane, 1-hexadecene, n-decylbenzene, n-decylcyclohexane, n-decylcyclopentane, and the variation of heat of combustion with chain length. *Journal of Research of the National Bureau of Standards*, 55 (6), 329.

Friedman, H.L., 1964. Kinetics of thermal degradation of char-forming plastics from thermogravimetry. Application to a phenolic plastic. *Journal of Polymer Science Part C: Polymer Symposia*, 6 (1), 183–195.

Galaska, M.L., Morgan, A.B., Schenck, K.A., and Stalter, J.G., 2014. Apparatus for the vertical orientation cone calorimeter testing of flexible polyurethane foams. *Fire and Materials*.

Gallagher, P.K., 1998. *Chapter 4 Thermogravimetry and Thermomagnetometry*. Handbook of Thermal Analysis and Calorimetry. Elsevier Masson SAS.

Galwey, A.K. and Brown, M.E., 1998. *Chapter 3 Kinetic Background to Thermal Analysis and Calorimetry*. Handbook of Thermal Analysis and Calorimetry. Elsevier Masson SAS.

Ghazi Wakili, K. and Hugi, E., 2009. Four Types of Gypsum Plaster Boards and their Thermophysical Properties Under Fire Condition. *Journal of Fire Sciences*, 27 (1), 27–43.

Ghazi Wakili, K., Hugi, E., Wullschleger, L., and Frank, T., 2007. Gypsum Board in Fire -- Modeling and Experimental Validation. *Journal of Fire Sciences*, 25 (3), 267–282.

Glassman, I. and Dryer, F.L., 1981. Flame spreading across liquid fuels. *Fire Safety Journal*, 3 (3), 123–138.

Gratkowski, M.T., Dembsey, N.A., and Beyler, C.L., 2006. Radiant smoldering ignition of plywood. *Fire Safety Journal*, 41 (6), 427–443.

Grønli, M.G., Várhegyi, G., and Di Blasi, C., 2002. Thermogravimetric Analysis and Devolatilization Kinetics of Wood. *Industrial & Engineering Chemistry Research*, 41 (17), 4201–4208.

Gustafsson, S.E., 1991. Transient plane source techniques for thermal conductivity and thermal diffusivity measurements of solid materials. *Review of Scientific Instruments*, 62 (3), 797–804.

Hadden, R., Alkatib, A., Rein, G., and Torero, J.L., 2012. Radiant Ignition of Polyurethane Foam: The Effect of Sample Size. *Fire Technology*.

Hadden, R.M., 2011. Smouldering and self-sustaining reactions in solids: an experimental approach. University of Edinburgh. PhD thesis.

Haines, P.J., Reading, M., and Wilburn, F.W., 1998. *Chapter 5 Differential Thermal Analysis and Differential Scanning Calorimetry*. Handbook of Thermal Analysis and Calorimetry. Elsevier Masson SAS.

Hakkarainen, T., 2001. Rate of Heat Release and Ignitability Indices in Predicting SBI Test Results. *Journal of Fire Sciences*, 19 (4), 284–305.

Hakkarainen, T. and Kokkala, M.A., 2001. Application of a one-dimensional thermal flame spread model on predicting the rate of heat release in the SBI test. *Fire and Materials*, 25 (2), 61–70.

Hakkarainen, T., Messerschmidt, B., Hansen, A.S., and Thureson, P., 1998. SP Report 1998:20 Comparison of Nordic Classification System for Surface Linings and Floor Coverings with the EU Euroclasses for Surface Linings and Floor Coverings.

Hall, K., 2013. An experimental investigation into the use of Hemp-lime as a fire protection material for structural steel. University of Edinburgh. MEng thesis.

Harmathy, T.Z., 1975. The role of thermal feedback in compartment fires. *Fire Technology*, 11 (1), 48–54.

Harmathy, T.Z., 1976. Design of buildings for fire safety — Part I. *Fire Technology*, 12 (2), 95–108.

Harmathy, T.Z., 1979. Effect of the nature of fuel on the characteristics of fully developed compartment fires. *Fire and Materials*, 3 (1), 49–60.

Haurie, L., Mazo, J., Delgado, M., and Zalba, B., 2014. Fire behaviour of a mortar with different mass fractions of phase change material for use in radiant floor systems. *Energy and Buildings*, 84 (December), 86–93.

Hawes, D.W., 1991. Latent Heat Storage in Concrete. Concordia University.

Hawes, D.W., Banu, D., and Feldman, D., 1992. The stability of phase change materials in concrete. *Solar Energy Materials and Solar Cells*, 27 (2), 103–118.

Hawes, D.W. and Feldman, D., 1992. Absorption of phase change materials in concrete. *Solar Energy Materials and Solar Cells*, 27 (2), 91–101.

He, Y., 2005. Rapid thermal conductivity measurement with a hot disk sensor: Part 1. Theoretical considerations. *Thermochimica Acta*, 436 (1-2), 122–129.

Hidalgo-Medina, J.P., 2015. Performance-based methodology for the fire safe design of insulation materials in energy efficient buildings. The University of Edinburgh. PhD thesis.

Hong, H., Kim, S.K., and Kim, Y.-S., 2004. Accuracy improvement of T-history method for measuring heat of fusion of various materials. *International Journal of Refrigeration*, 27 (4), 360–366.

Huggett, C., 1980. Estimation of Rate of Heat Release by Means of Oxygen Consumption Measurements. *Fire and Materials*, 4 (2), 61–65.

Ingberg, S., 1928. Tests of the severity of building fires. *NFPA Quarterly*, 22 (1), 43–61.

Ip, K. and Miller, A., 2012. Life cycle greenhouse gas emissions of hemp-lime wall constructions in the UK. *Resources, Conservation and Recycling*, 69, 1–9.

ISO Standards: *See British Standards Institution.*

Janssens, M., 2002. Calorimetry. *In*: P. DiNenno, ed. *SFPE Handbook of Fire Protection Engineering*. Quincy, Massachusetts: National Fire Protection Association, 3.38–3.62.

Janssens, M., 2011. Thermogravimetric Study of Dehydration and Thermal Degradation of Gypsum Board at Elevated Temperatures. *Fire Safety Science*, 10, 295–306.

Janssens, M.L., 1991. Measuring rate of heat release by oxygen consumption. *Fire Technology*, 27 (3), 234–249.

Jessup, B.R.S. and Prosen, E.J., 1950. Heats of Combustion and Formation of Cellulose and Nitrocellulose (Cellulose Nitrate). *Journal of Research of the National Bureau of Standards*, 44 (April), 387–393.

Johansson, P. and Van Hees, P., 2000. *SP Rapport 2000:26 Development of a Test Procedure for Sandwich Panels using ISO 9705 Philosophy - Nordtest project nr 1432-99*. Borås, Sweden.

Jowsey, A., 2006. Fire imposed heat fluxes for structural analysis. University of Edinburgh. PhD thesis.

Karkri, M., Lachheb, M., Albouchi, F., Nasrallah, S. Ben, and Krupa, I., 2015. Thermal properties of smart microencapsulated paraffin/plaster composites for the thermal regulation of buildings. *Energy and Buildings*, 88, 183–192.

Karlsson, B., 1993. A mathematical model for calculating heat release rate in the room corner test. *Fire Safety Journal*, 20 (2), 93–113.

Kashiwagi, T. and Nambu, H., 1992. Global kinetic constants for thermal oxidative degradation of a cellulosic paper. *Combustion and Flame*, 88 (3-4), 345–368.

Kawagoe, K., 1958. *Fire Behaviour in Rooms - Report No. 27*. The Building Research Institute, Ministry of Construction.

Kenisarin, M.M. and Kenisarina, K.M., 2012. Form-stable phase change materials for thermal energy storage. *Renewable and Sustainable Energy Reviews*, 16 (4), 1999–2040.

Khudhair, A., 2004. A review on energy conservation in building applications with thermal storage by latent heat using phase change materials. *Energy Conversion and Management*, 45 (2), 263–275.

Kifani-Sahban, F., Belkbir, L., and Zoulalian, A., 1996. Etude de la pyrolyse lente de l'Eucalyptus marocain par analyse thermique. *Thermochimica Acta*, 284 (2), 341–349.

Kikas, T., Tutt, M., Raud, M., Alaru, M., Lauk, R., and Olt, J., 2015. Basis of Energy Crop Selection for Biofuel Production: Cellulose vs. Lignin. *International Journal of Green Energy*, ((in press)).

Kissel, T., Maretschek, S., Packhauser, C., Schnieders, J., and Seidel, N., 2006.

Microencapsulation Techniques for Parental Depot Systems and Their Application in the Pharmaceutical Industry. *In*: S. Benita, ed. *Microencapsulation: Methods and Industrial Applications*. Boca Raton, USA: Taylor & Francis Group, 99–118.

Kokkala, M.A., Thomas, P.H., and Karlsson, B., 1993. Rate of heat release and ignitability indices for surface linings. *Fire and Materials*, 17 (5), 209–216.

Kolaitis, D.I., Asimakopoulou, E.K., and Founti, M. a, 2013. Gypsum plasterboards enhanced with phase change materials: A fire safety assessment using experimental and computational techniques. *MATEC Web of Conferences*, 9, 06002.1–06002.11.

Kontogeorgos, D.A., Mandilaras, I.D., and Founti, M.A., 2015. Fire behavior of regular and latent heat storage gypsum boards. *Fire and Materials*, 39 (5), 507–517.

Konuklu, Y. and Paksoy, H.O., 2009. Phase Change Material Sandwich Panels for Managing Solar Gain in Buildings. *Journal of Solar Energy Engineering*, 131 (4), 041012.1–041012.7.

Koschenz, M. and Lehmann, B., 2004. Development of a thermally activated ceiling panel with PCM for application in lightweight and retrofitted buildings. *Energy and Buildings*, 36 (6), 567–578.

Kośny, J., David W., Y., Timothy, R., Douglass, L., Jogn B., S., and Marcus, B., 2009. Development and testing of ignition resistant microencapsulated phase change material. *In*: *Proceedings of the Effstock 2009 - The 11th international conference on thermal energy storage*. Stockholm, Sweden.

Kuznik, F., David, D., Johannes, K., and Roux, J.-J., 2011. A review on phase change materials integrated in building walls. *Renewable and Sustainable Energy Reviews*, 15 (1), 379–391.

Kuznik, F. and Virgone, J., 2009. Experimental assessment of a phase change material for wall building use. *Applied Energy*, 86 (10), 2038–2046.

Kuznik, F., Virgone, J., and Johannes, K., 2010. Development and validation of a new TRNSYS type for the simulation of external building walls containing PCM. *Energy and Buildings*, 42 (7), 1004–1009.

Kuznik, F., Virgone, J., and Noel, J., 2008. Optimization of a phase change material wallboard for building use. *Applied Thermal Engineering*, 28 (11-12), 1291–1298.

Lamprecht, I., 1999. Combustion Calorimetry. *In*: *Handbook of Thermal Analysis and Calorimetry*. 175–218.

Lanas, J., Pérez Bernal, J.L., Bello, M.A., and Alvarez Galindo, J.I., 2004. Mechanical properties of natural hydraulic lime-based mortars. *Cement and Concrete Research*, 34 (12), 2191–2201.

Law, M., 1986. Translation Of Research Into Practice: Building Design. *Fire Safety Science*.

Laye, P.G., 2002. *Differential Thermal Analysis and Differential Scanning Calorimetry*. Principles of Thermal Analysis and Calorimetry. Cambridge, UK: Royal Society of Chemistry.

Lázaro, D., Puente, E., Lázaro, M., Lázaro, P.G., and Peña, J., 2015. Thermal modelling of gypsum plasterboard assemblies exposed to standard fire tests. *Fire and Materials*, n/a–n/a.

Lee, S.H., Yoon, S.J., Kim, Y.G., Choi, Y.C., Kim, J.H., and Lee, J.G., 2007. Development of building materials by using micro-encapsulated phase change material. *Korean Journal of Chemical Engineering*, 24 (2), 332–335.

Lee, S.H., Yoon, S.J., Kim, Y.G., and Lee, J.G., 2011. The utilization of microencapsulated phase change material wallboards for energy saving. *Korean Journal of Chemical Engineering*, 28 (11), 2206–2210.

Lee, T., Hawes, D.W., Banu, D., and Feldman, D., 2000. Control aspects of latent heat storage and recovery in concrete. *Solar Energy Materials*, 62 (3), 217–237.

Li, W., Zhang, X., Wang, X., Tang, G., and Shi, H., 2012. Fabrication and morphological characterization of microencapsulated phase change materials (MicroPCMs) and macrocapsules containing MicroPCMs for thermal energy storage. *Energy*, 38 (1), 249–

254.

Liang, C., Lingling, X., Hongbo, S., and Zhibin, Z., 2009. Microencapsulation of butyl stearate as a phase change material by interfacial polycondensation in a polyurea system. *Energy Conversion and Management*, 50 (3), 723–729.

Lin, K., Zhang, Y., Xu, X., Di, H., Yang, R., and Qin, P., 2005. Experimental study of under-floor electric heating system with shape-stabilized PCM plates. *Energy and Buildings*, 37 (3), 215–220.

Log, T. and Gustafsson, S., 1995. Transient plane source (TPS) technique for measuring thermal transport properties of building materials. *Fire and Materials*, 19 (August 1994), 43–49.

MacRitchie, F., 1969. Mechanism of interfacial polymerization. *Transactions of the Faraday Society*, 65, 2503–2507.

Magnusson, S.E. and Sundström, B., 1985. Combustible Linings and Room Fire Growth - A First Analysis. *In*: T.Z. Harmathy, ed. *Fire safety science and engineering, ASTM STP 882*. Philadelphia, PA: American Society for Testing and Materials, 45–69.

Majdalani, A.H., 2014. Compartment Fire Analysis for Contemporary Architecture. University of Edinburgh. PhD thesis.

Maluk, C., 2014. Development and Application of a Novel Test Method for Studying the Fire Behaviour of CFRP Prestressed Concrete Structural Elements. University of Edinburgh. PhD thesis.

Mankowski, J. and Kolodziej, J., 2008. Increasing Heat of Combustion of Briquettes Made of Hemp Shives. *International Conference on Flax and Other Bast Plants*, 344–352.

Manzello, S.L., Gann, R.G., Kukuck, S.R., and Lenhert, D.B., 2007. Influence of gypsum board type (X or C) on real fire performance of partition assemblies. *Fire and Materials*, 31 (7), 425–442.

Manzello, S.L., Grosshandler, W.L., and Mizukami, T., 2010. Furnace testing of full-scale gypsum steel stud non-load bearing wall assemblies: Results of multi-laboratory testing in Canada, Japan, and USA. *Fire Technology*, 46 (1), 183–200.

McGrattan, K., Hostikka, S., McDermott, R., Floyd, J., Weinschenk, C., and Overholt, K., 2014. *NIST Special Publication 1019. Sixth Edition: Fire Dynamics Simulator - User's Guide*.

Mehaffey, J.R., Cuerrier, P., and Carisse, G., 1994. A Model for Predicting Heat Transfer through Gypsum-Board/Wood-Stud Walls Exposed to Fire. *Fire and Materials*, 18 (5), 297–305.

Mehling, H. and Cabeza, L.F., 2008. *Heat and cold storage with PCM*. Berlin, Heidelberg: Springer.

Messerschmidt, B., 2008. The Capabilities and Limitations of the Single Burning Item (SBI) Test. *In*: *Fire and Building Safety in the Single European Market*. 70–81.

Messerschmidt, B., Van Hees, P., and Wickström, U., 1999. Prediction of SBI (Single Burning Item) test results by means of cone calorimeter test results. *In*: *Interflam '99*. 11–22.

van Mierlo, R. and Sette, B., 2005. The Single Burning Item(SBI) test method - a decade of development and plans for the near future. *Heron*, 50 (4), 191–207.

Mowrer, F. and Williamson, R., 1991. Flame Spread Evaluation For Thin Interior Finish Materials. *Fire Safety Science*, 3, 689–698.

Mowrer, F.W., 2004. Flammability of oil-based painted gypsum wallboard subjected to fire heat fluxes. *Fire and Materials*, 28 (5), 355–385.

Mowrer, F.W., 2005. An analysis of effective thermal properties of thermally thick materials. *Fire Safety Journal*, 40 (5), 395–410.

Mwaikambo, L.Y. and Ansell, M.P., 2002. Chemical modification of hemp, sisal, jute, and kapok fibers by alkalization. *Journal of Applied Polymer Science*, 84 (12), 2222–2234.

Ohlemiller, T. and Lucca, D., 1983. An experimental comparison of forward and reverse smolder propagation in permeable fuel beds. *Combustion and Flame*, 54 (1-3), 131–147.

Ohlemiller, T.J., 1985. Modeling of smoldering combustion propagation. *Progress in Energy and Combustion Science*, 11 (4), 277–310.

Ohlemiller, T.J., 2008. Smoldering Combustion. *In*: P. DiNenno, ed. *SFPE Handbook of Fire Protection Engineering*. Quincy, Massachusetts: National Fire Protection Association, 2.229–2.240.

Oliver, A., 2012. Thermal characterization of gypsum boards with PCM included: Thermal energy storage in buildings through latent heat. *Energy and Buildings*, 48, 1–7.

Ouajai, S. and Shanks, R. a., 2005. Composition, structure and thermal degradation of hemp cellulose after chemical treatments. *Polymer Degradation and Stability*, 89 (2), 327–335.

Ozawa, T., 1965. A New Method of Analyzing Thermogravimetric Data. *Bulletin of the Chemical Society of Japan*, 38 (11), 1881–1886.

Ozonur, Y., Mazman, M., Paksoy, H.O., and Evliya, H., 2006. Microencapsulation of coco fatty acid mixture for thermal energy storage with phase change material. *International Journal of Energy Research*, 30 (10), 741–749.

Park, S.H., L. Manzello, S., Bentz, D.P., and Mizukami, T., 2010. Determining thermal properties of gypsum board at elevated temperatures. *Fire and Materials*, 34 (5), 237–250.

Pasupathy, A., Velraj, R., and Seeniraj, R.V., 2008. Phase change material-based building architecture for thermal management in residential and commercial establishments. *Renewable and Sustainable Energy Reviews*, 12 (1), 39–64.

Pironi, P., 2009. Smouldering Combustion of Organic Liquids in Porous Media for Remediating NAPL-contaminated Soils. University of Edinburgh. PhD thesis.

Pironi, P., Switzer, C., Gerhard, J.I., Rein, G., and Torero, J.L., 2011. Self-sustaining smoldering combustion for NAPL remediation: laboratory evaluation of process sensitivity to key parameters. *Environmental science & technology*, 45 (7), 2980–6.

Pironi, P., Switzer, C., Rein, G., Fuentes, A., Gerhard, J.I., and Torero, J.L., 2009. Small-scale forward smouldering experiments for remediation of coal tar in inert media. *Proceedings of the Combustion Institute*, 32 (2), 1957–1964.

Prosen, E.J. and Rossini, F.D., 1945. Heats of combustion and formation of the paraffin hydrocarbons at 25 C. *Journal of Research of the National Bureau of Standards*, 34 (3), 263.

Putzeys, O.M., Fernandez-Pello, A.C., Rein, G., and Urban, D.L., 2008. The piloted transition to flaming in smoldering fire retarded and non-fire retarded polyurethane foam. *Fire and Materials*, 32 (8), 485–499.

Qiu, X., Li, W., Song, G., Chu, X., and Tang, G., 2012. Fabrication and characterization of microencapsulated n-octadecane with different crosslinked methylmethacrylate-based polymer shells. *Solar Energy Materials and Solar Cells*, 98 (2012), 283–293.

Quintiere, J., 1981. A simplified theory for generalizing results from a radiant panel rate of flame spread apparatus. *Fire and Materials*.

Quintiere, J., Harkleroad, M., and Walton, D., 1983. Measurement of Material Flame Spread Properties. *Combustion Science and Technology*, 32 (1-4), 67–89.

Quintiere, J.G., 2006. *Fundamentals of Fire Phenomena*.

Quintiere, J.G. and Harkleroad, M.T., 1985. New Concepts for Measuring Flame Spread Properties. *In*: T.Z. Harmathy, ed. *Fire safety science and engineering, ASTM STP 882*. Philadelphia, PA, 239–267.

Quintiere, J.G., Harkleroad, M.T., and Hasemi, Y., 1986. Wall Flames and Implications for Upward Flame Spread. *Combustion Science and Technology*, 48 (3-4), 191–222.

Rachini, A., Troedec, M. Le, Peyratout, C., and Smith, A., 2009. Comparison of the thermal degradation of natural, alkali-treated and silane-treated hemp fibers under air and an

inert atmosphere. *Journal of Applied Polymer Science*, 112, 226–234.

Ramachandran, V.S., Paroli, R.M., Beaudoin, J.J., and Delgado, A.H., 2003. Gypsum and gypsum products. *In*: *Handbook of Thermal Analysis of Construction Materials*.

Rasbash, D.J., 1975. Relevance of firepoint theory to the assessment of fire behaviour of combustible materials. *International Symposium on Fire Safety of Combustible Materials*, 169–178.

Rasbash, D.J., Drysdale, D.D., and Deepak, D., 1986. Critical heat and mass transfer at pilot ignition and extinction of a material. *Fire Safety Journal*, 10 (1), 1–10.

Rein, G., 2009. Smouldering combustion phenomena in science and technology. *International Review of Chemical Engineering*, 1, 3–18.

Rein, G., 2013. Smouldering Fires and Natural Fuels. *In*: C.M. Belcher, ed. *Fire Phenomena and the Earth System: An Interdisciplinary Guide to Fire Science*. Oxford: John Wiley & Sons, 15–33.

Rein, G., 2016. Smoldering Combustion. *In*: *SFPE Handbook of Fire Protection Engineering*. 581–603.

Rein, G., Carlos Fernandez-Pello, a, and Urban, D.L., 2007. Computational model of forward and opposed smoldering combustion in microgravity. *Proceedings of the Combustion Institute*, 31 (2), 2677–2684.

Rein, G., Cohen, S., and Simeoni, A., 2009. Carbon emissions from smouldering peat in shallow and strong fronts. *Proceedings of the Combustion Institute*, 32 (2), 2489–2496.

Rein, G., Lautenberger, C., Fernandezpello, a, Torero, J., and Urban, D., 2006. Application of genetic algorithms and thermogravimetry to determine the kinetics of polyurethane foam in smoldering combustion. *Combustion and Flame*, 146 (1-2), 95–108.

Reszka, P., 2008. In-Depth Temperature Profiles in Pyrolyzing Wood. University of Edinburgh.

Rich, D., Lautenberger, C., Torero, J.L., Quintiere, J.G., and Fernandez-Pello, C., 2007. Mass flux of combustible solids at piloted ignition. *Proceedings of the Combustion Institute*, 31 (2), 2653–2660.

Richardson, L. and Brooks, M., 1991. Combustibility of building materials. *Fire and Materials*, 15 (3), 131–136.

Rigips AG, 2015. Alba®balance brochure Version 2.0b [online]. Available from: www.rigips.ch.

de Ris, J.N., 1969. Spread of a laminar diffusion flame. *Symposium (International) on Combustion*.

Robertson, A. and Ohlemiller, T., 1995. Low heat-flux measurements: some precautions. *Fire Safety Journal*, 25 (2), 109–124.

Rozanna, D., Chuah, T.G., Salmiah, A., Choong, T.S.Y., and Sa'ari, M., 2005. Fatty Acids as Phase Change Materials (PCMs) for Thermal Energy Storage: A Review. *International Journal of Green Energy*, 1 (4), 495–513.

Salyer, I.O. and Sircar, A.K., 1990. Phase change materials for heating and cooling of residential buildings and other applications. *In*: P.A. Nelson, W.W. Schertz, and R.H. Till, eds. *25th Intersociety Energy Conversion Engineering Conference*. Reno, Nevada: American Institute of Chemical Engineers, 236–243.

Salyer, I.O., Sircar, A.K., and Dantiki, S., 1988. *Advanced phase change materials and systems for solar passive heating and cooling of residential buildings. Final Technical Report on DOE Grant DE-FG03-86SF16308*. Dayton, USA.

Sánchez, L., Sánchez, P., Lucas, A., Carmona, M., and Rodríguez, J.F., 2007. Microencapsulation of PCMs with a polystyrene shell. *Colloid and Polymer Science*, 285 (12), 1377–1385.

Sanders, J.P. and Gallagher, P.K., 2002. Kinetic analyses using simultaneous TG / DSC

measurements Part I : decomposition of calcium carbonate in argon. *Thermochimica Acta*, 388 (1–2), 115–128.

Sanders, J.P. and Gallagher, P.K., 2005. Kinetic Analyses using TG/DSC measurements. Part II: Decompostion of calcium carbonate having different particle sizes. *Journal of Thermal Analysis and Calorimetry*, 82 (3), 659–664.

Sari, A. and Alkan, C., 2012. Preparation and thermal energy storage properties of poly (n-butyl methacrylate)/fatty acids composites as form-stable phase change materials. *Polymer Composites*, 33 (1), 92–98.

Sarı, A., Alkan, C., Karaipekli, A., and Uzun, O., 2009. Microencapsulated n-octacosane as phase change material for thermal energy storage. *Solar Energy*, 83 (10), 1757–1763.

Sari, A. and Karaipekli, A., 2007. Thermal conductivity and latent heat thermal energy storage characteristics of paraffin/expanded graphite composite as phase change material. *Applied Thermal Engineering*, 27 (8-9), 1271–1277.

Sarier, N. and Onder, E., 2012. Organic phase change materials and their textile applications: An overview. *Thermochimica Acta*, 540, 7–60.

Scalat, S., Banu, D., Hawes, D., Paris, J., Haghighata, F., and Feldman, D., 1996. Full scale thermal testing of latent heat storage in wallboard. *Solar Energy Materials and Solar Cells*, 44 (1), 49–61.

Schartel, B. and Hull, T.R., 2007. Development of fire-retarded materials-Interpretation of cone calorimeter data. *Fire and Materials*, 31 (5), 327–354.

Schemel, C.F., Simeoni, A., Biteau, H., Rivera, J.D., and Torero, J.L., 2008. A calorimetric study of wildland fuels. *Experimental Thermal and Fluid Science*, 32 (7), 1381–1389.

Sharma, A., Tyagi, V., Chen, C., and Buddhi, D., 2009. Review on thermal energy storage with phase change materials and applications. *Renewable and Sustainable Energy Reviews*, 13 (2), 318–345.

Shields, T.J., Silcock, G.W., and Murray, J.J., 1993. The Effects of Geometry and Ignition Mode on Ignition Times Obtained Using a Cone Calorimeter and ISO Ignitability Apparatus. *Fire and Materials*, 17 (1), 25–32.

Simms, D.L., 1963. On the pilot ignition of wood by radiation. *Combustion and Flame*, 7, 253–261.

Spearpoint, M.J. and Quintiere, J.G., 2000. Predicting the burning of wood using an integral model. *Combustion and Flame*, 123 (3), 308–325.

Spearpoint, M.J. and Quintiere, J.G., 2001. Predicting the piloted ignition of wood in the cone calorimeter using an integral model — effect of species, grain orientation and heat flux. *Fire Safety Journal*, 36 (4), 391–415.

Steinhaus, T., 2010. Determination of Intrinsic Material Flammability Properties from Material Tests assisted by Numerical Modelling. University of Edinburgh.

Stritih, U. and Novak, P., 1996. Solar heat storage wall for building ventilation. *Renewable Energy*, 8, 268–271.

Su, J.-F., Wang, L.-X., and Ren, L., 2005. Preparation and characterization of double-MF shell microPCMs used in building materials. *Journal of Applied Polymer Science*, 97 (5), 1755–1762.

Su, J.-F., Wang, S.-B., Zhou, J.-W., Huang, Z., Zhao, Y.-H., Yuan, X.-Y., Zhang, Y.-Y., and Kou, J.-B., 2010. Fabrication and interfacial morphologies of methanol–melamine–formaldehyde (MMF) shell microPCMs/epoxy composites. *Colloid and Polymer Science*, 289 (2), 169–177.

Su, J.F., Wang, X.Y., Wang, S.B., Zhao, Y.H., Zhu, K.Y., and Yuan, X.Y., 2011. Interface stability behaviors of methanol-melamine-formaldehyde shell microPCMs/epoxy matrix composites. *Polymer Composites*, 32 (5), 810–820.

Sundström, B., 2007. The Development of a European Fire Classification System for Building Products Test Methods and Mathematical Modelling. Lund University. PhD thesis.

Sundström, B. and Axelsson, J., 2002. Development of a common European system for fire testing of pipe insulation based on EN 13823 (SBI) and ISO 9705 (Room/Corner Test).

Suppes, G.J., Goff, M.J., and Lopes, S., 2003. Latent heat characteristics of fatty acid derivatives pursuant phase change material applications. *Chemical Engineering Science*, 58 (9), 1751–1763.

Sutton, A., Black, D., and Walker, P., 2011a. *IP 14/11 Hemp lime: an introduction to low-impact building materials*. Bracknell, UK: IHS BRE Press.

Sutton, A., Black, D., and Walker, P., 2011b. *IP 18/11 Natural fibre insulation: an introduction to low-impact building materials*. Bracknell, UK: IHS BRE Press.

Switzer, C., Gerhard, J.I., Pironi, P., Rein, G., and Torero, J.L., 2009. Self-sustaining smouldering combustion: A novel remediation process for non-aqueous phase liquids in porous media. *Environmental Science and Technology*, 43 (15), 5871–5877.

Tewarson, A., 1980. Heat release rate in fires. *Fire and Materials*, 4 (4), 185–191.

Thomas, G., 2002. Thermal properties of gypsum plasterboard at high temperatures. *Fire and Materials*, 26 (1), 37–45.

Thomas, P.H. and Heselden, A.J.M., 1972. Fully developed compartment fires in a single compartment- A cooperative programme of the Conseil Interntational du Batiment. Fire Research Note 923.

Thomson, H.E. and Drysdale, D.D., 1987. Flammability of plastics I: Ignition temperatures. *Fire and Materials*, 11 (4), 163–172.

Thornton, W.M., 1917. XV. The relation of oxygen to the heat of combustion of organic compounds. *Philosophical Magazine Series 6*, 33 (194), 196–203.

Torero, J.L., 1992. Buoyancy Effects on Smoldering of Polyurethane Foam. University of California, Berkeley. PhD thesis.

Torero, J.L., 2008. Flaming Ignition of Solid Fuels. *In*: P.J. DiNenno, ed. *SFPE Handbook of Fire Protection Engineering*. Quincy, Massachusetts: National Fire Protection Association, 2.260–2.278.

Torero, J.L., 2013. Scaling-Up fire. *Proceedings of the Combustion Institute*, 34 (1), 99–124.

Torero, J.L., 2016. Flaming Ignition of Solid Fuels. *In*: *SFPE Handbook of Fire Protection Engineering*. New York, NY: Springer New York, 633–661.

Torero, J.L. and Fernandez-Pello, A.C., 1995. Natural convection smolder of polyurethane foam, upward propagation. *Fire Safety Journal*, 24 (1), 35–52.

Torero, J.L. and Fernandez-Pello, A.C., 1996. Forward smolder of polyurethane foam in a forced air flow. *Combustion and Flame*, 106 (1-2), 89–109.

Torero, J.L., Fernandez-Pello, A.C., and Kitano, M., 1993. Opposed Forced Flow Smoldering of Polyurethane Foam. *Combustion Science and Technology*, 91 (1-3), 95–117.

Torero, J.L., Majdalani, A.H., Abecassis-empis, C., and Cowlard, A., 2014. Revisiting the Compartment Fire. *In*: *11th International Symposium on Fire Safety Science*.

Tsai, K.C., 2009. Orientation effect on cone calorimeter test results to assess fire hazard of materials. *Journal of Hazardous Materials*, 172 (2-3), 763–772.

Tyagi, V.V. and Buddhi, D., 2007. PCM thermal storage in buildings: A state of art. *Renewable and Sustainable Energy Reviews*, 11 (6), 1146–1166.

Tyagi, V.V., Kaushik, S.C., Tyagi, S.K., and Akiyama, T., 2011. Development of phase change materials based microencapsulated technology for buildings: A review. *Renewable and Sustainable Energy Reviews*, 15 (2), 1373–1391.

Vivaldo-Lima, E., Wood, P.E., and Hamielec, A.E., 1997. An updated review on suspension polymerization. *Industrial & Engineering Chemistry Research*, 36 (4), 939–965.

Walker, R., Pavia, S., and Mitchell, R., 2014. Mechanical properties and durability of hemp-lime concretes. *Construction and Building Materials*, 61, 340–348.

Warrington, S.B., 2002. Simultaneous Thermal Analysis Techniques. *In*: *Principles of Thermal Analysis and Calorimetry*. Cambridge, UK: Royal Society of Chemistry, 166–189.

Wichman, I.S., 1992. Theory of opposed-flow flame spread. *Progress in Energy and Combustion Science*, 18 (6), 553–593.

Witkowski, A., Stec, A.A., and Hull, T.R., 2016. Thermal Decomposition of Polymeric Materials. *In*: *SFPE Handbook of Fire Protection Engineering*. New York, NY: Springer New York, 167–254.

Wright, A., 2013. Hempcrete: A Revolution in Fire Protection? University of Edinburgh. MEng thesis.

Wullschleger, L. and Ghazi Wakili, K., 2008. Numerical parameter study of the thermal behaviour of a gypsum plaster board at fire temperatures. *Fire and Materials*, 32 (2), 103–119.

Wuttig, M. and Yamada, N., 2007. Phase-change materials for rewriteable data storage. *Nature materials*, 6 (11), 824–832.

Xiao, W., Wang, X., and Zhang, Y., 2009. Analytical optimization of interior PCM for energy storage in a lightweight passive solar room. *Applied Energy*, 86 (10), 2013–2018.

Yang, H., Yan, R., Chen, H., Lee, D.H., and Zheng, C., 2007. Characteristics of hemicellulose, cellulose and lignin pyrolysis. *Fuel*, 86 (12-13), 1781–1788.

Yao, F., Wu, Q., Lei, Y., Guo, W., and Xu, Y., 2008. Thermal decomposition kinetics of natural fibers: Activation energy with dynamic thermogravimetric analysis. *Polymer Degradation and Stability*, 93 (1), 90–98.

Yermán, L., Hadden, R.M., Carrascal, J., Fabris, I., Cormier, D., Torero, J.L., Gerhard, J.I., Krajcovic, M., Pironi, P., and Cheng, Y.-L., 2015. Smouldering combustion as a treatment technology for faeces: Exploring the parameter space. *Fuel*, 147 (1 May 2015), 108–116.

Zalba, B., Marín, J., Cabeza, L.F., and Mehling, H., 2003. Review on thermal energy storage with phase change: materials, heat transfer analysis and applications. *Applied Thermal Engineering*, 23 (3), 251–283.

Zhang, H., Sun, S., Wang, X., and Wu, D., 2011. Fabrication of microencapsulated phase change materials based on n-octadecane core and silica shell through interfacial polycondensation. *Colloids and Surfaces A: Physicochemical and Engineering Aspects*, 389 (1-3), 104–117.

Zhang, H. and Wang, X., 2009a. Synthesis and properties of microencapsulated n-octadecane with polyurea shells containing different soft segments for heat energy storage and thermal regulation. *Solar Energy Materials and Solar Cells*, 93 (8), 1366–1376.

Zhang, H. and Wang, X., 2009b. Fabrication and performances of microencapsulated phase change materials based on n-octadecane core and resorcinol-modified melamine-formaldehyde shell. *Colloids and Surfaces A: Physicochemical and Engineering Aspects*, 332 (2-3), 129–138.

Zhang, H., Wang, X., and Wu, D., 2010. Silica encapsulation of n-octadecane via sol-gel process: a novel microencapsulated phase-change material with enhanced thermal conductivity and performance. *Journal of colloid and interface science*, 343 (1), 246–55.

Zhang, H., Xu, Q., Zhao, Z., Zhang, J., Sun, Y., Sun, L., Xu, F., and Sawada, Y., 2012. Preparation and thermal performance of gypsum boards incorporated with microencapsulated phase change materials for thermal regulation. *Solar Energy Materials and Solar Cells*, 102, 93–102.

Zhang, J., Delichatsios, M., and Colobert, M., 2008. Assessment of Fire Dynamics Simulator for Heat Flux and Flame Heights Predictions from Fires in SBI Tests. *Fire Technology*, 46

(2), 291–306.

Zhang, P., Hu, Y., Song, L., Ni, J., Xing, W., and Wang, J., 2010. Effect of expanded graphite on properties of high-density polyethylene/paraffin composite with intumescent flame retardant as a shape-stabilized phase change material. *Solar Energy Materials and Solar Cells*, 94 (2), 360–365.

Zhang, Y., Zhou, G., Lin, K., Zhang, Q., and Di, H., 2007. Application of latent heat thermal energy storage in buildings: State-of-the-art and outlook. *Building and Environment*, 42 (6), 2197–2209.

Zhang, Y.P., Lin, K.P., Yang, R., Di, H.F., and Jiang, Y., 2006. Preparation, thermal performance and application of shape-stabilized PCM in energy efficient buildings. *Energy and Buildings*, 38 (10), 1262–1269.

Zhang, Y.X. and Yang, C.H., 2009. Recent developments in finite element analysis for laminated composite plates. *Composite structures*, 88 (1), 147–157.

Zhou, D., Zhao, C.Y., and Tian, Y., 2011. Review on thermal energy storage with phase change materials (PCMs) in building applications. *Applied Energy*, 86.

Zhou, G., Yang, Y., and Xu, H., 2011. Performance of shape-stabilized phase change material wallboard with periodical outside heat flux waves. *Applied Energy*, 88 (6), 2113–2121.